XLIV CBrAVIC

Hotel Leão da Montanha, Campos do Jordão – SP, 25 a 29 de novembro de 2023

25 -29 NOVEMBRO DE 2023



CONGRESSO BRASILEIRO DE APLICAÇÕES DE VÁCUO NA INDÚSTRIA E CIÊNCIA

> HOTEL LEÃO DA MONTANHA CAMPOS DO JORDÃO/SP

ISBN: 978-65-01-61692-6 DOI: 10.17563/cbravic.2023

Book of Extended Abstracts 2023



XLIV CBrAVIC

Brazilian Congress on Vacuum Applications in Industry and Science

Book of Extended Abstracts 2023

edited by

Ana Carla de Paula Leite Almeida Rafael Resende Lucas Rogério Pinto Mota Nazir Monteiro dos Santos



Hotel Leão da Montanha - Campos do Jordão, SP, Brazil November 25-29, 2023

International Cataloging of Publication

B827 Brazilian Congress on Vacuum Applications in Industry and Science (44. : 2023 : Campos do Jordão, SP).

Book of extended abstracts of the XLIV CBrAVIC [electronic resource] / editors: Ana Carla de Paula Leite Almeida ... [et al.]. – Campos do Jordão, SP: CBrAVIC, 2023.

ISBN: 978-65-01-61692-6 DOI: 10.17563/cbravic.2023

1. Applied sciences. 2. Industry. 3. Technology. I. Almeida, Ana Carla de Paula Leite. II. Lucas, Rafael Resende. III. Mota, Rogério Pinto. IV. Santos, Nazir Monteiro dos. V. Brazilian Congress on Vacuum Applications in Industry and Science.

CDU 6 CDD 60

Prepared by the librarian Priscila Rodrigues dos Santos CRB1/3381

Sobre

Desde 1979, pesquisadores e instituições que atuam na área de Ciências, Tecnologia e Engenharia, juntamente com a Sociedade Brasileira de Vácuo (SBV) vêm organizando, anualmente, o Congresso Brasileiro de Aplicações de Vácuo na Indústria e na Ciência (CBrAVIC). Esse importante e tradicional evento conta com o apoio de universidade e instituições de pesquisa que congregam os principais segmentos da comunidade científica.

A organização do evento deste ano foi feita pela UNESP, agregando os campi de Bauru, Guaratinguetá e Sorocaba e Sociedade Brasileira de Vácuo (SBV).

O evento foi realizado entre os dias 25 e 29 de novembro de 2023 no Hotel Leão da Montanha em Campos do Jordão – SP e a programação contou com minicursos, palestras nacionais e internacionais e apresentações de trabalhos.

Em busca de complementar as capacidades nacionais por meio de atividades e projetos de cooperação, colaborações internacionais estão associadas ao evento através da "International Union for Vacuum Science, Technique and Applications (IUVSTA)".

A IUVSTA é uma união de 33 sociedades internacionais de ciências e tecnologia cujo papel é estimular a colaboração internacional nos campos da ciência, tecnologia e aplicações do vácuo, e tópicos multidisciplinares relacionados. Através desta colaboração, o CBrAVIC pretende aproximar ciência e tecnologia para satisfazer interesses acadêmicos e industriais.



REALIZAÇÃO:





ORGANIZADORES:





INSTITUIÇÕES PARCEIRAS:



























PATROCINADORES:











Preface

This year, the "CBrAVIC – Brazilian Congress on Vacuum Applications in Industry and Science" celebrates its forty-fourth edition, to be held at the Leão da Montanha Hotel in Campos do Jordão, São Paulo, from November 25 to 29, 2023.

This initiative highlights the maturity and dynamism of the National Scientific Community, engaged in various knowledge areas such as Physics, Chemistry, Engineering, Biology, Medicine, among others.

In accordance with the traditions of previous editions, the Organizing Committee sought to bring together national and international researchers from different fields of knowledge, aiming to enrich the event through invited lectures. The choice of a current theme in Science and Technology aims to contribute significantly to the personal and professional development of all participants.

The Organizing Committee has decided to give prominence to works in the form of posters, consequently reducing the number of oral presentations. This decision aims to revive the opportunity for more in-depth discussions between presenters and interested congress attendees. Thus, the "Poster Sections" now compete on equal footing for the attention of all congress participants.

The Organizing Committee expresses the hope that this initiative is well-received by participants of the XLIV CBrAVIC and that it becomes a tradition, acknowledging the effort and dedication of all involved in the preparation of their presentations.

Nazir Monteiro dos Santos Brazilian Vacuum Society President

Prefácio

Neste ano, o "CBrAVIC – Congresso Brasileiro de Aplicações de Vácuo na Indústria e na Ciência" celebra sua quadragésima quarta edição, a ser realizada nas instalações do Hotel Leão da Montanha, em Campos do Jordão, São Paulo, no período de 25 a 29 de novembro de 2023.

Essa iniciativa destaca a maturidade e o dinamismo da Comunidade Científica Nacional, engajada em diversas áreas do conhecimento, como Física, Química, Engenharia, Biologia, Medicina, entre outras.

Em conformidade com as tradições das edições anteriores, o Comitê Organizador buscou reunir pesquisadores nacionais e internacionais de diferentes campos do conhecimento, com o objetivo de enriquecer o evento por meio de palestras convidadas. A escolha de uma temática atual em Ciência e Tecnologia visa contribuir de maneira significativa para o desenvolvimento pessoal e profissional de todos os participantes.

Decidiu-se, por parte do Comitê Organizador, dar destaque aos trabalhos na forma de pôsteres, reduzindo, consequentemente, o número de apresentações orais. Essa decisão visa resgatar a oportunidade de debates mais aprofundados entre os apresentadores e os congressistas interessados. Assim, as "Seções de Pôsteres" passaram a competir em igualdade de condições pelo centro das atenções de todos os congressistas.

O Comitê Organizador expressa a esperança de que essa iniciativa seja bem recebida pelos participantes do XLIV CBrAVIC e que ela se torne uma tradição, em reconhecimento ao esforço e dedicação de todos os envolvidos na elaboração de suas apresentações.

Nazir Monteiro dos Santos Sociedade Brasileira de Vácuo Presidente

The main topics to be discussed at XLIV CBrAVIC are:

- Biomaterials, Biofilms and Bioprocesses: Science and Technology;
- Plasma Science and Tecnology;
- Science and Technology of Sensors and Devices;
- Vacuum Science and Technology;
- Materials Science and Technology;
- Energy: Renewable Sources and Technology;
- General and Applied Physics and Chemistry;
- Nanoscience, nanotechnology and Nanomaterials;
- Surfaces, Interfaces and Thin Films;
- Treatment and Modifications of Materials;
- Vacuum in Industry.

Palestrantes Convidados (Invited Speakers)

Invited Plenary Speakers:

- PhD Katsuyuki Fukutani Institute of Industrial Science, University of Tokyo
- Dr. Durval Rodrigues Júnior Universidade de São Paulo Escola de Engenharia de Lorena
- PhD Jean-Michel Pouvesle GREMI, UMR7344 CNRS/Orleans University, Université d'Orléans, Orléans, France
- Dr. Marcelo Juni Ferreira European Spallation Source
- PhD Rachael L. Myers-Ward U.S. Naval Research Laboratory, USA
- PhD Diana Grondona Universidad de Buenos Aires, Argentina
- Dr. Carlos Roberto Grandini UNESP/FC/Bauru, Brazil
- Dr. Waldemar A.A. Macedo Centro de Desenvolvimento da Tecnologia Nuclear, Brazil
- Dr. Paulo Noronha Lisboa-Filho São Paulo University, Bauru, SP, Brazil
- Dr. Alvaro José Damião Instituto de Estudos Avançados, CTA, Brazil

Invited Oral Presentations

- Prof. Konstantin Georgiev Kostov Development of atmospheric pressure plasma jets for large area surface treatment
- Prof. Luis César Fontana Effect of shape and asymmetry of the voltage pulse on plasma ionization rate
- Prof^a. Cristiane Yumi Koga Ito Helium cold plasma for the treatment of oral lesions in rats undergoing chemotherapy
- Dr. Pedro Augusto Nascente AISI 316L stainless steel coated with Ti-Nb-Zr ternaray alloys

- Prof^a. Elidiane Cipriano Rangel Properties of N95 respirators exposed to O2/SF6 desinfection plasma
- Prof. Clodomiro Alves Júnior Growth of salt flower in plasma-activated hypersaline water

ORGANIZAÇÃO

COORDENAÇÃO GERAL (OVERALL COORDINATION)

- Dr. Nilson Cristino da Cruz | UNESP Campus Sorocaba/SP Coordenador
- Dr. Rogério Pinto Mota | UNESP Campus Guaratinguetá/SP Coordenador Adjunto
- Dr. Carlos Roberto Grandini | UNESP Campus Bauru/SP Coordenador Adjunto
- Dr. Mauricio Antônio Algatti | UNESP Campus Guaratinguetá/SP Editor dos Proceedings
- Dr. Konstantin G. Kostov | UNESP Campus Guaratinguetá/SP Editor Associado
- Dra. Nazir Monteiro dos Santos | SBV / Fatec Editora Associada
- Ana Cristina Leme | UNESP Campus Guaratinguetá/SP Secretária

COMITÊ ORGANIZADOR (ORGANIZING COMMITTEE)

- Dra. Ana Paula Rosifini Alves | UNESP Campus Guaratinguetá/SP
- Dr. Angel Fidel Vilche Penha | UNESP Presidente Prudente/SP
- Dr. Carlos Alberto Fonzar Pintão | UNESP Campus Bauru/SP
- Dr. Carlos Roberto Grandini | UNESP Campus Bauru/SP
- Dra. Cristiane Yumi Koga Ito | UNESP Campus São José dos Campos/SP
- Dr. Diego Rafael Nespeque Correa | UNESP Campus Bauru/SP
- Dr. Durval Rodrigues Júnior | EEL/USP Campus Lorena/SP
- Dr. Edson Cocchieri Botelho | UNESP Campus Guaratinguetá/SP
- Dr. Elidiane Cipriano Rangel | UNESP Campus Sorocaba
- Dr. Felipe Vicente de Paula Kodaira | UNESP Campus Guaratinguetá/SP
- Dr. Fellype do Nascimento | UNESP Campus Guaratinguetá/SP
- Dr. Fernando Luiz de C. Carvalho | UNESP Campus São José dos Campos/SP
- Dr. Francisco Tadeu Degasperi | Fatec-SP / CEETEPS
- Dr. José Roberto Ribeiro Bortoleto | UNESP Campus Sorocaba
- Dr. Konstantin G. Kostov | UNESP Campus Guaratinguetá/SP
- Dr. Mauricio Antônio Algatti | UNESP Campus Guaratinguetá/SP
- Dra. Nazir Monteiro dos Santos | SBV / Fatec
- Dr. Nilson Cristino da Cruz | UNESP Campus Sorocaba/SP
- Dra. Olívia Maria Berengue | UNESP Campus Guaratinguetá/SP
- Dr. Paulo Noronha Lisboa Filho | UNESP Campus Bauru/SP
- Dra. Rita de Cássia Cipriano Rangel | UFABC Santo André/SP
- Dr. Rogério Pinto Mota | UNESP Campus Guaratinguetá/SP
- Dr. Steven Frederick Durrant | UNESP Campus Sorocaba/SP
- Dr. Teófilo Miguel de Souza | UNESP Campus Guaratinguetá/SP

Dr. William Chiappim Júnior | UNESP - Campus Guaratinguetá/SP

COMITÊ CIENTÍFICO (SCIENTIFIC COMMITTEE)

- Dra. Adriana de Oliveira Delgado Silva | UFSCar Campus Sorocaba
- Dr. Adriano Gonçalves dos Reis | UNESP Campus São José dos Campos/SP
- Dra. Ana Neilde R Silva | USP Campus São Paulo/SP
- Dr. André Luiz Rangel | UNESP Campus Guaratinguetá/SP
- Dr. André Ricardo Marcondes | INPE Campus São José dos Campos/SP
- Ms. Ângelo Luiz Gobbi | LNNano Campinas/SP
- Dr. Antonio Renato Bigansolli | UFRRJ Campus Seropédica/RJ
- Dr. Argemiro Soares da Silva | ITA/CTA São José dos Campos/SP
- Dr. Carlos Roberto Grandini | UNESP Campus Bauru/SP
- Dr. Cícero Rafael Cena da Silva | UFMS Campus Campo Grande/MS
- Dr. Clodomiro Alves Júnior | UFERSA Campus Mossoró/RN
- Dra. Cristiane Costa Wachesk | UNIFESP Campus São Paulo/SP
- Dra. Danieli Aparecida P. Reis | UNIFESP Campus São José dos Campos/SP
- Dra. Deborah Cristina Ribeiro dos Santos | SBV Guaratinguetá/SP
- Dra. Elaine Conceição de Oliveira | Fatec-Sorocaba/ CEETEPS
- Dra. Elidiane Cipriano Rangel | UNESP Campus Sorocaba/SP
- Dra. Érica Freire Antunes | INPE Campus São José dos Campos/SP
- Dr. Evaldo José Corat | INPE Campus São José dos Campos/SP
- Dr. Felipe Carneiro da Silva | Fatec-Cotia / CEETEPS
- Dr. Fernando Luiz de C. Carvalho | UNESP Campus São José dos Campos/SP
- Dr. Francisco Tadeu Degasperi | Fatec-SP / CEETEPS
- Dra. Gabriela Araújo Ranieri | UNIFEI Campus Itajubá/MG
- Dr. Gelson B. de Souza | UEPG Campus Ponta Grossa/PR
- Dr. Gilberto Petraconi Filho | ITA/CTA São José dos Campos/SP
- Dra. Graziela da Silva Savonov | INPE Campus São José dos Campos/SP
- Dr. João Moro | IFSP Campus Bragança Paulista/SP
- Dr. José Lucena Barbosa Júnior | UFRRJ Campus Seropédica/RJ
- Dr. Julio César Sagás | UDESC Campus Joinville/SC
- Dr. Konstantin G. Kostov | UNESP Campus Guaratinguetá/SP
- Dra. Luciana Sgarbi Rossino | Fatec-So / CEETEPS
- Dr. Luís César Fontana | UDESC Campus Joinville/SC
- Dr. Marcelo Juni Ferreira, European Spallation Source (ERIC-SUÉCIA)
- Dr. Marco Aurélio Alvarenga Monteiro | UNESP Campus Guaratinguetá/SP



- Dr. Marcos Dorigão Manfrinato | Fatec-So / CEETEPS
- Dra. Maria Lúcia Pereira da Silva | USP Campus São Paulo/SP
- Dra. Maria Margareth da Silva | ITA/CTA São José dos Campos/SP
- Dra. Marina Fuser Pillis | IPEN/CNEN Campus São Paulo/SP
- Dr. Mario Ueda | INPE Campus São José dos Campos/SP
- Dr. Mauricio Antônio Algatti | UNESP Campus Guaratinguetá/SP
- Dr. Michel Felipe Lima de Araújo | UDC Campus Foz do Iguaçu/PR
- Dr. Milton Eiji Kayama | UNESP Campus Guaratinguetá/SP
- Dr. Mostafa Dadashbaba | Yeditepe University Istambul/Turquia
- Dra. Neidenei Gomes Ferreira | INPE Campus São José dos Campos/SP
- Dr. Nilson Cristino Cruz | UNESP Campus Sorocaba/SP
- Dra. Odila Florêncio | UFSCar Campus Sorocaba
- Dr. Pedro Augusto de Paula Nascente | UFSCar Campus São Carlos/SP
- Dr. Pedro William Moreira Júnior | ITA São José dos Campos/SP
- Dr. Rafael Toledo | UNILA Campus Foz do Iguaçu/PR
- Dra. Renata Antoun Simao | UFRJ Campus Rio de Janeiro/RJ
- Dr. Roberto Yzumi Honda | UNESP Campus Guaratinguetá/SP
- Dr. Rodrigo Sávio Pessoa | ITA/CTA São José dos Campos/SP
- Dr. Rogério de Almeida Vieira | UNIFESP Campus São Paulo/SP
- Dr. Rogério Pinto Mota | UNESP Campus Guaratinguetá/SP
- Dr. Ronaldo C. Cozza | FEI Campus São Bernardo do Campo/SP / Fatec-Mauá
- Dr. Rui de Góes Casqueira | UFRRJ Campus Seropédica/RJ
- Dra. Samantha de Fátima M. Mariano | INPE Campus São José dos Campos/SP
- Dra. Silvia Pierre Irazusta | Fatec-So / CEETEPS
- Dr. Steven Frederick Durrant | UNESP Campus Sorocaba/SP

COMITÊ ACADÊMICO (ACADEMIC COMMITTEE)

- Me. Ana Carla de Paula Leite Almeida | UNESP Campus Guaratinguetá/SP
- Me. Ananias Alves Barbosa | UNESP Campus Guaratinguetá/SP
- Me. Bruna de Oliveira Pinto | UNESP Campus Bauru/SP
- Me. Bruno Henrique da Silva Leal | UNESP Campus Guaratinguetá/SP
- Me. Cesar Augusto Antônio Jr. | UNESP Campus Sorocaba/SP
- Me. Fernanda de Freitas Quadros | UNESP Campus Bauru/SP
- Me. Jhuliene Ellen Torrento | UNESP Campus Bauru/SP
- Dr. Jonas Frank Reis | UNESP Campus Guaratinguetá/SP
- Me. Kléber Alexandre Petroski | UNESP Campus Guaratinguetá/SP

Me. Luís Felipe Barbosa Marques | UNESP - Campus Guaratinguetá/SP

Dr. Pedro Akira Bazaglia Kuroda | UNESP - Campus Bauru/SP

Dr. Rafael Parra Ribeiro | UNESP - Campus Sorocaba/SP

Me. Rafael Resende Lucas | UNESP - Campus Guaratinguetá/SP

Thayna Fernandes Tavares | UNESP - Campus Guaratinguetá/SP

Me. Thiago de Sousa Pereira | UNESP - Campus Bauru/SP

Tuane Stephania Reis dos Santos | UNESP - Campus Guaratinguetá/SP



SOCIEDADE BRASILEIRA DE VÁCUO (BRAZILIAN VACUUM SOCIETY)

BIÊNIO 2023-2025 (BIENNIUM 2023-2025)

DIRETORIA EXECUTIVA

Presidente: Nazir Monteiro dos Santos (FATEC)

1º Vice Presidente: Luis Cesar Fontana (UDESC)

2º Vice Presidente: Maria Lucia Pereira da Silva (USP/FATEC)

1º Diretor Secretário: Carlos Roberto Grandini (UNESP)

2º Diretor Secretário: Francisco Tadeu Degasperi (FATEC)

1º Diretor Tesoureiro: Rogério Pinto Mota (UNESP)

2º Diretor Tesoureiro: Antonio Renato Bigansolli (UFRRJ)

Diretor Científico: Luciana Sgarbi Rossino (FATEC)

Diretor Cultural: Júlio César Sagas (UDESC)

CONSELHO DELIBERATIVO

- A) Sócios Efetivos e/ou Honorários
- 1. Alvaro José Damião (IEAv)
- 2. Mário Ueda (INPE)
- 3. Elidiane Cipriano Rangel (UNESP)
- 4. Érica Freire Antunes (INPE)

SUPLENTES:

1. Marcelo Azevedo (Agilent) 2. Marcelo Juni Ferreira (ESS ERIC)

B) Sócios Coletivos e/ou Mantenedores

1. Avaco 2. INPE 3. Agilent 4. Antoon Paar

SUPLENTE: IEAV

CONSELHO FISCAL

- 1. Angelo Luiz Gobbi (LNNano)
- 2. Mauricio Algatti (UNESP)
- 3. Luciano Rugério da Silva (Inert Solution)

SUPLENTES:

1. Carlos Fonzar Pintão (UNESP) 2. Rogério Gelamo (UFTM)

PROGRAMAÇÃO DAS PALESTRAS E APRESENTAÇÃO DE PÔSTERES

CONFERENCE'S TIMETABLE

	Friday (24/11)	Saturday (25/11)	Monday (27/11)	Tuesday (28/11)	Wednesday (29/11)
08:30/09:30		Minicourses: 1. "Plasma for the treatment and deposition of materials"	Registration	Plenary talk #5 PhD Rachael L. Myers-Ward	
09:30/10:00	Minicourse: "Introduction to Vacuum Science and	Unesp Campus de Guaratinguetá. 2."Active Learning: A	Opening Ceremony	Plenary talk #6 PhD Diana Grondona	Vacuum Metrology
10:00/10:50	Technology" Faculdade de Tecnologia de São	thought-provoking approach" Unesp Campus de Guaratinguetá.	Plenary talk #1 PhD Katsuyuki Fukutani	Refreashment break (10:10/10:20)	
10:50/11:10	Paulo - FATEC/SP -	3. "Introduction to	Refreashment break		Refreashment break
11:10/12:00	CEETEPS	Vacuum Science and Technology" Faculdade de Tecnologia de São Paulo - FATEC/SP - CEETEPS	Plenary talk #2 Dr. Durval Rodrigues Júnior		Plenary talk #9 Dr. Paulo Noronha Lisboa-Filho
12:00/12:20			Oral contribution #1 Prof. Konstantin Georgiev Kostov	Vacuum in Industry	Oral contribution #5 Prof ^a . Elidiane Cipriano Rangel
12:20/12:40			Oral contribution #2 Prof. Luis César Fontana		Oral contribution #6 Prof. Clodomiro Alves Júnior
12:40/14:00			Lunch	Lunch	Lunch
14:00/14:50		Minicourses:	Plenary talk #3 PhD Jean-Michel Pouvesle	Plenary talk #7 Dr. Carlos Roberto Grandini	Plenary talk #10 Dr. Alvaro José Damião
14:50/15:40	Minicourse: "Introduction to metrology and uncertainty calculation" Faculdade de Tecnologia de São Paulo - FATEC/SP – CEETEPS	un to Unesp Campus de Guaratinguetá. (14:00/ 18:00)	Plenary talk #4 Dr. Marcelo Juni Ferreira	Plenary talk #8 Dr. Waldemar A.A. Macedo	
15:40/16:00			Refreashment break	Refreashment break Poster Session	Poster Session #2
16:00/16:40		2. "Introduction to rarefied gas dynamics: Theory and applications to vacuum systems" Faculdade de Tecnologia de São Paulo - FATEC/SP – CEETEPS (13:30/17:30)	Poster Session #1	Oral contribution #3 Prof ^a . Cristiane Yumi Koga Ito Oral contribution #4 Dr. Pedro Augusto Nascente	Refreashment break (16:20/16:40)
16:40/17:40				Annual Meeting of the Brazilian Vacuum Society	Closing and awards
17:40/20:00	Minicourse:	Minicourse:			
20:00 /22:00	"Modeling and calculation of vacuum systems" Faculdade de Tecnologia de São Paulo - FATEC/SP — CEETEPS	1. "Introduction to vacuum metrology" Faculdade de Tecnologia de São Paulo - FATEC/SP – CEETEPS (19:00/22:00)		Conference Dinner	

PROGRAMAÇÃO COMPLETA

Horário	Sexta-feira (24/11/2023)
	Minicurso: Introdução à Ciência e Tecnologia do Vácuo
00 20 12 20	Instrutores:
08:30 – 12:30	Dr. Francisco Tadeu Degasperi Fatec-SP / CEETEPS Dr. Marcelo Juni Ferreira, European Spallation Source (ERIC-Suécia)
	Local: Faculdade de Tecnologia de São Paulo - FATEC/SP - CEETEPS -Avenida Tiradentes, 615. Bairro do Bom Retiro, São Paulo
	Minicurso: Introdução à metrologia e cálculo de incertezas
13:30 – 17:30	Instrutores: Me. Jackson da Silva Oliveira Dr. Luciano do Nascimento Batista
	Local: Faculdade de Tecnologia de São Paulo - FATEC/SP - CEETEPS -Avenida Tiradentes, 615. Bairro do Bom Retiro, São Paulo
	Minicurso: Modelagem e cálculo de sistemas de vácuo
19:00 – 22:00	Instrutores: Dr. Francisco Tadeu Degasperi Fatec-SP / CEETEPS Dr. Nilberto H. Medina – Instituto de Física da USP
	Local: Faculdade de Tecnologia de São Paulo - FATEC/SP - CEETEPS -Avenida Tiradentes, 615. Bairro do Bom Retiro, São Paulo

Horário	Sábado (25/11/2023)
	Minicurso: Plasma para o tratamento e deposição de materiais
08:00 – 12:00	Instrutores: Dr. Felipe Vicente de Paula Kodaira Dr. Fellype do Nascimento Me. Rafael Resende Lucas
	Local: Sala 8 do bloco 6, Unesp Campus de Guaratinguetá, Guaratinguetá/SP
	Minicurso: Aprendizagem Ativa: Uma abordagem que faz pensar
08:00 – 12:00	Instrutores: Dr. Álvaro José Damião Local: Anfiteatro Inovee, Faculdade de Engenharia e Ciência - Campus deGuaratinguetá
08:30 – 12:30	Minicurso: Introdução à Ciência e Tecnologia do Vácuo Instrutores: Dr. Francisco Tadeu Degasperi Fatec-SP / CEETEPS Dr. Marcelo Juni Ferreira, European Spallation Source (ERIC-Suécia) Local: Faculdade de Tecnologia de São Paulo - FATEC/SP - CEETEPS -Avenida Tiradentes, 615. Bairro do Bom Retiro, São Paulo
13:30 – 17:30	Minicurso: Introdução à dinâmica dos gases rarefeitos: Teoria e aplicaçõesaos sistemas de vácuo Instrutores: Dr. Feliz Sharipov – Departamento de Física – UFPR Local: Faculdade de Tecnologia de São Paulo - FATEC/SP - CEETEPS -Avenida Tiradentes, 615. Bairro do Bom Retiro, São Paulo



CONGRESSO BRASILEIRO DE APLICAÇÕES DE VÁCUO NA INDÚSTRIA E CIÊNCIA Campos do Jordão – SP| 25 – 29 de Novembro de 2023

	Minicurso: Introdução a Microfluídica: Teoria e Prática	
14:00 – 18:00	Instrutores: Dr. Angelo Luiz Gobbi	
	Local: Sala 8 do bloco 6, Unesp Campus de Guaratinguetá, Guaratinguetá/SP	
	Minicurso: Introdução à metrologia de vácuo	
19:00 – 22:00	Instrutores: Dr. Francisco Tadeu Degasperi Fatec-SP / CEETEPSDr. Luciano do Nascimento Batista	
	Local: Faculdade de Tecnologia de São Paulo - FATEC/SP - CEETEPS -Avenida Tiradentes, 615. Bairro do Bom Retiro, São Paulo	

Horário	Domingo (26/11/2023)
19:00	Instalação dos stands; Entrega de materiais relacionados ao XLIV CBrAVIC.

Horário	Segunda-feira (27/11/2023)
08:30 - 09:30	Registro dos participantes do XLIV CBrAVIC
09:30 - 10:00	Abertura
10:00 – 10:50	Chair: Pedro Augusto de Paula Nascente Vice: Felipe Vicente de Paula Kodaira Palestra 01: Hydrogen in materials toward energy applications: from storage tomaterials property tuning — PhD Katsuyuki Fukutani — Institute of Industrial Science, University of Tokyo
10:50 - 11:10	Coffee Break
11:10 – 12:00	Chair: Carlos Roberto Grandini Vice: Felipe Vicente de Paula Kodaira Palestra 02: Development of high-performance superconducting materials for practical applications – Dr. Durval Rodrigues Júnior - Universidade de São Paulo - Escola de Engenharia de Lorena
12:00 – 12:20	Chair: Pedro Augusto de Paula Nascente Vice: Felipe Vicente de Paula Kodaira Apresentação Oral 01: Prof. Konstantin Georgiev Kostov – Development ofatmospheric pressure plasma jets for large area surface treatment
12:20 – 12:40	Chair: Pedro Augusto de Paula Nascente Vice: Felipe Vicente de Paula Kodaira Apresentação Oral 02: Prof. Luis César Fontana — Effect of shape andasymmetry of the voltage pulse on plasma ionization rate
12:40 – 14:00	Almoço
14:00 – 14:50	Chair: Konstantin Georgiev Kostov Vice: Maurício Antônio Algatti Palestra 03: Plasma jet interactions with biological targets – PhD Jean- Michel Pouvesle - GREMI, UMR7344 CNRS/Orleans University, Universitéd'Orléans, Orléans, France
14:50 – 15:40	Chair: Konstantin Georgiev Kostov Vice: Maurício Antônio Algatti Palestra 04: ESS Neutron Instrument Vacuum System – Dr. Marcelo JuniFerreira – European Spallation Source
15:40 – 16:00	Coffee Break



CONGRESSO BRASILEIRO DE APLICAÇÕES DE VÁCUO NA INDÚSTRIA E CIÊNCIA Campos do Jordão – SP| 25 – 29 de Novembro de 2023

Horário	Segunda-feira (27/11/2023)		
		SEÇÃO PÖSTER 1 Chair: Carlos Roberto Grandini Vice: Elidiane Cipriano Rangel	
	01	ANALYTICAL, NUMERICAL AND EXPERIMENTAL ANALYSIS OF A TUBULAR HIGH VACUUM SYSTEM	
	02	ANTIMICROBIAL EFFICACY OF DENTAL POLY(METHYL METHACRYLATE) COATED WITH AL203 BY ATOMIC LAYERDEPOSITION	
	03	APLICAÇÃO DE HMDSO VIA PIIID PARA MELHORIA EM JUNTAS SOLDADAS POR RESISTÊNCIA ELÉTRICA	
	04	COMPARATIVE ANALYSIS BETWEEN PLASMA ACTIVATED WATER AND PLASMA ACTIVATED SALINE SOLUTION	
	05	COMPUTATIONAL ANALYSIS OF THE HEAT DISTRIBUTIONGRADIENT IN THE PEI/FIBERGLASS STRUCTURAL LAMINATE USING ANSYS COMPOSITE PREPPOST (ACP)	
	06	DIAMOND-LIKE-CARBON COATINGS DOPED WITH GADOLINIUM: STUDY OF MECHANICAL AND TRIBOLOGICAL PROPERTIES OF COATING PRODUCED BY HIPIMS	
	07	DISCHARGE POWER DISSIPATED IN DEVICES WITH DOUBLE PLASMA IGNITION	
	08	DISTRIBUTED GENERATION USING HYDROKINETIC SUBMERGED TURBINES IN NORTHERN BRAZILIAN RIVERS AS A SOLUTION FOREXPANDINGRENEWABLE ELECTRICITY GENERATION AND SERVING ISOLATED COMMUNITIES	
	09	EFFECT OF MULTICOMPONENT OXIDE COATINGS OBTAINED BY PEO ON THE ROUGHNESS AND WETTABILITY OF COMMERCIALLYPURE TITANIUM FOR BIOMEDICAL USE	
	10	EFFECT OF PLASMA NITRING ON WEAR RESISTANCE OF THE HADFIELD AUSTENITIC MANGANESE STEEL	
	11	EFFECT OF SURFACE ROUGHNESS OF TI6AL4V SAMPLES ON THE FORMATION OF OXIDE LAYERS PRODUCED BY ABIPPS PLASMA	
	12	EFFECT OF THE TWO-STEP ANODIZATION TIME ON THE SURFACE PROPERTIES OF NANOPOROUS ANODIC ALUMINA	
16:00 – 17:30	13	EXPLORING THE PHYSICAL AND CHEMICAL ATTRIBUTES OF PLASMA ACTIVATED WATER AND ITS ANTIMICROBIAL POTENTIAL	
	14	FULL AUTOMATION OF VACUUM, PLASMA AND DEPOSITION SYSTEMS USING FRIENDLY, LOW-COST AND OPEN-SOURCEHARDWARE AND SOFTWARE	
	15	METALLOGRAPHIC STUDY OF LOW-CARBON STEELS API 5L X70 MO AND API 5L MS	
	16	OPTIMIZATION OF ALUMINUM-THERMOPLASTIC COMPOSITE ADHESION THROUGH MICROARC OXIDATION TREATMENT	
	17	OPTIMIZING WETTING PROPERTIES OF POLYPROPYLENE NON-WOVEN VIA ATOMIC LAYER DEPOSITION OF TiO2	
	18	OVERVIEW OF BRAZILIAN NATIONAL WIND ENERGY, HIGHLIGHTING THE NORTHEAST REGION	
	19	PADRONIZAÇÃO E PROCESSO DE SOLDAGEM TIG, EM LIGA DE ALUMÍNIO 6063 PARA ULTRA- ALTO VÁCUO DO PROJETO SIRIUS.	
	20	PHASE AND CHEMICAL COMPOSITION EFFECT ON THE GROWTH OF MAO COATING IN NOVEL BIO-HEAS.	
	21	PHYSICAL AND CHEMICAL CHARACTERISTICS OF PLASMAACTIVATED WATER GENERATED BY A COMBINATION OF DIELECTRIC BARRIER DISCHARGE AND GLIDING ARC TECHNIQUES	
	22	PHYSICAL AND MATHEMATICAL MODELING AND MEASUREMENT OF VACUUM LEAK DETECTION SYSTEM	
	23	PLASMA POWER SOURCES INFLUENCE ON CARBON NANOTUBES FUNCTIONALIZATION	
	24	PRODUCTION AND CHARACTERIZATION OF NOVEL ZRTINB-BASEDHIGH-ENTROPY ALLOYS BY ARGON ARC MELTING FOR BIOMEDICAL APPLICATIONS	
	25	PRODUCTION OF ULTRATHIN FILMS AND NANOSTRUCTURES FROM CARBON DIOXIDE	
	26	PRODUCTION, CARACTERIZATION AND APLLICATION OF LOW-COST HIGH VOLTAGE POWER SOURCE IN PLASMA ACVATEDWATER (PAW)	



CONGRESSO BRASILEIRO DE APLICAÇÕES DE VÁCUO NA INDÚSTRIA E CIÊNCIA Campos do Jordão - SP| 25 - 29 de Novembro de 2023

27	PROMOTING MAKER AND STEAM EDUCATION ON VACUUM:EVALUATION OF COMPLEXMIDIA FOR HEARING AND DEAF STUDENTS IN AN INCLUSIVE AND MULTIMEDIA APPROACH
28	RECOVERING OF A VACUUM SYSTEM USED IN PLASMA TREATMENT
29	RESPOSTA ESPECTRAL DE DRONE UTILIZANDO ESPECTRORADIÔMETRO EEMISSÃODE INFRA VERMELHO PRÓXIMO
30	ROTATIONAL TEMPERATURES OF N2 MOLECULES PRODUCED BYCOLD PLASMA JETS INSIDE MONTGOMERY TUBES
31	SIMULAÇÃO DE PERDA DE REFLEXÃO DE MATERIAIS ABSORVEDORES DE RADIAÇÃO ELETROMAGNÉTICA
32	SIMULATION AND INVESTIGATION OF THE THICKNESS OF CARBONYL-IRON MATERIALS IN THE KU BAND
33	SIMULATION OF PLASMA GENERATION IN A CATHODIC CAGESYSTEM
34	SÍNTESE E ESTUDO DA ATIVIDADE ANTIMICROBIANA DA MOF DECOBALTO
35	SOUND WAVE PROPAGATION IN WET STEAM
36	STRUCTURAL ANALYSIS OF HEO-BASED COATING ON TI-6AL-4V ALLOY PRODUCED BY PEO FOR POTENTIAL BIOMEDICALAPPLICATION
37	STUDY OF HYBRID TIO2–WOX THIN FILMS DEPOSITED VIA CO-SPUTTERING: EVALUATION OF THE PHOTOCATALYTIC ACTIVITY
38	STUDY OF LOW-POWER DIELECTRIC BARRIER DISCHARGE AT ATMOSPHERIC PRESSURE AND CYTOTOXICITY TEST ANDANTIMICROBIAL ACTIVITY
39	STUDY OF NON-LINEAR OPTICAL PROPERTIES USING THE Z SCAN TECHNIQUE OF QDs NANOFLUIDS OBTAINED BY GREEN SYNTHESIS
40	COMPARATIVE STUDY OF POLYMERIC STRUCTURES OBTAINED BY FDM ADDITIVE MANUFACTURING FOR BIOMEDICALAPPLICATIONS
41	STUDY OF THE EFFECT OF GAS FLOW VARIATION ON THE WEAR RESISTANCE OF PLASMA NITRIDED ASTM F138 STAINLESS STEEL
42	STUDY OF THE ELECTRICAL PROPERTIES OF POLY-O-METHOXYANILINE (POMA) FOR APPLICATIONS IN ELECTRONIC DEVICES
43	STUDY OF THE INFLUENCE OF DC POWER ON THE PROPERTIES OF WO3 FILM GROWN BY MAGNETRON SPUTTERING
44	STUDY OF THE INFLUENCE OF O2 FLOW VARIATION ON THE DEPOSITION OF WO3 FILMS BY THE MAGNETRON SPUTTERING TECHNIQUE
45	STUDY OF THE PHYSICOCHEMICAL PROPERTIES OF BACTERIAL NANOCELLULOSE POLYMERIC FILMS PRODUCED FROM PHYTO THERAPEUTIC AGENTS.
46	STUDY OF THE PROPERTIES OF DLC THIN FILMS DEPOSITED IN TI- 6AL-4V BY THE PIII&D TECHNIQUE INSIDE TITANIUM TUBES OFDIFFERENT DIMENSIONS
47	SURFACE FUNCTIONALIZATION OF TI15ZR15MO ALLOY - INCORPORATION OF NANOPARTICLES
48	TEMPORAL EVOLUTION OF SPATIAL DISTRIBUTION OF HYDROGEN AT TCABR-UPGRADE
49	THERMAL PLASMA APPLICATION FOR METHANE REFORMING
50	THERMAL STUDY OF Fe3O4 MAGNETIC NANOFLUIDS USING TWO PHOTOTHERMAL TECHNIQUES FOR BIOMEDICAL APPLICATIONS
51	THERMAL TREATMENT OF DAIRY SLUDGE BY DC-TRANSFERRED ARC PLASMA DISCHARGE
52	TIME-RESOLVED DETECTION OF DIFFERENT SPECIES IN A CONICAL APPJ BY AN ICCD CAMERA
53	TITANIUM-TANTALUM ALLOYS OBTAINED BY LASER DEPOSITION FOR BIOMEDICAL APPLICATIONS
54	TRATAMENTO DE AMOSTRAS POLIMÉRICAS COM UM JATO DE PLASMA CÔNICO EM PRESSÃO ATMOSFÉRICA
55	TREATMENT OF COMMERCIAL FABRIC WITH A CONICAL-SHAPED ATMOSPHERIC PRESSURE PLASMA JET
56	TRIBOLOGICAL BEHAVIOR OF BORON DOPED DLC FILM GROWN VIA PULSED PECVD



CONGRESSO BRASILEIRO DE APLICAÇÕES DE VÁCUO NA INDÚSTRIA E CIÊNCIA Campos do Jordão – SP| 25 – 29 de Novembro de 2023

57	TRIBOLOGICAL BEHAVIOR OF THE HYBRID NANOSTRUCTURE OF CNTS AND DLC FILM OBTAINED BY PECVD
58	TRIBOLOGICAL STUDY OF AISI 304 NITROCEMENTED STEEL WITH DIFFERENT PERCENTAGES OF METHANE
59	UNDERSTANDING THE INTERACTION OF PLASMA JETS WITH THE HUMAN BODY FOR MEDICAL APPLICATIONS
61	USE OF HIGH-ENERGY BALL MILLING AND POROSITY CONTROL IN THE DEVELOPMENT OF ALLOYS OF THE MG-ZN SYSTEM AIMINGBIOMEDICAL APPLICATIONS
62	USING FOG COMPUTING: PROPOSING A PROBLEM-SOLVING ROADMAP FOR INDUSTRY 4.0 AND VACUUM TECHNOLOGY
63	VACUUM COMPONENTS OBTAINED BY 3D PRINTING USING BIODEGRADABLE PLASTIC
64	VACUUM PRESSURE METROLOGY BY THE STATIC EXPANSIONMETHOD - MORE RESULTS
65	ZINC OXIDE FILM ON GLASS SUBSTRATES BY MEANS OF PLASMA IMMERSION ION IMPLANTATION AND DEPOSITION

	IMPLANTATION AND DEPOSITION
Horário	Terça-feira (28/11/2023)
08:30 - 09:20	Chair: Luís César Fontana Vice: Pedro Augusto de Paula Nascente Palestra 05: Epitaxial graphene: properties and applications for the us navy – PhD Rachael L. Myers-Ward – U.S. Naval Research Laboratory, USA
09:20 – 10:10	Chair: Luís César Fontana Vice: Pedro Augusto de Paula Nascente Palestra 06: Trielectrode non-thermal plasma sources for gas and water remediation – PhD Diana Grondona – Universidad de Buenos Aires, Argentina
10:10 - 10:20	Coffee Break
	VÁCUO NA INDÚSTRIA
	Chair: Luciana S. Rossino
	Vice: Francisco T. Degasperi
	Abertura – Francisco T. Degasperi e Luciana S. Rossino (10:20 – 10:25)
	Características gerais dos sistemas de vácuo industriais. Achim Lessel – Busch do Brasil Ltda. (10:25 – 10:50)
	Detecção de vazamentos em sistemas de vácuo industrias. Fernando Zappelline – Ahestest Ltda. (10:50 – 11:15)
10:20 – 12:50	Sistemas de vácuo com vapor de água ou com vapores de solventes. Luis Almeida – Edwards Vácuo Ltda. (11:15 – 11:40)
	Bombas de pré-vácuo secas para processos industriais. Luciano Camacho – Leybold Vácuo Ltda. (11:40 – 12:05)
	Bombas turbomoleculares nas aplicações industriais. Rafael Shiguematsu Amaral – Avaco Ltda. (12:05 – 12:30)
	Bombas Difusoras: Há como substituí-las? Marcelo Azevedo – Agilent Vácuo Ltda. (12:30 – 12:50)
	Fechamento Vácuo na Indústria. Francisco Tadeu Degasperi e Luciana Sgarbi Rossini. (12:50)
12:50 - 14:00	Almoço
	Chair: Nazir Monteiro dos Santos
14:00 - 14:50	Vice: Paulo Noronha
	Palestra 07: Ti-10Mo-Mn system alloys for Biomedical – Dr. Carlos Roberto Grandini - UNESP/FC/Bauru, Brasil
	Chair: Rogério Pinto Mota Vice: Paulo Noronha Palestra 08: Interfacial effects in Fe-based layered magnetic nanostructures: depth-resolved investigations – Dr. Waldemar
14:50 – 15:40	A.A. Macedo – Centro deDesenvolvimento da Tecnologia Nuclear, Brasil
15:40 – 16:00	Coffee Break
16:00 – 16:20	Chair: Nazir Monteiro dos Santos Vice: Paulo Noronha Apresentação Oral 03: Prof ^a . Cristiane Yumi Koga Ito - Helium cold plasma forthe treatment of oral lesions in rats
16:20 – 16:40	undergoing chemotherapy Chair: Nazir Monteiro dos Santos Vice: Paulo Noronha Apresentação Oral 04: Dr. Pedro Augusto Nascente – AISI 316LSTAINLESS STEEL COATED WITH TI-NB-ZR
10020 10010	Apresentação Oral 04: Dr. Pedro Augusto Nascente – AISI 316LSTAINLESS STEEL COATED WITH TI-NB-ZR TERNARAY ALLOYS



CONGRESSO BRASILEIRO DE APLICAÇÕES DE VÁCUO NA INDÚSTRIA E CIÊNCIA Campos do Jordão – SP| 25 – 29 de Novembro de 2023

16:40 – 17:40	Assembleia SBV
20:00 - 22:00	Jantar de Confraternização

Horário	Quarta-feira (29/11/2023)		
	METROLOGIA DE VÁCUO		
	Chair: Francisco T. Degasperi		
	Vice: Marcelo Juni / Rogério Pinto Mota		
	Abertura – Francisco Tadeu Degasperi e Luciano do Nascimento Batista.		
	(08:30-08:35)		
08:30 – 11:00	Metrologia: Ciência, tecnologia e serviços. Jackson da Silva Oliveira –		
	LAPRE-INMETRO. (08:35 – 09:05)		
	A necessidade da metrologia de vácuo na indústria e na ciência. Luciano do		
	Nascimento Batista – LAPRE-INMETRO. (09:05 – 09:35)		
	Serviços de metrologia em geral e metrologia de vácuo. Hugo Alexandre Garrido		
	Aguiar – Empresa Centro Tecnológico de Metrologia - CTM. (09:35 – 10:05)		
	Oficina de Metrologia de Vácuo no Laboratório de Tecnologia do Vácuo – LTV da FATEC-SP. Francisco Tadeu Degasperi – FATEC-SP – CEETEPS e RodrigoArakawa – ETEC Professor Horácio Augusto da Silveira – CEETEPS. (10:05 – 10:35)		
	Construção de sistemas de vácuo. Fernando Arroyo - Empresa FCA Usinagem.		
	(10:35 – 11:00)		
	Fechamento da Metrologia de Vácuo. Francisco Tadeu Degasperi e Luciano		
	do Nascimento Batista. (11:00)		
11:00 – 11:20	Coffee Break		
	Chair: Nilson Cristino da Cruz Vice: William Chiappim Júnior		
11:20 - 12:10	Palestra 09: Biological Surface Science: A Review - Dr. Paulo NoronhaLisboa-Filho - São Paulo University,		
	Bauru, SP, Brazil		
	Chair: Nilson Cristino da Cruz		
12:10 – 12:30	Vice: William Chiappim Júnior		
	Apresentação Oral 05: Prof ^a . Elidiane Cipriano Rangel – Properties of N95 respirators exposed to O2/SF6 desinfection		
	plasma		
12:30 – 12:50	Chair: Nilson Cristino da Cruz Vice: William Chiappim Júnior		
	Apresentação Oral 06: Prof. Clodomiro Alves Júnior – Growth of salt flowerin plasma-activated hypersaline water		
12:50 – 14:00	Almoço		
14.00 14.70	Chair: Elidiane Cipriano Rangel Vice: Teófilo Miguel de Souza		
14:00 – 14:50	Palestra 10: Infrared Camera Calibration by ISO 12233 – Dr. Alvaro JoséDamião – Instituto de Estudos Avançados, CTA, Brazil		



CONGRESSO BRASILEIRO DE APLICAÇÕES DE VÁCUO NA INDÚSTRIA E CIÊNCIA Campos do Jordão – SP| 25 – 29 de Novembro de 2023

	Quarta-feira (29/11/2023)
	SEÇÃO PÔSTER 2 Chair: Elidiane Cipriano Rangel Vice: Teófilo Miguel de Souza
01	3D PRINTING FOR PRESSURE SENSOR PACKAGING
02	A COMBINED RAMAN, X-RAY AND FOURIER TRANSFORM INFRARED FOR INVESTIGATING THE COBALT OXIDE FILMS BYREACTIVE SPUTTERING
03	A WORLDWIDE PERSPECTIVE ON HYDROGEN PRODUCTION RESEARCH
04	AISI 316L STAINLESS STEEL COATED WITH TI-NB-ZR TERNARAY ALLOYS
05	ANALYSIS OF LIGNOCELLULOSIC BIOMASS GASIFICATION INSUPERCRITICAL WATER: EXPLORING KEY PARAMETERS AND PROCESS OPTIMIZATION STRATEGIES
06	ANTIMICROBIAL ACTIVITY EVALUATION OF BINARY AND TERNARY TITANIUM ALLOY
07	ANTIMICROBIAL EFFICACY ON ENTEROCOCCUS FAECALIS OF PLASMA-ACTIVATED WATER PRODUCED BY DIELECTRIC BARRIERDISCHARGE
08	APATITE FORMATION ON ALKALI-TREATED TI-7.5MO ALLOY AFTER TIO2 NANOTUBES GROWTH
09	APPLICATION OF ATMOSPHERIC PRESSURE PLASMAS ON WATER DECONTAMINATION AND DEPOLLUTION
10	ARC-MELTING PROCESS APPLIED TO PRODUCE NOVEL TITANIUM- BASED MATRIX COMPOSITES FOR BIOMEDICAL APPLICATIONS
11	AUTOMATED LASER CLADDING PROCESSING FOR OF CARBON FILMS DEPOSITION FOR TBC CLAD-COUPLER
12	BIFURCATION FROM HOMOCLINIC TO HETEROCLINIC TOPOLOGY IN TOKAMAK DISCHARGES
13	BIOCOMPATIBILIDADE DE NOVAS LIGAS A BASE DE TITÂNIO VISANDO APLICAÇÕES BIOMÉDICAS
14	BIOFILM INACTIVATION OF CANDIDA PARAPSILOSIS AND CANDIDA ALBICANS BY ARGON / AIR PLASMA
15	BIOFUNCTIONAL COATING OF STAINLESS STEEL SURFACES WITH CARVACROL- AND EUGENOL-DERIVED FILM USING DIELECTRIC BARRIER DISCHARGE PLASMA: AIMING FOR SUPPRESSION OF BIOFILM FORMATION AND CORROSION PROTECTION
16	CARACTERIZAÇÃO DA LIGA TI-20MO-15ZR-4,5CU VISANDO USO EM BIOMATERIAIS
17	CARACTERIZATION OF MONOCRYSTALLINE GRAPHITE FILM DEPOSITED BY PIII&D INSIDE
18	TITANIUM ALLOY TUBE CERIUM OXIDE NANOPARTICLE DEPOSITION ON PLA SCAFFOLDS USING HIGH-
10	VOLTAGE MODIFIED ELECTROPHORESIS
19	CHARACTERIZATION AND PLASMA SURFACE TREATMENT OF PHEROMONE- RELEASING SEPTA IN AGRICULTURE
20	STUDY OF PROCEDURES FOR 3D PRINTING OF POLYMERIC STRUCTURES AIMING BIOMEDICAL APPLICATIONS
21	COMPARATIVE WEAR BEHAVIOR OF DLC, DLCN AND DLC-SI FILM DEPOSITED BY PECVD
	ON AISI 321 STAINLESS STEEL COMPARISON OF THE ECOTOXICITY OF CARBON NANOTUBES OBTAINED BY CVD
22	AND PECVD
23	CONSTRUCTION AND VALIDATION TESTING OF A PLANETARY ROTATING SAMPLE HOLDER FOR THIN FILM DEPOSITION BY MAGNETRON SPUTTERING
24	CVD DIAMOND FILMS DEPOSITED ON INTRINSIC AND BORON-DOPED SILICON WAFER WITH CRYSTAL ORIENTATION (100) AND(111)
25	DENSIFICATION OF PLASMA DEPOSITED SIOX BY LOW ENERGY CHEMICAL REACTIONS
26	DEPOSITION OF GRAPHENE OXIDE ON METALLIC SUBSTRATE VIA CLASSICAL AND MODIFIED ELECTROPHORETIC DEPOSITION
	02 03 04 05 06 07 08 09 10 11 12 13 14 15 16 17 18 19 20 21 22 23 24 25



CONGRESSO BRASILEIRO DE APLICAÇÕES DE VÁCUO NA INDÚSTRIA E CIÊNCIA Campos do Jordão - SP| 25 - 29 de Novembro de 2023

27	DESENVOLVIMENTO DE UMA INTERFACE EM PYTHON PARASIMULAÇÃO DE MATERIAIS EM MULTICAMADAS PARA CONTROLE DE INTERFERÊNCIA ELETROMAGNÉTICA
28	DESIGN OF A VACUUM CHAMBER FOR FILM DEPOSITION BY MAGNETRON SPUTTERING
29	DETECTION BY RAMAN 2D SPECTROSCOPY OF MWCNT INGESTION BY EARTHWORMS LIVING IN CONTAMINATED SOIL
30	DETERMINAÇÃO DA VELOCIDADE DE DEPOSIÇÃO DO FILME DE DIAMANTE CVD POR PESAGEM
31	DEVELOPMENT OF A HYBRID ADDITIVE MANUFACTURING AND PLASMA JET EQUIPMENT FOR PLA SCAFFOLD CONSTRUCTION
32	DEVELOPMENT OF SODIUM AND HYDROGEN TITANATES FOR BIOCIDAL APPLICATIONS
33	EFFECT OF THERMOMECHANICAL TREATMENTS ON THE STRUCTURE, MICROSTRUCTURE AND SELECTED MECHANICAL PROPERTIES OF TI-25TA-XNB SYSTEM ALLOYS, AIMING ATBIOMEDICAL APPLICATIONS
34	EFFECT OF ULTRASOUND ON BENTONITE CLAY SURFACES.
35	ENHANCED HIPS WITH DLC SURFACE TREATMENT BY PLASMA
36	EVALUATION OF ANTITUMORAL EFFECTS OF RINGER LACTATE SOLUTION TREATED WITH PLASMA AT ATMOSPHERIC PRESSURE ON THEMIGRATION AND PROLIFERATION OF MURINE MELANOMA CELLS (B16F10) IN VITRO
37	EVALUATION OF THE ANTIMICROBIAL EFFECT OF WATER ACTIVATED PLASMA ON AMNIOTIC MEMBRANE CONTAMINATED BY ESCHERICHIA COLI AND STAPHYLOCOCCUS AUREUS
38	EVALUATION OF THE CORROSION BEHAVIOR OF BETA-PAHSED TITANIUM ALLOYS
39	AFTER EQUAL CHANNEL ANGULAR PRESSING EVALUATION OF THE INFLUENCE OF PLASMA TREATMENT ON POLYURETHANE ON THE SORPTION OF \$500 DIESEL OIL
40	EVALUATION OF THE MODIFICATION OF THE SURFACE OF NIOBIUM BY THE PROCESS OF OXIDATION BY ELECTROLYTICPLASMA
41	EVALUATION OF THE RELATIONSHIP BETWEEN ROUGHNESS AND WETTING OF DIFFERENT IMPLANTS SURFACES.
42	STUDY OF PROCEDURES FOR 3D PRINTING OF POLYMERIC STRUCTURES AIMING BIOMEDICAL APPLICATIONS
43	EXPLORING PHYSICOCHEMICAL PROPERTIES OF BACTERIAL NANOCELLULOSE POLYMERIC FILMS DERIVED FROM ORGANIC RESIDUES
44	COMPARISON OF THE ECOTOXICITY OF CARBON NANOTUBES OBTAINED BY CVD AND PECVD
45	CONSTRUCTION AND VALIDATION TESTING OF A PLANETARY ROTATING SAMPLE HOLDER FOR THIN FILM DEPOSITION BY MAGNETRON SPUTTERING
46	EXTRACTION OF LIGNIN FROM CORNCOB USING DEEP EUTECTIC SOLVENTS
47	DENSIFICATION OF PLASMA DEPOSITED SIOX BY LOW ENERGY CHEMICAL REACTIONS
48	FLUID SIMULATION OF GLOW DISCHARGES GENERATED BY BIPOLAR PULSED POWER SUPPLIES
49	THERMAL PLASMA APPLICATION FOR METHANE REFORMING
50	FUNCTIONALIZED MULTI-WALLED CARBON NANOTUBES POTENCIALIZE EFFECT OF PHOTODYNAMIC THERAPY OF MURINE MELANOMA IN 2D AND 3D CULTURE.
51	THERMAL TREATMENT OF DAIRY SLUDGE BY DC-TRANSFERRED ARC PLASMA DISCHARGE
52	TIME-RESOLVED DETECTION OF DIFFERENT SPECIES IN A CONICAL APPJ BY AN ICCD CAMERA
53	GROWTH OF BORON-DOPED DLC FILMS ON DIFFERENT SUBSTRATES
54	TRATAMENTO DE AMOSTRAS POLIMÉRICAS COM UM JATO DE PLASMA CÔNICO EM PRESSÃO ATMOSFÉRICA



CONGRESSO BRASILEIRO DE APLICAÇÕES DE VÁCUO NA INDÚSTRIA E CIÊNCIA Campos do Jordão - SP| 25 - 29 de Novembro de 2023

	55	HYPERSONIC HEAT FLUX EVALUATION FOR SHAPE MEMORY ALLOY THERMO MECHANICAL CHARACTERIZATION
	56	TRIBOLOGICAL BEHAVIOR OF BORON DOPED DLC FILM GROWN VIA PULSED PECVD
	57	HYPERSONIC PLASMA SETUP FOR OXIDATION TESTING OF ULTRA- HIGH TEMPERATURE CERAMIC COMPOSITES
	58	TRIBOLOGICAL STUDY OF AISI 304 NITROCEMENTED STEEL WITH DIFFERENT PERCENTAGES OF METHANE
	59	IMPACTS OF THE PRESENCE OF COMMERCIAL MWCNT ON THE TERRESTRIAL ECOSYSTEM
	61	USE OF HIGH-ENERGY BALL MILLING AND POROSITY CONTROL IN THE DEVELOPMENT OF ALLOYS OF THE MG-ZN SYSTEM AIMINGBIOMEDICAL APPLICATIONS
	62	INFLUENCE OF THE ABRASIVE WEAR MODES ON THE VOLUME OF WEAR OF THIN FILMS
	63	VACUUM COMPONENTS OBTAINED BY 3D PRINTING USING BIODEGRADABLE PLASTIC
	64	INTERACTION OF OXYGEN PLASMA ACTIVATED WATER WITH CALCITE
16:20 – 16:40	Coffee Br	reak
16:40 – 17:40	Encerram	ento e Premiações



Sumário:

HYDROGEN IN MATERIALS TOWARD ENERGY APPLICATIONS: FROM STORAGE TOMATERIALS PROPERTY TUNING
ANTIBACTERIAL AND BIOMIMETIC STRATEGIES APPLIED FOR COATINGS ON STABLE AND BIODEGRADABLE BIOMEDICAL IMPLANTS
PLASMA JET INTERACTIONS WITH BIOLOGICAL TARGETS
INFRARED CAMERA CALIBRATION BY ISO 12233
EPITAXIAL GRAPHENE: PROPERTIES AND APPLICATIONS FOR THE US NAVY20
TRIELECTRODE NON-THERMAL PLASMA SOURCES FOR GAS AND WATER REMEDIATION21 $$
REAL TIME MONITORING OF CALCIUM PHOSPHATE CEMENTS: AN INSIGHT INTO KINETICS ANDMECHANISMS
INTERFACIAL EFFECTS IN FE-BASED LAYERED MAGNETIC NANOSTRUCTURES:DEPTH-RESOLVED INVESTIGATIONS
BIOLOGICAL SURFACE SCIENCE: A REVIEW
ESS NEUTRON INSTRUMENT VACUUM SYSTEM
DEVELOPMENT OF ATMOSPHERIC PRESSURE PLASMA JETS FOR LARGE AREA SURFACE TREATMENT
EFFECT OF SHAPE AND ASYMMETRY OF THE VOLTAGE PULSE ONPLASMA IONIZATION RATE27
HELIUM COLD PLASMA FOR THE TREATMENT OF ORAL LESIONS IN RATS UNDERGOING CHEMOTHERAPY
Ti-10Mo-Mn SYSTEM ALLOYS FOR BIOMEDICAL APPLICATIONS
PROPERTIES OF N95 RESPIRATORS EXPOSED TO O2/SF6 DESINFECTION PLASMAS30
GROWTH OF SALT FLOWER IN PLASMA-ACTIVATED HYPERSALINE WATER31
3D PRINTING FOR PRESSURE SENSOR PACKAGING
A COMBINED RAMAN, X-RAY AND FOURIER TRANSFORM INFRARED FOR INVESTIGATINGTHE COBALT OXIDE FILMS BY REACTIVE SPUTTERING
A WORLDWIDE PERSPECTIVE ON HYDROGEN PRODUCTION RESEARCH
AISI 316L STAINLESS STEEL COATED WITH TI-NB-ZR TERNARAY ALLOYS38
ANÁLISE COMPUTACIONAL DO GRADIENTE DE DISTRIBUIÇÃO DE CALOR DO LAMINADO ESTRUTURAL PEI/FIBRA DE VIDRO POR MEIO DO ANSYS COMPOSITE PREPPOST (ACP)39
ANALYSIS OF LIGNOCELLULOSIC BIOMASS GASIFICATION IN SUPERCRITICAL WATER: EXPLORING KEY PARAMETERS AND PROCESS OPTIMIZATION STRATEGIES
ANALYTICAL, NUMERICAL AND EXPERIMENTAL ANALYSIS OF A TUBULAR HIGH VACUUM41
SYSTEM41
ANTIMICROBIAL ACTIVITY EVALUATION OF BINARY AND TERNARY TITANIUM ALLOY42
ANTIMICROBIAL EFFICACY OF DENTAL POLY (METHYL METHACRYLATE) COATED WITHAL2O3 BY ATOMIC LAYER DEPOSITION44
ANTIMICROBIAL EFFICACY ON <i>ENTEROCOCCUS FAECALIS</i> OF PLASMA-ACTIVATEDWATER PRODUCED BY DIELECTRIC BARRIER DISCHARGE
APATITE FORMATION ON ALKALI-TREATED Ti-7.5MO ALLOY AFTER TIO2 NANOTUBES GROWTH
APLICAÇÃO DE HMDSO VIA PIIID PARA MELHORIA EM JUNTAS SOLDADAS POR RESISTÊNCIA ELÉTRICA



CONGRESSO BRASILEIRO DE APLICAÇÕES DE VÁCUO NA INDÚSTRIA E CIÊNCIA

Campos do Jordão – SP| 25 – 29 de Novembro de 2023

APPLICATION OF ATMOSPHERIC PRESSURE PLASMAS ON WATER DECONTAMINATION AND DEPOLLUTION
ARC-MELTING PROCESS APPLIED TO PRODUCE NOVEL TITANIUM-BASED MATRIXCOMPOSITES FOR BIOMEDICAL APPLICATIONS49
BIFURCATION FROM HOMOCLINIC TO HETEROCLINIC TOPOLOGY IN TOKAMAK DISCHARGES53
BIOCOMPATIBILIDADE DE NOVAS LIGAS DE TITÂNIO VISANDO APLICAÇÕES BIOMÉDICAS 54
BIOFILM INACTIVATION OF CANDIDA PARAPSILOSIS AND CANDIDA ALBICANS BY ARGON / AIR PLASMA55
BIOFUNCTIONAL COATING OF STAINLESS STEEL SURFACES WITH CARVACROL- AND EUGENOL-DERIVED FILM USING DIELECTRICBARRIER DISCHARGE PLASMA: AIMING FOR SUPPRESSION OF BIOFILM FORMATION AND CORROSION PROTECTION
CARACTERIZATION OF MONOCRYSTALLINE GRAPHITE FILM DEPOSITED BY PIII&D INSIDE TITANIUM ALLOY TUBE
CERIUM OXIDE NANOPARTICLE DEPOSITION ON PLA SCAFFOLDS USING HIGH VOLTAGE- MODIFIED ELECTROPHORESIS59
CHARACTERIZATION AND PLASMA SURFACE TREATMENT OF PHEROMONE-RELEASING SEPTA IN AGRICULTURE
CHARACTERIZATION OF THE TI-20MO-15ZR-4.5CU ALLOY AIMING FOR BIOMATERIALS APPLICATIONS61
COMPARATIVE ANALYSIS BETWEEN PLASMA ACTIVATED WATER AND PLASMAACTIVATED SALINE SOLUTION62
COMPARATIVE STUDY OF POLYMERIC STRUCTURES OBTAINED BY FDM ADDITIVE MANUFACTURING FOR BIOMEDICAL APPLICATIONS63
COMPARATIVE WEAR BEHAVIOR OF DLC, DLCN AND DLC-SI FILM DEPOSITED BY PECVDON AISI 321 STAINLE55 STEEL
COMPARISON OF THE ECOTOXICITY OF CARBON NANOTUBES OBTAINED BY CVD ANDPECVD 65
COMPUTATIONAL ANALYSIS OF THE HEAT DISTRIBUTION GRADIENT IN THE PEI/FIBERGLASS STRUCTURAL LAMINATE USING ANSYS COMPOSITE PREPPOST (ACP)
CONSTRUCTION AND VALIDATION TESTING OF A PLANETARY ROTATING SAMPLEHOLDER FOR THIN FILM DEPOSITION BY MAGNETRON SPUTTERING67
CVD DIAMOND FILMS DEPOSITED ON INTRINSIC AND BORON-DOPED SILICON WAFERWITH CRYSTAL ORIENTATION (100) AND (111)68
DENSIFICATION OF PLASMA DEPOSITED SIOX BY LOW ENERGY CHEMICAL REACTIONS69
DEPOSITION OF GRAPHENE OXIDE ON METALLIC SUBSTRATE VIA CLASSICAL ANDMODIFIED ELECTROPHORETIC DEPOSITION70
DESENVOLVIMENTO DE UMA INTERFACE EM PYTHON PARA SIMULAÇÃO DE MATERIAISEM MULTICAMADAS PARA CONTROLE DE INTERFERÊNCIA ELETROMAGNÉTICA71
DESIGN OF A VACUUM CHAMBER FOR FILM DEPOSITION BY MAGNETRON SPUTTERING72
DETECTION BY RAMAN 2D SPECTROSCOPY OF MWCNT INGESTION BY EARTHWORMLIVING IN CONTAMINATED SOIL
DETERMINAÇÃO DA VELOCIDADE DE DEPOSIÇÃO DO FILME DE DIAMANTE CVD POR PESAGEM74
DEVELOPMENT OF A HYBRID ADDITIVE MANUFACTURING AND PLASMA JET EQUIPMENTFOR PLA SCAFFOLD CONSTRUCTION
DEVELOPMENT OF SODIUM AND HYDROGEN TITANATES FOR BIOCIDAL APPLICATIONS 77
DIAMOND-LIKE-CARBON COATINGS DOPED WITH GADOLINIUM: STUDY OF MECHANICALAND TRIBOLOGICAL PROPERTIES OF COATING PRODUCED BY HIPIMS78
DISCHARGE POWER DISSIPATED IN DEVICES WITH DOUBLE PLASMA IGNITION 79



CONGRESSO BRASILEIRO DE APLICAÇÕES DE VÁCUO NA INDÚSTRIA E CIÊNCIA

Campos do Jordão – SP| 25 – 29 de Novembro de 2023

BRAZILIAN RIVERS AS A SOLUTION FOR EXPANDING RENEWABLE ELECTRICITY GENERATION AND SERVING ISOLATED COMMUNITIES
EFFECT OF MULTICOMPONENT OXIDE COATINGS OBTAINED BY PEO ON THE ROUGHNESS AND WETTABILITY OF COMMERCIALLY PURE TITANIUM FOR BIOMEDICAL USE
EFFECT OF PLASMA NITRING ON WEAR RESISTANCE OF THE HADFIELDAUSTENITIC MANGANESE STEEL
EFFECT OF SURFACE ROUGHNESS OF TI6AL4V SAMPLES ON THE FORMATION OF OXIDE LAYERS PRODUCED BY ABIPPS PLASMA83
EFFECT OF THERMOMECHANICAL TREATMENTS ON THE STRUCTURE, MICROSTRUCTURE AND SELECTEDMECHANICAL PROPERTIES OF TI-25TA-XNB SYSTEM ALLOYS, AIMING AT BIOMEDICAL APPLICATIONS
EFFECT OF THE TWO-STEP ANODIZATION TIME ON THE SURFACE PROPERTIES OF NANOPOROUS ANODICALUMINA
EFFECT OF ULTRASOUND ON BENTONITE CLAY SURFACES
ENHANCED HIPS WITH DLC SURFACE TREATMENT BY PLASMA
EVALUATION OF ANTITUMORAL EFFECTS OF RINGER LACTATE SOLUTION TREATED WITH PLASMA AT ATMOSPHERIC PRESSURE ON THE MIGRATION AND PROLIFERATIONOF MURINE MELANOMA CELLS (B16F10) IN VITRO
EVALUATION OF THE ANTIMICROBIAL EFFECT OF WATER ACTIVATED PLASMA ON AMNIOTIC MEMBRANECONTAMINATED BY ESCHERICHIA COLI AND STAPHYLOCOCCUS AUREUS
EVALUATION OF THE CORROSION BEHAVIOR OF BETA-PAHSED TITANIUM ALLOYS AFTER EQUAL CHANNELANGULAR PRESSING90
EVALUATION OF THE INFLUENCE OF PLASMA TREATMENT ON POLYURETHANE ON THE SORPTION OF \$500 DIESEL OIL
EVALUATION OF THE MODIFICATION OF THE SURFACE OF NIOBIUM BY THE PROCESS OF OXIDATION BY ELECTROLYTIC PLASMA
EVALUATION OF THE RELATIONSHIP BETWEEN ROUGHNESS AND WETTING OFDIFFERENT IMPLANTS SURFACES
EXPLORING PHYSICOCHEMICAL PROPERTIES OF BACTERIAL NANOCELLULOSE POLYMERIC FILMS DERIVED FROM ORGANIC RESIDUES95
EXPLORING THE PHYSICAL AND CHEMICAL ATTRIBUTES OF PLASMA-ACTIVATED WATERAND ITS ANTIMICROBIAL POTENTIAL96
EXTRACTION OF LIGNIN FROM CORNCOB USING DEEP EUTECTIC SOLVENTS97
FLUID SIMULATION OF GLOW DISCHARGES GENERATED BY BIPOLAR PULSED POWER SUPPLIES99
FULL AUTOMATION OF VACUUM, PLASMA AND DEPOSITION SYSTEMS USINGFRIENDLY, LOW- COST AND OPEN-SOURCE HARDWARE AND SOFTWARE
FUNCTIONALIZED MULTI-WALLED CARBON NANOTUBES POTENCIALIZE EFFECT OF PHOTODYNAMIC THERAPY OF MURINE MELANOMA IN 2D AND 3D CULTURE
GROWTH OF BORON-DOPED DLC FILMS ON DIFFERENT SUBSTRATES
HYPERSONIC HEAT FLUX EVALUATION FOR SHAPE MEMORY ALLOY THERMO-MECHANICAL CHARACTERIZATION
HYPERSONIC PLASMA SETUP FOR OXIDATION TESTING OF ULTRA-HIGH TEMPERATURE CERAMIC COMPOSITES
IMPACTS OF THE PRESENCE OF COMMERCIAL MWCNT ON THE TERRESTRIAL ECOSYSTEM 106
INFLUENCE OF THE ABRASIVE WEAR MODES ON THE VOLUME OF WEAR OF THIN FILMS107
INTERACTION OF OXYGEN PLASMA ACTIVATED WATER WITH CALCITE



CONGRESSO BRASILEIRO DE APLICAÇÕES DE VÁCUO NA INDÚSTRIA E CIÊNCIA Campos do Jordão - SP| 25 - 29 de Novembro de 2023

INVESTIGATION OF POWDER METALLURGY TECHNIQUE FOR FABRICATING MG-ZN ALLOYS FOR BIOMEDICAL APPLICATIONS	
METAL ADSORPTION FROM CONTAMINATED SOIL USING SODIUM POLYACRYLATE	
METALLOGRAPHIC STUDY OF LOW-CARBON STEELS API 5L X70 MO AND API 5L MS	
METHODOLOGY FOR APPLYING SHAPE MEMORY ALLOY IN HYPERSONIC VEHICLES SIMULATED IN A PLASMA TUNELL	112
METROLOGY IN VACUUM TECHNOLOGY BY THE STATIC EXPANSION METHOD	
MICRO ABRASION WEAR OF HOMOGENEOUS AND GRADED TITANIUM NITRIDE FILMS	
Nb-DOPED TiO ₂ FILMS FOR APPLICATION AS TRANSPARENT CONDUCTIVE OXIDE	115
NITROGEN-DOPED DIAMOND FILMS APPLIED TO THIN-FILM TRANSISTORS	116
NUMERICAL EVALUATION OF PEROVSKITE SOLAR CELLS USING Nb ₂ O ₅ /AZO AS FRONT CONTACT LAYER	117
NUMERICAL MODELING OF A RESONANT CAVITY LINEAR ACCELERATOR USING MONTE CARLO METHOD	118
O IEAMAR NAS ESCOLAS DE ENSINO BÁSICO DA REDE PÚBLICA ESTADUAL	119
OPTIMIZATION OF ALUMINUM-THERMOPLASTIC COMPOSITE ADHESION THROUGH MICROA OXIDATION TREATMENT	
OPTIMIZING WETTING PROPERTIES OF POLYPROPYLENE NON-WOVEN VIA ATOMICLAYER DEPOSITION OF TiO2	121
OVERVIEW OF BRAZILIAN NATIONAL WIND ENERGY, HIGHLIGHTING THE NORTHEASTREGIC	
PESQUISA 3IP REALIZADAS NO BRASIL NAS ÚLTIMAS DUAS DÉCADAS	
PHASE AND CHEMICAL COMPOSITION EFFECT ON THE GROWTH OF MAO COATING IN NOVE BIO-HEAS.	
PHYSICAL AND CHEMICAL CHARACTERISTICS OF PLASMA ACTIVATED WATER GENERATED BY A COMBINATION OF DIELECTRIC BARRIER DISCHARGE AND GLIDING ARC TECHNIQUES	
PHYSICAL AND MATHEMATICAL MODELING AND MEASUREMENT OF VACUUM LEAK DETECTION SYSTEM	126
PLASMA POWER SOURCES INFLUENCE ON CARBON NANOTUBES FUNCTIONALIZATION	127
PRODUCTION AND CHARACTERIZATION OF NOVEL ZrTiNb-BASED HIGH-ENTROPY ALLOYS I ARGON ARC MELTING FOR BIOMEDICAL APPLICATIONS	
PRODUCTION OF ULTRATHIN FILMS AND NANOSTRUCTURES FROM CARBON DIOXIDE	129
PRODUCTION, CARACTERIZATION AND APLLICATION OF LOW-COST HIGH VOLTAGE POWER SOURCE IN PLASMA ACVATED WATER (PAW)	
PROMOTING MAKER AND STEAM EDUCATION ON VACUUM: EVALUATION OF COMPLEXMID FOR HEARING AND DEAF STUDENTS IN AN INCLUSIVE AND MULTIMEDIAAPPROACH	
RAMAN SPECTROSCOPY ANALYSIS OF $\alpha\text{-Bi}_2\mathrm{O}_3$ STRUCTURAL DEFECTS POST ATMOSPHERIC ARGON PLASMA EXPOSURE	135
RECOVERING OF A VACUUM SYSTEM USED IN PLASMA TREATMENT	136
RESPOSTA ESPECTRAL DE DRONE UTILIZANDO ESPECTRORADIÔMETRO E EMISSÃO DE INFRAVERMELHO PRÓXIMO	139
ROTATIONAL TEMPERATURES OF N2 MOLECULES PRODUCED BY COLD PLASMA JETS INSID MONTGOMERY TUBES	
SIMULAÇÃO DE PERDA DE REFLEXÃO DE MATERIAIS ABSORVEDORES DE RADIAÇÃO ELETROMAGNÉTICA	142
SIMULATION AND INVESTIGATION OF THE THICKNESS OF CARBONYL-IRON MATERIALS IN T	HE



CONGRESSO BRASILEIRO DE APLICAÇÕES DE VÁCUO NA INDÚSTRIA E CIÊNCIA

Campos do Jordão - SP| 25 - 29 de Novembro de 2023

SIMULATION OF PLASMA GENERATION IN A CATHODIC CAGE SYSTEM	144
SÍNTESE E ESTUDO DA ATIVIDADE ANTIMICROBIANA DA MOF DE COBALTO	145
SOUND WAVE PROPAGATION IN WET STEAM	146
STRUCTURAL ANALYSIS OF HEO-BASED COATING ON Ti-6Al-4V ALLOY PRODUCED BY PEO FOR POTENTIALBIOMEDICAL APPLICATION	147
STUDY OF HYBRID TiO2–WOX THIN FILMS DEPOSITED VIA CO-SPUTTERING: EVALUATION O THE PHOTOCATALYTIC ACTIVITY	
STUDY OF LOW-POWER DIELECTRIC BARRIER DISCHARGE AT ATMOSPHERIC PRESSUREANI CYTOTOXICITY TEST AND ANTIMICROBIAL ACTIVITY	
STUDY OF NON-LINEAR OPTICAL PROPERTIES USING THE Z SCAN TECHNIQUE OF QDs NANOFLUIDS OBTAINED BY GREEN SYNTHESIS	150
STUDY OF PROCEDURES FOR 3D PRINTING OF POLYMERIC STRUCTURES AIMINGBIOMEDICA APPLICATIONS	
STUDY OF THE EFFECT OF BORETATING AGENT 70%NA2B4O7 + 30%SIC ON THE MICROWEAR RESISTANCE OF AISI 420 STAINLESS STEEL	
STUDY OF THE EFFECT OF GAS FLOW VARIATION ON THE WEAR RESISTANCE OFPLASMA NITRIDED ASTM F138 STAINLESS STEEL	153
STUDY OF THE ELECTRICAL PROPERTIES OF POLY-O-METHOXYANILINE (POMA) FOR APPLICATIONS IN ELECTRONIC DEVICES	154
STUDY OF THE INFLUENCE OF DC POWER ON THE PROPERTIES OF WO3 FILM GROWN BY MAGNETRON SPUTTERING	155
STUDY OF THE INFLUENCE OF O ₂ FLOW VARIATION ON THE DEPOSITION OF WO ₃ FILMS BY T MAGNETRON SPUTTERING TECHNIQUE	HE
STUDY OF THE PHYSICOCHEMICAL PROPERTIES OF BACTERIAL NANOCELLULOSEPOLYMER FILMS PRODUCED FROM PHYTOTHERAPEUTIC AGENTS	
STUDY OF THE PROPERTIES OF DLC THIN FILMS DEPOSITED IN TI-6AL-4V BY THE PIII&D TECHNIQUE INSIDE TITANIUM TUBES OF DIFFERENT DIMENSIONS	158
SURFACE FUNCTIONALIZATION OF TI15ZR15MO ALLOY - INCORPORATION OF NANOPARTICLES	159
TEMPORAL EVOLUTION OF SPATIAL DISTRIBUTION OF HYDROGEN AT TCABR-UPGRADE	161
THERMAL PLASMA APPLICATION FOR METHANE REFORMING	162
THERMAL STUDY OF Fe ₃ O ₄ MAGNETIC NANOFLUIDS USING TWO PHOTOTHERMAL TECHNIQUES FORBIOMEDICAL APPLICATIONS	163
THERMAL TREATMENT OF DAIRY SLUDGE BY DC-TRANSFERRED ARC PLASMADISCHARGE	164
ΓΙΜΕ-RESOLVED DETECTION OF DIFFERENT SPECIES IN A CONICAL APPJ BY AN ICCD CAMERA	
TITANIUM-TANTALUM ALLOYS OBTAINED BY LASER DEPOSITION FOR BIOMEDICAL APPLICATIONS	
TRATAMENTO DE AMOSTRAS POLIMÉRICAS COM UM JATO DE PLASMA CÔNICO EM PRESSÃ ATMOSFÉRICA	
TREATMENT OF COMMERCIAL FABRIC WITH A CONICAL-SHAPED ATMOSPHERIC PRESSURE PLASMA JET	
TRIBOLOGICAL BEHAVIOR OF BORON DOPED DLC FILM GROWN VIA PULSED PECVD	169
TRIBOLOGICAL BEHAVIOR OF THE HYBRID NANOSTRUCTURE OF CNTS AND DLC FILM OBTAINED BY PECVD	170
TRIBOLOGICAL STUDY OF AISI 304 NITROCEMENTED STEEL WITH DIFFERENT PERCENTAGE OF METHANE	



NDERSTANDING THE INTERACTION OF PLASMA JETS WITH THE HUMAN BODY FOR MEDICA PPLICATIONS17
SE OF DUPLEX TREATMENT OF NITROCARBURIZING AND SILICON DOPED DLC FILM AS A MPROVEMENT OF USEFUL LIFE OF AISI M2 STEEL MACHINING TOOL17
SE OF HIGH-ENERGY BALL MILLING AND POROSITY CONTROL IN THE DEVELOPMENT OF LLOYS OFTHE MG-ZN SYSTEM AIMING BIOMEDICAL APPLICATIONS17
SING FOG COMPUTING: PROPOSING A PROBLEM-SOLVING ROADMAP FOR INDUSTRY 4.0 ANI ACUUM TECHNOLOGY17
ACUUM COMPONENTS OBTAINED BY 3D PRINTING USING BIODEGRADABLE PLASTIC17
ACUUM PRESSURE METROLOGY BY THE STATIC EXPANSION METHOD - MORE RESULTS 17
INC OXIDE FILM ON GLASS SUBSTRATES BY MEANS OF PLASMA IMMERSION ION



HYDROGEN IN MATERIALS TOWARD ENERGY APPLICATIONS: FROM STORAGE TO MATERIALS PROPERTY TUNING

Katsuyuki Fukutani

¹Institute of Industrial Science, University of Tokyo, Japan ²Advanced Science Research Center, Japan Atomic Energy Agency

Hydrogen is most abundant in the universe and a ubiquitous element in our society. Whereas hydrogen can be stored in hydrogen-absorbing metals as a clean energy carrier that does not release carbon dioxide, materials properties are potentially controlled by doping hydrogen in materials as demonstrated for high-temperature superconductivity and H-induced metal insulator transition. As hydrogen absorption occurs at materials surfaces, interaction of hydrogen with surfaces and diffusion of hydrogen across surfaces are of particular importance and interest. In this presentation, I report our studies on hydrogen absorption in metals andmetal oxides by in-situ observation with nuclear reaction analysis, which allows us to quantitatively measure the H depth distribution and H location in materials [1].

Palladium is a typical H-absorbing metal. We demonstrate the hydrogen diffusion across the Pd surface can be controlled by molecular cap and surface structural changes [2]. Furthermore, the H absorption is considerably enhanced by alloying the Pd surface with a small amount of Au, which is caused by a reduced penetration barrier due to destabilization of the surface adsorption [3]. At low temperature, on the other hand, theH diffusion is expected to undergo a crossover from a classical thermal regime to a quantum regime. By measuringthe temperature dependence of the H hopping rate, we reveal the quantum tunneling dominates the H diffusion atlow temperature [4].

Metal oxides exhibit fascinating functionalities including electronic, optical and catalytic properties. Wedemonstrate the effects of hydrogen on the electronic properties of TiO₂ surfaces (rutile and anatase). While atomic hydrogen adsorbs on TiO₂ surfaces, low-energy ion irradiation allows heavy H doping [5]. As observed by photoemission spectroscopy and transport measurements, it is shown hydrogen acts as an electron donor for rutile and anatase TiO₂ forming small and large polarons, respectively [5]. In contrast to TiO₂, rare-earth nickelates with a perovskite structure absorb substantial amounts of hydrogen upon atomic H dosage. Along with the hydrogen incorporation, the resistance of the film was substantially increased indicating hydrogen-induced metal-insulator transition (MIT). We discuss the mechanism of MIT based on the relation between the resistance and Honcentration [6].

References

- [1] M. Wilde and K. Fukutani, Surf. Sci. Rep. 69 (2014) 196; T. Ozawa et al., submitted.
- [2] K. Fukutani et al, Catal. Lett. 152, 1583 (2022); S. Ogura et al., J. Phys. Chem. C 117 (2013) 9366; J. Phys. Chem. C 120 (2016) 11481; J. Phys. Chem. C 121 (2017) 3373.
- [3] K. Namba et al., PNAS 115, 7896 (2018).
- [4] T. Ozawa et al., submitted.
- [5] Y. Ohashi et al., J. Phys. Chem. C 123, 10319 (2019); N. Nagatsuka et al., J. Chem. Phys. 152, 074708 (2020); Phys. Rev. B 105, 045424 (2022); Y. Yamashita et al., Phys. Rev. B 104, L041111 (2021).
- [6] I. Matsuzawa et al. Phys Rev Materials 7, 085003 (2023).

ANTIBACTERIAL AND BIOMIMETIC STRATEGIES APPLIED FOR COATINGS ON STABLE AND BIODEGRADABLE BIOMEDICAL IMPLANTS

Julietta V. Rau*

Instituto di Struttura della Materia, Consiglio Nazionale delle Ricerche (ISM-CNR), Via del Fosso del Cavaliere, 100 - 00133 Rome, Italy

In the next future, a significant increase of biomedical implants demand is prognosed due to rising of life expectancy. Nowadays, the main requests for implants are their good osteointegration, long term stability, and antimicrobial surface able to fight against infections. For these purposes, metallic implants are coated with biomimetic functional ceramic biomaterials substantially improving metal properties: creating a suitable bone-material interface, and, as a result, leading to a better integration into the surrounding bone tissue. Recent results obtained for biomaterials possessing multiple functional properties designed as coatings on titanium and on biodegradable metal alloy implants will be reported. In the case of Mg and Zn biodegradable alloy implants, the focus point is the control of their degradation rate and their bioactivity characteristics. The developed coating materials are mainly composed of multi-substituted biomimetic calcium phosphates and bioactive glass materials, containing trace ions with therapeutic functions, triggering the natural tissue response.

A crucial aspect of biomedical implants is the development of their antimicrobial characteristics – a challenging issue for a sustainable medical practice avoiding massive use of antibiotics. In this work, the synthesis of antimicrobial materials and the development of antimicrobial surfaces was carried out and their comprehensive characterization was performed. Their structural, morphological, and mechanical features, wetting contact angle, surface topography, and behaviour in model media will be reported. The results obtained for ion doped calcium phosphate bioceramics will be demonstrated. Such materials possess a broad range of specific functional properties, from antibacterial to magnetic ones. In vitro bioactivity, cell and microbiology tests data focused on material-cell interactions will be reported.

Nanostructured antimicrobial biomimetic materials developed in this work are promising for tissue replacement and regeneration, ensuring required structural, chemical, morphological and mechanical characteristics and improving performances of medical implant devices.

^{*} Corresponding author: giulietta.rau@artov.ism.cnr.it

PLASMA JET INTERACTIONS WITH BIOLOGICAL TARGETS

Jean-Michel Pouvesle, Augusto Stancampiano, Éric Robert

¹GREMI, UMR7344 CNRS/Orleans University, Université d'Orléans, Orléans, France

The two last decades have seen an impressive increase of the research dedicated to applications of low temperature atmopheric pressure plasmas, especially in biology and medicine related domains. Biological applications are also now extending to agriculture and, more recently, to cosmetic. Despite the huge number of in vitro and in vivo experiments, there are still numerous challenges to overcome linked to the nature of the encountered target (biological tissues and materials, organs and their direct environment, liquids) that have a direct effect on the produced plasma itself and on the generated species, that being especially true in the case of the use of plasma jets. The extremely strong coupling between the characteristics of the plasma and those of the target, as already shown (e.g. ref. [1, 2]), will play a very important role in the results observed during the treatments. A variation in the chemical or physical characteristics of the target will involve significant differences in the gas flow, the local temperature, or the induced electric field, resulting de facto in variations in the production of the reactive species. It also concerns the transposition of the results between the in vitro and the in vivo/in field experiments [3] that are carried out under extremely different conditions, especially concerning the equivalent electric circuit of the reactor / plasma / target assembly. That must therefore be taken into account in the applied treatments and it complicates the definition of a "plasma dose" expected by many. Development of Artificial Intelligence and Machine Learning can also bring new solutions in the quest of reliable routinely applied plasmas treatments. In this talk, after a presentation of the context, we will focus on the different problems linked to the plasma/target interaction, including treatments of tissues and liquids. We will emphasize on the fact that plasma diagnostics must be performed in real treatment conditions and discuss the main issues, challenges and opportunities linked to the control of the multimodal action of low temperature non-equilibrium plasmas.

References

- [1] Darny T, Pouvesle JM, Fontane J, (...), Robert E 2017 PSST 26 105 001
- [2] Darny T, Pouvesle JM, Puech V, (...), Robert E 2017 PSST 26 045 008
- [3] Stancampiano A, Chung TH, Dozias S, (...), Robert E 2020 IEEE TRPMS 4 355

Acknowledgments

The work realized at GREMI was supported in part by ANR BLANC 093003 PAMPA, by CNRS PEPS project ACUMULTIPLAS, by the ITMO Cancer in the frame of the Plan Cancer, project PLASCANCER N°17CP086-00, by ARD2020 Cosmetosciences project PLASMACOSM and by GDRs ABioPlas and HAPPYBIO. Involved PhD students have been supported by TFS INEL/Région Centre Val de Loire, MENSR, and ANRT/LVMH PhD fellowships

INFRARED CAMERA CALIBRATION BY ISO 12233

Alvaro José Damião¹*, Raphael Efísio da Silva ²

¹ Instituto Tecnológico de Aeronáutica & Instituto de Estudos Avançados- ITA&IEAv-SP-Brazil

² Instituto Tecnológico de Aeronáutica – ITA-SP-Brazil

1. Introduction

Camera calibration is essential for precise image use [1]. Once calibrated, the aging and other camera problems can be known and evaluated. ISO 12233 was applied to establish the main camera characteristics and range [2]. A commercial UAV, DJI Phantom 2, having an adapted FLIR infrared camera, was chosen for this study, and the Slanted Edge Method was applied. The results showed that the camera parameters were successfully obtained, and the camera was correctly characterized.

2. Experimental

A commercial UAV infrared camera, a FLIR Camera, and an Extended area CI Blackbody hollow plate pattern were used (FIG 1) to establish the Spatial resolution. Initially, it was verified if the camera's Automatic Gain Control could be disabled. As it was impossible, a hot source (70 °C) was placed in the camera's Field of View (FOV), so a more detailed image could be registered. The AGC spreads the camera's digital levels to its limits to enhance the contrast. Then, the camera responsivity, the Noise Equivalent Temperature Difference (NETD) and the Modulated Transfer Function were obtained [3]. Having this data, the MRTD – Minimum Resolvable Temperature Difference was estimated.

3. Results and Discussions

The camera responsivity was measured by obtaining the digital levels as a function of the Blackbody temperature (Fig. 2). Good linear agreement was obtained. Then, the NETD was calculated, with some other camera data being measured. Finally, the MRTD was calculated, and a value of 32 m was found. Latter field tests showed that this value was underestimated. The correct value was 35 m.



Fig. 1. Set up used for the camera Spatial resolution measurement.

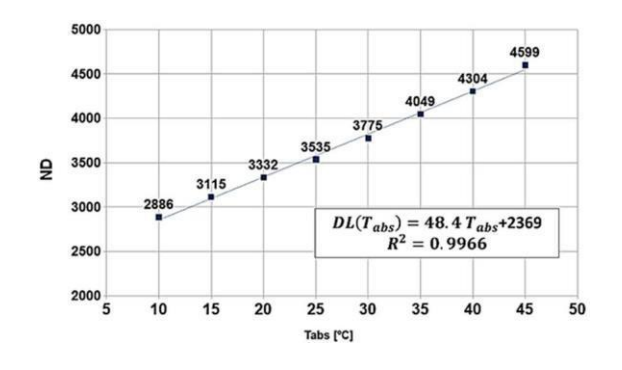


Fig. 2. The camera responsivity - Temperature (°C) xDigital Level (ND).

4. References

HOLST, G. C. Electro-optical Imaging System Performance. 5th ed. Bellingham: SPIE, 2008 BS ISO 12233:2023 Photography. Electronic still picture imaging. Resolution and spatial frequency responses. BOREMAN, G. D. Modulation Transfer Function in Optical and Electro-Optical Systems. Bellingham: SPIE,2001. 110 p.

Acknowledgments

To Marielcio Lacerda for UAV flight tests.

^{*} Corresponding author: alvarojd@ita.br

EPITAXIAL GRAPHENE: PROPERTIES AND APPLICATIONS FOR THE US NAVY

Rachael L. Myers-Ward

¹US Naval Research Laboratory

Since its discovery, graphene has been recognized for its exceptional physical, electronic and optical properties. While the lack of an energy gap has limited conventional device applications, our research has focused on its sensing abilities. Graphene is an attractive material to sense adsorbates which impact carrier concentration and leads to measureable variations in conductivity. Here, we report on epitaxial graphene sublimated from SiC substrates as the material of choice for sensor development, focusing on underwater, sulfur and biological sensors. In addition, the use of graphene to grow remote epitaxial films to impact power electronics and quantum science applications will be presented.

TRIELECTRODE NON-THERMAL PLASMA SOURCES FOR GAS AND WATER REMEDIATION

Diana Grondona

Instituto de Física Interdisciplinaria y Aplicada (INFINA) (UBA-CONICET)

A very active branch in plasma physics is the development of plasma sources operated at atmospheric pressure able to provide energetic electrons, which produce in turn highly active chemical reactive species, at relatively low gas temperature. This is due to a large number of applications of these sources in plasma technology and in particular for environmental challenges.

This work presents the study of trielectrode non-thermal plasma sources for water and gas treatment. The reactors combines a dielectric barrier discharge with a remote third electrode, designed to extend the non-thermal plasma region.

The reactor for gas treatment has a cylindrical geometry that provides a natural boundary for the gas flow, with low impedance. In the reactor for water treatment the non-thermal plasma extends towards the third electrode attached to a channel through which the water to be treated flows.

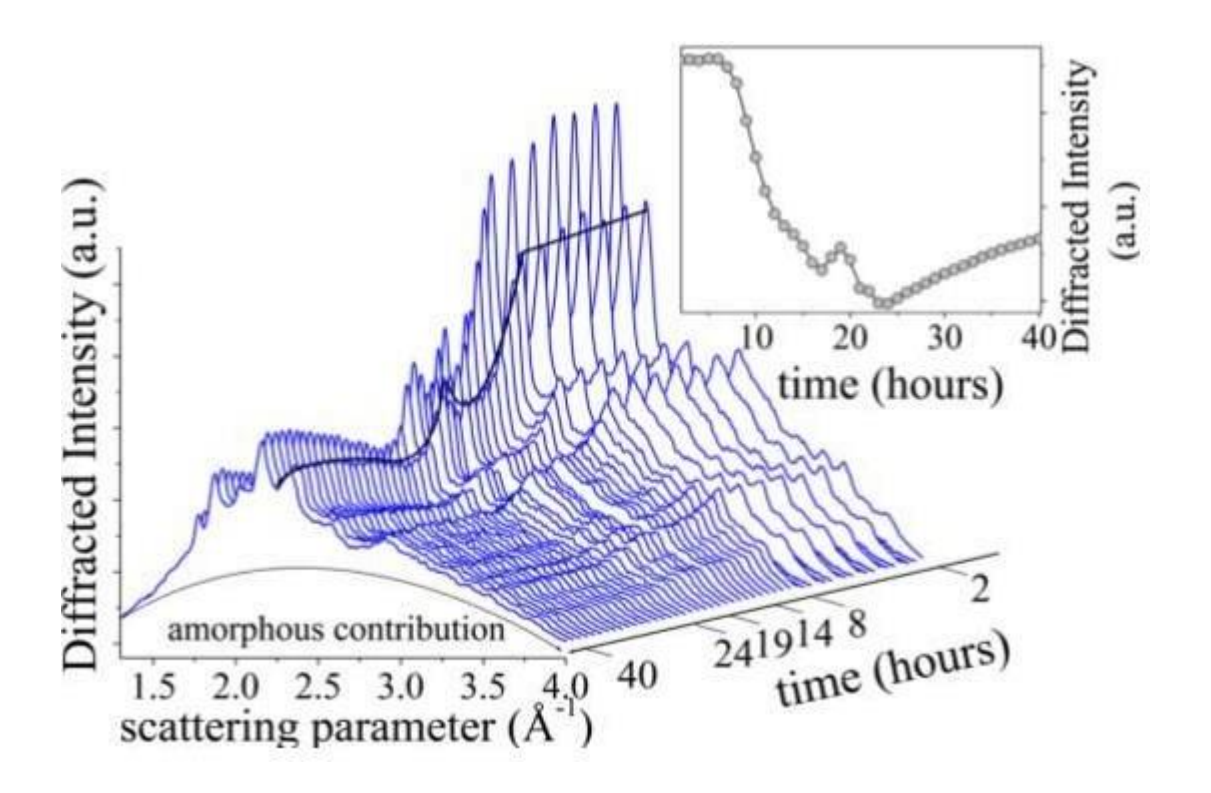
 $[\]hbox{*Corresponding author: grondona@df.uba.ar}\\$

REAL TIME MONITORING OF CALCIUM PHOSPHATE CEMENTS: AN INSIGHT INTO KINETICS ANDMECHANISMS

Marco Fosca* and Julietta V. Rau

Instituto di Struttura della Materia, Consiglio Nazionale delle Ricerche (ISM-CNR), Via del Fosso del Cavaliere, 100 - 00133 Rome, Italy

Calcium phosphates cements (CPC) have been used in the past years as second-generation biomaterial for bonedefect repair, bone regeneration and augmentation, mainly due to their chemical composition, similar to the one of natural bone. Besides this fundamental feature, they are also characterized by biocompatibility, injectability, self-setting properties at physiological temperatures, and biodegradability, with tailorable dissolution rate which depends on Ca/P ratio. Once into the physiological environment, CPC may promote osteoconduction and osteogenesis. After injection, CPCundergo setting and hardening processes where different changes, such as phase transformations, amorphous into crystalline transitions, primary and secondary crystallizations took place. Invitro, real-time monitoring of structural transformation of CPCs is performed mainly by Energy Dispersive X-Ray Diffraction technique (EDXRD) (see Figure below) due to its ability of fast collection of diffraction patterns in a spectroscopic fashion, providing time-resolved diffraction data. Quantitative analysis of time-resolved EDXRD patterns allows to define characteristic time of structural changes of CPCs. Furthermore, it also allows to observe such phenomena as the appearance and/or disappearance of transient or permanent new phase(s), which occur on a time scale that ranges from few minutes up to several weeks. Therefore, the EDXRD technique is able to provide insights into kinetics and mechanisms of CPC biomineralization process. Finally, complementary characterizations by other techniques (mainly SEM and FTIR) are performed to support and confirm the EDXRD structural outcomes.



^{*} Corresponding author marco.fosca@artov.ism.cnr.it

INTERFACIAL EFFECTS IN FE-BASED LAYERED MAGNETIC NANOSTRUCTURES: DEPTH-RESOLVED INVESTIGATIONS

Waldemar A. A. Macedo

Centro de Desenvolvimento da Tecnologia Nuclear 31270-901 Belo Horizonte, MG, Brazil

The study of layered magnetic nanostructures and interface-induced phenomena are of fundamental relevance in physics and materials science, due to the importance for spintronics and related areas, and the potential for new applications and disruptive technologies. For such systems, the possibility of conducting depth-resolved measurements and accessing buried magnetic interfaces is of vital relevance but can be challenging. This talk will address studies on the growth, structure, and magnetism of layered nanostructures (FM/AFM, FM/NM) prepared in ultra-high vacuum, by molecular beam epitaxy or by sputtering deposition. The potential offered by the application of isotope-selective measurements for the study of surfaces and interfaces will be illustrated with the application of isotope-enriched (57Fe) probe layers and conversion electron Mössbauer spectroscopy (CEMS) on the investigation of depth-dependent spin structures, magnetization reversal, and interfacial interdiffusion in different Fe-based exchange-biased FM/AFM bilayers grown by sputtering (FeCo/IrMn, Fe/FeMn, FeCo/Mn₂Au,...). For FM/NM systems, it will be discussed the influence of chemical order on the magnetic anisotropy of epitaxialFe/Co ultrathin films grown by MBE on Cu₃Au(001), and the induced magnetization in the non- magnetic surface atoms, investigated by combining conventional surface-sensitive techniques, X- ray magnetic circular dichroism (XMCD) measurements, and depth-resolved first-principles calculations.

BIOLOGICAL SURFACE SCIENCE: A REVIEW

Paulo Noronha Lisboa-Filho*

UNESP - São Paulo State University, Bauru, SP, Brazil

1. Introduction

Biological Surface Science (BioSS) can be defined as an interdisciplinary field that studies the properties and processes at interfaces between synthetic materials and biological environments [1]. These interfaces play a crucial role in various scientific, medical, and technological applications, as they determine the interactions and exchanges that occur between the biological and synthetic components.

Biointerfaces can exist at different scales, from the molecular level where proteins interact with surfaces,to the cellular level where cells interact with biomaterials, to the macroscopic level where medical devices or implants come into contact with tissues. The interactions at these interfaces can involve physical, chemical, and biological processes, and they have implications for fields like biomaterials, tissue engineering, drug delivery, medical diagnostics, and more. Understanding and engineering biointerfaces is essential for developing biocompatible materials and devices, as well as for improving the performance and safety of medical treatments and interventions. This contribution intends to describe the multifaceted realm of biointerfaces by delving into the intricateinteractions that transpire between biomolecules and surfaces at varying scales, discussing results of advanced surface science techniques, including X-ray photoelectron spectroscopy, atomic force microscopy and computational simulation, reviewing addresses in biomaterials and medical devices.

As representative illustrations of the field, findings for titania substrates modified with chemisorbed organophosphonates, will be discussed [2,3]. Firstly, modifications of surface properties caused by bisphosphonates' adsorption on smooth titanium dioxide were demonstrated, where the use of a smooth substrateaims to reduce the influence of the geometric surface area, which can increase the surface charge or even the interaction between layers and cells. In a more complex environment, the adsorption of bisphosphonates (BPs) on TiO2, hydroxyapatite (HA), and TiO2+HA composite surfaces were also investigated.

2. References

[1] B. Kasemo, Surface Science, **500**, 656-677, (2002).

L. F. G. Dias, et al., Chemistry Select, 7, e202200286, (2022).

L. F. G. Dias, et al., Surfaces and Interfaces, 39, 102964, (2023).

Acknowledgments

The author is grateful to the São Paulo Research Foundation FAPESP for the financial support through the grants 2014/26982-7; 2017/15035-5; 2018/07520-3 and 2019/13100-0

^{*}Corresponding author: paulo.lisboa@unesp.br

ESS NEUTRON INSTRUMENT VACUUM SYSTEM

Marcelo Juni Ferreira^{1*}, Laurence Page¹

 1 European Spallation Source – ERIC, Technical Division, Vacuum Group, Lund, Sweden

The European Spallation Source (ESS) is a multi-disciplinary research infrastructure for neutron, based on a 2GeV-5MW proton linear accelerator (LINAC), as a most updated version of vacuum science applied for accelerators [1]. The goal of ESS is to be the brightest neutron facility and to enable novel science in many fields such as biology research, environmental technologies and fundamental physics. The facility includes Super-Conductive Radio-frequency cavities (SRF) to accelerator a proton beam to produce neutron by spallation process on a helium-cooled tungsten wheel, possibility to host 42 neutron instruments [2]. The ESS Vacuum Group has the overall responsibility for all technical vacuum systems used on the Accelerator, Target and Neutron Scattering Instruments (NSS). An overview is provided of the 15 neutron beam instruments making up the initial instrument suite of the European Spallation Source (ESS), and being made available to the neutron user community. The ESS neutron source consists of a high-power accelerator and target station, providing a unique long-pulse time structure of slow neutrons. The initial first 15-instrument suite covering small-angle instruments, reflectometers, imaging, diffractometers; macromolecular crystallography, powder diffractometers, diffractometer, as well as inelastic instruments. The vacuum conceptual design, performance and specific technical solutions of these instruments are described.

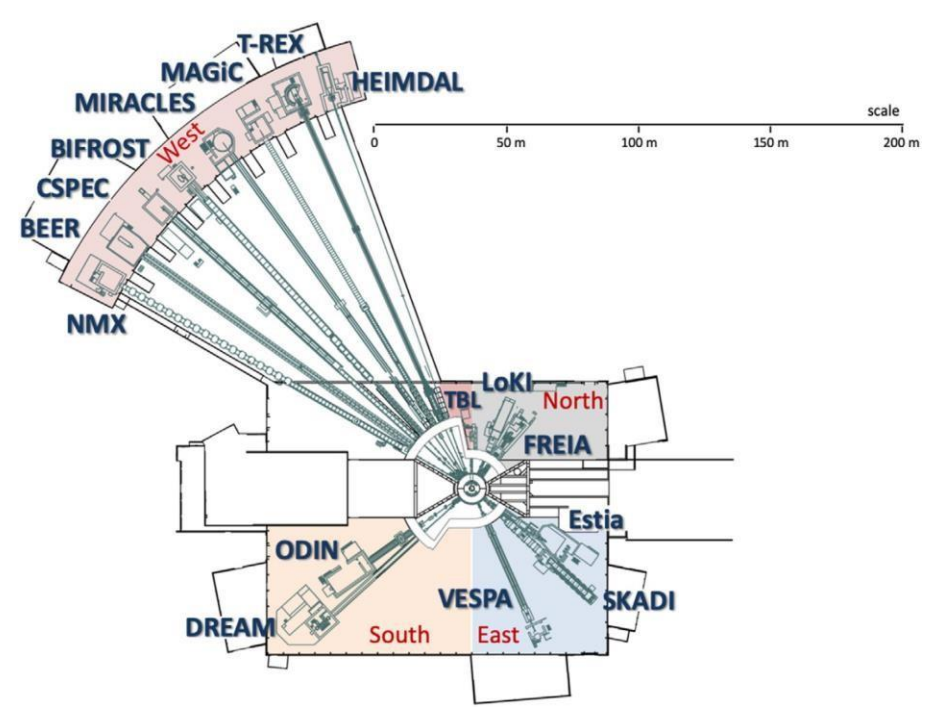


Fig. 1. *Instrument Suite distribution layout on the experimental halls [2].*

References

- [1] Roland Garoby and et all, Physica Scripta, 93, n.1 (2017).
- [2] K.H. Andersen and et all, Nuclear Inst. and Methods in Physics Research, A 957 (2020) 163402.

Acknowledgments

Special thanks for all ESS in-kind and project teams for the design, tests, and the Vacuum Group team interfacing all partners.

^{*}Corresponding author: marcelo.juniferreira@ess.eu

DEVELOPMENT OF ATMOSPHERIC PRESSURE PLASMA JETS FOR LARGE AREA SURFACETREATMENT

Konstantin G. Kostov^{1*}, Felipe V. P. Kodaira¹, Thayna F. Tavares¹, Luiz R. O. Hein¹ and Antje Quade²

¹FEG – UNESP, Guaratinguetá, 12516-410, SP, Brazil ²INP – Greifswald, Greifswald, 17489, Germany

1. Introduction

Atmospheric pressure plasma jets (APPJs) are low-cost systems where electric discharge is ignited in a noble gas that flows through a thin dielectric tube and the resulting plasma is ejected into the air. Normally, the APPJs generate severalcm-long plasma plumes that can be easily adapted to treat irregular 3D objects and internal surfaces of narrow tubes or cavities [1]. However, the plasma plume diameter is limited by the inner diameter of the dielectric tube thus resulting in a modified surface with small size (typically few cm²) [2]. In this work, we report on an APPJ terminating with a conical nozzlewith diameter of 7.0 cm.

2. Experimental

A schematic drawing of the plasma jet configuration employed in this work is shown in the Fig. 1. It consists of a pin electrode (2.4-mm-thick Tungsten rod) centered inside a 2.5-mm-thick quartz conical funnel, which has inner diameters of 4 mm at the straight part and 70 mm and at the funnel exit, respectively. The device was installed vertically with the exit pointing downward. The signal from a commercial high voltage generator was applied to the pin electrode and measured by P6015A Tektronix voltage divider (1×1000). Beneath the funnel was placed a grounded metal electrode (Ø 155 mm) covered by a 3-mm-thick glass. The charge transferred to the target and the discharge current were obtained by measuring the voltage drop across a serial capacitor of 10 nF or a serial resistor of 100 Ω , respectively. The device was operated with Ar gas using moderate flow rates between 1 and 5 slm. To identify the exited species produced by the plasma an Avantes spectrometer was used. As can be seen in the Fig. 2 the entire area below the jet exit nozzle is covered by plasma, which makes the device suitable for applications that require surface modification over larger area (tens of cm²) [3]. To confirm this large polymers samples were placed under the jet conical exit and plasma treated. To assess the polymers surface modification, we employed water contact angle (WCA) measurements and XPS analysis.

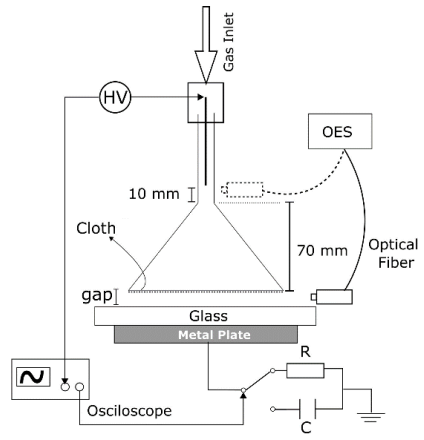






Fig. 2. Photo of the plasma jet device.

3. Results and Discussions

The proposed conical plasma jet with exit nozzle exhibited a stable operation over wide range of gas flow rates andgap distances. Depending on the operating conditions, the device mean power and rms current can be maximized. The plasmajet device has very simple construction, but it is able to promote a uniform surface modification over relatively large area, which was confirmed by the WCA and XPS measurements.

4. References

- [1] M. Laroussi, T. Akan, Plasma Process. Polymers 4, 777–788 (2007).
- [2] Ö. Birer, Appl. Surf. Sci., **354**, 420 (2015).
- [3] T. S. M. Mui, R. P. Mota, A. Quade, L. R. H. Oliveira, K. G. Kostov, Surf. Coat. Technol., **352**, 338 (2018) **Acknowledgments:** Financial support from the FAPESP under grant 2019/05856-7 is acknowledged.

^{*}Corresponding author: konstantin.kostov@unesp.br

EFFECT OF SHAPE AND ASYMMETRY OF THE VOLTAGE PULSE ON PLASMA IONIZATION RATE

Luis César Fontana

Universidade do Estado de Santa Catarina UDESC

Several dc, pulsed, and radiofrequency (RF) stabilized plasma power supplies have been developed over a wide range of frequencies and voltage waveforms. However, the influence of voltage waveform on the plasma ionization, mainly due to the secondary electron emission from the electrodes, has not been quite explored. The present paper will present preliminary results of plasma generation through asymmetric pulsed bipolar power supply. Short period positive pulses, between longer negative pulses, increase greatly the secondary electron emission from the electrodes and, consequently, the plasma ionization rate. Short pulses (with period of nanoseconds) are obtained by the phase shift between each carrier, and the high-intensity pulses are obtained by cascading the cell submodules in a half-bridge cascade topology, using a modular half-bridge converter configuration. The intensity of the positive and negative pulses can be varied independently. The plasma generated in this way is free of electric arc and can be kept stable within a broader range of operating parameters, mainly the voltage and the working gas pressure. Some application of this technology for materials treatment are showed in this paper.

Acknowledgements:

This work was supported by the FAPESC/CNPq [PRONEM 2020TR730] and FAPESC-UDESC PAP 2023TR000258

^{*}Corresponding author: luis.fontana@udesc.br

HELIUM COLD PLASMA FOR THE TREATMENT OF ORAL LESIONS IN RATS UNDERGOING CHEMOTHERAPY

Aline da Graça Sampaio¹, Noala Vicensoto Moreira Milhan¹, Fellype do Nascimento², Konstantin GeorgievKostov², Cristiane Yumi Koga Ito^{1*}

¹ Institute of Science and Technology, São Paulo State University (Unesp), SP, Brazil. ² Guaratinguetá Faculty of Engineering, São Paulo University (Unesp), SP, Brazil. e-mail: cristiane.koga-ito@unesp.br

1. Introduction

Chemotherapy for the treatment of cancer in the head-neck region shows high toxicity that results in adverse effects, such as oral lesions. This clinical condition is responsible for significant clinical[1] and economic negative consequences[2], increased risk of systemic fungal infections and morbidity[3]. Clinical practice guidelines indicate palliative care for the treatment of these lesions. However, an evidence-based study highlights that the existing therapeutic alternatives have limitations [4]. Low-temperature atmospheric pressure plasma (LTAPP) generates reactive oxygen and nitrogen species (RONS) that have promising antifungal and anti-inflammatory effects[5]. The objective of the study was to evaluate the application of Helium LTAPP (He-LTAPP) jet for the treatment of oral lesions infected by *Candida albicans* in rats undergoing chemotherapy.

2. Experimental

Male rats (*Rathus norvegicus*) received a single dose of cisplatin (7 mg/kg) and 4 consecutive doses of 5-fluorouracil, followed by inoculation of *C. albicans* suspension (10^8 cells/ml), intraorally, on days 2, 3 and 5. After, oral lesion was induced on the side of the tongue (4th day), with the aid of a swab soaked in 50% acetic acid. For treatment, the animals were anesthetized, and the lesions were treated with He-LTAPP jet for 5 min, at a distance of 1.5 cm, on days 4 and 5. Control group was not exposed to LTAPP. The animals were sacrificed after 24 and 72 h, the tongue was removed in an aseptic environment, weighed, and homogenized in saline solution. Afterwards, an aliquot of $100 \,\mu\text{L}$ was plated in Sabouraud dextrose agar and incubated at 37°C for 24h. The number of colonies was determined by the weight of the tongue (CFU/mg). The results were compared between test and control group by the appropriate statistical tests, at the level of significance of 5%.

3. Results and Discussions

Significant reduction in fungal counts was detected in He plasma group in relation to control after 24 h (p = 0.0101, Mann-Whitney test) (3.32 x $10^3 \pm 5.01$ x 10^3 and 1.68 x $10^3 \pm 4.23$ x 10^3 CFU/ mg, respectively). These findings demonstrate the promising application of He-LTAPP for the treatment of infected oral lesions.

4. References

- [1] Sonis, S.T.; Tracey, C.; Shklar, G.; Jenson, J.; Florine, D. Oral Surgery, Oral Medicine, Oral Pathology (1990).
- [2] Peterman, A.; Cella, D.; Glandon, G.; Dobrez, D.; Yount, S. J Natl Cancer Inst Monogr (2001).
- [3] Vargas-Espíndola, L.A.; Cuervo-Maldonado, S.I.; Enciso-Olivera, J.L.; et al. Journal of Fungi. (2023).
- [4] Daugėlaitė, G.; Užkuraitytė, K.; Jagelavičienė, E.; Filipauskas, A. Medicina (Kaunas) (2019).
- [5] Borges, A.C.; Morais, G.G.L.; Mayumi, T.C.N.; Gontijo, A.V.L.; Kostov, K.G.; Koga-Ito, C.Y. PLoS One (2018).

Acknowledgments

This work was supported by FAPESP 2019/25652-7 and 2019/05856-7.

^{*}Corresponding author: cristiane.koga-ito@unesp.br

Ti-10Mo-Mn SYSTEM ALLOYS FOR BIOMEDICAL APPLICATIONS

Mariana Luna Lourenço and Carlos Roberto Grandini*

UNESP – Universidade Estadual Paulista, Lab. Anelasticidade e Biomateriais, 17.033-360, Bauru, SP, Brazil

1. Introduction

Ti alloys are being extensively studied as a biomaterial, mainly β -type, because they have a low modulus of elasticity, which avoids the "stress shielding" effect, causing loss of bone density around the implanted material [1]. Ti has become famous for its use as a biomaterial due to its excellent combination of mechanical strength, elastic modulus, and biocompatibility. Mo increases the material's mechanical strength and is among the most popular elements for forming β -type alloys. Mn increases corrosion resistance, decreases the modulus of elasticity, is an essential element for the human body, has good biocompatibility, and has a low cost compared to Mo. Giventhe good properties of the elements, a ternary system was made for study. The present study aimed to prepare alloys of the Ti-10Mo-xMn system (x = 0, 2, 4, 6, 8 wt%) and to analyze the influence of some thermal treatments in the structure, microstructure, some mechanical properties, and its cytotoxic nature.

2. Experimental Part

The alloys were obtained by arc-melting and submitted to thermomechanical processes, such as homogenization, hot-rolling, and annealing. Subsequently, they were characterized in terms of chemical, structural, microstructural, electrochemical, mechanical, and cytotoxic aspects, with the aim of better understanding the relationship betweenmicrostructure and properties of the alloys [2,3].

3. Results and Discussions

The alloys showed a metastable β crystalline structure, obtaining the β , α and α " phases depending on the concentration of the alloying elements and the processing conditions. Preliminary cytotoxicity tests indicated no deleterious effects on cell viability with osteoblastic cells in all alloys [2,3].

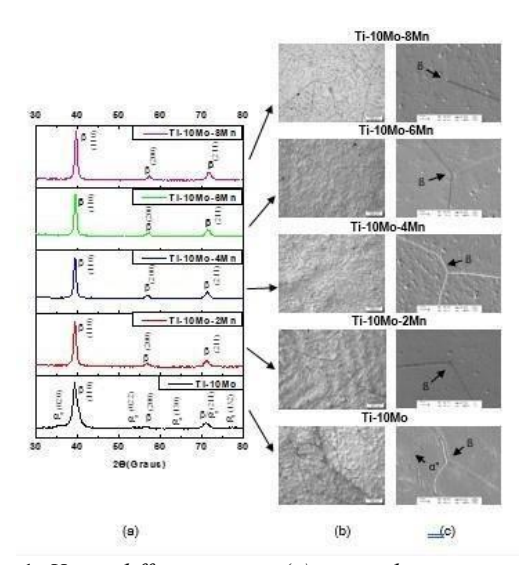


Fig. 1. X-ray diffractograms (a), optical microscopy (b) and scanning electron microscopy (c) for as-cast Ti-10Mo-Mn alloys.

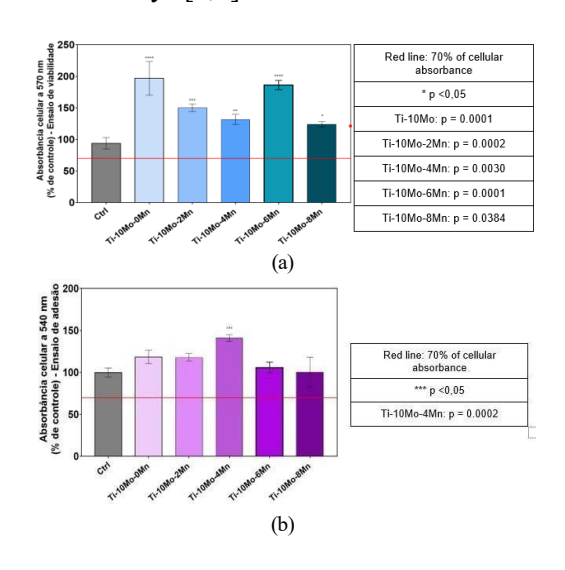


Fig. 2. Cellular viability (a) and cellular adhesion (b) for as-cast Ti-10Mo-Mn alloys.

4. References

- [1] R.P. Kolli, A.A. Devaraj, Metals 8, 506 (2018);
- [2] M.L. Lourenço et al. Scientific Reports 10, 6298 (2020).
- [3] M.L. Lourenço, F.M.L. Pontes, C.R. Grandini, Metals 12, 527 (2022).

Acknowledgments: The authors thank Capes, CNPq (grant # #314.810/2021-8) and FAPESP (grant #2015/50280-5) for financial support.

^{*}Corresponding author: carlos.r.grandini@unesp.br

PROPERTIES OF N95 RESPIRATORS EXPOSED TO O2/SF6 DESINFECTION PLASMAS

Julia Kolowrotkiewicz¹, Rafael P. Ribeiro², Nilson C. Cruz², Elidiane C. Rangel^{2*}

 Production Engineering at Mechanical Department, Cracow University of Technology
 Technological Plasma Laboratory - São Paulo State University (UNESP), Institute of Science and Technology, Sorocaba

1. Introduction

In the last few years there was a growing demand for sterilization in different kinds of applications, including dry food surfaces, medical items, body implants, drugs packages, probes and extra-planetary probes andsamples [1]. The necessity for the development of new disinfection methodologies that better attend the specific requests of each case was thus created. Amongst the different possibilities, low pressure plasma processes rise as a promising alternative since they allow the synergetic combination of the physical (UV-radiation, ion and electron bombardment) and chemical (reactive species erosion) processes of conventional methodologies in a simple, clean and environmentally correct. Owing to that, it was evaluated here the possibility of using an innovative plasma sterilization route for disinfection of N95 commercial mask fabrics, based on O₂ and SF6 mixtures. Specifically, it was investigated the effect of the proportion of SF₆ incorporated to O₂ atmosphere on the properties of the fabric fibers, to evaluate if the tissue functionality is preserved upon the plasma exposure.

2. Experimental

Polypropylene (PP) samples from N95 masks were submitted, for 10 min, to low pressure radiofrequency (13.56 MHz, 100 W, 9.3 Pa) plasmas established from mixtures of O_2 and SF_6 . Samples were treated in both the grounded (upper) and driven (lower) electrodes of a capacitively coupled reactor. It was evaluated the effect of the O_2 (100-0%) dilution with SF_6 (0-100%) on the chemical structure and composition, surface microstructure and wettability of the fabric fibers. Besides the properties of the material, the cytotoxicity of the disinfected fabricwas also accessed.

3. Results and Discussions

The pristine PP fabric, a super-hydrophilic material that fast absorbs the water droplet, presented essentially C-H groups in the infrared spectrum and 100% of C from the energy dispersive spectroscopy, what isin good agreement with the chemical formula of the PP (C_6H_3). In this material the fibers, with an average diameter of 15 μ m, are reticulated to each other. Upon plasma exposure, there was no changes in the overall fiber morphology and dimension. The infrared spectra also revealed the same chemical structure as the control PP, suggesting that plasma exposure will not affect the material operationality and usability. However, contact angle, that is a surface sensitive probe, changed after the plasma treatments. The super-hydrophilic pristine samples became hydrophobic (108-115°) upon plasma exposure indicating F incorporation only on the surface of the fibers. The mentioned results were obtained for the samples treated in the grounded (upper) and in the driven (lower) electrodes, showing that chemical reactions are more prominent than the electrical configuration.

4. References

[1] FIEBRANDT, M. et al. Journal of Physics D: Applied Physics, v. 51, n. 4, p. 045401, 2018.

Acknowledgments

Authors thank to MNF laboratory of LNNano/CNPEM, FAPESP (2017/21034-1;2020/06448-7), CNPq (48437/2018 and 47114/2018) and CAPES (1766917).

^{*}Corresponding author: elidiane.rangel@unesp.br

GROWTH OF SALT FLOWER IN PLASMA-ACTIVATED HYPERSALINE WATER

Lucas Cabral Rocha¹, Jussier de Oliveira Vitoriano², Rodrigo Sávio Pessoa³, Clodomiro Alves Junior^{4*}

¹Federal Rural University of Semiarid, UFERSA-PPGCEM ²Federal Rural University of Semiarid, UFERSA-Labplasma ³Technological Institute of Aeronautics, ITA-LPP ⁴Technological Institute of Aeronautics, ITA-LPP/FAPESP

Abstract

Under condition still unknown, crystals called salt flower can be formed on the surface of seawater during evaporation. With the aim of investigating the effect of plasma activation on the formation of these crystals, the current study was conceived. The mechanism of growth and morphology of salt flower crystals produced through natural evaporation was compared with those produced in plasma-activated hypersaline water. The growth mechanisms, morphology, and microstructure of the salts obtained during the evaporation of residual solution (hypersaline solution), initial density of 28°Be (1,23g/cm³), by a fixed thermal gradient and humidity were studied. The size and mass of the salt flower film in plasma activated water (PAW) was higher than one obtained in natural evaporation (NPAW). It was also observed that the coated area and the total mass of the saltflower produced in the PAW were greater than in the NPAW. A mechanism for salt flower production was proposed based on the generation of air bubbles as nucleation sites, with the coalescence of crystals occurring through salt bridges.

Keywords: salt flower, crystals growth; PAW; mechanism

1. Introduction

During the process of obtaining NaCl in salt pans through the evaporation of seawater, crystal growth on the water's surface is observed under specific conditions of temperature, humidity, and winds [1]. These crystals are called 'flower of salt' and possess a high added value due to their purity, extreme whiteness, and crunchy texture, which contribute to quality in the gourmet universe. The presence of scientific studies explaining the role of thermodynamic factors involved in the process of crystal formation, as well as their morphology and chemical composition, is limited [2-3]. It is difficult to pinpoint which of these factors is the most important, but it is presumed that the phenomenon depends mainly on a thermal and chemical gradient between the liquid phase and the external environment.

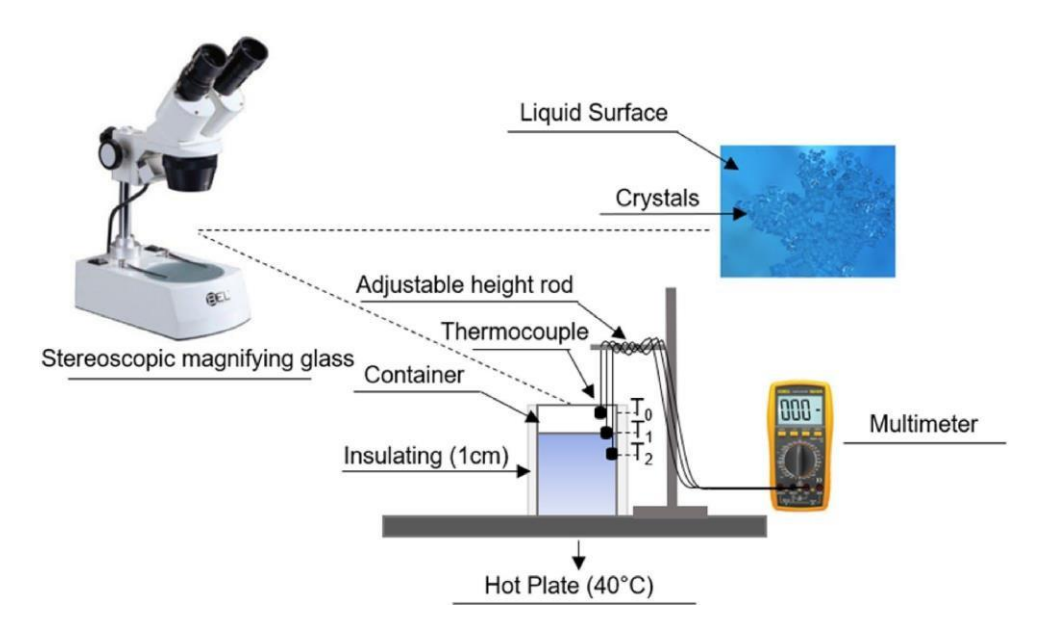
By applying plasma to the surface of hypersaline water, thermal and chemical modifications are expected to occur in subsurface regions. Theoretical models studying the effect of the external electric field on the water's surface and the analysis of interfacial mobilities of salt ions at the liquid-vapor interface, or the effect of ohmic heating, already exist and can be validated with the present study [4-6]. In the present work, the growth kinetics of the salt flower on the surface of hypersaline water was investigated. The effect of growth through natural evaporation was compared with growth activated by plasma.

2. Experimental

Samples of residual water collected at Salina F. Souto Ind, Grossos-RN, with a density of 1.224 g/cm3, were used as the starting material for this study. The formation of salt flower was experimentally simulated in the laboratory by introducing 200 ml of the residual water into a becker, insulated by a 1cm-thick layer of Styrofoam to prevent radial temperature variations. The becker was placed on a heated plate at 40°C to maintain the average water temperature constant and at 35°C (Figure 1). Three thermocouples were used to measure temperature variations on the surface (T1) and 10 mm above and below the surface (T0 and T2, respectively). During the 18-hour observation period, corresponding to a density change from 1.224 to 1.235 g/cm3, the experiment was conducted as illustrated in Fig. 1. Plasma corona activation was performed using the same experimental apparatus as depicted schematically in the Figure 1. A stainless-steel needle (1.20 mm x 40.0 mm) with a conical end (tip radius 0.27 mm), negatively polarized was positioned 3.0 mm above the bittern surface. A grounded copper plate (1.0 mm x 100.0 mm x 100.0 mm) was positioned inside of the becker. A corona discharge using a pulsed voltage source set at 11.5 kV, repeated with a frequency of 450 Hz was triggered to generate the plasma over the bittern during 10 s to start the plasma activation experiment. The process was recorded by a video camera for 1 hour, starting from the moment the water reached a temperature of 40 ° C. Onehour after the start of the naturally evaporated hypersaline water (NPAW) and plasma-activated hypersaline water (PAW) experiments, fleur de sel was collected for weighing and chemical analyses. Images was extracted from this video at different instants for subsequent image analysis. The total area of

the salt flower produced with and without plasma activation was compared through image analysis.

To prevent the dissolution of the salts due to atmospheric moisture, vacuum filtration was employed as the method for collecting the salt flower samples. Subsequently, the crystals were dehydrated in a 60°C oven for the necessary duration until complete dryness was achieved. They were then weighed, packaged in plastic bags, and prepared for analysis using Scanning Electron Microscopy (SEM) and Energy-Dispersive X-ray Spectroscopy (EDS).



3. Results and Discussions

For both the natural evaporation condition and the plasma-activated condition, temperature values of 27 ± 0.34 °C, 32.5 ± 0.25 °C, and 34.8 ± 0.50 °C were observed for T0, T1, and T2, respectively. The first visible nucleation sites under the microscope are observed after 1 hour from the start of the experiment. In Figure 2, images extracted from the video are illustrated, showing the crystals formed at moments 0s, 10s, 20s, and 27s after the emergence of the first crystals. It is observed that in the PAW, a thin film grows on the surface, unlike the NPAW, where the grains appear dispersed. Probably due to the larger grain size, it appears whiter than inthe PAW. It was also noted that in the NPAW, crystals are also precipitated in the volume and sedimented at thebottom of the beaker making it difficult to distinguish between the images of grains on the surface and those on the bottom of the beaker. The mechanism by which this film is formed on the surface is not yet well known, although it is known that temperature, wind speed and relative humidity are important variables in the process [7-8].

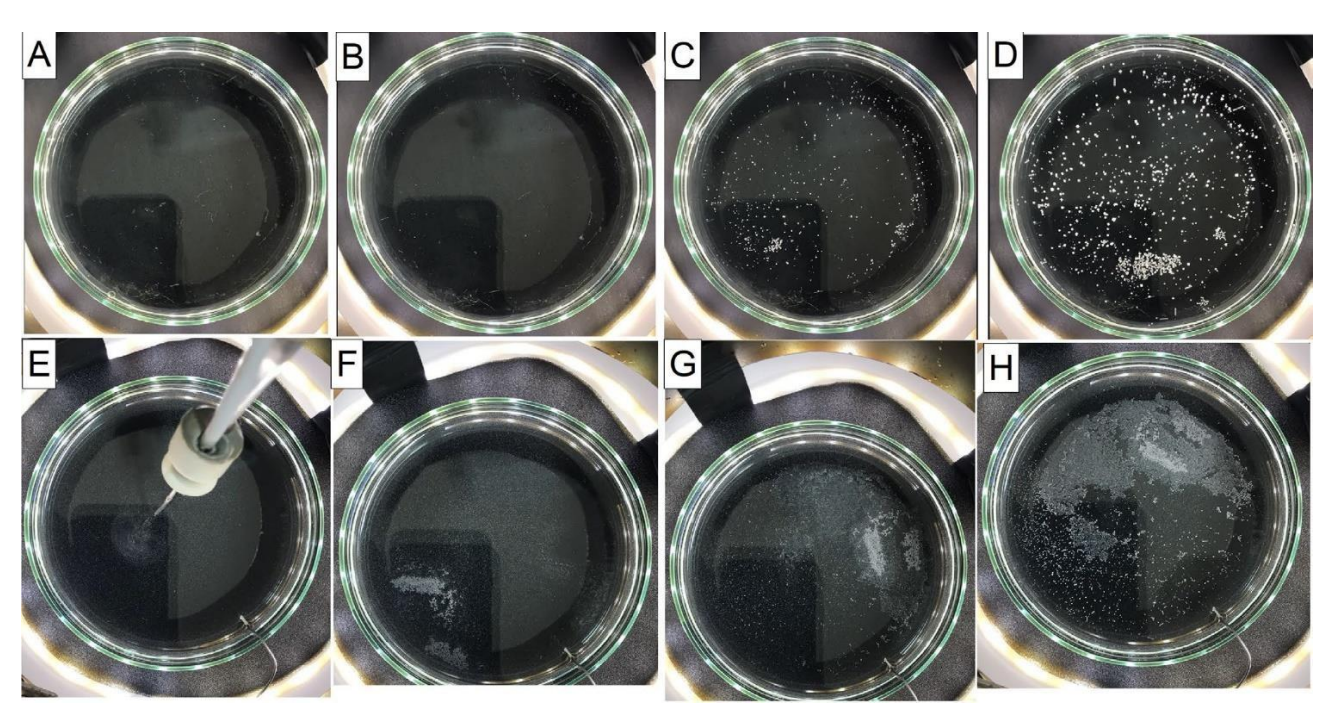


Figure 2. Images taken at 0 s, 25 s, 50 s, and 67 s for NPAW (A-D) and PAW samples (E-H), respectively.

During the process, the presence of bubbles was observed, in a convection movement produced by the thermal gradient from the bottom to the surface (Fig. 3). There is a correlation between the reduction of bubbles and the appearance of salt flower crystals. It is possible that the presence of these bubbles is essential for the formation of crystals on the surface since they are preferred sites for the nucleation of salts. In the case of PAW, which have a higher nucleation speed, confirmed by the smaller size of the grains, it is clear that the plasma also influences the precipitation mechanism. So far, little attention has been paid to understanding the mechanism of flower of salt formation, either in saltwork or laboratory. Some authors point out that the phenomenon occurs only on warmer days, with reduced humidity and wind speed [7]. Despite the importance of these variables, there is still a shortage of evidence on mechanism of the crystallization. We observed that during the evaporation of the liquid there was a convection movement of black dots (Fig. 3A) that we assume are air bubbles produced by heating the solution. We also found that the number of these bubbles was reduced as crystallization progressed (Fig. 3B), confirming research results in which the greater volume of air is entrained insalt than in freshwater to generate many more bubbles in salt water, but in very concentrated solutions the size and mobility of the bubbles are reduced. We hypothesized that floating salts are produced following the same principle as floation extraction, that is, only hydrophobic particles tend to attach with bubbles after collision. Once that dissolved ions in solutions may alter the water structure, particle surface wettability and colloidal interactions between bubbles and particles, we expect the extraction process to be strongly dependent on the concentration of solutes in the solution, that is, on its density [9]. Based on the knowledge of the literature and our experimental observations, a model of nucleation and growth of grains of flower of salt was proposed. During the heating of the solution, air bubbles are released from water to to the surface. Along the way they can collide with different solvated ions, or even particles of salts, which will be attached if they are hydrophobic [10-11]. The compression of the electrical double layer in saline water enhances the thinning and rupture of the wetting film between bubbles and salt particles which are a critical step in the formation of a stable bubble-salt crystal, an important phenomenon in flower of salt production [12]. The coalescence of the crystals is done through capillarity bridges (Fig. 3C,7D) produced under drying conditions, resulting in a crystal film. In thecase of PAW, the process is increased by the action of the plasma.

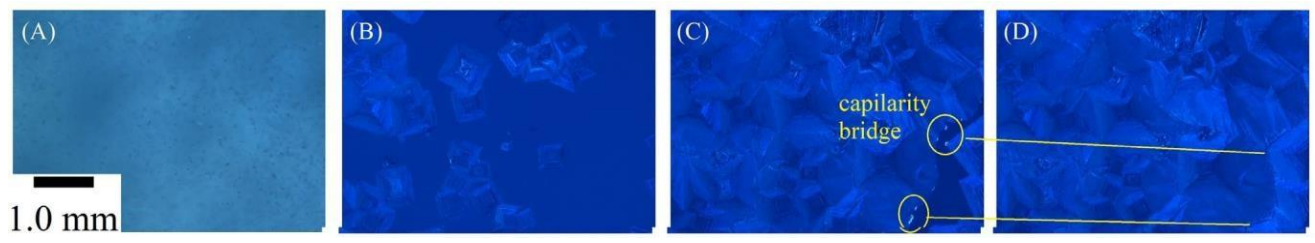


Figure 3. Mechanism of salt flower growth. Nucleation sites formed by bubbles emerge on the surface (A), producing the initial crystals (B), which coalesce through the salt bridge mechanism (C-D).

The areas covered by the salt flower, calculated from image processing, show that in the PAW, the area is nearly four times larger. This difference becomes smaller when we consider the weight. The weight of the salt flower in the PAW was 0.629 g, while the one produced in the NPAW was 0.330 g. This difference can be attributed to the smaller thickness of the salt flower film in the PAW, which is approximately one-fourth the thickness of the salt flower in the NPAW.

4. Conclusion

The main goal of the current study was to assess the effect of plasma on mechanism and kinetics of flower ofsalt crystallization. Hypersaline solutions from effluents from the salt industry, called bittern, were treated by plasma, using pulsed corona discharge. From this treatment, three types of samples were collected, namely: (i) salt crystals (SED) produced by supersaturation, sedimented at the bottom of the container; (ii) Flower of salt (FS) crystals, floating films formed in regions without plasma action; (iii) Dense Flower of salt (DFS), formed under the action of plasma. The findings from this study make several contributions to the current literature. First, it contributes to our understanding of the mechanism of formation of the flower of salt, even under the action of plasma. It also shows that it is possible to extract salts, by dissolved air flotation, from hypersaline waters, at a rate higher than that of natural evaporation. It also shows that plasma can be used to enhance the extraction and selectivity of salts. These results add to the rapidly expanding field of desalination and wastewater treatment technology.

5. References

process, Saline Systems. 7 (2011) 1-14.

J.B.F. de O. Barauna, C.S. Pereira, I.A. Gonçalves, J.O. Vitoriano, C. Alves-Junior, Sodium chloride crystallization by electric discharge in brine, Mater. Res. 20 (2017) 215–220.

L.F.A. Almada, K.E.S. Fontes, J.O. Vitoriano, V.R.M. Melo, F.E.N. Fraga, C. Alves-Junior, Applyingpulsed corona discharge in hypersaline droplets, J. Phys. D. Appl. Phys. 54 (2021) 055202

Giwa, A., Dufour, V., Al Marzooqi, F., Al Kaabi, M., & Hasan, S. W. (2017). Brine management methods: Recent innovations and current status. Desalination, 407, 1–23

Silsby, J. A., Dickenson, A., Walsh, J. L., & Hasan, M. I. (2022). Resolving the spatial scales of mass and heat transfer in direct plasma sources for activating liquids. Frontiers in Physics, 10

Silsby, J. A., Simon, S., Walsh, J. L., & Hasan, M. I. (2021). The Influence of Gas-Liquid Interfacial Transport Theory on Numerical Modelling of Plasma Activation of Water. Plasma Chemistry and Plasma Processing, 41(5), 1363–1380

Sainz-López N, Boski T, Sampath DMR. Fleur de Sel Composition and Production: Analysis and Numerical Simulation in an Artisanal Saltern. J Coast Res 2019;35:1200–14

Donadio C, Bialecki A, Valla A, Dufossé L. Carotenoid-derived aroma compounds detected and identified in brines and speciality sea salts (fleur de sel) produced in solar salterns from Saint-Armel (France). J Food Compos Anal 2011;24:801–10.

Shokri-Kuehni SMS, Norouzi Rad M, Webb C, Shokri N. Impact of type of salt and ambient conditions on saline water evaporation from porous media. Adv Water Resour 2017;105:154–61.

Wang B, Peng Y. The effect of saline water on mineral flotation - A critical review. Miner Eng2014;66:13–24. Wu Z, Wang X, Liu H, Zhang H, Miller JD. Some physicochemical aspects of water-soluble mineral flotation. Adv Colloid Interface Sci 2016;235:190–200

Vanraes P, Bogaerts A. Plasma physics of liquids — A focused review. Appl Phys Rev 2018;5:031103-1-56

^{*}Corresponding author: clodomiro.jr@hotmail.com

3D PRINTING FOR PRESSURE SENSOR PACKAGING

Henrique Chaves Gulino¹, Francisco Tadeu Degasperi², Marcelo Bariatto Andrade Fontes³

^{1,2} Laboratório de Tecnologia do Vácuo - LTV/DSE – Faculdade de Tecnologia de São Paulo - CEETEPS ³ Laboratório de Processos e Dispositivos - LPD/DSE – Faculdade de Tecnologia de São Paulo - CEEETPS

1. Introduction

The 3D printing, or additive manufacturing, is a technology that transforms digital designs into physical objects, through 3D modeling and slicing software. This manufacturing method is much more agile and flexible compared to traditional ones, as 3D printing does not rely on molds to generate new objects [1]. In this work, an packaging will be developed for a previously developed pressure microsensor [2].

2. Experimental

The proposed packaging in this study is based on the FDM (Fused Deposition Modeling) 3D printing technique. Initially, the packaging was designed to meet all mechanical requirements to accommodate the chip with the pressure microsensor in its internal cavity. Autodesk Inventor software was used at this stage. After the CAD design, the manufacturing process started, using a commercial 3D printer, PLA (polylactic acid) as the filament, with the extrusion temperature calibrated to 200°C, table temperature to 60°C, and filling at 100%. It isworth mentioning that the total manufacturing time was 10 minutes.

3. Results and Conclusions

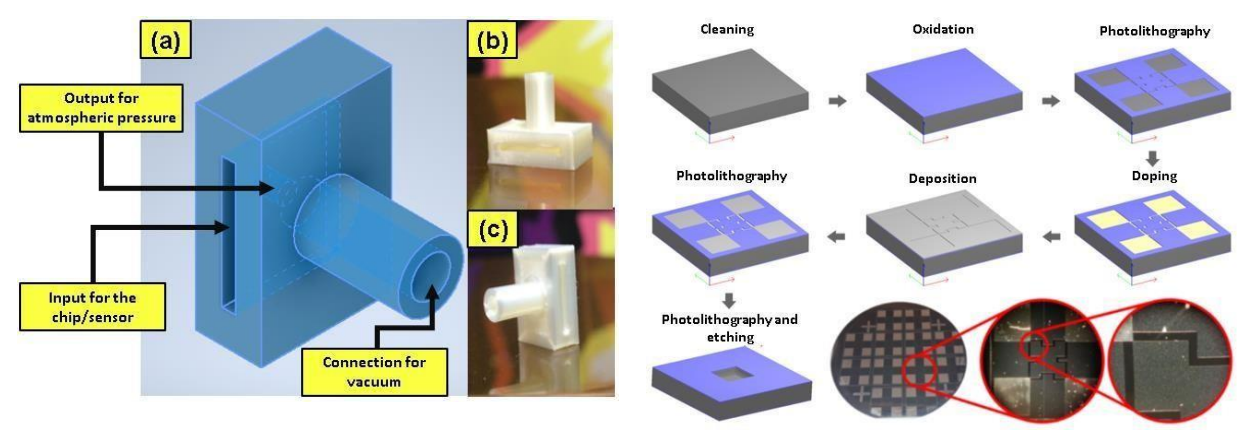


Fig. 1. (a) CAD design of the proposed packaging, (b) and (c) Final results of the obtained packaging.

Fig. 2. Design and manufacturing of a pressure microsensor.

Packaging pressure sensors through 3D printing involves creating protective casings that protect the sensor's core components. This approach offers customized, efficient, and cost-effective packaging solutions for pressure sensors across several areas, including automotive, aerospace, healthcare, industrial applications, and educational purposes.

4. References

- [1] https://encr.pw/bKBTx, accessed on 04/11/2023.
- [2] Sanches, K. F.; et al. **Desenvolvimento de um Microssensor de Pressão Microeletromecânico**. BoletimTécnico da Faculdade de Tecnologia de São Paulo, v. 47, p. 17-22, 2019.

Acknowledgments

The infrastructure of the LPD (Processes and Devices Laboratory) and LTV (Vacuum Technology Laboratory)laboratories of the Department of Electronic Systems (DSE) at FATEC-SP. To CNPq for the PIBIC scholarship.

^{*}Corresponding author: henriquegulino550@gmail.com

A COMBINED RAMAN, X-RAY AND FOURIER TRANSFORM INFRARED FOR INVESTIGATING THE COBALT OXIDE FILMS BY REACTIVE SPUTTERING

Nilton Francelosi A. Neto^{1*}, Antonio Ricardo Zanatta² and José H. Dias da Silva³

¹Instituto Tecnológico de Areronáutica ²Universidade Estadual Paulista ³Universidade de São Paulo

1. Introduction

Most of the information regarding the structure of Co₃O₄ and CoO has been based on X-ray diffraction (XRD) and Raman scattering spectroscopy (RS) that, not rarely, can show some discrepancies. Typically, RS can provide details regarding the composition, stress and disorder of different classes of materials. In certain cases, however, the experimental conditions during the RS measurements can influence either the response of some phonon modes (laser wavelength) or alter the samples structure or local temperature (laser power). In fact, the RS of Co₃O₄ following excitation with 532 and 785 nm photons has shown variations in certain peak positions, that has been correlated with the optical absorption in the Vis and NIR regions. When increasing laser powers are used instead, RS results show a CoO-to-Co₃O₄ phase transition, in a clear reference to the local heating of the samples. In this case, allied to the extra temperature, it is believed that the room (atmospheric) oxygen present on the surface of the samples increases the oxidation rate. Considering that cubic CoO presents a few Raman inactive modes, and the possible development of Co₃O₄ isolated islands due to local heating–oxidation processes, it is important to further explore the phenomenon [1].

2. Experimental

The cobalt oxide films were deposited fused silica (SiO₂) substrate by DC magnetron sputtering a solid Co target (99.995% pure) in a plasma reactive atmosphere made of Ar and O₂ gases. The films were deposited using 80 and 240 W discharge power. The XRD of the films was performed with $Cu_{K\alpha}$ radiation (λ = 1.54 Å) under grazing (1.5°) incidence, from 15° to 80° (0.02° step size), in a Rigaku Ultima 2000+ commercial system. RS measurements were achieved by exciting the films with 632.8 nm radiation (spot size ~ 0.8 μ m², average power ~ 0.25 mW) with a typical 2 cm⁻¹ spectral resolution (Renishaw RM2000). IR spectra of the films deposited were obtained in Fourier transform infrared (FTIR) by based spectrometer (Bruker Vertex 70) in the range 350 – 1000 cm⁻¹.

3. Results and Discussions

The XRD measurements showed that the film deposited with 80 W has the Co3O4 spinel cubic phase, while the increase in deposition power to 240 W is observed only diffraction peaks related to the CoO cubic phase. The RS spectra of the films show five phonon modes of Co_3O_4 (with typical spinel structure): F_{2g} (at ~ 194.4 , 521.6, and 618.4 cm⁻¹), E_g (at ~ 482.4 cm⁻¹), and A_{1g} (at ~ 691.0 cm⁻¹). Besides, considering that the CoO-related Raman signal is weak and, sometimes, coincident with that of Co_3O_4 , the spectra of the film 240W is made of a mixture of Co_3O_4 and CoO crystallites (of various sizes) embedded in an amorphous matrix. The spectra IR of 80 W showed three distinctive bands of Co_3O_4 phase. By comparing the spectra of the films in the region between 600 and 350 cm⁻¹, there is a wide absorption band at 594 cm⁻¹, in 240 W film. The CoO has a band of medium-to-weak intensity at 630-600 cm⁻¹ and medium bands at 570-440 cm⁻¹. Therefore, the CoO phase led to the formation of a broad band that overlaps with the assigned band of the Co_3O_4 phase. The FTIR analysis confirmed the RS results and clearly showed that at 240 W the film exhibited a presence of Co_3O_4 phase [1].

4. References

[1] N. F. Azevedo Neto, A. R. Zanatta and J.H Dias da Silva, Vib. Spectrosc., 126, 103524-103530, (2023).

Acknowledgments

We acknowledged the financial support of the São Paulo Research Foundation (FAPESP), grant #2023/02268-2, 2023/02273-6 and Conselho Nacional de Desenvolvimento Científico e Tecnológico (CNPq), grant #304569/2021-6.

^{*}Corresponding author: nilton.azevedo@unesp.br

A WORLDWIDE PERSPECTIVE ON HYDROGEN PRODUCTION RESEARCH

Gustavo Henrique Romeu da Silva^{1*}, Andreas Nascimento^{1,2}

¹Faculty of Engineering and Sciences of Guaratinguetá, São Paulo State University (UNESP) ²Institute of Engineering and Mechanics, Federal University of Itajubá (UNIFEI)

1. Introduction

The growing demand for sustainable energy sources and the need to decarbonize the global energy mix have driven interest in hydrogen production technologies. Therefore, in the search for more efficient and sustainable energy distribution and storage resources, hydrogen is a choice of paramount importance to be studied and evaluated [1]. Although electrolysis and thermochemical processes are presently the costliest approaches to hydrogen production, they arise as a viable alternative to fossil fuels and, in conjunction with other energy sources, exhibit significant potential for sustainable development [2]. Through a bibliometric approach to scientific publications and emerging trends, this study aims to map and analyze the research landscape in global hydrogen production, providing an in-depth view of the trends, challenges, and advancements in this critical field.

2. Theory

This study is based on a literature review of scientific articles related to the research topic, obtained from the Scopus database. The document set was restricted to cover the period from 2018 to 2022, including articles and reviews in the English language. Moreover, for the bibliometric analysis, the bibliometrix tool was applied, which is integrated within the R programming language and executed through the RStudio software.

3. Results and Discussions

Figure 1 provides a comprehensive overview of global research publications on hydrogen production, highlighting the contributions of various countries to this pivotal field of study. The global research landscape in hydrogen production is dynamic and diverse, encompassing a wide array of technologies, approaches, and applications. From water electrolysis to methane reforming, from solar energy to wind energy, numerous strategies are being explored to produce hydrogen more efficiently and sustainably. As environmental pressures mount and governments seek cleaner energy solutions, the role of hydrogen in the global energy matrix continues to evolve.

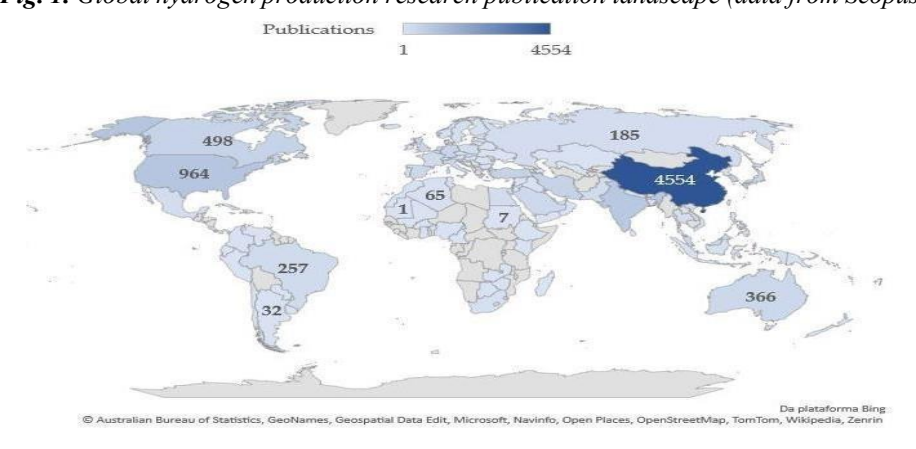


Fig. 1. Global hydrogen production research publication landscape (data from Scopus).

References

[1] SILVA, G. H. R.; NASCIMENTO, N.; NASCIMENTO, A. Hydrogen related perspectives in Brazil. In: World Conference on Mechanical Engineering, 1st., 2022, Berlim, Alemanha. **Anais** [...]. 2022. p. 16-25.

[2] SILVA, G. H. R.; NASCIMENTO, N. Comparative study of various methods of hydrogen production based on costs and environmental impact. **SODEBRAS**, v. 18, n. 211, p. 120-124, jul. 2023.

Acknowledgments: This work is financially supported by ANP, FINEP, and MCTI through the PRH 34.1 FEG/UNESP program.

^{*} Corresponding author: gustavo.romeu@unesp.br

AISI 316L STAINLESS STEEL COATED WITH TI-NB-ZR TERNARAY ALLOYS

Pedro A. P. Nascente^{1*}, Lucas L. D. Lemos¹, Sidney C. Z. Costa¹, Angelo L. Gobbi², Valmor R. Mastelaro³

¹Federal University of Sao Carlos, Department of Materials Engineering, 13565-905, Sao Carlos, SP, Brazil. ²Brazilian Center for Research in Energy and Materials, Brazilian Nanotechnology National Laboratory, 13083-970, Campinas, SP, Brazil.

³University of Sao Paulo, Sao Carlos Institute of Physics, 13560-590, Sao Carlos, SP, Brazil.

1. Introduction

AISI 316L stainless steel (SS) is one of the most used metallic biomaterials in implants, in spite of a significant disadvantage: the cytotoxicity caused by the release of Cr and Ni ions. Ti, Nb, and Zr are non-toxic and non-allergenic biocompatible metals, and the β phase Ti-Nb-Zr alloys present an elastic modulus as low as 50 GPa, making them very promising for biomedical application [1]. However, these alloys are much more costly than the 316L SS. To overcome this limitation, an economical option is to coat a SS implant with Ti-Nb-Zr thin film that has adequate composition and thickness [2]. Magnetron sputtering has shown to be an adequate technique to coat SS surfaces with Ti-base alloys. The main goal of this study is to produce and characterize Ti-Nb-Zr coatings sputter deposited on AISI 316L SS.

2. Experimental

Ti, Nb, and Zr disks with 2 in. diameter, 3 mm thickness, and 99.99% purity were used as targets. The substrates were made of 1 mm thick AISI 316L SS sheet, and 15 mm diameter disks were cut from this sheet to produce the substrates. An AJA Orion 8 Phase II J magnetron sputtering system was used to deposit six coatings with different compositions. The physicochemical characteristics of the Ti-Nb-Zr coatings were characterized by x-ray fluorescence spectroscopy (XRFS), x-ray diffraction (XRD), and x-ray photoelectron spectroscopy (XPS), using a Shimadzu 720 spectrometer, a Bruker diffractometer (model D8 Advance ECO), and a Scienta-Omicron spectrometer, respectively.

3. Results and Discussions

Elemental analysis was performed by XRFS, giving the following compositions (at.%): $Ti_{76}Nb_{10}Zr_{14}$, $Ti_{62}Nb_{26}Zr_{12}$, $Ti_{62}Nb_{26}Zr_{12}$, $Ti_{62}Nb_{20}Zr_{18}$, $Ti_{59}Nb_{19}Zr_{22}$, and $Ti_{53}Nb_{34}Zr_{13}$. In contrast, surface analysis by XPS of the same samples gave: $Ti_{60}Nb_8Zr_{32}$, $Ti_{50}Nb_{16}Zr_{34}$, $Ti_{45}Nb_{25}Zr_{30}$, $Ti_{43}Nb_{17}Zr_{40}$, $Ti_{38}Nb_{16}Zr_{46}$, and $Ti_{49}Nb_{20}Zr_{31}$, indicating a Zr surface enrichment and a Ti depletion. High resolution XPS Ti 2p spectra revealed the presence of mainly Ti^{4+} , with smaller contribution of Ti^{3+} , Ti^{2+} , and Ti^{0} . Nb 3d spectra showed a predominance of Nb^{5+} , but with important contributions of Nb^{4+} , Nb^{2+} , and Nb^{0} . Zr 3d spectra had only two doublets, the main one due to Zr^{4+} and a minor one to Zr^{0} . These results indicated that the coating surfaces were oxidized, and the predominant phases were TiO_2 , Nb_2O_5 , and ZrO_2 . These oxidized surface layers provide better corrosion protection and are beneficial for biomedical applications. XRD detected only the β (BCC) phase for the $Ti_{76}Nb_{10}Zr_{14}$, $Ti_{62}Nb_{26}Zr_{12}$, and $Ti_{53}Nb_{34}Zr_{13}$ coatings, and a minor contribution of the martensitic α phase in addition to the β phase for the other three coatings. These characteristics suggest that the Ti-Nb-Zr coatings are good candidates to be used in dental and orthopedic prosthetic devices.

4. References

- [1] E.D. Gonzalez et al., Mater. Today Comm., 32, 104069, (2022).
- [2] E.D. Gonzalez *et al.*, Thin Solid Films, **721**, 138565 (2021).

Acknowledgments

This work was supported by FAPESP (process 2017/25983-8), CNPq (process 302450/2017-3), CAPES (Finance Code 001), and CNPEM/LNLS.

^{*}Corresponding author: nascente@ufscar.br

ANÁLISE COMPUTACIONAL DO GRADIENTE DE DISTRIBUIÇÃO DE CALOR DO LAMINADO ESTRUTURAL PEI/FIBRA DE VIDRO POR MEIO DO ANSYS COMPOSITE PREPPOST (ACP)

Tuane Stefania Reis Santos*1; Rogério Pinto Mota¹, Erick Siqueira Guidi¹, Luís Felipe Barbosa Marques¹, Rafael Resende Lucas¹, Jonas Frank Reis¹

¹Faculty of Engineering and Sciences of Guaratinguetá, São Paulo State University (UNESP)

1. Introdução

Materiais compósitos possibilitam a combinação de baixa densidade com elevada resistência estrutural, o que os tornaram bastante utilizados em toda indústria global. Para facilitar o estudo desta classe de materiais, pode-se utilizar a análise computacional, que fornece dados por simulação do comportamento dos materiais em condições de trabalho diversas, como uma análise térmica para avaliação dos fenômenos térmicos derivados de um processo de soldagem [1]. O ANSYS Composite PrepPost (ACP) fornece todas as funcionalidades necessárias para a análise de estruturas compostas em camadas [2], utilizando-o, este trabalho visa avaliar o gradiente de distribuição de calor no compósito PEI/Fibra de Vidro oriundo do processo de soldagem oxiacetileno para união hibrida entre o compósito termoplástico de matriz polimérica e alumínio 2024-T3.

2. Modelagem Estrutural

Utilizando o módulo ACP do programa ANSYS, foi elaborado o modelo em formato de laminado sanduiche, considerando as configurações do material fornecido pela empresa TORAY, de 8HS, (0/90)5s contendo aproximadamente 50% em volume de matriz de poli(éter-imida) reforçado com fibras de vidro. A geometria adotada para simulação foi somente da área da junta soldada de 25 mm por 25mm, para diminuir o tempo de processamento, obtendo uma espessura de 2,89 mm ao final da configuração do modelo pelo ACP(Prep).

2.1 Análise Térmica Transitória

Para simulação, a temperatura aferida na área de contato (junta) do compósito com alumínio é de 378 °C, já a temperatura aferida na parte inferior da amostra é 136,33 °C, dados obtidos experimentalmente. O intervalo de exposição foi de 120 s, tempo que é empregado durante o processo de soldagem.

3. Resultados e discussões

Os resultados da simulação mostram que o máximo gradiente de distribuição de calor do compósito é de aproximadamente 0,01545, o que significa que a amostra se expandirá em cerca de 1,545% de sua dimensão original devido à variação de temperatura, com esses dados de simulação futuramente será a realizada de aferições experimentas do processo para validar o modelo e assim e constatar as melhores condições de soldagem considerando o comportamento térmico do compósito.

4. Referências

- [1] ABDULLA, Kareem Abdulghafour; SAFEENYASEENEZDEEN; AMS, Alfons. EXPERIMENTAL AND HARMONIC MODAL ANALYSIS OF COMPOSITE SPUR GEAR USING ANSYS ACP. International Journal Of Mechanical And Production Engineering Research And Development (Ijmperd). Índia, p. 15401-15416. 08 jun. 2020.
- [2] HASSAN, Najibah Binti. Thermal Analysis of Carbon Fiber Composite Structure by Finite Element Analysis. 2013. 45 f. Dissertação (Mestrado) Curso de Mechanical Engineering, Universiti Teknologi Petronas, Tronoh, 2013. Disponível em: https://utpedia.utp.edu.my/id/eprint/13688/1/DISSERTATION%2013275.pdf. Acesso em: 02 out. 2023.
- [3] KUMBHARE, Niraj; MOHEIMANI, Reza; DALIR, Hamid. Analysis of Composite Structures in Curing Process for Shape Deformations and Shear Stress: basis for advanced optimization. Journal Of Composites Science, [S.L.], v. 5, n. 2, p. 63, 23 fev. 2021. MDPI AG. http://dx.doi.org/10.3390/jcs5020063.
- [4] XIONG, Xuefeng; LI, Li; LI, Hong; ZAN, Peng. Thermal Stress Analysis for Carbon/Carbon Material Throat Lining Based on Finite Element Analysis. Journal Of Physics: Conference Series, [S.L.], v. 2338, n. 1, p. 012046, 1 set. 2022. IOP Publishing. http://dx.doi.org/10.1088/1742-6596/2338/1/012046.

^{*} Corresponding author: tuane.stefania@unesp.br

ANALYSIS OF LIGNOCELLULOSIC BIOMASS GASIFICATION IN SUPERCRITICAL WATER: EXPLORING KEY PARAMETERS AND PROCESS OPTIMIZATION STRATEGIES

Thiago Averaldo Bimestre^{1*}, Eliana Vieira Canettieri², Ana Maria Ramos da Silva³, Lília dos Anjos de Freitas⁴

^{1,2,3,4} Chemistry and Energy Department, School of Engineering and Science, UNESP, Guaratinguetá, SP, Brazil.

1. Introduction

In recent years, the growing demand for sustainable and clean energy sources has provided significant advances in renewable energy technologies. Hydrogen, as a versatile and environmentally friendly fuel, has received substantial attention as a potential solution to reduce greenhouse gas emissions and mitigate the effects of climate change [1]. Among the various hydrogen production methods, biomass gasification in supercritical water (SCWG) stands out as a promising and innovative approach as it is a combined thermal decomposition and hydrolysis process that converts biomass feedstock into hydrogen-rich synthesis gas. This work aims to investigate and understand how the main influencing factors in the biomass gasification process with supercritical water, such as temperature, pressure and residence time influence the gasification efficiency and hydrogen production. This work is expected to provide important information for the development of more efficient and sustainable strategies in biomass conversion.

2. Theory

The supercritical water gasification system operates at temperatures and pressures above the critical point of water (374°C and 22.1 MPa), where water exhibits unique properties. Due to its low dielectric constant, low number of hydrogen bonds and low strength, supercritical water has neither surface tension nor phase boundaries, making it a solvent with high solubility, mobility, diffusivity, and mass transfer capacity [2]. This process allows higher biomass conversion rates, better hydrogen yields and reduced tar formation compared to conventional gasification techniques [3].

3. Results and Discussions

This study of gasification of lignocellulosic biomass with supercritical water found that temperature is one of the most important process parameters. High temperatures favor hydrogen production while milder temperatures favor methane yields. The research range is generally 400°C-600°C. An increase in temperature decreases the dielectric constant of water, increases the dissolution of organic matter, decreases the density and ionic product of supercritical water, promotes free radical reactions, and facilitates the formation of gaseous products during gasification. However, high temperatures inevitably increase operating costs and energy consumption. The use of catalysts can reduce the operating temperature, increase hydrogen production, and reduce coke tar production. It has also been found that biomasses with a high cellulose content are easier to gasify and break down during the reaction, while lignin and phenol are more difficult. Pressure has little influence on the overall reaction, but it is necessary to keep the pressure at supercritical levels (>22 MPa-30MPa). The reaction time plays a crucial role: too short a period does not favor the development of the reaction and the production of gas, while an excessively long period does not contribute significantly to the intensification of gasification in supercritical water. In practice, the selection of the appropriate reaction time must be determined according to the different operating conditions.

4. References

[1] Barros, T. V., Lopez, G. de S., Santos, R. J., Parizi, M. P. S., Cardozo-Filho, L., Ferreira L. (2022). Gasification biomass in supercritical water as hydrogen production technology. *Research, Society and Development, 11*(9). [2] Qing W., Xu Z., Da C., Jingru B., Zhichao W., Faxing X., Zhenye W. (2023). Advances in supercritical water gasification of lignocellulosic biomass for hydrogen production. *Journal of Analytical and Applied Pyrolysis*, 170. [3] Haoyang L., Yulin H., Haoyu W., Xue H., (2022). Supercritical water gasification of lignocellulosic biomass: Development of a general kinetic model for prediction of gas yield, *Chemical Engineering Journal*, 433(2).

Acknowledgments: This work greatly acknowledges CAPES Brazil and FEG/UNESP.

^{*}Corresponding author: thiago.bimestre@unesp.br

ANALYTICAL, NUMERICAL AND EXPERIMENTAL ANALYSIS OF A TUBULAR HIGH VACUUM **SYSTEM**

Francisco Tadeu Degasperi, Regina Maria Ricotta* and Vinicius Carvalho de Morais

Faculdade de Tecnologia de São Paulo – FATEC SP – CEETEPS

1. Introduction

In high vacuum systems whose vacuum chambers are formed by predominantly tubular geometry, the determination of the pressure field along the entire structure of the vacuum chamber is essential for the proper realization of the project. Particle accelerators, elementary particle storage rings and electronic microscopes are examples where this type of arrangement occurs. This work presents the construction of a tubular system for which direct experimental measurement of the pressure field can be made along the structure. The main objective of the work is to verify the results obtained by modeling this tubular system, [1] and the results obtained through the Monte Carlo Method, using the Molflow simulation program, [2].

2. Modeling, Simulation and Experimental Analysis

Figure 1 and Figure 2 show the scheme of the high vacuum system that consists of four cylindrical tubes of length l and diameter D in series, connected to pumps of vacuum on the left side and gauges along the tubes. The modeling performed assumes that the transport of gases occurs in the molecular gas transport regime (free particles) and that it can be considered a diffusive phenomenon, [1], with 1 > 5D. The general differential equation of the diffusive process for obtaining the pressure field in the steady state is given by $c(x) \frac{d^2 p(x)}{dx^2} + \frac{dc(x)}{dx} \frac{dp(x)}{dx} = -q(x)$

$$c(x)\frac{d^2p(x)}{dx^2} + \frac{dc(x)}{dx}\frac{dp(x)}{dx} = -q(x) \tag{1}$$

where c(x) is the specific conductance and q(x) is the function that represents the gas sources present in the system. The general solution of equation (1) is

 $p(x) = -\frac{q}{2c} \cdot x^2 + A \cdot x + B$

valid to the whole tube unit. The constants A and B are solved by applying the appropriate boundary conditions at the ends of the tube. The pressure field along the tube increases parabolically and is maximum at the right end. The simulation was performed using the Monte Carlo Method with the Molflow program, [2].

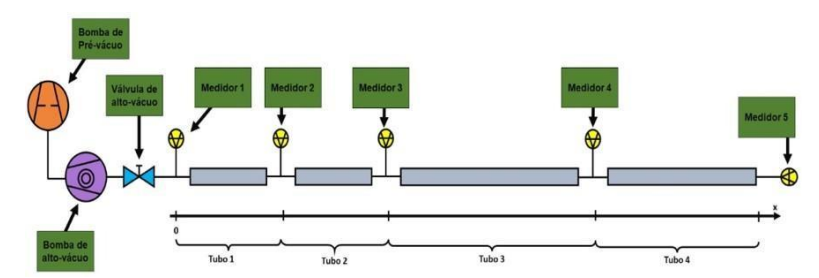


Fig. 1. Scheme of the high vacuum system.

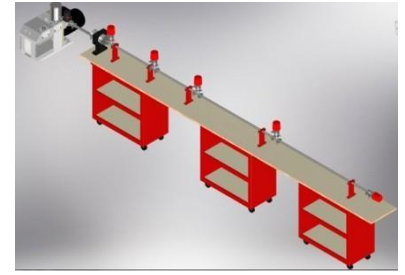


Fig. 2. Experimental design.

4. Results and Discussions

The analytic result for the pressure field of the composition has been evaluated and the boundary conditions have been applied. The simulation results agree with the analytical result, showing that the behavior is typical of pumped vacuum systems and must be considered in all high vacuum tube system designs to achieve the expected performance results. Work with the measurements is in progress.

5. References

- [1] F. T. Degasperi, R. M. Ricotta, Vacuum, 188C, p. 1-30, (2021).
- [2] R. Kersevan, J.-L. Pons, J. Vac. Sci. Technol. A 27, 1017 (2009).
- [3] F. T. Degasperi, R. M. Ricotta, Braz. J. Phys. 53 (2023) 44.

^{*}Corresponding author: regina@fatecsp.br

ANTIMICROBIAL ACTIVITY EVALUATION OF BINARY AND TERNARY TITANIUM ALLOY

Patricia Capellato ^{2*}, Filipe Bueno Vilela¹, Ana Paula Rosifini Alves Claro², Daniela Sachs¹

¹Centre for Studies and Innovation in Biofunctional Advanced Materials, Institute of Physics and Chemistry, Unifei-Federal University of Itajubá, Av. BPS, 1303, Cep-37500 903, Itajubá, MG, Brazil. ²Department of Materials, Faculty of Engineering, UNESP—University Estadual Paulista, Av. Ariberto Pereira da Cunha, 333, Pedregulho, Guaratinguetá 12516-410, SP Brazil

1. Introduction

Estimate that the global dental implants market reach \$6.95 billion by 2030 [1]. However, the field present problems that decrease the useful life of dental implant [2]. Among the problems, failure and infections of dental implant has been the leading causes of dental implant loss [3]. So, in this study we investigated the antimicrobial activity of two types of titanium alloy. The binary Ti30Ta alloy and the ternary Ti10Mo8Nb alloy surfaces were evaluated with gram positive bacteria S Aureus.

2. Experimental

The binary Ti30Ta alloy and the ternary Ti10Mo8Nb alloy were obtained as describe into previous work by Capellato et al 2021 and 2022 [4] [5]. The antimicrobial activity was evaluated by Staphylococcus aureus strain (ATCC 6538). Initially, a sterile solution of BHI for brain and heart was prepared using 52 g of BHI diluted in 1000 ml of distilled water. Sterilize the BHI solution in an autoclave at 127 °C for 1 hour. After this process, inoculate the strains into tubes containing 3 ml BHI and place them in an oven at 37 °C for 2 h. After the incubation period, 10 µL of the solution prepared with the strain was used to streak the petri dishes previously prepared with agar. The plates were taken to a oven at 37 °C for a period of 24 h for biofilm growth. Finally, an aliquot of the cultured bacterial colony was added to a test tube with 3 mL of 0.9% NaCl solution until the concentration of the liquid medium was on the McFarland scale 0.5 (1.5 x 108 cells/mL). The total of 10 samples were used for the test, which were divided into two groups, namely: group 1 - Ti30Ta alloy and group 2- Ti10Mo8Nb. Both groups were sterilized for 30 minutes. Then place group 1 and 2 in the well plate and cover with 3 mL of BHI and add 100 µL of 0.5 McFarland suspension per well and in the oven at 37°C for 8 hours. After incubation, group 1 and 2 was placed in a test tube containing 3 mL of saline solution, vortexed for 3 minutes and ultrasonically cleaned for 10 minutes in order to disperse the formed biofilm and obtained a liquid pure bacterium. Make five dilutions of this solution in 0.9% saline. A drop of each dilution was then inoculated into a Petri dish prepared with agar, and finally the plate was placed in an oven at 37°C for 2 hours. At the end of the process, colony growth on the surface of the plate was evaluated. The results obtained were log10 transformed and analyzed using Student's T test. Calculations were performed using GraphPad Prism software. P < 0.05 was considered to indicate a statistically significant difference between group 1 and 2.

3. Results and Discussions

In order to investigated the antimicrobial activity was evaluated the bacterial proliferation of grampositive bacteria S Aureus on binary Ti30Ta alloy and the ternary Ti10Mo8Nb alloy surfaces. This assessment is relevant as an indication of the possible infectious process after dental implant surgery that can leading a implant loss. The Figure 1 shows the concentration of colony-forming units on surfaces of the group 1 and 2 was similar. The results do not present significant statistical differences for bacterial adhesion of S aureus on both groups.

4. References

- [1] Table of Content Dental Implants Market | Fortune Business Insights. (n.d.). Retrieved August 21, 2023, from https://www.fortunebusinessinsights.com/industry-reports/toc/dental-implants-market-100443
- [2] Yang, X., Li, X., Li, X., Chen, W., Shen, L., Li, X., & Deng, Y. (2023). Two-Stream Regression Network for Dental Implant Position Prediction.
- [3] Samuel S. Malheiros, Bruna E. Nagay, Martinna M. Bertolini, Erica D. de Avila, Jamil A. Shibli, João Gabriel S. Souza & Valentim A. R. Barão (2023) Biomaterial engineering surface to control polymicrobial dental implant-related infections: focusing on disease modulating factors and coatings development, Expert Review of Medical Devices, 20:7, 557-573,
- [4] Patricia Capellato, Lucas V B Vasconcelos et al. Titanium-Tantalum Alloy Surface Modification by Hydroxyapatite Layer on TiO 2 Nanotubes: Effect on Microbial Activity.Materials Research, 24, 6, 2021 [5] Capellato, P.; Vilela, F.B.; Fontenele, A.H.P.; Silva, G.; da Silva, K.B.; Carobolante, J.P.A.; Bejarano, E.G.M.; de Lourdes Noronha Motta Melo, M.; Claro, A.P.R.A.; Sachs, D.Evaluation of Microstructure and Mechanical Properties of a Ti10Mo8Nb Alloy for Biomedical Applications. Metals 2022, 12, 1065.

Acknowledgments

The authors would like to thank partial funding support for this work provided by the Brazilian federal government and the National Council for Scientific, Technological Development (CNPq) via Award Number 201271/2010-9 and Fapesp 2014/14533-3.

^{*} corresponding author pat_capellato@yahoo.com.br

ANTIMICROBIAL EFFICACY OF DENTAL POLY (METHYL METHACRYLATE) COATED WITH AL_2O_3 BY ATOMIC LAYER DEPOSITION

Lady D. P. Leite, 1*, William Chiappim³, Rodrigo S. Pessoa² and Cristiane Y. Koga Ito¹

¹Department of Environmental Engineering/ Science Applied to Oral Health Graduate Program, Institute of Science and Technology, São Paulo State University (UNESP), São José dos Campos, Brazil.

² Plasmas and Processes Laboratory, Technological Institute of Aeronautics (ITA), São José dos Campos, Brazil.

³Department of Physics, Faculdade de Engenharia de Guaratinguetá, São Paulo State University (UNESP), Guaratinguetá, Brazil.

1. Introduction

Poly (methyl methacrylate) (PMMA) is a material that is widely used in dentistry. However, like all materials, PMMA has some limitations, especially regarding its biological properties. One such limitation is its susceptibility to microbial adhesion, which can result in infections [1]. In this study, the surfaces of PMMA substrates were functionalized using ALD Al_2O_3 thin films to inhibit or mitigate the adhesion of microorganisms.

2. Experimental

In this study, colorless thermosetting acrylic resin was used, prepared according to the manufacturer's recommendations. The specimens were made in the shape of a disk, measuring 2 mm in height x 9 mm in diameter. After the polymerization process, all the samples were sanded and polished. The Al₂O ₃ films were deposited on the samples using a cross-flow ALD reactor operating in thermal mode at 100 °C. The deposition process was carried out by varying the number of reaction cycles, where the specimens were classified as untreated (control) and coated with Al₂O₃(Al₂O₃:250 cycles, Al₂O₃:500 cycles, Al₂O₃:1000 cycles, Al₂O₃:1500 cycles, Al₂O₃:2000 cycles and Al₂O₃:3000 cycles). The reference strain of *C. albicans* ATCC 18804 was used to evaluate the antibiofilm properties [1]. The experiments were performed in triplicate (n=9). Data was compared by One-way ANOVA and post hoc Tukey (5%). Microstructural characterization was performed using scanning electron microscopy (SEM).

3. Results and Discussions

C. albicans adhesion to surfaces is pivotal for its pathogenicity due to its role in initiating colonization and subsequent biofilm formation. The control group, devoid of Al₂O₃ coating, exhibited a mean CFU/mL of 8.00 x 10⁵, providing a benchmark for assessing the efficacy of the Al₂O₃-coated samples. Compared to this control, samples coated with Al₂O₃ at 250 and 500 cycles demonstrated a 50% reduction in mean CFU/mL. This significant decrease suggests that, during these specific ALD cycles, alterations in the surface characteristics be it topographical, chemical, or a combination there of might deter C. albicans attachment. Hence, ALD at these cycles appears to engender surface properties that impede the yeast's primary adhesion.

Group	Mean CFU/m L	SD	
Control	8.00 x 10 ⁵	3.71 x 10°	
Al ₂ O ₃ (250 cycles ALD)	4.00 x 10 ⁵	3.87 x 10°	
Al ₂ O ₃ (500 cycles ALD)	4.00 x 10 ⁵	2.80 x 10°	
Al ₂ O ₃ (1000 cycles ALD)	5.00 x 10 ⁵	2.87 x 10 ⁵	
Al ₂ O ₃ (1500 cycles AL D)	5.00 x 10 ⁵	3.80 x 10°	
Al ₂ O ₃ (2000 cycles AL D)	6.00 x 10 ⁵	3.28 x 10 ⁵	
Al ₂ O ₃ (3000 cycles AL D)	8.00 x 10 ⁵	4.12 x 10 ⁵	

Table 1. Mean CFU/mL of the tested groups

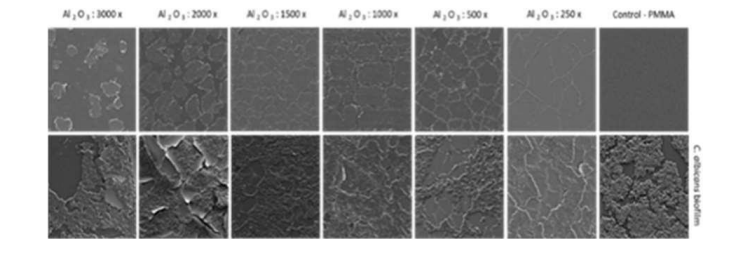


Fig. 1. SEM micrographs of the PMMA samples, controland coated with Al_2O_3 , before and after colonization with C. albicans after 24 hours (scale = $50 \mu m$).

4. References

[1] B. R. C. Menezes; et al. Applied Surface Science, v. 543, p. 148830, (2021).

Acknowledgments: Coordenação de Aperfeiçoamento de Pessoal de Nível Superior – Brasil (CAPES) – Finance Code 001.Fundação de Amparo à Pesquisa do Estado de São Paulo (FAPESP), 2019/05856-7.

^{*}Corresponding author: lady.leite@unesp.br

ANTIMICROBIAL EFFICACY ON ENTEROCOCCUS FAECALIS OF PLASMA-ACTIVATED WATER PRODUCED BY DIELECTRIC BARRIER DISCHARGE

Victória K.F.Tavares^{1*}, Felipe S. Miranda², Rodrigo S. Pessoa, ² and Cristiane Y. Koga Ito¹

¹Department of Environmental Engineering/ Science Applied to Oral Health Graduate Program, Institute of Science and Technology, São Paulo State University (UNESP), São José dos Campos, Brazil.

² Plasmas and Processes Laboratory, Technological Institute of Aeronautics (ITA), São José dos Campos, Brazil.

1. Introduction

The persistence of microorganisms in the root canals is a challenge for the endodontic treatment. *Enterococcus faecalis* is a bacterial species often related to persistent endodontic infections [1]. The study evaluated the antimicrobial effect of plasma-activated water (PAW) produced by dielectric barrier discharge (DBD) on *E. faecalis*.

2. Experimental

Sterile deionized water (DI) was activated for 10 minutes using a coaxial DBD type reactor. Compressed air was used as the working gas (5 L/min). For microbiological assay, suspension of *E. faecalis* (ATCC 29212) containing 10⁶ cells/mL was exposed to PAW or DI (negative control) for 45 seconds, 1 minute and 1 minute 30 seconds. After the contact time, the suspensions were diluted, plated in culture medium and incubated at 37 °C for 24 hours. Colony counts (CFU/mL) and percentage reduction were determined. The experiments were performed in triplicate (n=9) and the data was compared by One-way ANOVA and post hoc Tukey (5%).

3. Results and Discussions

Before plasma activation, DI water had a pH of 8.81, and after activation, it dropped to 2.29. This pH decrease can influence positively the antimicrobial effectiveness of PAW due to physicochemical reactions and the production of reactive species [2]. Significant reductions in *E. faecalis* counts were observed after 45 s, 1 min, and 1 min 30 s of PAW exposure, with percentage reductions of 59.09%, 67.77%, and 71.98%, respectively. The exposure time did not influence the results. It suggests great potential for the application of PAW as an antimicrobial irrigating solution and its use in endodontics, moreover, another study that required 2 min of exposure and direct application of plasma discharge for reductions of up to 3-log [3].

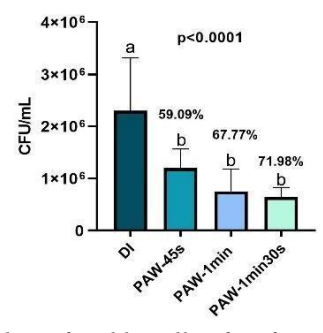


Fig. 1. Number of viable cells of <u>E. faecalis</u> (CFU/mL) following exposure to PAW for 45 s, 1 min and 1 min 30 s compared to negative control (DI).

4. References

[1] A. B. Muniz et al. Biomedicines, vol. 11, no. 5, pp. 1–13, 2023.

[2] Y. M. Zhao et al., Comprehensive Reviews in Food Science and Food Safety, vol. 19, no. 6, pp. 3951–3979,2020.

[3] Y. Wen et al. Journal of Physics D: Applied Physics., vol. 55, no. 36, 2022.

Acknowledgments

Fundação de Amparo à Pesquisa do Estado de São Paulo (FAPESP), 2019/05856-7 and 2021/14181-3 Coordenação de Aperfeiçoamento de Pessoal de Nível Superior – Brasil (CAPES) – Finance Code 001.

 $[\]hbox{*Corresponding author: Victoria.kelly@unesp.br}\\$

APATITE FORMATION ON ALKALI-TREATED Ti-7.5MO ALLOY AFTER TIO2 NANOTUBES GROWTH

Ana Lúcia do Amaral Escada¹, Ana Paula Rosifini Alves Claro²

¹Universidade Estadual de São Paulo (Unesp), Faculdade de Engenharia, Departamento de Física e Química-IlhaSolteira

² Universidade Estadual de São Paulo (Unesp), Faculdade de Engenharia e Ciências, Departamento deMateriais e Tecnologia, Guaratinguetá, SP, Brasil.

1. Introduction

Titanium and its alloys are widely used to manufacture dental implants and orthopedic prostheses due to their excellent mechanical properties, low specific weight, high resistance to corrosion, and high biocompatibility. Recent studies have shown that human cells interact with nanostructured surfaces such as nanorough surfaces, and nanoparticles or nanostructured metal oxides based on the self-organization electrochemical process [1]. Anodization is an electrolytic passivation technique used to increase the thickness of the natural oxide layer on metal surfaces [2]. The purpose of this work was surface modification of Ti-7.5Mo alloy from the growth of TiO₂ nanotubes, alkaline treatment and SBF immersion.

2. Experimental or Theory

The Ti-7.5Mo alloy was produced from sheets of commercially pure titanium (99.9%) and molybdenum (99.9%). Samples were melted in an arc furnace and ingots were homogenized under vacuum. They were cold worked by swaging and bars with 13 mm of diameter were produced and discs with 4 mm of thickness were cut. The electrolyte used for anodization was glycerol containing 0.25% NH₄F and the discs were anodized at 30V for 24h and calcined at 450 °C. The samples were treated with 5M NaOH at 80 °C for 1hour and immersed in SBF for 24 hours. The surfaces of samples were characterized by scanning electron microscopy and DRX.

3. Results and Discussions

Figure 1 shows the samples images anodized at 30V for 24h and calcined at 450 $^{\circ}$ C containing TiO₂ nanotubes with 120 nm diameter (Fig.1a) and immersed in SBF for 24 hours forming a continuous apatite film (Fig.1b). The TiO2 nanotubes growth and the apatite film were confirmed by XRD in wich we observed the anatase and apatite peaks (Fig 2).

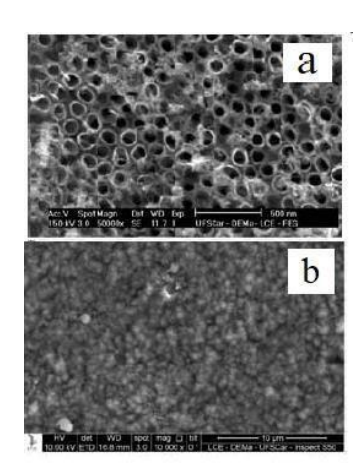


Fig.1.TiO₂ nanotubes (a), Apatite (b)

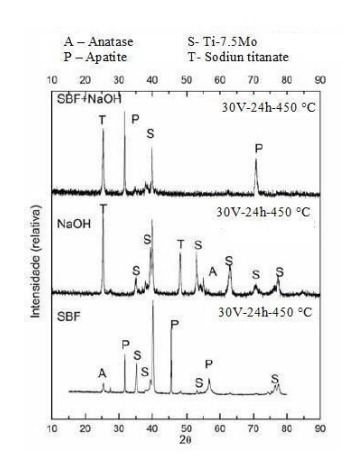


Fig.2. DRX

4. References

[1] Mohan L, Anandan C, Rajendran N. Electrochemical behavior and effect of heat treatment on morphology, crystalline structure of self-organized TiO2 nanotube arrays on Ti–6Al–7Nb for biomedical applications. *Materials Science and Engineering: C*, **50**:394-401(2015).[2] Regonini D, Bowen CR, Jaroenworaluck A, Stevens R. A review of growth mechanism, structure and crystallinity of anodized TiO₂ nanotubes. *Materials Science and Engineering: R: Reports*, 74(12):377-406 (2013).

APLICAÇÃO DE HMDSO VIA PIIID PARA MELHORIA EM JUNTAS SOLDADAS POR RESISTÊNCIA ELÉTRICA

Luís Felipe Barbosa Marques*, Jonas Frank Reis¹, Rafael Rezende Lucas¹, Felipe Vicente de Paula Kodaira¹, Rogério Pinto Mota¹, Edson Cocchieri Botelho¹

¹ Universidade Estadual Paulista "Júlio de Mesquita Filho" - Campus de Guaratinguetá

1. Introdução

O método de união por resistência elétrica oferece uniões de alta qualidade e rápidas quando comparado a outros métodos de uniões [1,2]. A aplicação de filmes e tratamentos superfície vem sendo investigada para a melhoria da interação de juntas. Com isso, o presente estudo investigou a aplicação de filmes finos de HMDSO aplicado por plasma em baixa pressão no elemento resistivo.

2. Experimental

O compósito utilizado no presente estudo foi o termoplástico PEI/fibra de vidro em tipo 8HS, configuração (0/90)5s. Os parâmetros ideais para a soldagem por resistência elétrica em compósitos PEI/fibra de vidro foram previamente investigados em um estudo anterior [3]. As melhores condições para a deposição do HMDSO foram determinadas através de um planejamento estatístico. O elemento resistivo utilizado para a soldagem foi uma malha metálica de aço inoxidável AISI 304, com diâmetro do fio de 0,04 mm e abertura de 0,08 mm.

3. Resultados e discussões

A melhor condição foi tomada com base na resposta ao ensaio de *Lap Shear Strength* (LSS), sendo os melhores parâmetros determinados: tempo de deposição (40 min), composição do gás (40% argônio e 60% HMDSO) e potência (30 W). A figura 1 ilustra os resultados obtidos.

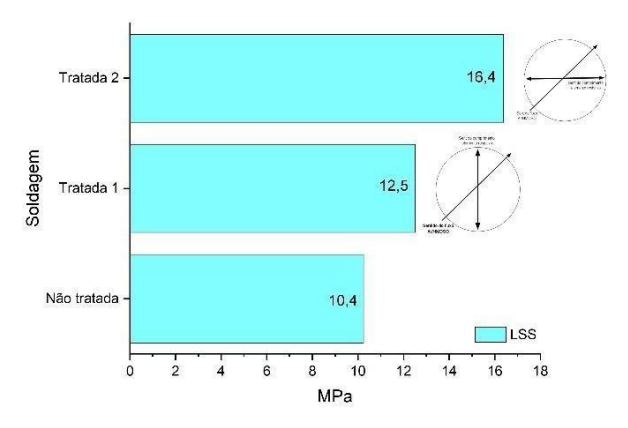


Fig. 1. Relação do resultado de LSS.

A melhora observada de 58% está relacionada a formação de ligações covalentes que melhoram a adesão e interação entre a superfície metal/polímero com maior homogeneidade no sentido do fluxo do gás.

4. Referências

- [1] Xiong et al. 2021 Resistance welding technology of fiber reinforced polymer composites a review pt-BR n.d.
- [2] Totla HS, Gupta A, Mishra S, Sharma S, Selvaraj SK. Resistance welding analysis of thermoplastic composite structures in aeronautical applications. International Journal on Interactive Design and Manufacturing 2023. https://doi.org/10.1007/s12008-022-01151-1.
- [3] Barbosa Marques LF, Frank Reis J, Ramos Moreira Abrahão AB, Oliveira Hein LRD, Cocchieri Botelho E, Costa ML. Interfacial, mechanical, and thermal behavior of PEI/glass fiber welded joints influenced by hygrothermal conditioning. J Compos Mater 2022;56:239–49. https://doi.org/10.1177/00219983211055826.

Agradecimentos

Os autores agradecem a CAPES, em especial ao processo 88887.663597/2022-00.

APPLICATION OF ATMOSPHERIC PRESSURE PLASMAS ON WATER DECONTAMINATION AND DEPOLLUTION

Elidiane C Rangel, Nilson C Cruz Laboratory of Technological Plasmas – Unesp, Sorocaba, SP, Brazil

1. Introduction

The interaction of plasmas with the surrounding atmosphere may result on the formation of a myriad of reactive species mostly containing oxygen and nitrogen. Since such species can react with a material nearby the discharge, atmospheric pressure plasmas (APP) can be a very interesting tool for the incorporation of reactive species into liquids. In this work, APP have been applied to decontaminate and depollute water. It has been evaluated the effect of the exposure on the inhibition of bacteria and on the degradation of indigo carmine dye.

2. Experimental

The experiments have been performed using a homemade dielectric barrier discharge device. Essentially, it is composed by an adjustable frequency oscillator and a high voltage transformer able to deliver up to 15 kV totwo grid electrodes separated by a glass tube fed with compressed air.

3. Results and Discussions

In figure 1 are shown pictures of agar plates incubated with water samples as a function of exposure time to plasma generated species. As it can be observed, exposures longer than 5 minutes inactivated all the microorganisms present in water. In addition, as observed in Figure 2, the dye was degraded after the water being exposed to plasma for only a few seconds.

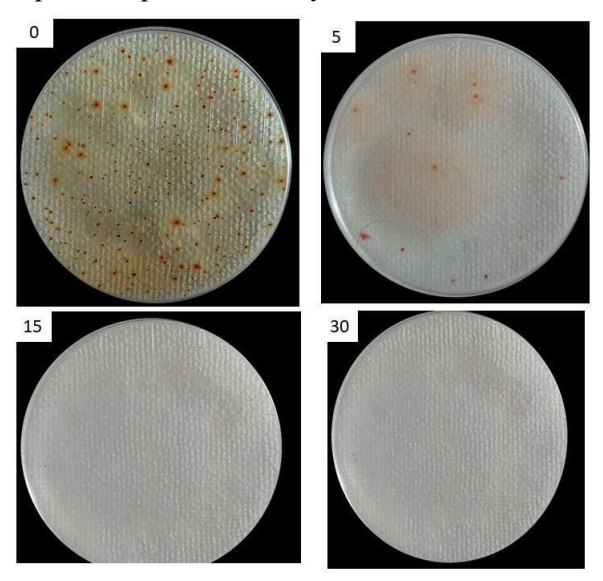


Fig. 1. Pictures of agar petri dishes after inoculation with contaminate water exposed to plasma with different exposure times

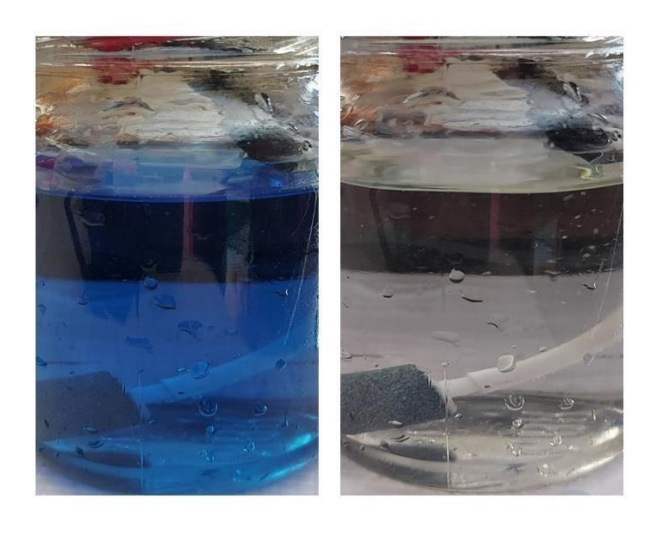


Fig. 2. Pictures of beaker with indigo carmine water solution before (left) and after exposure for 25 s to plasma generated species

Acknowledgments

The authors thank Fapesp for financial support through process. 2020/06448-7

^{*}Corresponding author: nilson.cruz@unesp.br

ARC-MELTING PROCESS APPLIED TO PRODUCE NOVEL TITANIUM-BASED MATRIX COMPOSITES FOR BIOMEDICAL APPLICATIONS

Vinícius R. M. Gonçalves^{1*}, Diego R. N. Corrêa¹, Tiago S. P. Sousa¹, Carlos A. F. Pintão¹, Conrado R. M. Afonso², Paulo N. Lisboa-Filho¹, and Carlos R. Grandini¹

¹São Paulo State University (UNESP), School of Science, Bauru, SP, 17033-360, Brazil. ²Federal University of São Carlos (UFSCar), Dep. of Materials Engineering, São Carlos, SP, 3565-905, Brazil.

1. Introduction

Titanium (Ti) alloys are considered attractive metallic materials for long-term bone implant applications [ref number 1]. However, metallic implants generally present poor wear resistance, and the degradation process can be intensified with the friction occurring in corrosive body fluids, such as joint prostheses [ref number 2]. Tibased matrix composites (TMCs) represent promising alternatives for wear-resistant applications because the addition of hard ceramic particles enables to achieve the desired combination of properties. Indeed, the degree of adhesion at the matrix/reinforcement interface is the main factor for achieving the properties, and it can be designed during the composite fabrication when chemical reactions are directly involved in the manufacturing steps, defined as in-situ reactions [ref number 3]. Therefore, the present study aimed to produce novel in-situ TMCs with arc-melting process in order to deliver promising wear-resistant materials for biomedical applications.

2. Experimental

Initially, two metallic ingots including commercially pure (cp) Ti and Ti-40wt.%Nb alloy were produced by arc-melting. As the second melting step, the TMCs were prepared by adding 5 vol.% of B₄C ceramic powder. The as-cast unreinforced cp Ti and Ti-40Nb alloy, along with the TMCs Ti+5B₄C and Ti-40Nb+5B₄C were investigated with optical and electronic microscopy, X-ray diffraction, and Vickers hardness measurements. Furthermore, preliminary tribocorrosion tests were performed in a phosphate-buffered solution, while an alumina ball was the counter body used to promote friction. In addition, a sensor, PASCO, was connected to the tribometer to calculate the coefficient of friction (COF) values, and all tribocorrosion tests were performed under open circuit potential (OCP), such as the Ag/AgCl saturated electrode as the reference.

3. Results and Discussions

The XRD diffractogram indicated that in-situ composites were obtained after arc-melting. For both Ti and Ti-40Nb alloy, the addition of B₄C promoted chemical reactions during the process, such as B diffused to precipitate TiB whiskers and C diffused to precipitate TiC particles, both embedded into the metallic matrix. Microstructures analyzed by SEM confirmed the XRD statements. The composites presented slightly higher hardness values in comparison to unreinforced materials. In other words, the reinforcing phase increased the hardness, indicating an effect of load-carrying hard ceramic phase. Consequently, the TMCs demonstrated higher tribocorrosion resistance than the unreinforced metallic materials. Therefore, the present study proposed promising TMCs as candidates for wear-resistant biomedical applications.

4. References

- [1] S. S. Sidhu, et.al, Mater. Sci. Eng. C, 111661 (2020).
- [2] N. Diomidis, S. Mischler, N. S. More, and M. Roy, Acta Biomater., 8, 852 (2012).
- [3] V. R. M. Gonçalves, et.al, Mater. Chem. Phys., 301, 127597 (2023).

Acknowledgments

The authors acknowledge São Paulo Research Foundation, FAPESP (grant #2018/00746-6), and Coordenação de Aperfeiçoamento de Pessoal de Nível Superior, CAPES (grant #88887.890647/2023-00) for the financial support.

^{*}Corresponding author: vinicius.manso@unesp.br

AUTOMATED LASER CLADDING PROCESSING FOR OF CARBON FILMS DEPOSITION FORTBC CLADCOUPLER

Paulo P. O. L. Dyer^{1*}, Silvelene A. Silva², Maria Margareth da Silva³, Anderson K. Hirata⁴, Helder P. Vicente¹, Aroldo M. P. Neto⁵, Getúlio de Vasconcelos¹

¹Instituto de Estudos Avançados, Dep. Fotônica, São José dos Campos, São Paulo, Brasil
²Instituto Nacional de Pesquisas Espaciais, Dep. Materiais, São José dos Campos, São Paulo, Brasil
³Instituto Tecnológico de Aeronáutica, Dep. Materiais, São José dos Campos, São Paulo, Brasil
⁴Instituto Federal do Estado de São Paulo, Dep. Controle Automação, São José dos Campos, São Paulo,
BrasilInstituto Militar de Engenharia, Dep. Materiais, Rio de Janeiro, Brasil

1. Introduction

The laser deposition are widely versatile to materials improvements [1, 2]. Specifically, the laser claddingsystem optimize this process [3, 4]; since, the irradiation is carried out with coating supplying [4]. In addition, according to Vilar (1999) [4], the technique are effectiveness for only irradiation processing. I this way, aiming part (or substrate) surface improvements, by phase changing; or pre-deposited film remelting process, improving surface or acting as a "cladding coupler" for thermal barrier coating (TBC) composites. Due to its high capacity for parameters controlling; including variable parameters, such as power efficiency "E" and beam velocity of scanning " v_s ". As function of fixed parameters, such as beam diameter " b_d " and maximum power "P". Under the focal distance between the substrate surface and "headstock laser cladding" (or laser beam emission system).

In this horizon, the beam profile - pulsed or continuous - brings or not advantages [5-8]; particularly for pre-deposited films, as Vanalakar et al. (2015) [9] reiterate. According to Keist and Palmer (2016) [8], Gaussian transfer twice P under 30% of central beam profiling. As a result, its crucial the pulsed-beam use, highlights Rodeet al. (1999) [5]; allowing the control of intensity between irradiation cycles. In other side, the top-hat profiling can transfer a uniform energy, over entire incidence spot; corresponding to b_d diameter [7]. Concluding that this profiling type; associated to continuous beam; could be suitable for a uniform film remelting process [6, 7]. However, as Tenbrock et al. (2020) [10] points, in practice occur a small Gaussian central region. Where, a highenergy density transference may be causing some adverse effects under substrate film, such as ablation; considering the correct focal length between headstock and surface.

The last 30' years to currently, literature shown good results for laser irradiation films; such as carbon films and Diamond-like growth [11-14]. However, despite the top-hat continuous laser possibilities, Gaussian-pulsed lasers are the most studied [9]. In the same way, there are also no specific studies about TBC cladding couplers. Where, although proven the importance of controlling experimental parameters for films, were few studies pointing procedures, explain Wang et al. (2023) [15]. In addition, an automated experimental set up; such a robotic arm operating the laser headstock, imbued with a programming routine; are also rarely observed [16].

According to Torims (2013) [16], automation can be compensating some outside effects; and allow its reproducibility. Where, in the field of carbon films for clad coupling, Ya et al. (2016) [17] points out its role of top-hat controlling for a uniform irradiation; including some points, of experiment, for laser beam to move out the focus, maximizing the substrate irradiation covering. Likewise, in the spectrum of top-hat profiles, the programroutine execution can be absented for adverse effects from little Gaussian region. Where, possible paths avoiding beam focal distance are included at beam pass programming; considering determined experimental time up.

2. Experimental

For processing, were tested 3 film types: carbon black soot (CBS) with 95% (C) and 5% (O, H and N) with particle size of 50-100 nm; commercial graphite spray – GS (ORBI Química) with 99% (C) and 1% (trace elements with residual oils); and graphite powder – GP: 98% (C) and 2% (contaminants) with particle size of 4-40 μm. Under a 4340-steel discoidal samples (25X5mm) with 0.5% (C), 96% (Fe) and 3.5% (Ni, Cr, Mn and Mo). The carbon black soot film were obtained, positioning the sample 60 mm from the flame top (Homemade lamp) for 18 s. For the spray can or pneumatic gun (APREX-Hobby Jet) the film were made by positioning samples at 10 cm, spraying for 30 s and 4 bar. To analyze the film as a cladding coupler role in TBC, was used: NiCrAlY powder (PRAXAIR) with 30.1% (Ni), 10.5% (Al), 0.4% (Y) and 0.06% (H and O) with particle size of 15-22 μm; and Zirconia powder (PRAXAIR) with 7.3% (Y2O₃), Bal. (ZrO₂) and 4.3% (traces) with part. size of 11-22 μm. Under a copper discoidal sample (25X5 mm) with 95% (Cu) and 5% (traces); containing or not an irradiated film.

Firstly, 20 mm line tracks were made under CBS samples; using manual parameters controlling of v_s and coordinate. Throughout YaskawaCL25 robotic arm pendant controller. Likewise, E parameters were manually adjusted using a P = 1500W Ytterbium IPG fiber laser. Next, GS and GP films were then irradiated throughout rectilinear and area programmed tracks; using RoboDK software. In this case, the processing automation assured perpendicular beam incidence, as well correct track definition; an impossible adjustment under a manual execution. Finally, the sectional of samples were optical microscopy (OM) analyzed; using a Zeiss microscope. In order to evaluate the process automation impact throughout a process chart containing parameters variation: TK1- δ , as shown in Fig. 1; where also specifies the programming type: 20 mm line or 25X8 mm area or when notused (manual) and focal up length. With Argon gas flow " s_g " of 7 l/min; using a continuous laser beam.

With best result definition, this parameter were repeated; evaluating this efficiency as a TBC clad-coupling. NiCrAlY and zirconia deposition. To this end, NiCrAlY was firstly deposited, acting as a "bond-coating" for ZrO₂ above; both deposited at " μ " rate and charged by " s_t " argon flow of 7 l/min. According to parameters showed in Fig. 2; including the program routine of 20X20 mm area and static laser for certain period (Sl). Noting that, TBC was deposited with and without film. Parallelly, best TK result was analyzed; evaluating its friction coefficient " θ ", wear resistance rate "W", Vickers microhardness (MHV) and "RA" roughness average index; using an Anton Paar TRB³ tribometer; according the following parameters of: 6 mm sphere tip of 440C inox, amplitude " Δ " of 10 mm, linear speed " l_s " of 4.7 cm/s, normal load " N_l " of 5 N for maximum period "t" of100 s with frequency "f" of 1.5 Hz. Likewise, a micro–Vickers Hardness tester F700 with 100 gf applied for 15 sat surface film or substrate; and a Taylor Hobson roughness meter at 1.5 mm/s of speed and 2.5 mm of length.

Track	v_s	E	Program	Focus	Film
	mm/s	%		mm	
TK-1	18	50	no	on	CBS
TK-2	18	70	no	on	CBS
TK-3	10	50	line	on	GS
TK-4	10	70	line	on	GS
TK-5	10	50	line	20	GP
TK-6	10	70	line	20	GP
TV 7	10	50	area	30	CBS
TK-7	0	75	Sl 5 m	70	CBS
TVO	10	60	area	30	CBS
TK-8	0	75	Sl 5 m	70	CBS

Track	v_s	E	μ	Prog.	Focus	Powder
	mm/s	%	g/min		mm	
TK-9	6	50	0	area	on	none
No fikm	6	50	0	area	on	none
	6	50	9	area	on	NiCrAlY
	0	40	0	Sl 32 s	112	none
	0	40	6	Sl 25 s	112	ZrO_2
TK-10	6	30	0	area	on	none
film	6	30	0	area	on	none
	6	55	9	area	on	NiCrAlY
	6	30	0	area	9	none
	6	50	2	area	9	ZrO_2

Fig. 1. Film irradiation parameters.

Fig. 2. TBC deposition parameters.

3. Results and Discussions

"TK-5" parameter shown best tribological properties with a " θ " 74% lower than sample surface without film, as Fig. 3 graph shown. In addition, this film showed a 22% of reduction in "W", according to the mass losses between wear pair: surface and ball, as Fig. 4 micrographs illustrates. Furthermore, the automatization role was crucial under the processing. Evolving from an irregular and discontinuous film; as Fig. 5 process-chart shown; to a uniform-well-cladded film, as Fig. 6 process chart shown. Consequently, was observed an improvement of NiCrAlY bond-coating anchoring; due to a RA increase: 3.2 μ m against 1.8 μ m. Thus, Zirconia deposition was improved; facilizing the fixation by covalent bonds under NiCrAlY surface oxides, as Fig. 7 photographs shown.

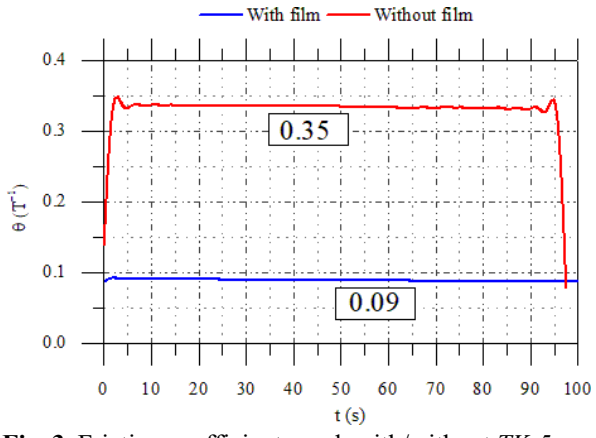


Fig. 3. Friction coefficient graph with/without *TK-5*.

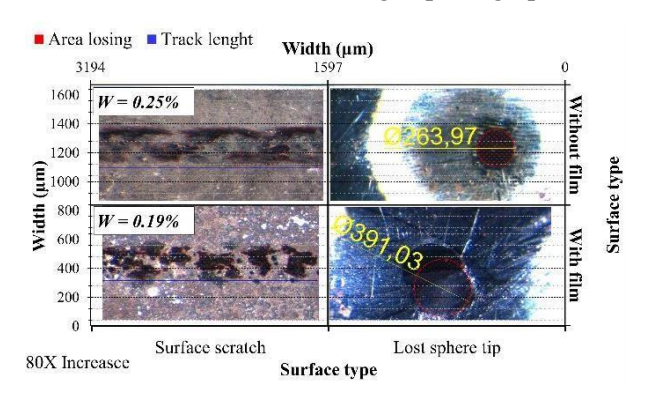
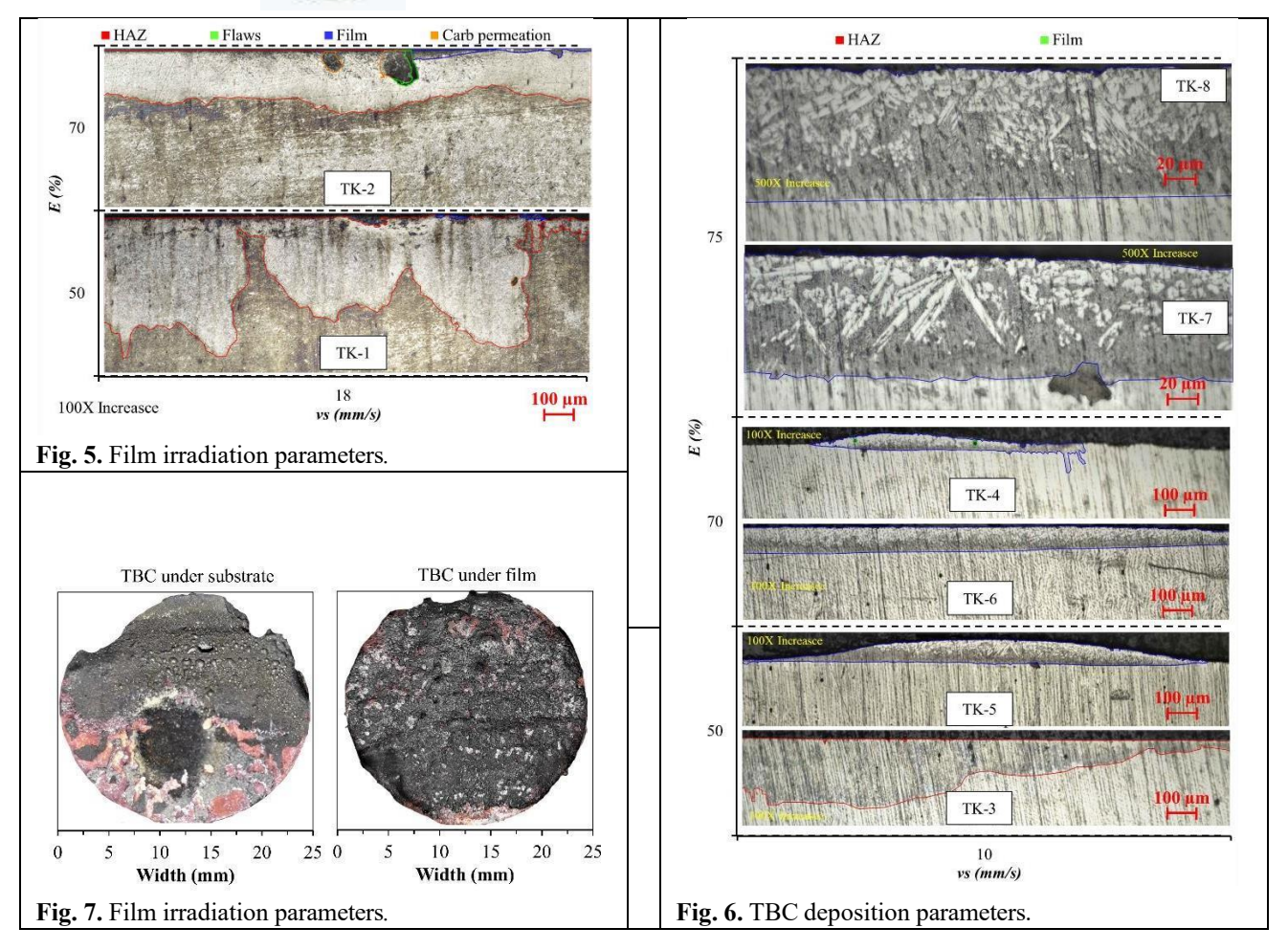


Fig. 4. Micrographs of pair mass losing.



Concluding that the laser irradiated carbon films, act as a cladding-coupler for TBC. Likewise, the processautomation improves the film fixation quality; controlling the parameters and equipment precision of set-up.

4. References

- [1] M. N. R. Ashfold, F. Claeyssens, G. M. Fuge and Simon J. Henley, Chem. Soc. Rev. 33, 23-31, (2004).
- [2] Q. Bao, C. Chen, D. Wang, Q. Ji, T. Lei, Applied Surface Science, 252, 1538–1544, (2005).
- [3] F. J. Decker, In *Proceedings of the AIP Conference Proceedings*, (1995).
- [4] R. Vilar, 1999, Journal of Laser Applications, 11, pp. 346, (1999).
- [5] A. V. Rode, B. Luther-Davies and E. G. Gamaly, Journal of Applied Physics, 85, 4222-4230, (1999).
- [6] G. Sreekumar et al., J. Opt. A: Pure Appl. Opt., 11, (2009).
- [7] O. Homburg and T. Mitra, In *Proceedings of the LIMO Lissotschenko Mikrooptik GmbH*, (2012).
- [8] J. S. Keist and T. A. Palmer, Materials Design, (2016).
- [9] S. A. Vanalakar et al., Journal of Alloys and Compounds, 619, 109–121, (2015).
- [10] C. Tenbrock et al., Journal of Materials Processing Tech., 278, pp. 116514,
- (2020).[11] D. L. Pappas et al., J. Appl. Phys. 71, 5675-5684, (1992).
- [12] D. He, S. Zheng, J. Pu, G. Zhang and L. Hu, Tribology International, (2015).
- [13] G. Huang et al., Journal of Physics: Conference Series, 1775, (2021).
- [14] Y. Lu, et al., Applied Surface Science, (2020).
- [15] K. Wang., et al., Coatings, 13, pp. 496, (2023).
- [16] T. Torims, Chapter 32 In "DAAAM International Scientific Book 2013", 587-608, (2013).
- [1] W. Ya, B. Pathiraja and S. Liu, Journal of Materials Processing Technology, 230, pp. 232, (2016).

Acknowledgments

CNPq grant: 405624/2022-0. Finep grant: 25670-SUB-1 and IEAv.

BIFURCATION FROM HOMOCLINIC TO HETEROCLINIC TOPOLOGY IN TOKAMAK DISCHARGES

André Carlos Fraile Jr.^{1*}, Marisa Roberto², Iberê Luiz Caldas³

¹Divisão de Aerotermodinâmica e Hipersônica, IEAv, DCTA, São José dos Campos ²Departamento de Física, ITA, DCTA, São josé dos Campos ³Departamento de Física Aplicada, Instituto de Física, USP, S. Paulo

1. Introduction

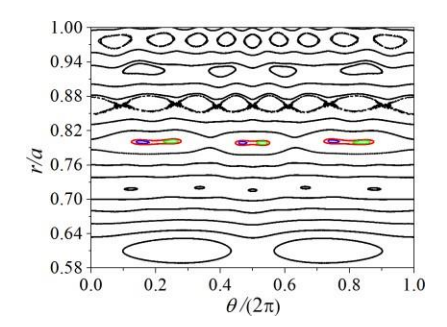
Topological bifurcations have been the subject of recent studies in plasma confinement in order to improve regimes of operation for tokamaks. We present a model of resonant magnetic perturbations for a cylindrical plasma with toroidal correction in which heteroclinic bifurcations around rational surfaces are induced. In this model, a perturbation generated by a pair of resonant helical windings (RHWs) located on the external wall is superposed to a helical current sheet (HCS) located on a rational surface. We show that heteroclinic islands are created when the perturbation current associated to the HCS is increased, which is consistent to bifurcations reported in resistive mhd simulations for the NSTX-U and in experiments for the DIII-D tokamak.

2. Theory

We present a model that is capable of generating heteroclinic bifurcations applying two resonant magnetic perturbations (RMPs) superposed for a cylindrical plasma with toroidal correction. The first perturbation is created by a pair of resonant helical windings (RHWs) on the external wall, which is usually studied in order to reduce wall erosion by generating a chaotic layer near the plasma edge [1-2]. The second one is a helical current sheet (HCS) located on a rational flux-surface, acting like a plasma current perturbation around this region [3]. We have identified four topological bifurcations located around rational flux-surfaces, all of them modifying the distribution of field lines similarly to the heteroclinic bifurcations observed in resistive mhd simulations and in experiments.

3. Results and Discussions

We present new topological bifurcations that are generated when the current I_s is increased. In all cases considered here, the perturbation is generated by RHWs and HCS.



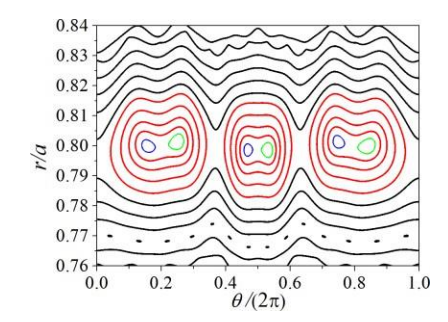


Fig.1: Poincaré plots of field lines considering RHWs resonant to mode $(m_h, n_h) = (2, 1)$ with $I_h = 1\%I_p$ and HCS resonant to mode $(m_s, n_s) = (8, 2)$ with $I_s = 0.628\%I_p$, showing region (a) around $r_h/a = 0.610$, associated to safety factor $q(r_h) = 2$, and (b) zoom around r/a = 0.800, associated to safety factor r/a = 3. The interior of red magnetic islands contains two islands (blue and green).

4. References

- [1] S. S. Abdullaev, *Magnetic Stochasticity in Magnetically Confined Fusion Plasmas*, 1st edn. (Springer, Berlin, 2014), pp. 227-262.
- [2] M. Lehnen, S.S. Abdullaev, W. et al, "First results from the dynamic ergodic divertor at TEXTOR," *J. Nucl. Mater.*, **337-339**, pp. 171-175, 2005.
- [3] M.S.P.Araujo, A.Vannucci, K.A. Oliveira. "Toroidal geometry and plasma column displacement corrections in the analyzes of Mirnov oscillations". Brazilian Journal of Physics, **32**, 1, pg. 131,138, 2002.

^{*}Corresponding author: r.marisa@gmail.com

BIOCOMPATIBILIDADE DE NOVAS LIGAS DE TITÂNIO VISANDO APLICAÇÕES BIOMÉDICAS

Mariana Rocha Corrêa^{1*}, Anderson Moreira Gomes², Willian Fernando Zambuzzi², Carlos Roberto Grandini¹

¹ UNESP - Universidade Estadual Paulista, Lab. Anelasticidade e Biomateriais, 17.033-360, Bauru, SP ² UNESP - Universidade Estadual Paulista, Departamento de Ciências Químicas e Biológicas, 18618-689, Botucatu, SP

1. Introdução

O titânio e suas ligas desempenham um papel crucial em implantes ortopédicos e odontológicos devido às suas notáveis características de biocompatibilidade, resistência à corrosão e uma excelente relação entre resistência mecânica e densidade, quando comparados a outras ligas utilizadas na área biomédica (1). No entanto, a amplamente utilizada liga Ti6Al4V contém elementos considerados citotóxicos, como o vanádio e o alumínio (2).Portanto, a pesquisa está focada no desenvolvimento de ligas que não contenham esses elementos, como nióbio, zircônio, molibdênio, manganês e tântalo, que são reconhecidos como β-estabilizadores. São realizadas avaliações de citotoxicidade in vitro para determinar a adequação desses novos materiais para aplicações biomédicas, com ênfase na sua capacidade de não interferir no crescimento celular.

2. Parte Experimental

Foram utilizadas amostras de titânio comercial e ligas a base de titânio no estudo. Esses materiais passaram por um processo de decapagem e lavagem para remover impurezas superficiais. Em seguida, foram fundidos em umforno de arco-voltaico com atmosfera controlada de argônio para evitar contaminações. Posteriormente, foram submetidos a processos adicionais, como tratamento térmico, laminação a quente e solubilização. Após a preparação dos lingotes, foram cortados, lixados, polidos e limpos para análises futuras.

Os ensaios de citotoxicidade foram realizados no Instituto de Biociências da UNESP. As amostras das ligas forampesadas e autoclavadas, e um meio de cultivo adequado foi preparado. As células pré-osteoblásticas (MC3T3-E1)foram transferidas para placas de 96 poços com uma densidade de 5x10⁴ células/ml, 24 horas antes dos ensaios de MTT. Cada amostra foi avaliada em duas placas diferentes, uma para o período de 24 horas e outra para o período de 72 horas. O meio de cultivo condicionado com as amostras foi adicionado às células na placa. Em seguida, foi conduzido o ensaio de MTT indireto para avaliar a citotoxicidade das amostras em relação às célulasem cultivo, tanto após 24 horas quanto após 72 horas.

3. Resultados e Discussões

As Figs. 1 e 2 mostram os resultados das análise de adesão e proliferação celular em algumas ligas de Ti.

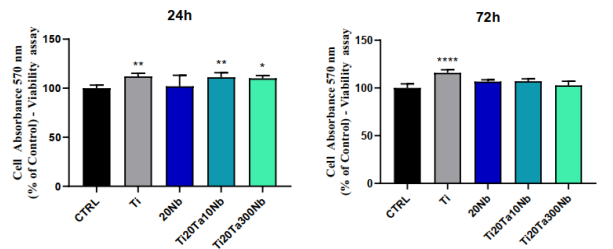


Figura 1: Gráfico representando a análise das ligas Ti20TaxNb (x=10,20 e 30) no período de 24 e 72 horas.

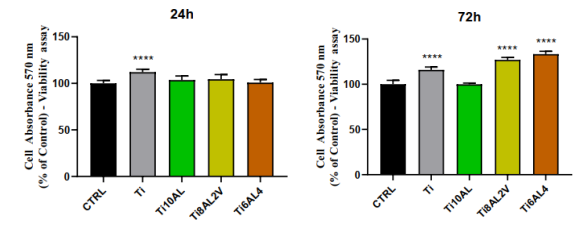


Figura 2: Gráfico representando a análise das ligas Ti6Al4V, Ti8Al2V e Ti10Al no período de 24 e 72 horas.

Os resultados da análise das ligas de titânio desenvolvidas pelo Laboratório de Anelasticidade e Biomateriais revelam consistência com valores superiores ou estatisticamente equivalentes ao grupo de controle

Agradecimentos

Os autores agradecem a FAPESP e ao CNPq pelo suporte financeiro.

Referências

- 1. Sidhu SS, Singh H, Gepreel MA-H. Materials Science and Engineering C. 2021;121:111661.
- 2. Park Y-J, Song Y-H, An J-H, Song H-J, Anusavice KJ. Journal of Dentistry. 2013;41(12):1251-8.

^{*}Corresponding author: mr.correa@unesp.br

BIOFILM INACTIVATION OF CANDIDA PARAPSILOSIS AND CANDIDA ALBICANS BY ARGON / AIR PLASMA

Anelise Cristina Osorio Cesar Doria¹, Felipe Santos de Almeida¹, Sonia Khouri Sibelino¹, Rodrigo Sávio Pessoa²

¹UNIVAP – Universidade do Vale do Paraíba ²ITA – Instituto Tecnológico de Aeronáutica

1. Introduction

Candida yeasts are the fourth most prevalent cause of hospital-acquired infections globally. Although they are generally considered benign in humans, they have the potential to cause opportunistic infections, often associated with the development of biofilms. This kind of microbial organization complicates the treatment process and leads to worrying mortality rates [1]. Given the critical medical significance of this organization of microorganisms, the adoption of new technologies is imperative for their control or elimination. Low temperature atmospheric pressure plasmas (LTAPP) are gaining growing recognition as a potential method for eradicating and managing infections, as well as bacterial or fungal contamination [2,3].

2. Experimental

In this study, Low Temperature Atmospheric Pressure Plasmas (LTAPP) were produced in a gliding reactor using 6L/min of Argon and 4L/min of Argon. The objective was to apply LTAPP for the inactivation of standard ATCC® strains and clinical strains of *Candida parapsilosis* and *Candida albicans*, cultivated in vitro on polyurethane substrates. To achieve this, the treatment was conducted for a duration of 10 minutes at 3 cm distance. The composition of the plasma was examined through Optical Emission Spectroscopy, while the presence of biofilm was confirmed via Scanning Electron Microscopy. To quantify the reduction in colony forming units, all samples were plated on Sabouraud Dextrose Agar using the Spread Plate technique. Additionally, cell viability was assessed using Confocal Laser Scan Microscopy, using the markers SYTO9 and propidium iodide.

3. Results and Discussions

The Optical Emission Spectroscopy showed the presence of NO, OH, NH, and N₂ in the plasma plume, in which the OH system emissions were the highest [4]. Scanning Electron Microscopy confirmed the presence of biofilm in the samples and the Spread Plate technique showed for *C. parapsilosis* a 91.5% and 90.1% reduction in Colony Forming Units for the standard and clinical strains, respectively. In the other hand, for *C. albicans* the reduction was 88.8% and 83.3% respectively. The evaluation of cell viability by Confocal Laser Scan Microscopy, verified that the treated samples presented internalization of Propidium Iodide, demonstrating cell membrane damage. The reduction in *Candida sp* contamination varies due to species-specific morphological, physiological, biofilm-forming, and extracellular matrix capabilities. These distinctions account for CFU reduction percentage differences, highlighting the challenge of devising a universal methodology for different species and an even greater hurdle for diverse clinically relevant microorganisms [5].

4. References

- [1] C.G. Pierce, A.K. Chaturvedi, A.L. Lazzell, A.T. Powell, S.P. Saville, S.F. McHardy, et al. BiofilmsMicrobiomes. 2015 Aug 12;1:15012.
- [2] Y-O. Park, C-M. Lee, M-S. Kim, S-C. Jung, S-W. Yang, M-S. Kook, et al. Jpn J Appl Phys. 2017 Jan1;56(1S):01AC01.
- [3] P. Puligundla, C. Mok. J Appl Microbiol. 2017 Jan.
- [4] M. Moisan, P. Levif, J. Séguin, J. Barbeau. J.Phys.D:Appl.Phys.47(2014)
- [5] M. Cavalheiro, M.C. Teixeira. Front. Med., 13 February 2018

Acknowledgments

We would like to express our gratitude to FAPESP (2015/10876-6) for their financial support. Our thanks also extend to UNIVAP and to the entire BIOTECPLASMA - Univap team for their valuable support.

^{*}Corresponding author: ferder017@gmail.com

BIOFUNCTIONAL COATING OF STAINLESS STEEL SURFACES WITH CARVACROL- AND EUGENOL-DERIVED FILM USING DIELECTRICBARRIER DISCHARGE PLASMA: AIMING FOR SUPPRESSION OF BIOFILM FORMATION AND CORROSION PROTECTION.

Tsegaye G. Getnet¹*, Elidiane C. Rangel², Nilson C. Cruz², Milton E. Kayama³.

¹Department of Chemistry, College of Science, Bahir Dar University, Ethiopia, ²Technolog Plasmas Laboratory, São Paulo State University, Brazil, ³Labolaboratory of Plasma and Applications, São Paulo State University, Brazil.

1. Introduction

The increased adoption of implantable medical devices (IMDs) in modern medicine and healthcare is due to their capacity to repair and replace damaged tissues or organs [1][2]. However, careful consideration is necessary when selecting the materials for IMDs to ensure optimal performance within a biological environment. Besides exhibiting biocompatibility and chemical stability, the ideal materials should possess the ability to prevent bacterial colonization on the implants[3]. Although bacterial infections can be addressed with antibiotics, their excessive use has contributed to the emergence of antibiotic-resistant microorganisms. Additionally, bacteria can create biofilms, which are clusters of cells that shield them from external factors, when they adhere to surfaces[4].

2. Experimental

In this particular situation, the potential solution to address the challenges related to implants involves modifying the surfaces of biomaterials using natural antimicrobial compounds. To explore this approach, we conducted an experiment involving the deposition and characterization of polymeric thin films derived from carvacrol and eugenol monomers using a Dielectric Barrier Discharge (DBD) plasma reactor, as illustrated in Figure 1. The electrical discharge properties were assessed by measuring voltage drop across a resistor and capacitor, while theapplied voltage was determined using a voltage divider. The maximum applied voltage reached 14.4 kV peak-to-peak, with a power level of approximately 1.2 W. The study also involved analyzing the structural properties of the films through techniques such as infrared reflectance spectroscopy, scanning electron microscopy, atomic force microscopy, profilometry, and contact angle measurements. Furthermore, we evaluated the effectiveness of these films in inhibiting biofilm formation of *Staphylococcus aureus*, *Pseudomonas aeruginosa*, *Escherichia coli*, and *Candida albicans* on stainless steel surfaces.

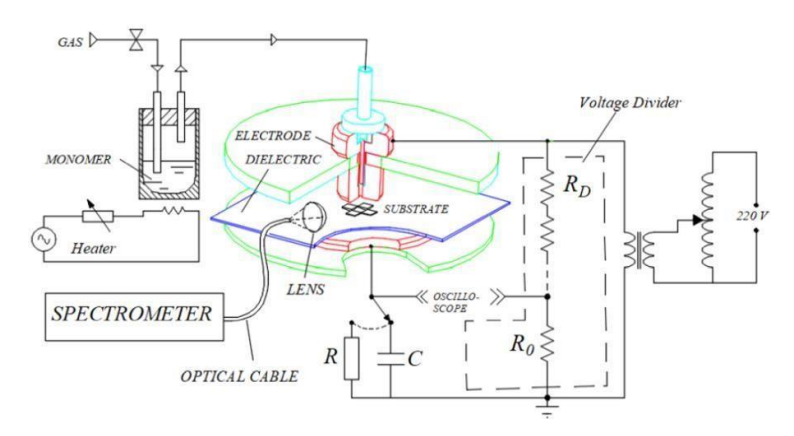


Figure 1. The experimental setup used for film deposition and discharge characterization.

3. Results and Discussions

The resultant films were found to possess a uniform, smooth, and dense structure that closely resembled the chemical composition of the respective monomers. In terms of their antimicrobial properties, the coatings derived from carvacrol were observed to completely inhibit the adhesion of *E. coli*, while reducing the proliferation of *S.aureus* by 90%. Furthermore, these coatings inhibited the adhesion of *P. aeruginosa* and *C. albicans* by up to 44% and 60%, respectively. Similarly, films produced in plasmas containing eugenol demonstrated strong antimicrobial capabilities, inhibiting the adhesion of *E. coli* and *S. aureus* by more than 75% and 65%, respectively, and reducing the adhesion of *P. aeruginosa* and *C. albicans* by more than 30% and 40%, respectively. Additionally, electrochemical impedance spectroscopy and potentiodynamic results indicated that both carvacrol- and eugenol-derived films significantly increased the corrosion resistance of stainless steel in NaCl solution by at least 10 times.

4. References

- [1] D.D. Kiradzhiyska, R.D. Mantcheva, Folia Med. 61, 34–40 (2019).
- [2] S. Chatterjee, M. Saxena, D. Padmanabhan, M. Jayachandra, H.J. Pandya, Biosens. Bioelectron., 142 (2019).
- [3] J.D. Caplin, A.J. García, Acta Biomater., 93, 2–11 (2019).
- [4] I. Francolini, C. Vuotto, A. Piozzi, G. Donelli, Apmis. 125, 392–417 (2017).

Acknowledgments

The authors express their gratitude to CNPq-TWAS and FAPESP (Proc. 190896/2015 and 302992/2017-0) for providing financial support for this study.

^{*}Corresponding author: tsegshchem2004@gmail.com

CARACTERIZATION OF MONOCRYSTALLINE GRAPHITE FILM DEPOSITED BY PHI&D INSIDE TITANIUM ALLOY TUBE

Nazir.M. Santos^{1*}, Beiker .M. Rueda², Fernando V. Santos², Diego.F.G. Silva², Mário Ueda¹,

¹National Institute for Space Research (INPE), São José dos Campos, SP, Brazil ²Federal University of Latin American Integration (UNILA), Foz do Iguaçu, PR, Brazil

1. Introdution

Monocrystalline graphite films have interesting properties for technological applications, such wear resistance and low friction coefficient [1]. Using monocrystalline graphite films as protective coatings can increase the lifetime of the tubes used in propulsion of spacecrafts and thermal control systems of satellites and inhibit the permeation of corrosive species from the fuels and the cooling fluids through the film-metal interface. The properties of the films deposited by Plasma Immersion Ion Implantation and Deposition (PIII&D) system generally depend on the deposition conditions, which determine their microstructure, especially the respective proportions of sp³ and sp² carbon site [2, 3]. Therefore, the objectives of this work were the production of monocrystalline graphite films inside metal tubes to increase the useful lifetime in the applications of the aerospace, oil and gas sectors, taking advantage of the plasma ejected from the interior of the tube for the coating of flat samples and to investigate the properties of these films.

2. Experimental Procedure

The films were produced by PIII&D system using acetylene plasma, by driving Hollow Cathode (HC) discharges inside the tube attached to the top part of the chamber, in a stainless-steel cylindrical vessel with a volume of 20 liters. The tube used was titanium alloy (Ti6Al4V), with 15 cm length and small internal diameter of 1.1 cm, with one side closed configuration. Polished samples of Ti6Al4V (TAV), and pieces of p-type silicon, were fixed along the inner tube wall for subsequent analysis of the monocrystalline graphite coatings. The material expelled by the HC driven tube was deposited in a commercial Si-wafer disc target, placed 7 cm from the tube exit. Prior to each deposition, the tubes were further cleaned in argon plasma for 10 min (4kV, 15A, 20μs, 500Hz). Acetylene plasma was generated by the application of pulses of 2kV, 15A, 20μs, 500 Hz rate, reaching temperatures of about 1000°C quickly. Deposition time varied from 30 to 240 minutes. Chemical structure of films were analyzed by Raman Spectroscopy and the film thicknesses were measured by Field Emission Gun – Secondary Electron Microscopy (FEG/SEM/EDS), and the topography was evaluated from surface images.

3. Results and Discussions

The ID/IG value proved the existence of monocrystalline graphite on the film. The internal wall of the tube was completely covered by these films, as well as the samples placed inside the tube, and revealed to be of quite a good quality, totally adhered, with thickness between 2 to 25 μ m. It was found that the plasma ejected from the tube has also good properties, such as high density, stability of the discharge, uniform plasma and with high rates of implantation and deposition. Finally, it can be used for coating planar components with success.

4. Reference

[1] S.F.M. Mariano, M. Ueda, R.M. Oliveira, E.J.D.M. Pillaca,; **N.M. Santos**, Magnetic-field enhanced plasma immersion ion implantation and deposition (PIII&D) of diamond-like carbon films inside tubes. Surface & Coatings Technology. v. 312, p. 47-54, 2017.

[2] Y. Lifshitz, "Diamond-like carbon present status", Diamond and Related Materials, v.8, p. 1659, 1999. [3]J. Robertson, Diamond-like amorphous carbon. Materials Science and Engineering R v. 37, p. 129-281 (Reports: A review journal), 2002.

Acknowledgements

The authors thank the CNPq for financial support.

^{*}Corresponding author: nazirmonteiro@gmail.com

CERIUM OXIDE NANOPARTICLE DEPOSITION ON PLA SCAFFOLDS USING HIGH VOLTAGE-MODIFIED ELECTROPHORESIS

Luis Guilherme Silva Rosa^{1*}, Daniela Becker¹, Luis César Fontana¹, Eduardo H. Backes², Lidiane C. Costa², Samarah V. Harb², Luiz H. Pessan²

¹Santa Catarina State University (UDESC), Joinville-SC, Brazil ²Federal University of São Carlos (UFSCar), São Carlos-SP, Brazil

1. Introduction

In scaffold engineering, PLA is used as a substitute for metallic bone implants, but its low surface energy and hydrophilicity hinder bone cell growth. To address this issue, bioagents can be incorporated into the polymer matrix or deposited on the scaffold's surface [1]. Cerium oxide, known for scavenging reactive oxygen species, is promising for overcoming these challenges. This work focuses on depositing cerium oxide nanoparticles using modified electrophoretic deposition techniques, including short-timed pulsed voltages and mechanical agitation for stabilizing colloidal suspensions.

2. Experimental

0.1% (m/v) aqueous suspension of cerium oxide nanoparticles was prepared using a tip sonicator for 30 minutes to ensure complete dispersion. The reactor configuration is shown in Figure 1, consisting of a copper vessel acting as the polarized electrode and a grounded mechanical rod, which was set to rotate at 2340 rpm [2]. The scaffolds were immersed and freely moving in the suspension during the electrophoretic deposition. The experiment was performed for 10 minutes. The pulse configuration consists of two alternating positive and negative pulses, 2.5 µs of pulse width, and 1000 V amplitude (not shown here) [3]. The time between the pulse's sequence (time-off) was 250 µs to avoid excess medium heating.

3. Results and Discussions

Figure 2 shows the SEM analysis of the surface and inside the pores (cross-section) of the scaffolds. First, the constant mechanical agitation did not damage the scaffolds severely. Second, the highlighted agglomerates may indicate the presence of cerium oxide nanoparticles, due to their similarities with the morphology of the agglomerated nanoparticles (not shown here). Finally, the deposition was more efficient on the surface than on the inside of the scaffolds, probably because of the agglomerates' size and inability to diffuse through the pores.

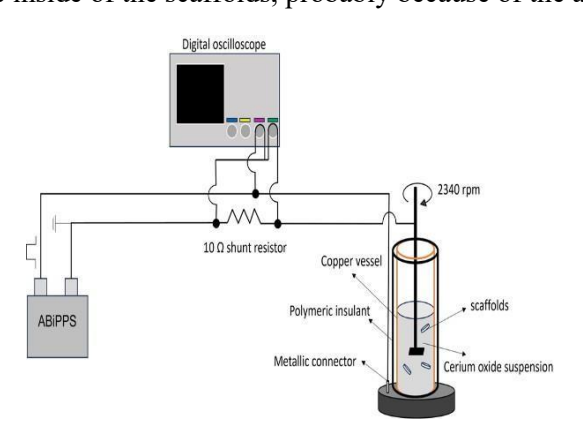


Fig.1. Representation of the reactor used in the high-voltage pulsed electrophoresis.

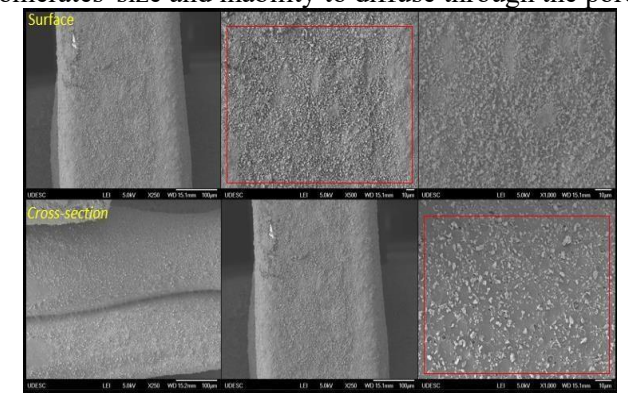


Fig. 2. SEM images of the scaffolds, with the cerium oxide agglomerates highlighted in red.

4. References

- [1] E. H. Backes et al, J. App. Pol. Sci, 138, 49759, (2021).
- [2] E. H. Segundo et al, Mater. Chem. Phys, 217, 1-4, (2018).
- [3] V. F. dos Santos et al, J. Appl. Phys, 129, 123302, (2021).

Acknowledgments

The authors thank CAPES, FAPESP, and FAPESC for the financial support and the Multi-User facility (UDESC).

^{*}Corresponding author: lguilhermesrosa@gmail.com

CHARACTERIZATION AND PLASMA SURFACE TREATMENT OF PHEROMONE-RELEASING SEPTA IN AGRICULTURE

Maura de Almeida Bueno¹, José Roberto Ribeiro Bortoleto¹, Maria Carolina Blassioli Moraes², Nilson C. Cruz¹, Leonardo F Fraceto¹, Elidiane C. Rangel¹

¹Universidade Estadual Paulista Júlio de Mesquita Filho (UNESP – Campus Sorocaba), ²Empresa Brasileira de Pesquisa Agropecuária (Recursos genéticos e biotecnologia).

1. Introduction

Butyl rubber is a copolymer of isobutylene + isoprene characterized by high resistance to gas and liquid permeability and used for various applications such as sealing rings, tires. In agriculture the material is used as a pheromone releaser through septa as a safer and more sustainable alternative to conventional pesticides [1]. To improve the release rate, atmospheric plasma surface treatment technique is a viable option. The plasma generator source KINPen IND, is an atmospheric plasma jet developed for sensitive surface treatment at atmospheric pressure and room temperature with optimized parameters for polymers.

2. Experimental

The characterization techniques used in this work include Scanning Electron Microscopy, Energy Dispersive X-Ray Spectroscopy, Fourier Transform Infrared Spectroscopy and Contact Angle, before and after treatment, to compare and evaluate the surface modification.

3. Results and Discussions

A jet of argon plasma with 2% oxygen under different conditions was used to treat the substrate reducing the contact angle up to 25°, enhancing its wettability.

4. References

1. Borges M, Moraes MCB, Peixoto MF, Pires CSS, Sujii ER, Laumann RA. Monitoring the Neotropicalbrown stink bug Euschistus heros (F.) (Hemiptera: Pentatomidae) with pheromone-baited traps in soybean fields. Journal of Applied Entomology. 2011 Feb;135(1–2):68–80.

Acknowledgments

We thank the collaborating professors of the project, as well as the institutions, the State University of Júlio de Mesquita Filho (UNESP), Sorocaba campus, for providing their laboratories, and Embrapa for supplying research materials and expertise in the field."

^{*}Corresponding author: maura.bueno@unesp.br

CHARACTERIZATION OF THE TI-20MO-15ZR-4.5CU ALLOY AIMING FOR BIOMATERIALS APPLICATIONS.

Danilo C. Mauricio¹, Israel R. Rodrigues¹, Carlos R. Grandini¹

¹São Paulo State University (UNESP), School of Science, Bauru, SP, 17033-360, Brazil.

1. Introduction

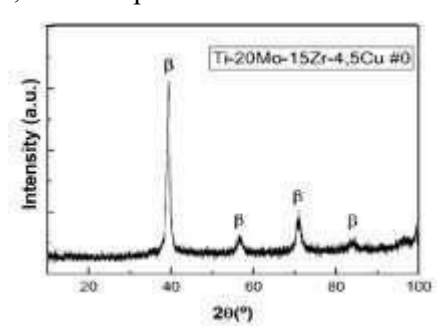
Titanium is a lightweight material, abundant on Earth, and biocompatible due to its corrosion resistance and physical and chemical properties. Similarly, molybdenum, zirconium, and copper are also biocompatible [1]. Zirconium, molybdenum, and copper are typically used to enhance corrosion resistance and, most importantly, the properties of titanium alloys, which do not possess the best mechanical properties on their own for use in prosthetics [2]. A noteworthy property of molybdenum and copper is that they act as β -stabilizers for titanium. Therefore, in this biomaterial application project, the alloy utilized was Ti-20Mo-15Zr-4.5Cu, where its characterization was conducted, and some of its properties were obtained.

2. Experimental

Metals were initially weighed and then taken to an electric arc furnace for melting. In the furnace, under an argon atmosphere, an inert gas, there was no reaction with the alloy. Subsequently, the sample was poured five times to achieve better homogeneity. After melting, the sample is transferred to the heat treatment furnace, which is heated and then slowly cooled to room temperature for 24 hours. At each stage of the alloy, where it is sanded with various sandpapers, polished, and chemically attacked with Kroll solution [3], optical and scanning electron microscopy analyses, as well as X-ray testing, are performed, in addition to the microhardness test, which was also conducted.

3. Results and Discussions

During and after the melting process, it was observed in the sample that there was no contamination within the furnace under the argon atmosphere; therefore, the sample was suitable for the subsequent steps and analyses. The density and hardness analyses of the alloy show that the results are very close to alloys commonly used in the field of biomaterials and implants, thus making it viable for use in biomaterials. Furthermore, in the images obtained from optical microscopy, a characteristic morphology of the beta phase is observed in some areas, with axial grains and a 120-degree angle between grain boundaries. The presence of the beta phase is also evident in the samples' X-ray diffraction (XRD) analyses. Additionally, scanning electron microscopy (SEM) provides greater detail on grain boundaries and the presence of heavy elements in the darker regions, such as copper and titanium in lighter regions. Finally, the presence of the beta phase (body-centered cubic) in the alloy is indeed confirmed, which is preferable for biomedical applications due to its theoretically low modulus of elasticity.



 $Fig.\ 1-DRX\ for\ Ti\mbox{-}20Mo\mbox{-}15Zr\mbox{-}4.5Cu\ alloy$

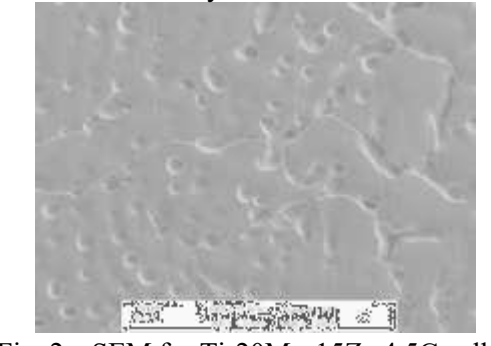


Fig. 2 – SEM for Ti-20Mo-15Zr-4.5Cu alloy

4. References

- [1] Chun-Te, W. et al., Materialia, v. 21, p. 101313, 2022.
- [2] Pires, A.L.R.; Bierhalz, A.C.K.; Moraes, Â.M. Química nova, v. 38, p. 957-971, 2015.
- [3] Rodrigues, I.R.; Lopes, R.E.L.; Grandini, C.R. Materials Research, v. 24, p. e20210503, 2021.

Acknowledgments

The authors acknowledge São Paulo State University (UNESP) and the National Council for Scientific and Technological Development (CNPq) for the laboratory space, equipment, and financial support

^{*}Corresponding author: danilo.mauricio@unesp.br

COMPARATIVE ANALYSIS BETWEEN PLASMA ACTIVATED WATER AND PLASMA ACTIVATED SALINE SOLUTION

Luan Gonçalves de Lima¹, Michaela Shiotani Marcondes¹, Felipe de Souza Miranda^{1,2}, Benedito Donizeti Botan Neto², Clodomiro Alves Junior^{1,3}, Rodrigo Sávio Pessoa¹

¹ Aeronautics Institute of Technology (ITA), São José dos Campos-SP, Brazil ² São Paulo State University (UNESP), São José dos Campos-SP, Brazil ³ UFERSA, Mossoró-RN, Brazil

1. Introduction

Among the different applications of plasma technology, plasma activated water (PAW) and plasma activated saline solution (PASS) have attracted significant attention for their potential applications. [1,2] Some of the numerous applications include the inactivation of microorganisms, the sterilization of medical equipment, the improvement of plant growth, surface treatment, among others. The liquid plasma interaction triggers a series of chemical and physical reactions that result in the generation of certain species and the alteration of some properties of the liquid, such as pH, conductivity, Total Dissolved Salts (TDS) and Salinity. Having control over the levels of these parameters is essential to optimize the plasma activation process and maximize its benefits in your applications, since in applications such as the food industry, the requirements may be different from those used in disinfection processes.

2. Experimental

Two different types of liquids, deionized water (DI) and saline solution (SS), were activated in periods of 10, 15, 20, 30 and 40 minutes, each in a volume of 40ml. Subsequently, a multiparameter meter (Metrohm 913) was used to measure pH, total distributed salts (TDS), conductivity, and salinity of each activated solution. Additionally, to account for potential evaporation during each activation, the final volume of each sample was measured. Furthermore, the experiment employed a Surfatron (SWD) microwave plasma jet utilizing surfacewave technology, operating at 2.45 GHz, with a continuous flow of argon gas. Using a solid-state power supply, experiments were performed at 70 W.

3. Results and Discussions

According to the measured parameters, as shown in Figure 1, it was possible to notice that the deionized water had a smaller volume loss, just as the other measured parameters were smaller, but its pH was close. On the other hand, when analyzing the percentage increase in TDS, conductivity and salinity of the last activation time, in relation to the control, it is possible to notice a significant difference, as shown in Figure 2. TDS has a synergistic effect on the production of IONs, for example high concentrations of TDS, may indicate the presence of ions that can participate in the formation of reactive oxygen species (ROS).

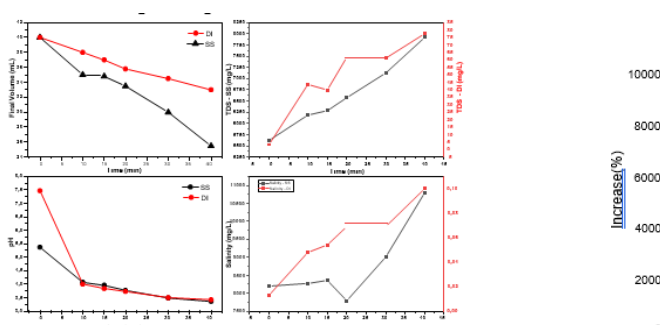


Fig 1 Final Volume, TDS, pH and Salinity of plasma

activated salinity solution and deionized water as a function

Fig 2 Percentage increase in TDS, conductivity and salinity parameters for PAW and PASS.

10346

of the time. **4. References**

- [1] Oztan MO, Ercan UK, Aksoy Gokmen A. Sci Rep. 2022 Mar 7;12(1):3646.
- [2] W. Chiappim. A. Sampaio. F. Miranda. G. Petraconi, *Plasma Process. Polym.* 18.11 (2021)

Acknowledgments

The authors acknowledge financial support from The São Paulo State Research Foundation (FAPESP, grants 2019/05856-7 and 2022/13141-0).

^{*}Corresponding author: luanlgl@outlook.com

COMPARATIVE STUDY OF POLYMERIC STRUCTURES OBTAINED BY FDM ADDITIVE MANUFACTURING FOR BIOMEDICAL APPLICATIONS

Fábio H. C. Bernardes*, Vinicius dos Santos, Durval Rodrigues Junior.

Department of Materials Engineering (DEMAR), Lorena School of Engineering (EEL)University of São Paulo (USP), Lorena-SP-Brazil

1. Introduction

Bone defects can cause aesthetic problems, impair mobility or even put a person's life at risk. One of the possibilities for restoring skeletal functions is the application of scaffolds made from synthetic materials. These scaffolds act as three-dimensional structures with adequate porosity to allow the growth of cells inside, as well as withstanding the mechanical stresses present at the site where they are applied. For this application, scaffolds could be produced with biopolymers such as PLA by FDM additive manufacturing using DICOM tomography images. However, we need to study and understand the behavior and influence of the geometries that can be applied in relation to compressive strength and inserted porosity [1,2].

2. Experimental

Cylindrical samples were obtained by FDM additive manufacturing using a GTMax H4 3D printer using PLA biopolymer with a variation in volume filled by 70% and 40%, inserting porosity into probable geometries that could be used to make scaffolds, which were characterized in SEM, subjected to compression tests and density tests using the Archimedes method with a vacuum applied to the samples for a more accurate result.

3. Results and Discussions

The samples submitted to the compression test initially showed linear-elastic behavior. Subsequently, the elastic limit of the polymer is exceeded, generating a permanent and irreversible deformation when loading ends. Based on the ASTM D695 standard, the point where the analytical line was projected outside the linear behavior was considered the useful stress point.

The compressive strength showed coherent and proportional values when tested at 70% and 40% infill, due to the reduction in density and increase in apparent porosity.

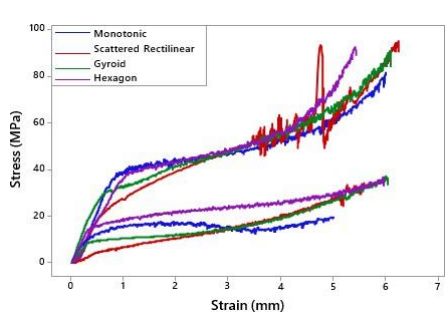




Fig. 1. Compression test Geometry in 70% and 40% Infill

Fig. 2. Geometry: (1) scattered rectilinear; (2) gyroid; (3) Hexagon; (4) monotonic.

Fig. 3. Vacuum application for density testing.

4. References

[1] ALONZO, Matthew et al. Bone tissue engineering techniques, advances, and scaffolds for treatment of bone defects. Current Opinion in Biomedical Engineering, [S. 1.], v. 17, mar. 2021.

[2] SHANMUGAM, Vigneshwaran et al. The mechanical testing and performance analysis of polymer-fibrecomposites prepared through the additive manufacturing. Elsevier Science Direct, v. 93, 2021.

Acknowledgments: Thanks to the USP Master's Program, CNPq and CAPES, Brazil, for the laboratory infrastructure and technical support for graduate students.

^{*}Corresponding author: bernardesfh@usp.br, durvalrj@usp.br

COMPARATIVE WEAR BEHAVIOR OF DLC, DLCN AND DLC-SI FILM DEPOSITED BY PECVDON AISI 321 STAINLE55 STEEL

Alex Rodrigues da Silva¹, João Gabriel Velo Danesi¹, Larissa Solano de Almeida², Marcos Dorigão Manfrinato², Luciana Sgarbi Rossino^{1,2}

¹ Faculdade de Tecnologia do Estado de São Paulo - Fatec Sorocaba,

1. Introduction

The DLC film deposited on 321 stainless steel aims to improve surface properties such as high wear resistance and low friction coefficient. The doping of DLC film with chemical elements such as nitrogen or siliconcan improve the film properties such as adhesion to the metal surface or structural stability of this film [1]. The objective of this work is to evaluate the effect of doping DLC films with nitrogen and silicon deposited by the Plasma Enhanced Chemical Vapor Deposition (PECVD) technique in the wear behavior of the AISI 321 stainlesssteel.

2. Experimental

The DLC films were deposited by PECVD on AISI 321 stainless steel (BM), initiating with plasma ablation process using 80% Ar and 20% H_2 at a pressure of 2.0 torr for 2 hours. After that, an interlayer of organosilicon was deposited using hexamethyldisioxane (HMDSO) (70%) as a precursor and Ar (30%) with a total gas flow of 0.06 torr for 25 minutes. The DLC films were deposited with the parameters shown in Tab1. Thetribological property of the films was characterized by the wear test by fixed ball, with variation in the test time with a contact load of 8N and a ball rotation frequency of 40 Hz.

Tab. 1. Deposition parameters of the DLC, DLCN and DLC-Si films by PECVD.

Samples	Gases	Voltage (V)	Time (h)	Temperature (°C)			
DLC	90% CH ₄ + 10% Ar (40sccm)						
DLCN	70% CH ₄ + 30% N ₂ (40sccm)	500	2	± 200			
DLC-Si	90% CH ₄ + 8% Ar + 2% HMDSO (40sccm)						

3. Results and Discussions

We can observe in Fig.1 that the untreated material (BM) showed the worst wear resistance compared to all treated materials. The DLC film showed a low wear volume at a shorter sliding distance, sharply decreasing the wear resistance for longer sliding distances. The good adhesion of the DLCN on the metal substrate corroborates with the high and stable wear resistance of this film. The higher wear resistance was observed for the DLC doped with silicon due to the stabilization of the film structure in high temperature situations that occurin the wear test.

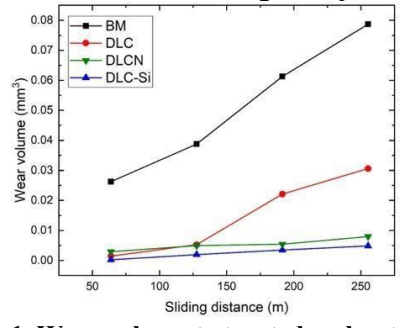


Fig. 1. Wear volume to treated and untreated material.

4. References

- [1] ALMEIDA, L. S. et al. Materials Research, v. 25, (2022).
- [2] WU, W.-J.; HON, M.-H. Surface and Coatings Technology, v. 111, n. 2–3, 134–140, (1999).

Acknowledgments

The authors acknowledge CEETEPS/CPS (Centro Paula Souza) by financial support.

² Universidade Federal de São Carlos -UFSCar Campus Sorocaba

^{*}Corresponding author: alexrodrigues203040@gmail.com

COMPARISON OF THE ECOTOXICITY OF CARBON NANOTUBES OBTAINED BY CVD AND PECVD

Rhaysla Thaiane Rodrigues Nunes¹, Larissa Solano de Almeida^{2*}, Luciana Sgarbi Rossino^{1,2}, Silvia Pierre Irazusta¹

1. Introduction

The carbon nanotube (CNTs) is a carbon nanostructure that has electrical, thermal, and mechanical properties, attractive for various applications. However, conventional CNT synthesis methods, such as chemical vapor deposition (CVD), require temperatures above 1000° C. In order to minimize this limitation, the combination of plasma and the CVD technique shows promise [1]. On the other hand, CNTs applied in differentareas at the end of the use cycle can interact with biological systems and generate toxicological effects. Therefore, it is important to study the ecotoxicity of these carbon nanostructures [2]. The objective of this work is to compare the ecotoxicity of CNTs obtained by CVD and Plasma Enhanced Chemical Vapor Deposition (PECVD) techniques using the *R. subcapitata* as bioindicator.

2. Experimental

The CNTs obtained by PECVD used the precursor gases of methane (CH₄), H₂ and Ar at a total gas pressure of 1.50 torr, with 800 V for 30 minutes. As for the CNTs obtained by CVD, the nanotubes commercial Helix® were used. Both CNTs were characterized by Raman spectrometry. For toxicity test it was carried out a Chronic Toxicity Test according to ENVIRONMENT CANADA, EPS 1/RM/27 (1992) using green algae of thespecies *R. subcapitata* exposed to concentrations of 0.1 to 100 mg/L of NTC.

3. Results and Discussions

The material obtained by the PECVD technique presented a Raman spectrum with D, G, D+D' and 2D bands, characteristic of Multi-Walled Carbon Nanotubes (MWCNTs) as shown in Fig.1. In Fig. 2, the E₅₀ concentrations obtained by exposing algae to CVD-CNT and PECVD-CNT are shown, respectively black and blue lines. It is observed that in both materials the inhibition rate increases with increasing concentrations. However, the PECVD-CNT presents E₅₀ of 161.209 mg/L and the CVD-CNT E₅₀ of 86.017 mg/L. This indicates that the CNTs obtained by PECVD were almost twice as toxic than the CNTs obtained by CVD (conventional technique) in this experimental contamination.

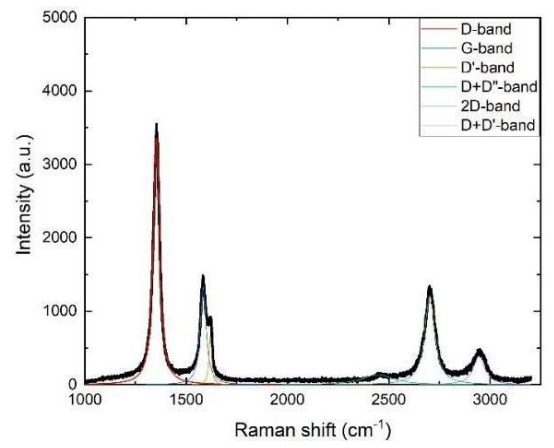


Fig. 1. MWCNTs obtained by PECVD Raman spectrum.

Fig. 2. Inhibition ratio of algae at concentrations from 0.1 to 100mg/L.

4. References

- [1] TAILLEUR, A. et al. Surface and Coatings Technology, v. 211, p. 18–23, (2012).
- [2] BONCEL, S. et al. Chemosphere, v. 136, p. 211–221, (2015).

Acknowledgments

The authors thank Prof. Leonilda Maria B. dos Santos for CNTs Helix®, UNICAMP, and UFPI for Raman and SEM analyses, and CAPES (001) for financial support.

¹ Faculdade de Tecnologia do Estado de São Paulo - Fatec Sorocaba

² Universidade Federal de São Carlos -UFSCar Campus Sorocaba.

^{*}Corresponding author: solano.larissa@gmail.com

COMPUTATIONAL ANALYSIS OF THE HEAT DISTRIBUTION GRADIENT IN THE PEI/FIBERGLASS STRUCTURAL LAMINATE USING ANSYS COMPOSITE PREPPOST (ACP)

Tuane Stefania Reis Santos*¹, Rogério Pinto Mota¹, Erick Siqueira Guidi¹, Luís Felipe Barbosa Marques¹, Rafael Resende Lucas¹; Jonas Frank Reis¹

1 UNESP FEG. Av. Ariberto Pereira da Cunha, 333 - Portal das Colinas - Guaratinguetá/SP

1. Introduction

Composite materials enable the combination of low density with high structural strength, making them widely used throughout the global industry. To facilitate the study of this class of materials, computational analysis can be employed, providing data through simulation of material behavior under various working conditions, such as thermal analysis to assess thermal phenomena derived from a welding process [1]. The ANSYS Composite PrepPost (ACP) provides all the necessary functionalities for the analysis of layered composite structures [2]. In this work, we aim to evaluate the heat distribution gradient in the PEI/Fiberglass composite resulting from the oxyacetylene welding process for hybrid bonding between the thermoplastic composite with a polymeric matrix and aluminum 2024-T3.

2. Structural Modeling

Using the ACP module of the ANSYS program, a sandwich laminate model was developed, considering the material configurations provided by TORAY, specifically 8HS, (0/90)5s, containing approximately 50% by volume of poly(ether-imide) matrix reinforced with fiberglass. The geometry adopted for simulation focused only on the welded joint area of 25 mm by 25 mm to reduce processing time, resulting in a thickness of 2.89 mm at the end of the model configuration by ACP (Prep).

2.1. Transient Thermal Analysis

For simulation, the measured temperature at the contact area (joint) of the composite with aluminum is 378 °C, while the temperature recorded at the bottom of the sample is 136.33 °C, based on experimental data. The exposure interval was 120 seconds, a duration corresponding to the welding process.

3. Results and Discussions

The simulation results indicate that the maximum heat distribution gradient of the composite is approximately 0.01545, implying that the sample will expand by about 1.545% of its original dimension due to temperature variation. With these simulation data, future experimental measurements of the process will be conducted to validate the model and determine the optimal welding conditions, taking into account the thermal behavior of the composite.

4. References

- [1] ABDULLA, Kareem Abdulghafour; SAFEENYASEENEZDEEN; AMS, Alfons. EXPERIMENTAL AND HARMONIC MODAL ANALYSIS OF COMPOSITE SPUR GEAR USING ANSYS ACP. International Journal Of Mechanical And Production Engineering Research And Development (Ijmperd). Índia, p. 15401-15416. 08 jun. 2020.
- [2] HASSAN, Najibah Binti. Thermal Analysis of Carbon Fiber Composite Structure by Finite Element Analysis. 2013. 45 f. Dissertação (Mestrado) Curso de Mechanical Engineering, Universiti Teknologi Petronas, Tronoh, 2013. Disponível em: https://utpedia.utp.edu.my/id/eprint/13688/1/DISSERTATION%2013275.pdf. Acesso em: 02 out. 2023.
- [3] KUMBHARE, Niraj; MOHEIMANI, Reza; DALIR, Hamid. Analysis of Composite Structures in Curing Process for Shape Deformations and Shear Stress: basis for advanced optimization. Journal Of Composites Science, [S.L.], v. 5, n. 2, p. 63, 23 fev. 2021. MDPI AG. http://dx.doi.org/10.3390/jcs5020063.
- [4] XIONG, Xuefeng; LI, Li; LI, Hong; ZAN, Peng. Thermal Stress Analysis for Carbon/Carbon Material Throat Lining Based on Finite Element Analysis. Journal Of Physics: Conference Series, [S.L.], v. 2338, n. 1, p. 012046, 1 set. 2022. IOP Publishing. http://dx.doi.org/10.1088/1742-6596/2338/1/012046.

^{*}Corresponding author: tuane.stefania@unesp.br

CONSTRUCTION AND VALIDATION TESTING OF A PLANETARY ROTATING SAMPLE HOLDER FOR THIN FILM DEPOSITION BY MAGNETRON SPUTTERING

Julio César de Oliveira Fermino^{1,2*}, Rubens Hesse¹, Julio César Sagás²

¹Instituto Federal de Educação, Ciência e Tecnologia de Santa Catarina, Joinville-SC ²Universidade do Estado de Santa Catarina, Laboratório de Plasmas, Filmes e Superfícies, Joinville-SC

1. Introduction

To achieve film uniformity on complex surfaces industrial PVD deposition systems use substrate movement strategies, such as double or even triple rotation. In this way, the sample trajectory is circular and double-circular respectively, which allows a more uniform thickness distribution, since the flow of sputtered atoms has a fixed nascent angular distribution during deposition [1]. In this work, we developed a rotating sample holder for film deposition by magnetron sputtering to analyze the effects of substrate movement on film thickness uniformity.

2. Experimental

The experiment was carried out in a cylindrical deposition chamber at the Laboratory of Plasmas, Films, and Surfaces of the Santa Catarina State University. The deposition system is a direct current unbalanced type II grid-assisted magnetron sputtering. The system was modified to include a rotating sample holder, consisting of a planetary gearbox with a low-cost rotational mechanical through-hole (figure 1). The sample holder system is placed in a face-to-face configuration with the target at a distance of 74 mm. Ti films were deposited on silicon substrates at room temperature for 10 minutes, at a constant current of 2.00 A and an average discharge voltage of 365 V at a working pressure of 0.40 Pa. Three different sample movement conditions were tested: stationary, rotating, and planetary rotating.

3. Results and Discussions

Figure 2 represents the thickness profile of the Ti films obtained through a profilometer. An average thickness of (611±49) nm was observed for the stationary sample, (598±51) nm for the rotating sample, and (583±6) nm for the planetary rotating sample, which results in standard deviations of 16%, 17%, and 2% respectively. In other words, the film thickness uniformity is 8 times higher in the planetary rotating sample compared to the other configurations tested.



Fig. 1. Planetary rotating sample holder and low-cost rotational mechanical through-hole.

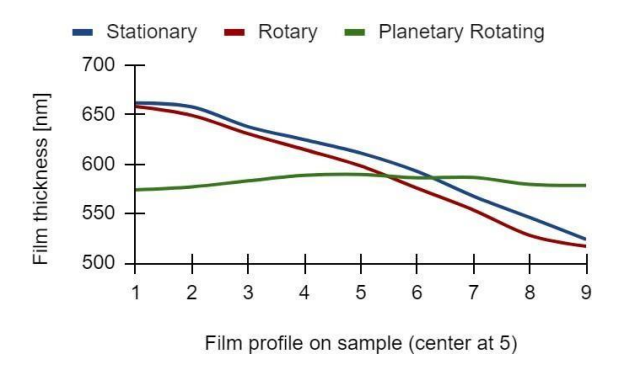


Fig. 2. *Ti film thickness onto Sis under the conditions: stationary, rotating, and planetary rotating.*

4. References

[1] PANJAN, M., ČEKADA, M., PANJAN, P., ZUPANIČ, F., & KÖLKER, W. (2012). Dependence of microstructure and hardness of TiAlN/VN hard coatings on the type of substrate rotation. Vacuum.

Acknowledgments

The authors thank FAPESC (PAP-UDESC) for financial support.

^{*}Corresponding author: julio.fermino@udesc.br

CVD DIAMOND FILMS DEPOSITED ON INTRINSIC AND BORON-DOPED SILICON WAFERWITH CRYSTAL ORIENTATION (100) AND (111)

Teófilo Miguel de Souza¹, Joelma de Oliveira¹, Evaldo Chagas Gouvêa¹, Raphaela Carvalho Machado¹

¹UNESP-DEE, Campus Guaratinguetá

1. Introduction

Synthetic diamond films deposited by CVD method comes from a gas mixture containing methane (CH₄)and hydrogen (H₂). Methane is responsible for producing methyl radical, which is the precursor of the diamond film formation. The growth technique used was Hot Filament Assisted Chemical Vapor Deposition (HFCVD)[1].

2. Experimental

A multifilament hot filament has been used to obtain CVD film. The gas flow, temperature, heating rate, pressure and time conditions were the adjusted parameters based on previous experiments. Intrinsic and boron-doped silicon wafer with crystal orientation (100) and (111) were employed as substrate after it has been polished with diamond paste (Struers $0.25~\mu m$) and cleaned up in ultrasound bath. Conditions of pressure and temperature were defined in previous step as 50 torr of pressure and substrate temperature of $800^{\circ}C$ During the optimization it was used a deposition time ranging from 120 to 180 minutes and gases flow of 100 to 200 sccm [2].

3. Results and Discussions

The obtained CVD diamond films were observed using a high-resolution scanning electron microscope model JEOL 7500F field emission (FEG-SEM) and a high resolution CCD camera installed at the Institute of Chemistry of Araraquara (IQ-UNESP), operating in secondary electrons (BSE). The micrographs were made in the normal plan to film for observation of diamond CVD crystals size and distribution and also in longitudinal plan for the film thickness observation. Results showed that the total flow value of 125 sccm and deposition time 120 minutes were sufficient to achieve films with thickness between 4 and 5.5 micrometers (Fig. 1).

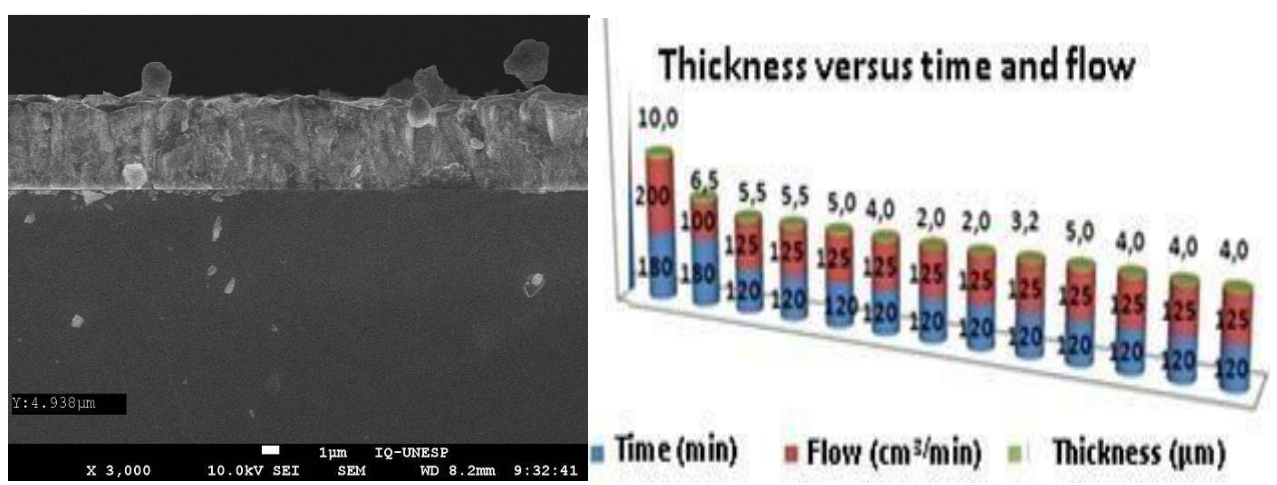


Fig 1.Electron micrographs thickness of CVD diamond film samples obtained with SEM. 3000x

This work presented the micro structural characterization produced by hot-filament assisted chemical vapour deposition (HFCVD). The 111 and 100 oriented crystal silicon wafers were used as the substrate. Diamond films were characterized by scanning electron microscope (SEM). Research suggests that doping has no interference in the morphology and thickness. Substrate crystallographic orientation presented no interference to film depositionor growing rate, but a deeper study is necessary to final conclusions.

4. References

[1] A. Götze, N. Striegler, A. Marshall, P. Neumann, C. Giese, P. Quellmalz, P. Knittel, *Phys. Status Solidi RRL*. 2021, 2100373

[2] P. Schätzle, A. Götze *Phys. Status Solidi A* 2023,220, 2200351

Acknowledgments

Acknowledgment: FAPESP and EDP.

^{*}Corresponding author: teofilo.souza@unesp.br

DENSIFICATION OF PLASMA DEPOSITED SIO_X BY LOW ENERGY CHEMICAL REACTIONS

Rita de Cássia C. Rangel^{1*}, Elidiane C. Rangel², Nilson C. Cruz², Maria Eliziane P. Souza³

¹Federal University of ABC - UFABC, ²Technological Plasma Laboratory, Paulista State University - UNESP ³Technological Center, Federal University of Maranhão

1. Introduction

Although several works in literature report on the effect of the plasma excitation parameters on the properties of Si based layers deposited from hexamethyldisiloxane (HMDSO) plasmas, the effects of homogenous reactions and heterogeneous high energy interactions are still under discussion. Considering that, this work aimedto investigate the possibility of inducing structural crosslinking and densification of SiO_x networks by controllinglow energy reaction mechanisms.

2. Experimental

Films were deposited for 300 s from 2% of HMDSO, 86% of O₂ and 12% of Ar mixtures at a working pressure of 9.5 Pa. Radiofrequency signal was used to excite the plasma in a way to not deliberately induce ion bombardment of the growing layers. The power of the radiofrequency excitation signal, P, was changed from 100to 300 W to alter the plasma energetics while preserving the oxide nature of the coatings. Film thickness and deposition rate were determined from data acquired by profilometer. Molecular structure and elemental composition were evaluated by infrared and X-ray photoelectron spectroscopies. Surface topography and roughness were determined by atomic force microscopy. Nanoindentation and scratching tests were employed toevaluate the mechanical and tribological properties of the films. Electrochemical impedance spectroscopy enabled the determination of the corrosion current density and potential as well as the layer porosity.

3. Results and Discussions

Non-stoichiometric SiOx films were homogeneously deposited on the surface of the substrates with the content of organic and hydroxyl contaminants dependent on P. The structure crosslinking and the quality of the oxide were observed to scale with the proportion of OH groups. Mechanical, tribological and barrier properties improved with the increment of crosslinking and with moieties elimination.

Acknowledgments

The authors thanks to Fapesp (2020/06448-7) and to ABC Federal University for financial support.

^{*}Corresponding author: rita.rangel@gmail.com

DEPOSITION OF GRAPHENE OXIDE ON METALLIC SUBSTRATE VIA CLASSICAL AND MODIFIED ELECTROPHORETIC DEPOSITION

Bruna Segat^{1*} and Daniela Becker¹

¹Laboratory of Plasmas, Films and Surfaces, Santa Catarina State University (UDESC), Joinville, Brazil.

1. Introduction

Electrophoretic deposition (EPD) is an important technology for coating surfaces with thin films from suspensions. However, when the process is conducted with water and high voltages are used, bubbles can form on the working electrode, creating a heterogeneous, weak, and porous deposit [1]. An efficient way to reduce gas bubbles on electrodes using aqueous suspensions is to carry out the EPD process under modulated electric fields, such as alternating current (AC) [2]. This work aims to evaluate the deposition of graphene oxide on a flat metallic substrate through the classical (direct electric current and low voltage) and modified electrophoretic deposition process with high-voltage pulses, using aqueous suspension.

2. Experimental

Before the EPD process, graphene oxide (GO) suspension was prepared in aqueous medium with 1 mg/mL. The suspension was sonicated for 1 hour and 20 min. For the depositions, the Supplier DC Power Source (ABiPPS) electrical source was used. The distance between the electrodes in the reactor was 4 cm. Classical deposition was conducted under direct electric current with a voltage of 10 V. The modified deposition was conducted with alternating positive pulses of +600 V and negative pulses of -600 V. The pulse train was composed of two pulses (2p+ and 2p-) and lasted 1 μs, with the interval between each pulse train being 20 μs. Depositions were conducted for 5 min. During the EPD process, an ultrasonic bath at 30 kHz was used to stir the suspension. The samples were characterized by scanning electron microscopy (SEM).

3. Results and Discussions

Fig. 1 shows the voltage waveform for the modified deposition process, in which high-frequency bipolar pulses with high voltages are used. Fig. 2A shows the SEM result for classical deposition and it is possible to observe regions without deposition (red circle), while for modified deposition (Fig. 2B) the entire surface was covered by GO. Furthermore, even using water and high voltage, the deposition did not show cracks, probably due to the high frequency, so there is no time for water electrolysis to occur. Thus, the electrophoretic deposition process with high voltage pulses resulted in a more homogeneous deposition.

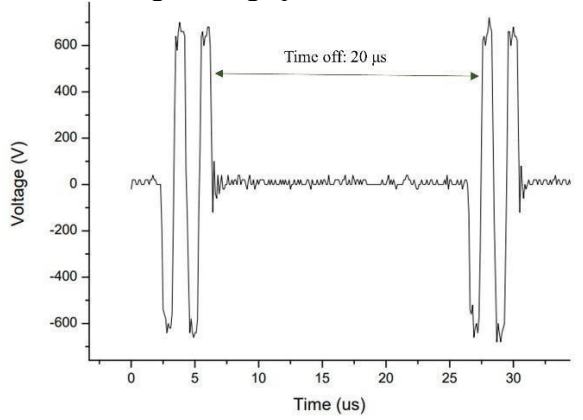


Fig. 1. Voltage waveforms of positive and negative pulses observed in modified EPD process.

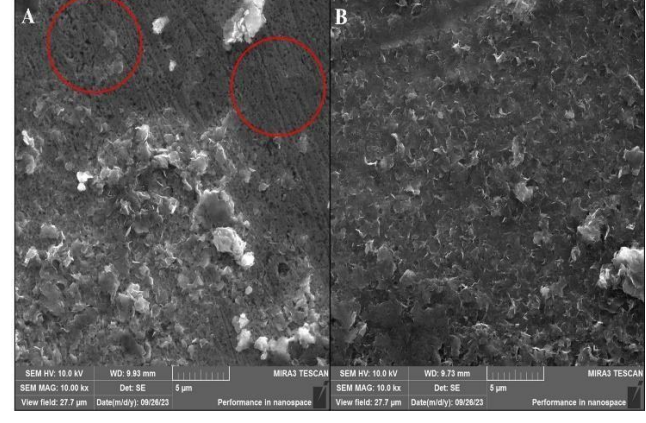


Fig. 2. SEM of GO deposition by A) classical and B) modified electrophoresis.

4. References

- [1] M. Diba et al, Progress in Materials Science, **82**, 83-117, (2016).
- [2] M. Ammam, RSC Advances, 2, 7633-7646, (2012).

Acknowledgments

The authors are thankful for the Multi-User Facility infrastructure from Santa Catarina State University's Technological Sciences Center for analysis, FAPESC and CAPES for the financial support.

^{*}Corresponding author: brusegat@gmail.com

DESENVOLVIMENTO DE UMA INTERFACE EM PYTHON PARA SIMULAÇÃO DE MATERIAIS EM MULTICAMADAS PARA CONTROLE DE INTERFERÊNCIA ELETROMAGNÉTICA

Glauber Rogério Lanziloti Alves^{1,2}, Mariana Aparecida de Assis Souza^{1,2}, Ana Paula Oliveira¹, Braulio Haruo Kondo Lopes¹, Mauricio Ribeiro Baldan^{1*}, Divani Carvalho Barbosa²

¹Instituto Nacional de Pesquisas Espaciais, Av. dos Astronautas, 1758, Jardim da Granja, São José dos Campos, SP, Brasil

1. Introdução

Esse trabalho tem como foco a linha de pesquisa e desenvolvimento de materiais para controle e Interferência EletroMagnética (EMI). O estudo da prevenção e mitigação de EMI é de grande interesse científico, pois, refere-se ao controle, através de revestimento de diferentes materiais, da interferência indesejada de sinais eletromagnéticos em eletrônicos e antenas, o que pode ocasionar distorções ou mau funcionamento em sistemas de comunicação como exemplo: ruídos, perda da qualidade de sinal, mau funcionamento, superaquecimento e atémesmo danos permanentes em ambientes sensíveis e críticos. Aqui propõe-se o desenvolvimento de um softwareem linguagem de programação Python que seja capaz de simular diferentes materiais com diferentes estruturas para controle e interferência eletromagnética (EMI).

2. Experimental e Teórica

Inicialmente as amostras são analisadas através do equipamento VNA (Analisador de Rede Vetorial) paraa obtenção dos parâmetros eletromagnéticos experimentais, essa análise fornece os dados que serão usados como parâmetros de entrada no software. O software retorna de resultado a plotagem de gráficos com as propriedades eletromagnéticas do material como: permeabilidade magnética relativa, permissividade elétrica relativa e a perdapor reflexão que são calculadas inicialmente em função da frequência e espessura. Posteriormente, o software simula computacionalmente a perda por reflexão em função da espessura do material, bem como, simula diferentes materiais em distintas camadas e sequência de empilhamento (multicamadas) de maneira que o usuáriopossa definir qual apresentaria melhor absorção de EMI de acordo com a aplicação desejada.

3. Resultados e Discussões

A Figura 1 apresenta o equipamento VNA onde são obtidas as propriedades do material como frequência, permeabilidade magnética relativa e permissividade elétrica relativa. A Figura 2 apresenta a interface do software desenvolvido nesse trabalho, onde tem-se o gráfico representando a perda de reflexão calculada versus a frequência e três barras de rolamento. A princípio esse gráfico é plotado com a espessura de camadas da amostraobtida experimentalmente, as barras de rolamento permitem ao usuário a simulação de diferentes espessuras de cada camada individualmente obtendo automaticamente a plotagem do gráfico na tela. Assim, o usuário conseguesimular qual apresentaria melhor absorção de EMI, ou seja, onde se tenha menor perda por reflexão.

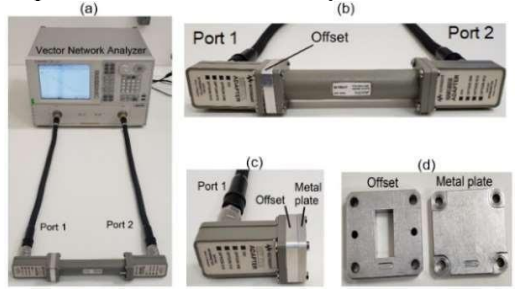


Fig. 1. (a) Equipamento VNA, (b) Sistema de montagem do guia de onda, (c) e (d) Vista frontal e individual do offset e da placa metálica, respectivamente.

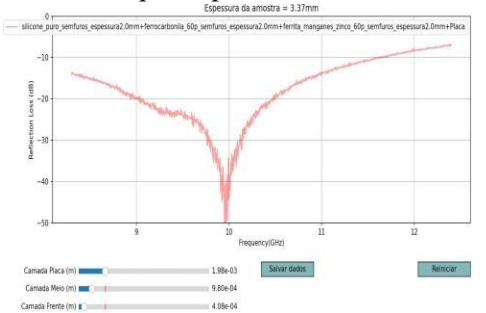


Fig. 2. Frequência (GHz) versus Perda por Reflexão (dB) simulada computacionalmente para uma amostra composta por três camadas de materiais diferentes.

Agradecimentos

Programa PIBIC/INPE 2023-2024 do CNPq.

²Faculdade de Tecnologia de Taubaté, Av. Tomé Portes Del Rei, 525, Vila São José, Taubaté, SP, Brasil

^{*}Autor correspondente: mauricio.baldan@inpe.br

DESIGN OF A VACUUM CHAMBER FOR FILM DEPOSITION BY MAGNETRON SPUTTERING

Eduardo Kressin¹, Elvis B. Silva¹, Cléber S. Kruger¹, Luiz E. Prince Goehr², Francisco Alfaro^{1, 2*}, Julio C. Sagás³ and Diego A. Duarte²

¹Centro Universitário SENAI de Santa Catarina, Campus Jaraguá do Sul.

²Universidade Federal de Santa Catarina, Joinville Center of Technology, Laboratory of Surface Treatments.

³Universidade do Estado de Santa Catarina, Laboratory of Plasmas, Films and Surfaces.

1. Introduction

Magnetron sputtering is a traditional thin film deposition method, suitable for processing of wide range of materials and scalable for industrial applications [1]. In this technique, a high vacuum level for optimal and contamination-free processing is mandatory, requiring a vacuum chamber composed of materials with chemical stability and mechanical resistance. Among the options available, stainless steel is the most used due to its inert surface and resistance to high-pressure gradients [2]. Thus, this work presents details of a vacuum chamber made in stainless steel for film deposition by magnetron sputtering, focusing on design and material selections.

2. Experimental

The cylindrical chamber, with 400 mm diameter and height, 4.25 (side) and 10.00 mm (top and base) wall thicknesses, was designed in *SolidWorks* and evaluated wall deformation under 1 atm pressure gradient. The position of the flange for the vacuum system and other features such as flow and energy of the sputtered particles, as a function of the target-to-substrate distance, were evaluated through SIMTRA software [3].

3. Results and Discussions

Fig. 1 shows that the highest deformation, lower than the yield limit, was observed in the center of the top plate where the magnetron will be installed, indicating the mechanical stability of the chamber. Fig. 2 shows the number of particles reaching the substrate holder (12 cm diameter) as a function of the target-to-substrate distance, with the flange of the pumping system positioned at different places, being two positions at the base plate (blue, centered flange; red, off-center flange) and one position at the side wall (orange). The particle flow toward the centered flange decreases as the target-to-substrate increases, decreasing losses for the pumping system.

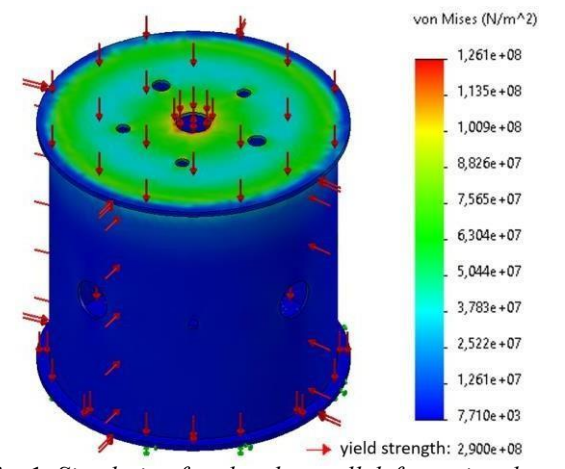


Fig. 1. Simulation for chamber wall deformation due to a 1 atm pressure difference.

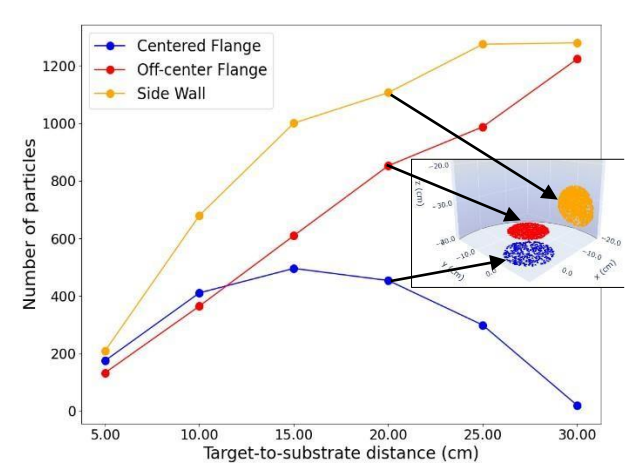


Fig. 2. Number of particles reaching key places as a function of the target-to-substrate distance.

4. References

- [1] J. T. Gudmundsson, D. Lundin, High power impulse magnetron sputtering, Elsevier (2020) 1-48.
- [2] D. M. Mattox, Handbook of physical vapor deposition processing, William Andrew Publishing (2010) 73-145.
- [3] K Van Aeken, S Mahieu and D Depla, J. Phys. D: Appl. Phys. 41 (2008) 205307.

Acknowledgments

The authors thank CNPq for the financial support (grants 307408/2021-3 and 406376/2022-0).

^{*}Corresponding author: alfaro.professor@gmail.com

DETECTION BY RAMAN 2D SPECTROSCOPY OF MWCNT INGESTION BY EARTHWORMLIVING IN CONTAMINATED SOIL

Vitória C. Pereira^{1*}, Alana M. Corá¹, Larissa S. Almeida², Gabriel A. C. Gonçalves³, Luciana S. Rossino^{1,2}, Idalina V. Aoki³, Silvia P. Irazusta^{1,4}.

¹Faculdade de Tecnologia de Sorocaba - FATEC; ²Universidade Federal de São Carlos - UFSCar Sorocaba ³Departamento de Engenharia Química da EscolaPolitécnica -USP ⁴ Programa de Mestrado Profissional em Gestão e Tecnologia em Sistemas Produtivos.

1. Introduction

There is a crescent use for multi-walled carbon nanotubes (MWCNTs) due to their high mechanical resistance, capillarity, optical and electronic properties [1]. Although the great production volume and use, the environmental impact still unknown [2]. This studies aim is to validate the application of 2D Raman Spectroscopyto validate the presence of MWCNT on earthworms.

2. Experimental

The exposed subjects were removed from the assay after 14 days, had the clitellum removed and preserved in paraformal paraformal dehyde to posterior histological sections. Once the slides were obtained, their were analyzed by 2DRaman Spectroscopy to assess the presence of MWCNT at the earthworms. The scheme made by BioRender (Fig.1) represent the process.

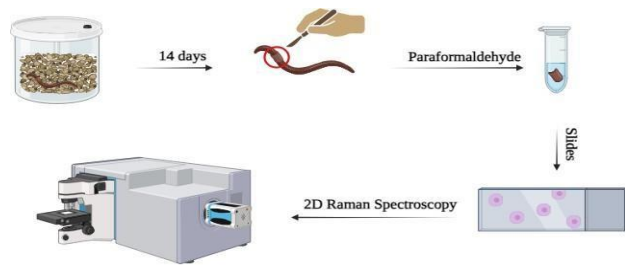


Fig. 1. *Process used to obtain the slides for 2D Raman Spectroscopy analysis.*

3. Results and Discussions

The 2D Raman analysis scheme (Fig. 2) shows the Raman spectrum for both samples, pure MWCNTs and the histological slides containing transversal section of *E. andrei* after MWCNT exposure. The Raman spectrum of the gastrointestinal tract lumen is compatible with the presence of MWCNT, the spectrum shows a peak next to 1300 cm⁻¹, characteristic band of MWCNT. Although the results are preliminary the 2D Raman Spectroscopy can be used as a valuable tool to detect the presence of these contaminants in bioindicators tissues, such as in the earthworms.

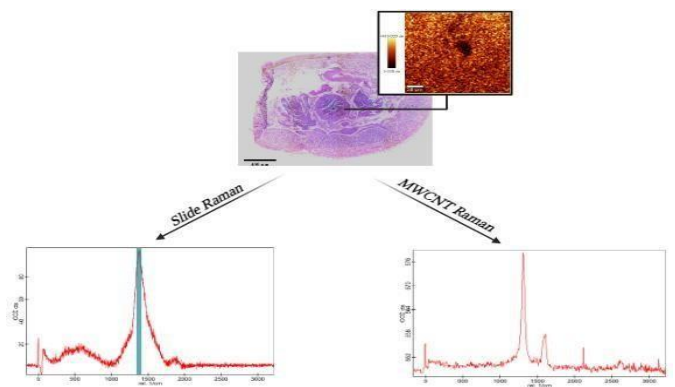


Fig. 2. Raman results from MWCNT and slides analysis.

4. References

- [1] T. L. A. Montanheiro, et al. Journal of Materials Research, 30, 55-65, (2015).
- [2] A. Albini, et al. International Journal of Nanomedicine, 10, 6133-3145, (2015).

Acknowledgments: To Instituto de Patologia e Citologia de Sorocaba for making the histological slides.

^{*}Corresponding author: vitoriapereira409@gmail.com

DETERMINAÇÃO DA VELOCIDADE DE DEPOSIÇÃO DO FILME DE DIAMANTE CVD POR PESAGEM

Raphaela Carvalho Machado¹, Teófilo Miguel de Souza¹, Evaldo Chagas Gouvêa¹

¹Universidade Estadual Paulista - UNESP-DEE, Campus de Guaratinguetá

1. Introdução

Um método alternativo ao microscópio eletrônico de varredura para se determinar a velocidade de deposição da amostra é o método da pesagem. A medida da massa da amostra é feita antes e após a deposição, supondo filme homogêneo em espessura sobre toda a superfície superior do substrato [1].

2. Procedimento

A espessura média do filme de diamante e_{filme} , conhecendo-se as densidades do filme e do substrato e a espessura do substrato, medida por um micrômetro digital, é dada pela Equação 1.

$$=_{\text{filme}} - \frac{\frac{m_{\text{filme}}}{P_{\text{filme}}}}{m_{\text{sub}} \sqrt{\frac{1}{e_{\text{sub}}}}}$$
(1)

Onde:

 e_{filme} é a espessura do filme de diamante em μm ; m_{filme} é a massa do diamante em gramas; ρ_{filme} é a densidade do diamante em g/cm 3 ; m_{sub} é a massa do substrato em gramas; ρ_{sub} é a densidade do material do substrato; e_{sub} é a espessura do substrato em μm .

Os valores de densidade adotados são valores já tabelados, onde a densidade do filme de diamante é ρ_{filme} = 3,51524 g/cm³ e a densidade do substrato usando a liga Ti6Al4V é ρ_{sub} = 4,38252 g/cm³. A espessura do substrato é e_{sub} = 5 μ m. Por sua vez, a massa do diamante depositada, m_{filme} , é calculada com uma incerteza sobre a pesagem de $4x10^{-5}$ g.

Uma incerteza sobre a densidade do diamante de 0,05g/cm³ é levada em consideração devido a variação da qualidade dos filmes, que podem apresentar uma razoável proporção de fases sp² e ter influência sobre a densidade. Ainda, uma incerteza média de 5% na espessura do filme é devido ao filme ser muito fino (<10µm).

Assim, a velocidade de crescimento do material é obtida dividindo a espessura calculada do filme de diamante pelo tempo de deposição do material. Duas grandezas alternativas para representar a velocidade de crescimento do material são em espessura por tempo de deposição, µm/h, ou em massa por tempo de deposição µg/(h. cm²). Uma vantagem desta representação é que ela independente das características dos filme, apenas de sua densidade.

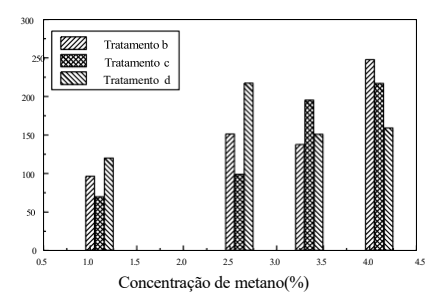
3. Resultados Experimentais

Os resultados experimentais foram obtidos usando uma balança com precisão de 2x10⁻⁵ g. Um reator de filamento quente foi utilizado com uma temperatura constante de 600°C e variação da concentração de metano de 1,0% a 4,0% dentro da mistura gasosa hidrogênio-metano, fluxo de 200sccm, com um tempo de crescimento de 8 horas.

De acordo com os resultados obtidos, foi observado que existe limpeza da superfície para o tratamento do substrato somente com Al₂O₃ e ácido oxálico, porém não produz os núcleos de iniciação do crescimento do filme de diamante. Entretanto, em 8 h há um acréscimo de massa do substrato, de acordo com o aumento da porcentagem de metano na mistura gasosa, sendo 0,06943% para 1% de CH₄, 0,08665% para 2,5% de CH₄ e 0,09639% para 4% de CH₄, pela difusão de átomos de carbono e hidrogênio na liga.

As Figuras 1 e 2 mostram as velocidades de deposição do filme de diamante, em μm/h e μg/(h. cm²) respectivamente. Verifica-se que a maior velocidade de crescimento é para uma mistura gasosa com 4% de metano, com morfologia não homogênea e sempre há descolamento do filme para maiores tempos de deposição. Há também o maior acréscimo na massa da amostra. Uma concentração de 2,5% de metano apresenta uma velocidade de

deposição relativamente alta e menor descolamento do filme para o tempo de deposição de 8 horas.



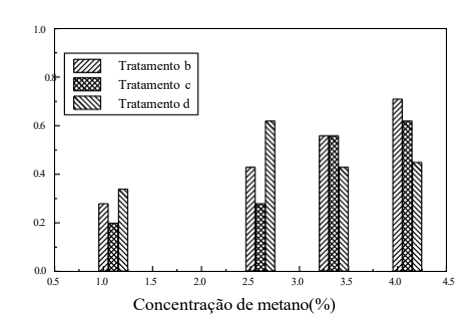


Fig. 1. Velocidade de deposição da amostra em $\mu g/(h.cm^2)$.

Fig. 2. Velocidade de deposição da amostra em μm/h.

Portanto, os resultados obtidos apresentados neste trabalho são considerados satisfatórios, visto que foi possível determinar, como método alternativo, a velocidade de deposição do material a partir da massa e espessura do filme de diamante. Futuramente, pretende-se utilizar o microscópio eletrônico de varredura e comparar com os resultados obtidos neste trabalho.

4. Referências

[1] A. Götze et al. Preferential Placement of Aligned NV Centers in CVD-Overgrown Diamond Microstructures, Physica Status Solidi (RRL), (2021).

Agradecimentos

Os autores agradecem a FAPESP (Fundação de Amparo à Pesquisa do Estado de São Paulo) e EDP São Paulo pelo suporte financeiro.

^{*}Corresponding author: raphaela.machado@unesp.br

DEVELOPMENT OF A HYBRID ADDITIVE MANUFACTURING AND PLASMA JET EQUIPMENTFOR PLA SCAFFOLD CONSTRUCTION

Anderson de Carvalho Fernandes¹, ^{2*}, Lais Bastos da Silva Lima², Julio César Sagás², Daniela Becker²

¹Centro Universitário SENAI/SC Campus Joinville ²Laboratório de Plasmas, Filmes e Superficies, Centro de Ciências Tecnológicas, Universidade do Estado de Santa Catarina - UDESC

1. Introduction

Additive Manufacturing (AM) is a layer-by-layer manufacturing process [1] with promising applications like the construction of biological supports (scaffolds). Some requirements for scaffolds are biocompatibility, mechanical strength, and cell adhesion. PLA, a thermoplastic polymer, meets some requirements but has low bioactivity. The surface treatment using a plasma jet can increase hydrophilicity and surface energy, crucial factorsfor improving cell adhesion and proliferation. Our goal is to couple of a remote plasma jet [2] with an AM equipment to activate the PLA surface in-line.

2. Experimental

The AM equipment is a Creality Ender 5 plus with a print area of 350x350x400mm. We change the extrusion system as well as the printing table to couple the plasma jet system. An Ar dielectric barrier discharge is generated between a high-voltage electrode coated with glass and a copper wire inserted inside a plastic tube. The Ar gas flows through the tube with the wire, that is connected to the AM equipment. A remote plasma jet is formed between the wire tip and the table.

3. Results and Discussions

In the first tests, the plasma jet interfered with the AM equipment, triggering the motor and pulling it closer to the extrusion nozzle. To address this issue, we modified the electrical network and eliminated potential sources of noise. In the initial tests, the table consisted of a grounded aluminum electrode covered with a glass plate. However, the plasma jet was not directed toward the table as intended but transferred to the AM equipmentnozzle. Removing the glass plate, the system operated without interference, generating the plasma jet (Fig. 1) overthe aluminum surface and producing a test specimen (Fig. 2).

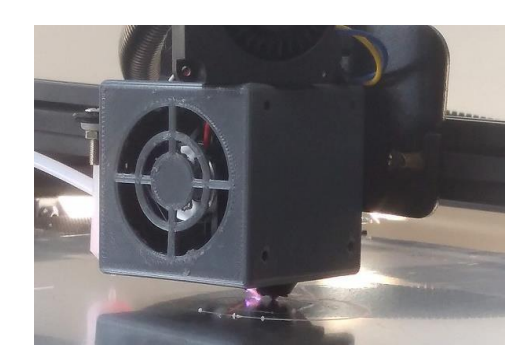


Fig. 1. Plasma jet during the AM process



Fig. 2. Test specimen

Based on preliminary tests, the hybrid additive manufacturing and plasma jet equipment proved viable, operating without interference during the fabrication of the test specimen with the assistance of the plasma jet.

4. References

[1] Gibson, I., Rosen, D. W., & Stucker, B. (2014). Additive manufacturing technologies: 3D printing, rapid prototyping, and direct digital manufacturing. Springer.

[2] K.G. Kostov, M. Machida, V. Prysiazhnyi, R.Y. Honda. Plasma Sources Sci. Technol. 24 (2015).

Acknowledgments

The authors would like to thank the funding agencies FAPESP (2019/27415-2) and FAPESC (2020TR1450 and 2021TR000563) for the financial support provided for this research.

^{*}Corresponding author: andersoncafer@gmail.com

DEVELOPMENT OF SODIUM AND HYDROGEN TITANATES FOR BIOCIDAL APPLICATIONS

Premiado _{2º Lugar} Bruno de Vasconcellos Averaldo Hangai*, Alexandre Zirpoli Simões

Faculdade de Engenharia e Ciências, UNESP-Campus de Guaratinguetá, Av. Ariberto P. Cunha 333, 12516-410 Guaratinguetá, SP, Brazil

1. Introduction

The propose is the synthesis of heterojunctions (Na_xH_{2-x}Ti₃O₇, $0 \ge x \ge 2$) - both in their pure form and with the presence of CTAB - and their subsequent modification using femtosecond laser and electron beam techniques to enhance the biocidal activity of these semiconductors. In this initial stage, the synthesis and characterization of the heterojunctions were carried out, along with the study of photoluminescence assays to understand the distribution of defects in the structure. To confirm the successful synthesis of the heterojunctions (both pure and with CTAB surfactant), analyses were performed using X-ray Diffraction (XRD) and Raman spectroscopy. Scanning Electron Microscopy (SEM) images provided data to identify the obtained morphology. Finally, photoluminescence assays and their deconvolutions were conducted to identify the type of defect present in the structures.

2. Experimental

For the synthesis of the heterojunction, initially, a 1M NaOH solution was prepared with a volume of 100 ml. Titanium IV butoxide, with a purity of 97% (Aldrich Chemistry), was used as the precursor. At this stage, two samples were prepared, one bare sample and one with CTAB surfactant. The samples were stirred for 30 minutes and then placed in the microwave for 8 minutes at 160°C, with a heating ramp of 10°C/min. After this process, they were removed from the reactor, centrifuged, and washed with H₂O until reaching pH 7. Finally, they were placed in an oven for approximately 18 hours at a temperature of 80°C until they dried. The samples were then ground into powder using a mortar and pestle. After synthesis, the samples were subjected to X-ray Diffraction (XRD) analysis, Raman spectroscopy, Scanning Electron Microscopy (SEM), and photoluminescence assays.

3. Results and Discussions

The X-ray Diffraction (XRD) patterns clearly indicate the formation of the heterojunction by comparing the diffraction planes of each phase. It's important to note that the addition of the CTAB surfactant resulted in the formation of a new plane (002), indicating structural changes. Raman spectroscopy provides results that are in agreement with the XRD findings, confirming the formation of the heterojunctions. Scanning Electron Microscopy (SEM) images reveal that the obtained morphology is in the form of nanosheets. Finally, the photoluminescence assays show differences in intensity and associated energy, indicating variations in the defect distribution among the samples. Based on the obtained wavelengths, it is possible to predict a higher presence of shallow defects in the CTAB-treated sample when compared to the bare sample.

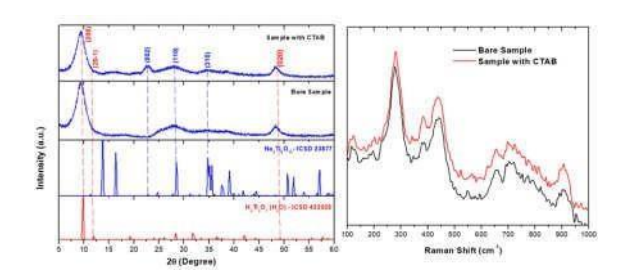


Fig. 1. Diffractogram and Raman spectra of the samples, left and right respectively.

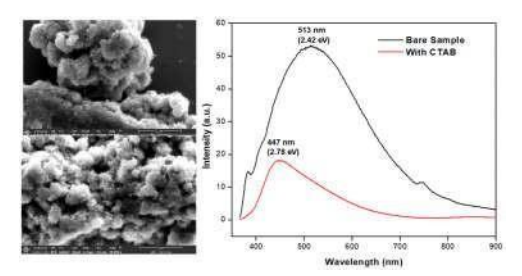


Fig. 2. Image bare sample left up, image sample with CTAB left down and photoluminescence spectra bare sample black trace and sample with CTAB red trace.

4. Reference

[1] Chrystopher A.M. Pereira, et al. "Effect of chemical potential on the structural modification of titanate-based photocatalysts: Fast dye degradation efficiency and adsorption power, J. of Alloys and Compounds, **947**, 169691, (2023).

Acknowledgments: Special thanks to FAPESP (Project number: 2021/12370-3) for supporting the research.

^{*}Corresponding author: bruno.hangai@unesp.br

DIAMOND-LIKE-CARBON COATINGS DOPED WITH GADOLINIUM: STUDY OF MECHANICAL AND TRIBOLOGICAL PROPERTIES OF COATING PRODUCED BY HIPIMS

Marcos Alves Fontes^{1*}, Fábio Emanuel de Sousa Ferreira², Albano Cavaleiro²

¹Instituto Federal de Educação, Ciência e Tecnologia de São Paulo, campus Sertãozinho ²Universidade de Coimbra, CEMMPRE (Centre for Mechanical Engineering Materials and Processes, Department of Mechanical Engineering)

1. Introduction

Diamond-like-Carbon (DLC) films have been used as coatings due to their low friction coefficient and high wear resistance and hardness (CoF) [1]. Despite the excellent tribological and mechanical properties, several studies have been carried out regarding the doping of films with different metallic elements to improve some properties [2,3]. The Gd, a rare metal element, can be introduced in the DLC matrix, incorporated as a single atom, and improve the surface adsorption and reactivity of ionic liquids. However, many demanding applications require good performance across the different regimes (from boundary to hydrodynamic). Acrossall regimes, the boundary regime is the most demanding, where metal-to-metal contact occurs. Therefore, it is essential to study the influence of the doping elements (Gd) on the performance of the doped-DLCs under the boundary regime. In this study, the Gd-DLC tribological systems were characterized by pin-on-disk test in dry conditions and by scratch test, and the mechanical properties were studied through nano-indentation.

2. Experimental

DLC films were deposited by High-Power Impulse Magnetron Sputtering (HiPIMS) technology. Different atomic concentrations of Gd in the doped-DLC coatings were obtained (1.0%, 1.4%, 2.3%, 3.7%, 5.5% and 5.8% at. concentration). Dry sliding tests in a pin-on-disk configuration at room temperature were used to evaluate the tribological properties. To evaluate the films' adhesion, the scratch test was performed using an automatic scratch tester, and the films' hardness was measured by nano-indentation.

3. Results and Discussions

The hardness and the adhesion resistance, measured by the critical load (Lc), are directly associated with the atomic % of doping element (Fig.1). For high atomic %, the hardness is below 14 GPa, and the critical load is below 20 N. Samples with higher atomic % failure much earlier compared to the other specimens. Regarding friction coefficient (Fig.2), a pure-DLC has better results than other doped samples.

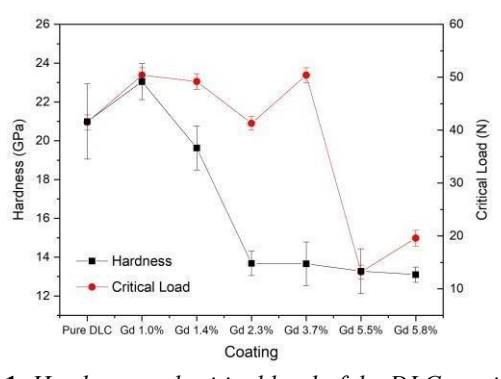


Fig. 1. Hardness and critical load of the DLC coatings.

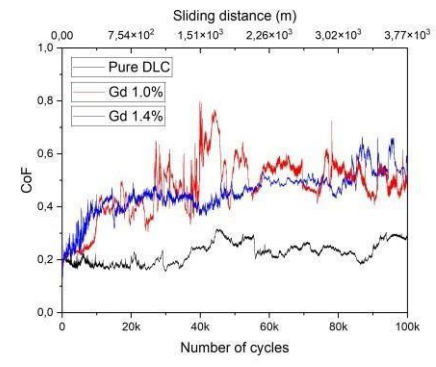


Fig. 2. The CoF of DLC films.

The difference found for hardness and adhesion resistance, can be explained by the film's morphology. A higher sp³ hybridization and a denser film, are responsible to promote a hardest coating [4].

4. References

- [1] P.S. Martins et al., Wear, 498–499, (2022).
- [2] M. Evaristo, T. Polcar and A. Cavaleiro, Lubrication Sci, 26(6), 428–439, (2014).
- [3] M.Y. Ming et al., Appl Surf Sci, 379, 424–432, (2016).
- [4] M. Evaristo, F. Fernandes and A. Cavaleiro, Coatings, 10(4), 319, (2020).

^{*}Corresponding author: marcos.fontes@ifsp.edu.br

DISCHARGE POWER DISSIPATED IN DEVICES WITH DOUBLE PLASMA IGNITION

Fellype do Nascimento¹, Kleber A. Petroski¹, Thalita M. C. Nishime², Konstantin G. Kostov¹

¹Faculty of Engineering in Guaratinguetá, São Paulo State University–UNESP, Guaratinguetá, Brazil ²Plasma Quellen, Leibniz Institute for Plasma Science and Technology–INP, 17489 Greifswald, Germany

1. Introduction

Most atmospheric pressure plasma devices work in a way that only one plasma discharge is ignited. However, some devices employ the jet transfer technique (JTT) in their design with two series discharges being ignited, usually a primary discharge (PD) and a plasma jet [1,2]. In the first case, the discharge powermeasurement is quite simple. However, in the second case, it is possible to measure only the total power dissipated in both discharges, without knowing how much is dissipated in each one. In this work, discharge power measurements were performed in a device that employs JTT, and it was possible to separate the power fraction dissipated in both PD and plasma jet.

2. Experimental

The experimental setup used in the experiments is depicted in Fig. 1. The plasma source is composed of a dielectric barrier discharge (DBD) reactor to which a long and flexible plastic tube is attached. A detailed description of the plasma source can be found in [1]. Measurements of discharge power in the PD (P_{PD}) were carried out by extinguishing the plasma jet through O_2 injection at the end of the long tube while the total power (P_T) dissipated in both discharges was measured with the plasma jet on.

3. Results and Discussions

The results of P_{PD} and P_{T} as a function of the gas flow rate (Q) is presented in Fig. 2. It can be seen that the P_{PD} does not change significantly as Q is incremented. On the other hand, the P_{T} curve presents a monotonic growth as a function of Q. This means that as Q is increased, most of the discharge power is dissipated in the plasma jet. The difference between P_{T} and P_{PD} can be attributed to the plasma jet. In most working conditions, varying parameters such as tube length, distance to target and applied voltage, it was observed that the ratio P_{T}/P_{PD} is higher than 1.0, that is, the power dissipation in the plasma jet is higher than in the PD in most cases.

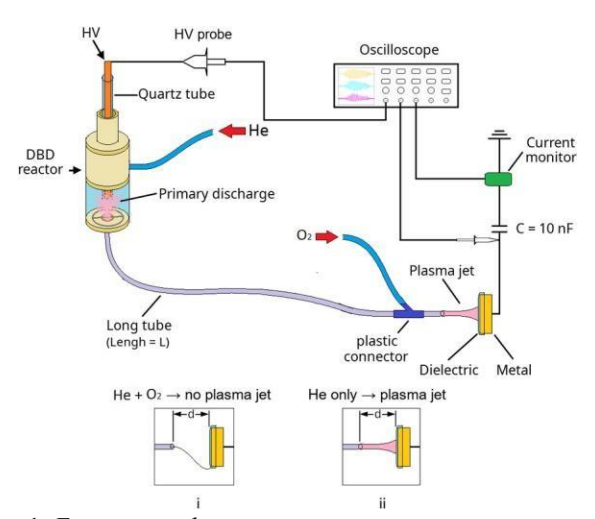


Fig. 1. Experimental setup overview.

Fig. 2. Discharge power vs gas flow rate.

4. References

- [1] K. G. Kostov et al, Plasma Sources Sci. Technol. 24, 025038, (2015).[2]
- O. Bastin et al., PMED, 10, 71–90, (2020).

Acknowledgments

This work was supported by FAPESP (grants #2019/05856-7 and #2020/09481-5) and CAPES.

^{*}Corresponding author: fellype@gmail.com

DISTRIBUTED GENERATION USING HYDROKINETIC SUBMERGED TURBINES IN NORTHERN BRAZILIAN RIVERS AS A SOLUTION FOR EXPANDING RENEWABLE ELECTRICITY GENERATION AND SERVING ISOLATED COMMUNITIES

Rogério P. Mota¹; Rafael R. Lucas¹; Carlos E. Chiaradia^{1*}, Luiz G. C. Silva¹, Felipe L. P. Rita¹, Raiane Cavadas¹

¹Faculty of Engineering and Science of Guaratinguetá, São Paulo State University (FEG/UNESP), Av. Dr. Ariberto Pereira da Cunha, 333, Guaratinguetá, São Paulo, Brazil.

1. Introduction

In Brazil, renewable sources accounted for 78.1% of the generated electricity, primarily from hydroelectric plants, which constituted 57% of the total generation [1]. An alternative is to harness the hydroelectric potential of rivers in the northern part of the country, utilizing innovative technologies that eliminate the need for dams, thereby reducing environmental impact [2]. Thus, this study aims to select hydrokinetic turbine models for electricity generation in communities within the state of Amazonas, which currently rely on diesel generators for their electricity supply.

2. Experimental

In this study, power coefficient equations, as described by Botan et al. (2016), were employed to identify the most suitable hydrokinetic turbines for the Amazon region. This process facilitated the generation of performance curves for different turbine types, including Crossflow, Savonius, Darrieus, 3-Blade Axial, 2-Blade Axial, and 1-Blade Axial (Figure 1). Through an analysis of the velocity and depth profile of the Amazon River, a more suitable area for turbine installation could be determined.

3. Results and Discussions

After evaluating the parameters of rotation range and water flow velocity of the river, it is possible to specify four types of turbines (Figure 1). Four types of hydrokinetic turbines are recommended for use in stretches of the Amazon River with flow velocities exceeding 1.5 m/s for at least 70% of the year: (1) Crossflow turbines; (2) Darrieus turbines; (3) 3-Blade Axial turbines; and (4) 2-Blade Axial turbines.

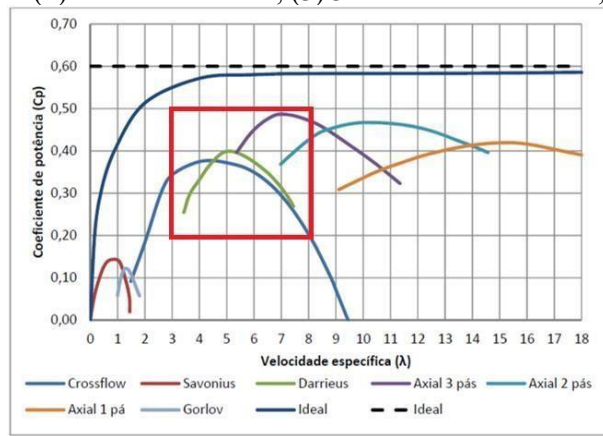


Fig. 1. Hydrokinetic turbines suitable for operation in stretches of the Amazon River with flow velocities exceeding 1.5 m/s for 70% of the year.

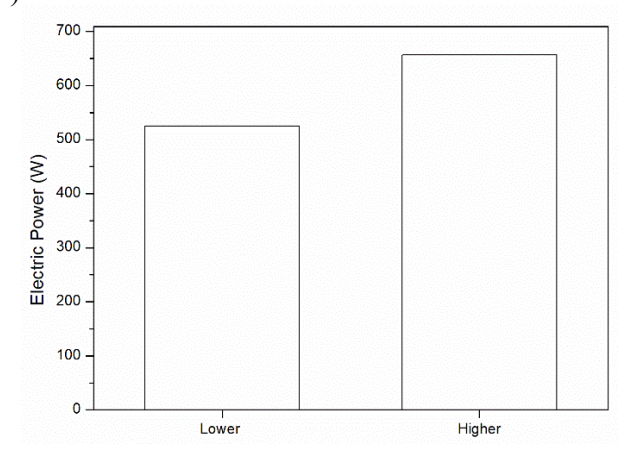


Fig. 2. Operating power range of a 3-blade turbine in regions of the Amazon River.

4. References

- [1] BOTAN F. *et al.* IFS Energia hidrocinética: aproveitamento em correntes de baixas velocidades. In: X Congresso Brasileiro de Planejamento Energético. 2016.
- [2] VITORIANO, J., ROCHA, A., & NETO, J. Production of blade for hydrokinetic turbine: High tech innovation fron low tech. *DAT Journal*, 7(1), (2022), 307–321. https://doi.org/10.29147/datjournal.v7i1.585

^{*}Corresponding author: rogerio.mota@unesp.br

EFFECT OF MULTICOMPONENT OXIDE COATINGS OBTAINED BY PEO ON THE ROUGHNESS ANDWETTABILITY OF COMMERCIALLY PURE TITANIUM FOR BIOMEDICAL USE

<u>Lauri Ruberti¹</u>, Nilson Cristino da Cruz¹, Diego Rafael Nespeque Corrêa¹ and Elidiane Cipriano Rangel¹

¹Technological Plasma Laboratory

1. Introduction

Among biomaterials options, titanium and its alloys stand out due to their favorable osteointegration and some important factors that influence this characteristic are roughness and wettability [1]. A parameter indicating the degree of roughness is the arithmetic mean of the surface topography, Ra, and the wettability parameter is the contact angle. PEO has proven to be an interesting alternative for modifying the surface of commercially pure Titanium (Ticp) due to its control and productivity. Although the corrosion resistance of Ti-cp is already high, the deposition by PEO of Zr oxides and Tantalum hydroxides can improve this virtue a little further. The objective of this work is to complement the characterization of these modifications and enrich the initial feasibility study of this process for this biomaterial.

2. Experimental

Thirty Ti-cp samples; circular in shape, 24 mm in diameter and 4 mm thick; were cut from a cylindrical billet and their circular face sanded until to 600 grit before oxidation via electrolytic plasma, PEO. Three samples were kept as a control reference without PEO treatment and the others were treated by PEO for 420 s, with voltage controlled at 500 V, pulsed at 1000 Hz in square wave with 50% duty cycle. Three types of electrolytes were used with: ZrO₂, Ta(OH)₅ and a 50/50% mixture of these two compounds. For each type of electrolyte, three concentrations were used: 2, 4 and 6 g/l. After then, the samples were analyzed by FTIR, XRD, Wettability and Roughness tests.

3. Results and Discussions

PEO treatments with a 50/50% mixture of ZrO2 and Ta(OH)5, at concentrations of 4 and 6 g/l produced superhydrophilic surfaces (Fig. 1) and the highest degrees of roughness (Fig. 2).

COMPOSITION	SAMPLE		MEAN ANGLE (°)			DROP SHAPE
		#00	78	T	-	v
Ti - CP	CONTROLE	#10	71	77	±	5
	2003/00/00/00/00/00	#20	81	1,500,00		
		#01	82	2200		
	2 g/l	#02	91	84	±	7
		#03	78	100000		
		#04				U U
ZrO ₂	4 g/l	#05	80	77	±	5
•		#06	74			, 4
	6 g/l	MO7	64			
		#08	68	66	±	3
	100000	#09				
		#11 42			U	
	2 g/1	#12	54	47	±	6
	5-20	#13	46			
	-	#14		2000000	-	ti ii
Ta(OH) _s	4 g/l	#15	30	26	±	5
		#16	22			
	6 g/l	#17	38			
		#18	50	44	±	9
		#19	8		_	
	2 g/1	#21	12			ų.
		#22	16	14	±	2
		#23	13			
	4 g/l	#24				U
ZrO2 + Ta(OH)5		#25	10	5	±	6
		#26	1			
	6 g/l	#27	1			
		#28	1	1	±	0
		#29				

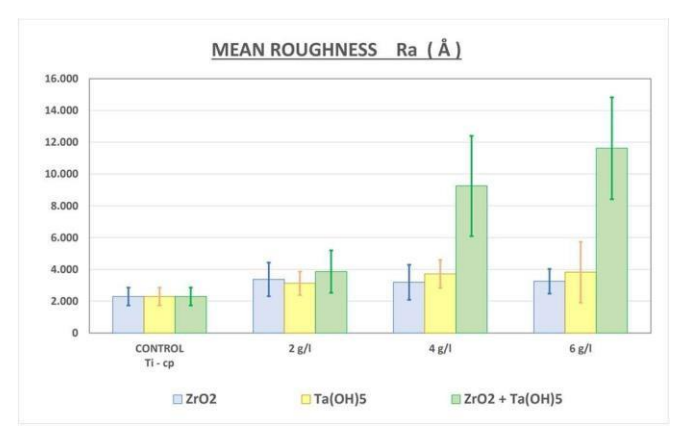


Fig. 2.

4. References

[1] ELIAS CN, MEIRELLES L. Improving osseointegration of dental implants. Expert review of medical devices, v. 7, n. 2, p. 241–256, 2010

Acknowledgments

We are grateful to the entire LaPTec's team for their support and dedication to this work.

^{*}Corresponding author: lauri.ruberti@unesp.br

EFFECT OF PLASMA NITRING ON WEAR RESISTANCE OF THE HADFIELD AUSTENITIC MANGANESE STEEL

João Vinicius Pinto da Silva¹, Miguel Rubira Danelon², Luciana Sgarbi Rossino^{1,2}, Marcos DorigãoManfrinato^{1,2}

¹ FATEC Sorocaba ² UFSCar Sorocaba

1. Introduction

The hadfield austenitic manganese steel is used in situations of high mechanical stress and wear resistance, being used in mining equipment, mainly in crusher jaws. To improve its wear resistance, plasma nitriding is the most recommended treatment, that it can be carried out at low temperatures and for short times. The nitrided layer formed by a compound layer and a diffusion layer, being responsible for increasing resistance to abrasive wearand increasing corrosion resistance in hadfield steels [1]. The objective of this work is to study the wear resistance of the hadfield steels nitreded by plasma at different temperatures.

2. Experimental

The plasma nitriding treatment was carried out using 80% of N₂ and 20% H₂ at 400°C, 450°C and 550°C by 2hours. The analysis of the treated and untreated material was performed by metallography and microhardness Vickers. The wear tests were carried out using etched ball fixed to the system that rotates in contact with a staticsample, using load of 8N, 150 RPM and time variation of 2, 5, 10, 15, 20, 25 and 30 minutes.

3. Results and Discussions

The thickness of the nitrided layer formed at 400° C, 450° C and 500° C were, respectively, $4.55 \pm 1.2 \, \mu m$, $8.5 \pm 1.2 \, \mu m$ and $20.8 \pm 1.1 \, \mu m$. The surface microhardness of the base metal, and nitrided at 400° C, 450° C and 550° C, are, respectively, 326HV, 488HV, 765HV and 641HV. The Fig 1 shows the nitrided layers. Fig. 2 showsthe wear volume as a function of sliding distance. The higher wear resistance was obtained by the nitrided sampleat 450° C. The wear mechanism was characterized by adhesion of the abrasive particles that were supposed to increase wear, which is directly linked to the surface hardening characteristic of manganese steel, the increase instrength can be improved due to nitrogen diffusion.

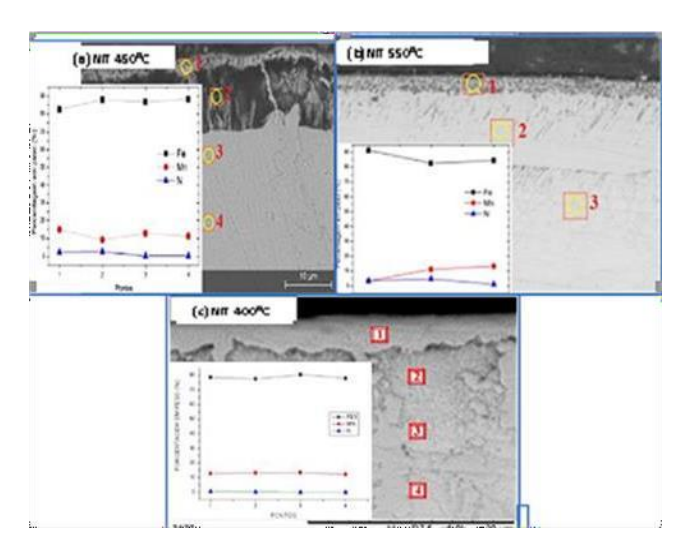


Figure 1 Micrography of the formed layer showing the punctual chemical composition by MEV/EDS

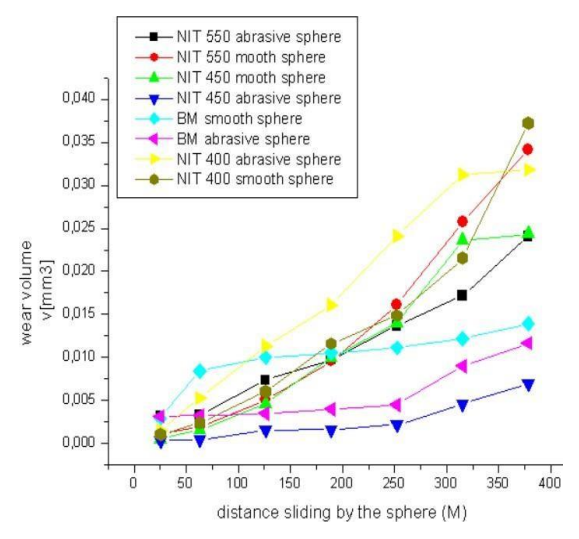


Figure 2 Wear volume of the treated and untreated hadfield steel

4. References

[1]. Sabzi, M.; Farzam, M. Materials Research Express, v. 6, n. 10, 2019.

Acknowledgments: To the CPS for the scholarship.

^{*}Corresponding author: Jvps1976@gmail.com

EFFECT OF SURFACE ROUGHNESS OF TI6AL4V SAMPLES ON THE FORMATION OF OXIDE LAYERS PRODUCED BY ABIPPS PLASMA

João Paulo Montalván Shica*, Luis César Fontana, Julio César Sagás Abel André Candido Recco

Laboratório de Plasmas, Filmes e Superfícies, Universidade do Estado de Santa Catarina – UDESC

1. Introduction

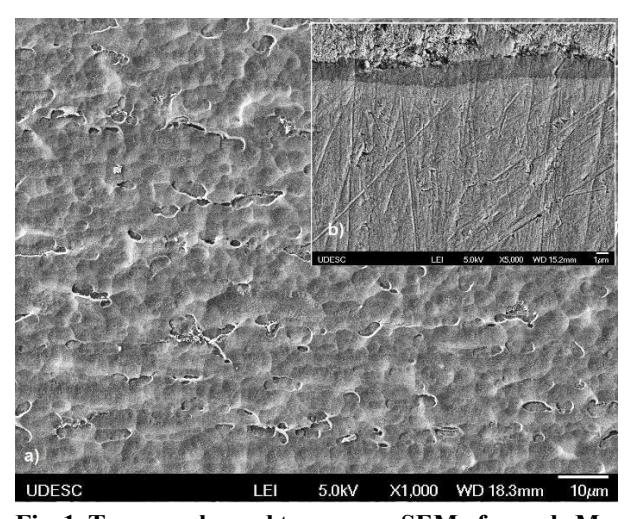
The Ti6Al4V alloy is widely used in dental implants. One of the factors that influence implantation success is osseointegration (OI). This is influenced by several factors, such as roughness. In this research, Ti6Al4V samples were oxidized by plasma using an asymmetric bipolar plasma power supply (ABiPPS). Samples with two different surface finishes were tested: machined (M) and acid-etched (AE).

2. Experimental

Plasma treatment was carried out in a 304 stainless steel reactor with mechanical pump; in an atmosphere of 70% Ar and 30% O₂. An ABiPPS power supply was used for the ignition and maintenance of the plasma. The treatment temperature was 500°C and the time was 180 minutes at a working pressure of 3.0 Torr. The characterizations presented are from SEM and XRD.

3. Results and Discussions

The topography of sample M has few machining grooves and some points with microfractures (fig. 1a), in addition, the layer formed is (1.7 ± 0.3) µm thick (fig. 1b). The roughness was (0.4 ± 0.1) µm (without treatment it was 0.6 ± 0.1 µm), indicating that there was a smoothing on the surface. For sample AE, it is possible to observe that the microcavities generated by the original chemical attack were filled, and the sharp edges were oxidized (fig. 2a). In this case, the thickness was (0.4 ± 0.2) µm (fig. 2b) and the roughness was (1.8 ± 0.4) µm (before treatment it was 1.14 ± 0.02 µm), indicating that there was an increase in roughness. The diffractogram showed the presence of anatase and rutile. A qualitative analysis of the phases fraction was carried out using the Spurr method [1], indicating that in sample U there was only formation of rutile (100%) and in sample AQ there was formation of anatase (66%) and rutile (34%).



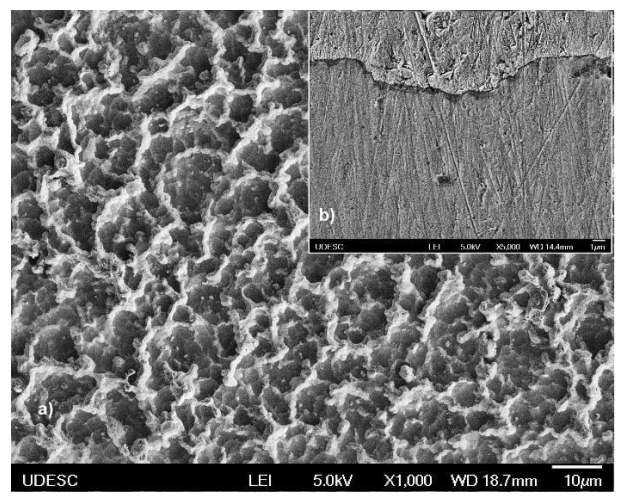


Fig. 1. Topography and transverse SEM of sample \boldsymbol{M}

Fig. 2. Topography and transverse SEM of sample AE

4. References

[1] SPURR, R. A., MYERS, H., "Quantitative analysis of anatase-rutile mixtures With an X-Ray diffractometer", Analytical Chemistry, v. 29, n. 5, pp. 760–762, May. 1957.

Acknowledgment

Thanks to CAPES, UDESC and FAPESC for financial support.

^{*}Corresponding author: eng.montalvan@gmail.com

EFFECT OF THERMOMECHANICAL TREATMENTS ON THE STRUCTURE, MICROSTRUCTURE AND SELECTEDMECHANICAL PROPERTIES OF TI-25TA-XNB SYSTEM ALLOYS, AIMING AT BIOMEDICAL APPLICATIONS

Fernanda de Freitas Quadros^{1*} and Carlos Roberto Grandini²

UNESP - Univ. Estadual Paulista, Laboratório de Anelasticidade e Biomateriais, Bauru, SP, Brazil

1. Introduction

Due to good corrosion resistance and excellent biocompatibility, titanium is widely used in biomaterials. Among titanium prostheses, alloys with a body-centered cubic structure (type β) are the most sought-after because they have better mechanical properties [1]. Like some other metals, niobium, and tantalum are excellent β stabilizing elements, capable of reducing the β transus temperature of titanium (882°C). However, the β phase structure can also be obtained through thermomechanical treatments such as solubilization. [2].

2. Experimental

The Ti-25Ta-xNb alloys (x=10,20,30 and 40% by weight) were melted in an arc furnace with an argon-controlled atmosphere under a water-cooled copper crucible. Afterward, all conditions were subjected to a homogenization heat treatment at 1000°C for 24 hours with slow cooling. To obtain samples that are appropriate for measuring elastic modulus, it is crucial to ensure that they have the proper shape; the alloys were hot rolled, reducing the thickness of the material to 4mm. Then, to relieve stress and retain the beta phase, the alloys underwent the solubilization process with rapid cooling. The samples were subjected to XRD and microscopy measurements to verify the alloys' structure and microstructure. The mechanical properties were analyzed using Vickers hardness and elastic modulus measurements.

3. Results and Discussions

The data represented in Figure 2 has been carefully examined and analyzed. It is noted that the value of the modulus of elasticity and Vicker microhardness (consider the error) of the three-phase Ti-25Ta-10Nb alloy is the highest due to the presence of the α ' and α " phases. It was verified through the X-ray diffractogram (Figure 1). From DRX, it can be seen that the Ti-25Ta-10Nb alloy was sensitive to thermomechanical treatments. This same result was also observed in other conditions.

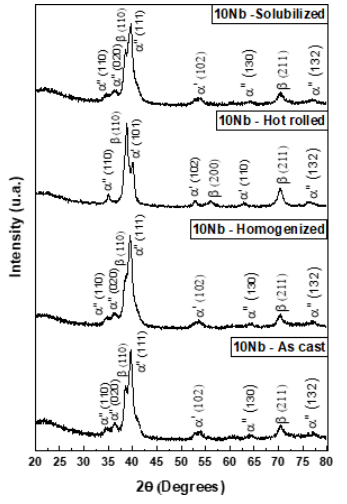


Fig. 1. X-ray diffraction pattern of the Ti-25Ta-10Nb alloy in the raw melt, homogenized, rolled, and solubilized conditions.

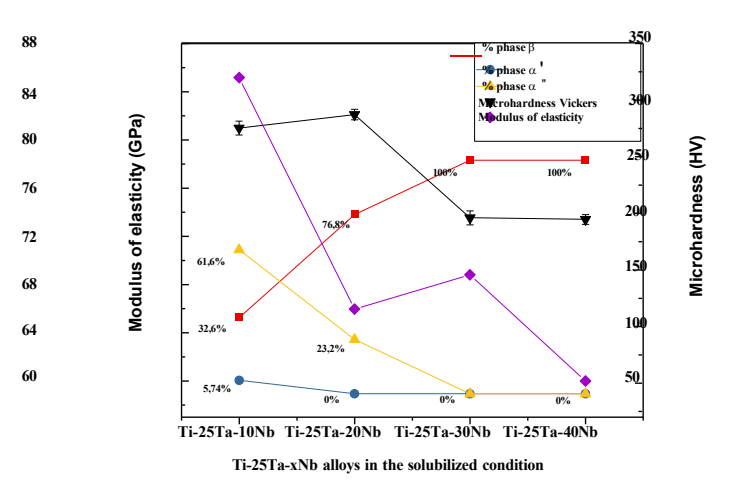


Fig. 2. Analysis between modulus of elasticity, Vickers microhardness, and percentage of phases

4. References

- [1] Pesode, P. and S. Barve, *A review—metastable β titanium alloy for biomedical applications*. Journal of Engine ering and Applied Science, 2023. **70**(1): p. 1-36.
- [2] de Freitas Quadros, F., et al., *Preparation, structural and microstructural characterization of Ti-25Ta-10Zr alloy for biomedical applications.* Journal of Materials Research and Technology, 2019. **8**(5): p. 4108-4114.

Acknowledgments: The authors thank CNPq for financial support.

^{*}Corresponding author: ff.quadros@unesp.br

EFFECT OF THE TWO-STEP ANODIZATION TIME ON THE SURFACE PROPERTIES OF NANOPOROUS ANODICALUMINA

Leandro S. Oliveira¹, Olandir V. Correa¹, Bento, R.T. ^{1,2} and Marina F. Pillis^{1*}

¹Energetic and Nuclear Research Institute, IPEN/CNEN-SP ²São Judas Tadeu University

1. Introduction

Nanoporous anodic alumina (NAA) has attracted interest due to the regular arrangement of nanopores, large specific surface area and biocompatibility, which allows its use in applications such as filtration processes, biosensors, biomaterials, catalysis, photocatalysis and humidity sensors. The geometric arrangement of the nanopores makes it possible to use NAA as a template for the synthesis of various nanostructures, such as nanotubes, nanorods and nanowires. The process is conducted through two-step anodization. On the 1st. stage there is the growth of an oxide of irregular morphology on the surface and for this reason it is necessary to have its chemical removal that results in the formation of nanoconcavities on the surface. On the 2nd. step there is regular growth of NAA and the flow of the oxide perpendicularly to the surface is observed, which results in the generation of nanotubes. The goal of this work was to produce a layer of nanoporous anodic alumina on the AA 1050 alloy and to study the influence of the anodization time on the distribution and morphology of the nanopores in the 2nd. anodizing step.

2. Experimental

Samples of 50 x 20 x 2 mm of AA1050 alloy were electrolytically polished and anodized at a constant voltage of 25 V. The electrolyte was an aqueous solution of $0.45 \, \mathrm{M} \, \mathrm{H}_2\mathrm{SO}_4$ at $20^{\circ}\mathrm{C}$. On the 1st. step of the process the samples were anodized for 60 min. Then, the irregular oxide layer was removed in an aqueous solution of $6^{\circ}\mathrm{p}$ H $_3\mathrm{PO}_4$ and $1.8^{\circ}\mathrm{p} \, \mathrm{H}_2\mathrm{CrO}_4$ at $60^{\circ}\mathrm{C}$ for 30 min. The samples were washed in abundant deionized water and dried. On the 2nd. step of the process, the samples were anodized for 2, 4, 5 and 6 h. The other parameters adopted in the 1st anodizing step were maintained. Scanning electron microscopy with a field emission gun, atomic force microscopy, X-ray diffraction and contact angle analyses were applied to characterize the samples.

3. Results and Discussions

All samples showed hydrophilic characteristics and the contact angle is smaller the longer the anodizing time. Increasing the anodizing time also resulted in an increase in the average size of nanopores, but with greater variability, as shown in Fig 1. The aluminum oxide layer is amorphous and presents a hexagonal arrangement (Fig 2). This layer is formed by nanotubes parallel to each other, with an average diameter ranging between 39 and 45 nm, and which grow perpendicular to the surface of the substrate. The thickness of the anodic alumina layer varied between 46 and 195 µm.

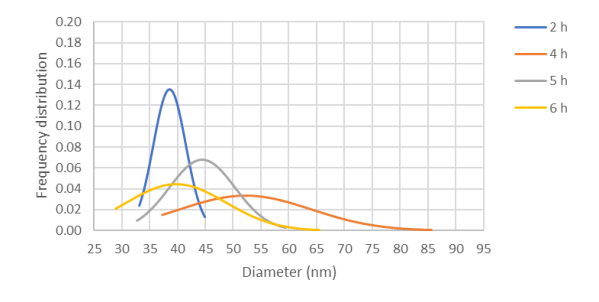


Fig. 1. Diameter nanopores dimensional analysis from test in 0.45 M H_2SO_4 aqueous solution.

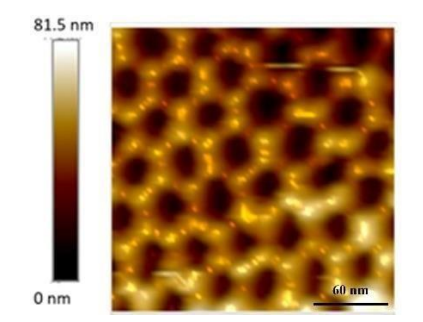


Fig. 2 AFM image of the sample surface anodized for 4h in 0.45 M H_2SO_4 aqueous solution.

Acknowledgments

The authors are grateful to the Brazilian agency CNPq (National Council for Scientific and Technological Development), grant No. 168935/2018-0.

^{*}Corresponding author: mfpillis@ipen.br

EFFECT OF ULTRASOUND ON BENTONITE CLAY SURFACES.

Beatriz Mendes Pessoa^{1*}, Marcel Guimarães Martins², Antonio Renato Bigansolli¹, João Victor Nicollini¹, Celio Lucas Valente Rodrigues², Wesley Brito Jalil da Fonseca², and Renata Nunes Oliveira¹.

¹ Universidade Federal Rural do Rio de Janeiro – UFRRJ, Seropédica - RJ ²Centro Brasileiro de Pesquisas Físicas – CBPF, Rio de Janeiro - RJ

1. Introduction

The modification of clay surfaces is a widely discussed process in the literature. Several techniques have been developed and patented for the characterization and synthesis of clays, which may or may not involve physical treatments such as freeze-drying, ultrasound, and plasma. [1] [2]

2. Experimental

Initially, 1g of the bentonite clay was weighed. This quantity is dispersed in 10 ml of deionized water, and the mixture is placed in an ultrasonic bath (Nova Instruments) for 30 minutes. After the ultrasonic bath, a sonicator (Hielscher, model UP200S) with a microtip is used to disperse the clay for 30 minutes. Next, the clay suspension is centrifuged (Eppendorf, model 5804R) for 5 minutes at a speed of 5000 rpm. After centrifugation, the clays are dried in an oven at a temperature of 80°C for 48 hours. All procedures were conducted at room temperature. Finally, the samples can be ground and used for the determination of CEC, as well as for characterization using X-ray Diffraction (XRD), Scanning Electron Microscopy (SEM).

3. Results and Discussions

The effect of exfoliation on the clay mineral is evident in the d(001) plane of the diffractogram, as demonstrated in Fig. 1. A decrease in the basal spacing was observed in the exfoliated material compared to the pure samples of BVA and BV. The use of the sonicator for clay dispersion resulted in a more pronounced basal spacing. However, it is important to mention that it was not possible to identify the d(001) peak in the sonicated BVA+S sample, as it appears amorphous, suggesting greater disorder of the lamellae. Morphological analysis demonstrates that significant changes occurred in their surfaces after exfoliation, as can be seen in Fig. 2. The applied treatment resulted in the exfoliation of the clay layers, leading to an increase in their surface area.

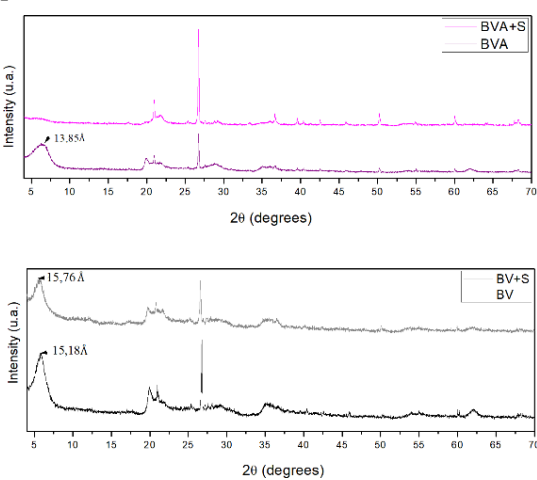


Fig. 1. Diffractometric analysis of the clay minerals BVA+S, BV+S, in their natural form compared to the sonicated form.

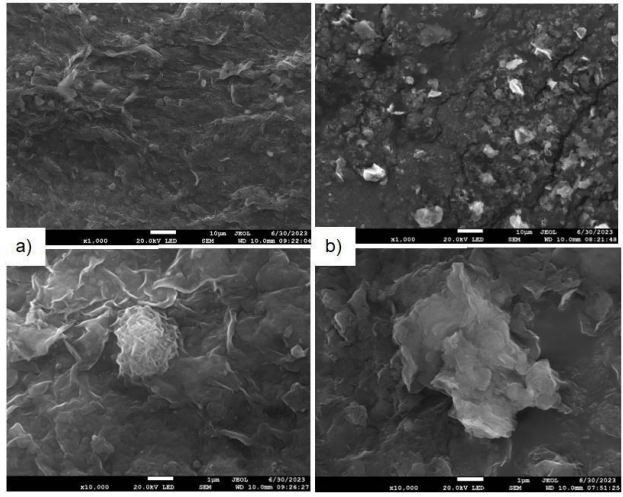


Fig. 2. Imagens de MEV para as argilas BVA+S (a), BV+S (b) (1.000x e 10.000x).

4. References

[1] SANTOS, P. S. Ciência e Tecnologia de Argilas. V. 1, ed. 2. SP: Edgard Blucher *Ltda*, 1989, 408 p. [2] TEIXEIRA-NETO, E., TEIXEIRA-NETO, A. A. "Modificação química de argilas: desafios científicos etecnológicos para obtenção de novos produtos com maior valor agregado." Química Nova 32 (2009): 809-817.

Acknowledgments: The authors are thankful to the CBPF for characterizing the clays and to Buntech Company for providing them.

^{*}Corresponding author: biamenddes@ufrrj.br

ENHANCED HIPS WITH DLC SURFACE TREATMENT BY PLASMA

Michel F. R. da Rosa^{1*}, Alana M. Corá¹, Larissa S. Almeida², Marcos D. Manfrinato¹, Luciana S. Rossino^{1, 2}

¹Faculdade de Tecnologia de Sorocaba ²Universidade Federal de São Carlos - UFSCar Sorocaba

1. Introduction

Diamond-Like-Carbon (DLC) is a thin film that can be produce by a surface treatment based on hydrocarbon precursor using plasma to their deposition, compound by ionized molecules of methane and argon, resulting in the formation of an amorphous carbon layer with sp² and sp³ hybridization. This treatment provides excellent surface properties to the treated substrate [1]. The objective of this work is to deposit the DLC film by plasma using DC-pulsed source supply on high impact polystyrene (HIPS) and determine the wear resistance of the material with and without the superficial treatment.

2. Experimental

The samples of HIPS with 12x12x2 mm dimension were treated by Plasma Enhanced Chemical Vapor Deposition (PECVD). The treatment started with ablation process using 20% H₂ and 80% Ar by 10 minutes. Subsequently, the interlayer was deposited with 70% HMDSO and 30% Ar by 30 minutes. After that, the DLC film was deposited with 90% CH₄ and 10% Ar by 130 minutes. The HIPS was treated in contact with ceramic insulation and non-insulated. The treated and untreated material was characterized by Fourier Transformed Infra- Red (FTIR) and wear test. The wear test was carried out with 1 N load and 150 RPM varying the testing time. The ATR-FTIR spectrum analyzed were performed from 400 cm⁻¹ to 4000 cm⁻¹.

3. Results and Discussions

In the FTIR result (Fig.1), the HIPS with DLC film shows the characteristic peaks between 3025 cm⁻¹ and 2850cm⁻¹, those appear on HIPS without treatment, but less intensive, because of the material chemical compound. The peaks between 1028 cm⁻¹ and 692 cm⁻¹ characterize amorphous carbon, in the HIPS with DLC sample on metallic plate probably the intense peak observed can by explained for the rise interaction between oxygen and the silicon add by the treatment. [1]. On HIPS sample without treatment is possible to observe less intense peaks, while on HIPS with DLC intense peaks are seen, possibly explained for the DLC film formation, such as the appearance of new peaks between 2000 cm⁻¹ and 1500 cm⁻¹, that possibly means that the carbon-oxygen interaction increased. Figure 2 shows that the sample treated on ceramics insulator present stable results and higher wear resistance while both samples, non-isolated and pure HIPS, showed wear volume variation.

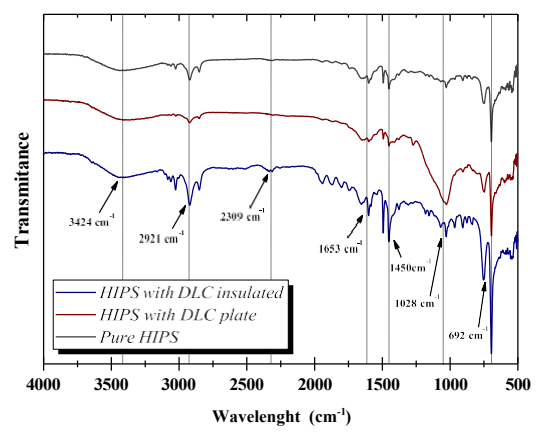


Fig. 1. FTIR samples with and without DLC film deposition.

Fig. 2. Wear test on HIPS with and without DLC film deposition.

4. References

[1] L. S. Almeida, et al. Rev. Bras. Apl. Vac., 39, 42-55, (2020).

Acknowledgments

To Faculdade de Tecnologia de Sorocaba for provide the necessary equipment.

^{*}Corresponding author: michel.rosa@fatec.sp.gov.br

EVALUATION OF ANTITUMORAL EFFECTS OF RINGER LACTATE SOLUTION TREATED WITH PLASMA AT ATMOSPHERIC PRESSURE ON THE MIGRATION AND PROLIFERATIONOF MURINE MELANOMA CELLS (B16F10) IN VITRO.

Diego V. Neves¹, Kaique G. Hergesel¹, Daiane M. Lima¹, Maria V. F. Fragoso¹, Keren A. S. Moura¹, Juliana P. Santos^{1,4}, Amanda D. R. Lima³, Breno B. Ferrari³, Fernando Pradela³, Leonilda M. B. Santos³, Elidiane C. Rangel², Nilson C. Cruz², Elaine C. Oliveira^{1,3}

¹ImunnoCell Laboratory – FATEC, CEETEPS-SP ²UNESP – Paulist State University ³University of Campinas – UNICAMP, ⁴UNIP – Paulist University

1. Introduction

Atmospheric Pressure Plasma (APP) are produced applied high voltages to a gas in ambient pressure. Owing to their high concentrations of reactive oxygen- and nitrogen- reactive species (RONS), APP has shown to be a promising anti-cancer therapy.[1]. Melanoma is the most aggressive cancer, resulted from accumulative UV exposure, which induces DNA damage altering the production and liberation of melanin [2]. Although it is the least common among skin cancers, it accounts for 75% of skin cancer deaths due to its high ability to spread to lymphatic tissue and blood vessels. In this work, it has been evaluated the effects of the exposure of Ringer Lactate (Rilac) solutions to APP on migration and proliferation of Murine Melanoma B16F10 cells.

2. Experimental

Rilac solution has been activated with APP for different times (30, 45 and 60 minutes), Murine melanoma B16F10 was cultured in a complete culture medium (DMEM supplemented with 10% of fetal bovine serum, 2% glutamine and 1% antibiotic). After that cells were plated in 96 wells plate at concentration $1x10^4$ cells/ml, and incubated for 30, 60, and 120 minutes in contact with 200 μ l of Rilac. Thereafter Rilac was replaced by a complete culture medium and cells were incubated for 24 hours. Spectrophotometry was used to identify differences in the solutions as a function of treatment times and MTT assay for cell viability.

3. Results and Discussions

Differences in absorbance of the solutions are observed after the exposure to plasma (figure 1). As the exposure time is increased, the absorption peak become more pronounced and dislocated to higher wavelength. As it can be noticed in Fig. 2. the modifications induced in Rilac decreased murine melanoma B16F10 cell viability. The best results were observed in 45 and 60 minutes of APP activation and cell contact for 60 and 120 minutes.

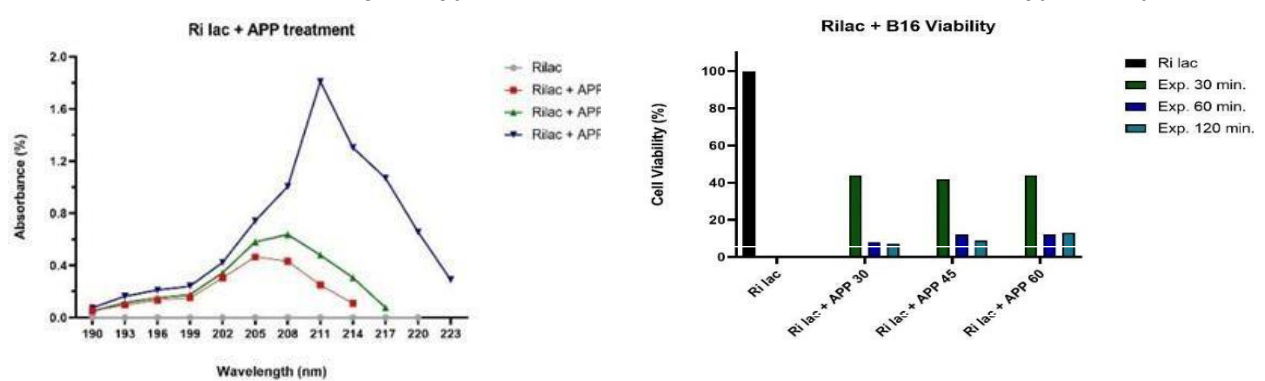


Fig. 1. Absorbance spectra of Rilac solution exposed toapp treatment for different times.

Fig. 2 Murine Melanoma B16F10 cell viabilityafter contact with APP activated Rilac. solution

4. References

[1] D. Yan, J. H. Sherman and M. Keidar, *OncoTarget, vol 8 (No. 9), Impact Journals, USA (2017).*[2] G. C. Leonardi, L Falzone, R. Salemi, A. Zanghì, D. A. Spandidos, J A. Mccubrey, S. Candido and M. Libra "Cutaneous Melanoma", *International journal of oncology 52, USA (2018).*

Acknowledgments: The authors acknowledge CPS, CNPq and Fapesp for the financial support.

^{*}Corresponding author: diegoverduino@hotmail.com

EVALUATION OF THE ANTIMICROBIAL EFFECT OF WATER ACTIVATED PLASMA ON AMNIOTIC MEMBRANECONTAMINATED BY ESCHERICHIA COLI AND STAPHYLOCOCCUS AUREUS

Felipe Santos de Almeida, Anelise Cristina Osório Cesar Doria, Luciana Barros Sant'Anna

UNIVAP – Universidade do Vale do Paraíba

1. Introduction

Extensive research has been conducted on the potential applications of the Amniotic Membrane (AM), and ensuring the sterility of this material is important for its utilization [1, 2]. The technique most widely used forits sterilization is Gamma radiation, but due to the characteristics of radiation, it can cause damage the AM layers[3]. An alternative technique to be studied for amniotic membrane sterilization is plasma activated water (PAW). Due to the formation of reactive species during the water activation process, and its low pH, PAW has shown a good antimicrobial effect [4]. Considering the biomedical applications of plasma and plasma activated water, suchas disinfection and sterilization [5], the aim of study is to evaluate the antimicrobial action of plasma activated water on Amniotic Membrane.

2. Experimental

This study was approved by the Ethics Committee of UNIVAP (n° 5.277.784). The AM remained in contact for 3 minutes with an *Escherichia coli* (ATCC® 25922) and *Staphylococcus aureus* (ATCC® 6538) inoculum at a concentration of 1x10⁶ CFU/ml in saline solution. After this period, the PAW was brought into contact with the AM for 90 minutes. The water activation was generated in a gliding arc system, using 6 L/min of argon and 4 L/min of compressed air for 30 minutes. Following the contact between AM and PAW a 1:1 solution of bacterial suspension and 2% Trypan Blue was prepared and incubated for 15 minutes, in order to studythe cell viability after exposing the AM samples to PAW. After the incubation process, a 10 μl volume was analyzed in a Neubauer® Chamber for cell viability quantification.

3. Results and Discussions

In a study involving the utilization of PAW generated by gliding arc plasma in *S. aureus* and *E. coli*, was obtained a 3 log reduction of both bacteria, but E. coli showed a greater effect to the antimicrobial effects of PAW[6], this reduction was observed in this study however the bacteria that showed a higher susceptibility to the effects of PAW was S. aureus, this finding can be explained by the use of argon and a different bacteria incubation timeand the antimicrobial effects of AM. *E. coli* and *S. aureus* were both susceptible to PAW, but it was not enoughfor sterilization. In studies that complete stopped bacteria growth the pH obtained was 2.1 and 2.3 [7] witch is significantly lower than the one obtained in this study, that was 3.41. In conclusion, the PAW had a good antimicrobial action on the microorganisms studied, although it did not stopped bacterial growth in contaminated AM.

4. References

- [1] M.S. Murri, M. Moshirfar, O.C. Birdsong, Y.C. Ronquillo, Y. Ding, P.C. Hoopes. Clin Ophthalmol. 2018;12:1105–12.
- [2] E. Jung, R. Romero, B.H. Yoon, K.R. Theis, D.W. Gudicha, A.L. Tarca. J Perinat Med. 2021;49(9):1103–21.
- [3] A.K. Riau, R.W. Beuerman, L.S. Lim, J.S. Mehta. Biomateriais. 2010;31(2):216–25.
- [4] Y. Gorbanev, D. O'Connell, V. Chechik. Chem A Eur J. 2016;22(10):3496-505.
- [5] N.K. Kaushik, B. Ghimire, Y. Li, M. Adhikari, M. Veerana M, N. Kaushik. 2018;400(1):39–62.
- [6] W. Chiappim, A.G. Sampaio, F. Miranda, M. Fraga, G. Petraconi, A. Silva Sobrinho. Water (Switzerland). 2021;13(11):1–16.
- [7] T.P Chen, J. Liang, T.L. Su. Environ Sci Pollut Res. 2018;25(27):26699-706.

Acknowledgments

We would like to express our gratitude to Coordenação de Aperfeiçoamento de Pessoal de Nível Superior - Brasil (CAPES) - Finance Code 001", process number 88887.649566/2021-00. Our thanks also extend to UNIAP and to the entire Biotec plasma for their valuable support.

^{*}Corresponding author: ferder017@gmail.com

EVALUATION OF THE CORROSION BEHAVIOR OF BETA-PAHSED TITANIUM ALLOYS AFTER EQUAL CHANNELANGULAR PRESSING

Celso Bortolini Júnior^{1*}, Tayslâine Borges Nascimento¹, João Pedro Aquiles Carlobolante¹, Roberto Zenhei Nakazato¹, Ana Paula Rosifini Alves¹

¹UNESP – Universidade Estadual Paulista, Faculdade de Engenharia e Ciências, Guaratinguetá

1. Introduction

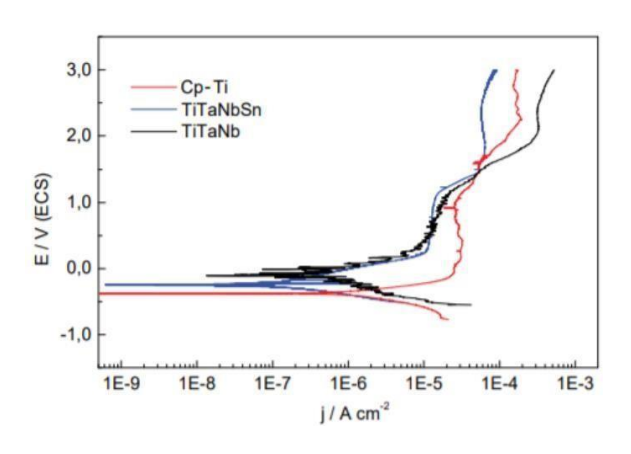
According to Williams (1987), biomaterials are natural or synthetic substances that can replace or aid any system, tissue, organ or body function [1]. Metallic biomaterials are used mostly to replace hard tissues and the production of pins and orthodontic screws, however, this class has the lowest biocompatibility among all the synthetics due to their corrosion resistance when in contact with human physiologic environment. Many metallic alloys such as Titanium alloys, which forms a passive oxide layer that protects the surface, stainless steel and cobalt-chromium alloys presents higher corrosion resistance but still are susceptible to the corrosion process which can lead to the release of ions or oxides toxics to the human body [2]. The Ti25Ta25Nb3Sn is a suitable alternative with an Elastic Modulus (E) close to the human bone's E but its mechanical resistance is below the desired level for hard tissue replacement. As a way to increase the mechanical properties the Equal Channel Angular Pressing (ECAP) was applied due to its grain reduction mechanism which increases the mechanical resistance without any alteration to the elastic modulus or chemical composition [3]. The corrosion behavior of the alloy was evaluated after the ECAP processing and compared with CP Ti and the Ti25Ta25Nb alloy.

2. Experimental

The Ti25Ta25Nb3Sn alloy was subjected to ECAP via route B_c at 773 K using samples with 40 mm length and 10 mm diameter in an L-shaped split-die with an internal channel angle, Φ , of 90° and an outer arc of curvature, Ψ , of 20.6° as shown on Fig 1. For this study the samples were subjected to 4 ECAP passes. To evaluate the corrosive behavior of the Ti25Ta25Nb3Sn alloy, an open circuit potential (OCP) and potentiodynamic polarization tests were performed in a fluorinated physiological medium, composed of 0.15 M NaCl and 0.03 MNaF, at a temperature of 37°C (± 0.5 °C) and pH of 6.0. A conventional three-electrode cell was employed, containing a platinum electrode as the counter electrode and a saturated calomel electrode (SCE) as the reference electrode. The alloy discs, with a diameter of 10 mm and thickness of 3 mm, were used as the working electrode, positioned on a sample holder with an exposed area of approximately 0.8 cm². OCP and potentiodynamic polarization measurements were performed in triplicate.

3. Results and Discussions

Comparing the corrosion current density (Jcorr) values, it is possible to observe that, the lower current passing through area unit of the alloy, the lower the breaking speed of the passive layer formed on the surface and higher will be its corrosion resistance. For this study, the Ti25Ta25Nb3Sn alloy showed a higher corrosion resistance than the Ti25Ta25Nb alloy and CP Ti.



	EOCP (V)	Ecorr(V)	J _{corr} (A/CM ²)
CP Ti	-0,39	-0,38	1,4 .10 ⁻⁶
TiTaNbSn	-0,31	-0,24	1,9 .10 ⁻⁷
TiTaNb	-0,18	-0,13	6,7 .10 ⁻⁷

Fig.1. Potentiodynamic Polarization for the Ti25Ta25Nb3Sn alloy, Ti25Ta25Nb alloy and CP Ti

Fig. 2. The corrosion parameters obtained for the Ti25Ta25Nb3Sn alloy, Ti25Ta25Nb alloy and CP Ti

4. References

[1] WILLIAMS, D. F. Tissue-biomaterial interactions. Journal of Materials science, v. 22, n. 10, p. 3421-3445,

1987.

- [2] SINHORETI, Mário Alexandre Coelho; VITTI, Rafael Pino; CORRER-SOBRINHO, Lourenço. Biomateriais na Odontologia: panorama atual e perspectivas futuras. Revista da Associação Paulista de Cirurgiões Dentistas, v. 67, n. 4, p. 256-261, 2013.
- [3] SILVA JR, Gilson et al. Estudo da influência do processo ECAP (Equal Channel Angular Pressing) nas propriedades mecânicas e características microestruturais do aço SAE 1020. 2017.

Acknowledgments

This study was financially supported by CNPq.

 $[\]hbox{* Corresponding author: $celso.bortolini@unesp.br}\\$

EVALUATION OF THE INFLUENCE OF PLASMA TREATMENT ON POLYURETHANE ON THE SORPTION OF \$500 DIESEL OIL

Lucas Cortat da Silva^{1*}, Fillip Cortat Alves², Carlos Eduardo Moraes², Rafael Resende Lucas², Edson Cocchieri Botelho² and Michelle Leali Costa^{2,3}.

 1 Department of Chemistry and Environmental, Rio de Janeiro State University (UERJ), Resende, Brazil.

1. Introduction

Oil spillage is considered one of the most serious threats to the marine and coastal ecosystem. Polyurethane (PU) has proven to be effective in oil removal due to its characteristics: being porous, oleophilic, and hydrophobic [1]. One possible way to enhance the characteristics of polyurethane is subjecting it to plasma treatment, which involves a process that modifies the material's surface through interaction with an ionized plasma, potentially improving its wettability and contributing to the enhancement of oil sorption efficiency [2]. Therefore, the aim of this study was to evaluate the influence of plasma treatment on polyurethane in the sorption of S500 diesel oil.

2. Experimental

The PU was synthesized from the polyol derived from castor oil and methylene diphenyl diisocyanate (MDI). The reagents were mixed in a 1:1 (w/w) ratio. After curing (24h), the foams were cut into dimensions of (80 x 10) mm (diameter x height). The sample identifications were as follows: PU(A), untreated polyurethane; PU(B), and PU(C), polyurethane treated with plasma for 20 and 40 minutes, respectively. Under the following conditions: Argon gas / 35W power, 1 mTorr pressure. Static sorption: The samples in triplicate were placed in beakers containing S500 diesel oil, the experiment lasted for 336 hours. At specific time intervals, the samples were removed and drainage for mass measurement. The sorption capacity of the PUs was calculated using Eq. 1. $C_S(\%) = \frac{M_f - M_i}{M_i} x \ 100$

$$C_S(\%) = \frac{M_f - M_i}{M_i} x \ 100 \tag{1}$$

Where C_S is sorption capacity, M_f and M_i are the final and initial weight.

3. Results and Discussions

As shown in Figure 1, sorption capacity was influenced by the experiment time and plasma treatment. It was noted that PU(A) exhibited significantly lower sorption capacity compared to PU(B) and PU(C), which underwent the plasma treatment. During the 336-hour test, the samples were observed to be approaching saturation, with minimal variations noted in the final measurements. The influence of plasma treatment time on the sorption difference between PU(B) and PU(C) was evident, possibly associated with surface modification of the material. When examining the FTIR of the samples, a decrease in the intensity of the characteristic -OH band (3330cm⁻¹) was observed for PU(B) and a more pronounced decrease for PU(C), indicating that plasma treatment reduces the surface polarity of the polyurethane, thus contributing to the interaction of the material with nonpolar oil.

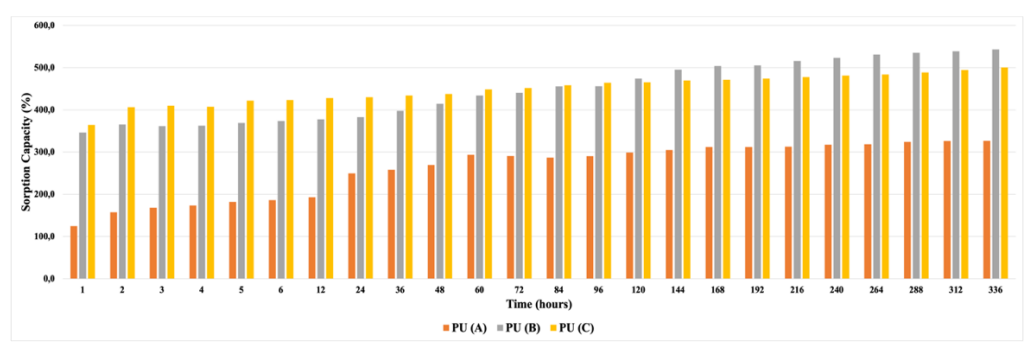


Fig. 1. Sorption capacity versus time.

4. References

- [1] F. Alves, et al. Efficiency of castor oil-based polyurethane foams for oil sorption S10 and S500: Influence of porous size and statistical analysis. Polymers and Polymer Composites. 1063-1074 (2021).
- [2] A. Uricchio, et al. Atmospheric pressure plasma treated polyurethane foam as reusable absorbent for removal of oils and organic solvents from water. Materials. 7948-7964 (2022).

Acknowledgments: The authors are grateful for the research support by CAPES – Finance Code 001; UNESP and

 $^{^2}$ Department of Materials and Technology, São Paulo State University (UNESP), Guaratinguetá, Brazil.

³Lightweight Structures Laboratory, Institute for Technological Research (IPT), São José dos Campos, Brazil.

^{*}Corresponding author: lucas.silva@discentes.fat.uerj.br

EVALUATION OF THE MODIFICATION OF THE SURFACE OF NIOBIUM BY THE PROCESS OF OXIDATION BY ELECTROLYTIC PLASMA.

Jorge Luiz Rosa^{1*}, Maria Carolina Ferraz Romão², Cristian Cley Paterniani Rita e Sergio Roberto Montoro⁴

¹Escola de Engenharia de Lorena – EEL-USP ^{1;2,3,4}Faculdade de Tecnologia – Fatec Pindamonhangaba-SP.

1. Introduction

Brazil is the world's largest producer of niobium (Nb) and niobium iron, responsible for 75% of world production. Although these alloys contain a maximum of 0.1% of niobium, this small percentage gives[1]. Recently, Niobium has aroused interest in exploring its applications in the area of biomaterials, as it presents properties in a biological environment that are biocompatible with the human body. However, its bioinert characteristics require changes in its surface properties to make it bioactive and improve its osseointegration [2]. Some techniques are very promising in modifying and improving the surface properties applied to implants, improving the relationship with bone tissue, and can be used in medical applications and mainly in the replacementof human bone and surgical elements. Due to the interesting characteristics of niobium in the technological area, it has recently aroused interest in the area of surface engineering by applying the Plasma Electrolytic Oxidation (PEO) process to promote changes in morphology and coatings [3]. This work was proposed to study the application of PEO in Niobium samples, using a DC source ranging from (0-20 A) and (0-1000 V). For electrolytic solutions, mixtures with Glycerol ($C_3H_8O_3$)+ NH₄F or propanetriol were used. Morphological analyzes were carried out by SEM and EDS.

2. Experimental

For the development of this ICTI, the premises of the Electrolytic Plasma Laboratory (LaPE), located at FATEC – Pindamonhangaba-SP, will be used. The electrolytic system that will be used in the plasma anodizing processes is shown in figure 1. The material used in this work was rectangular niobium sheets (124mm x 45mm x 02mm). Donated by the University of São Paulo (EEL-USP), figure 2.

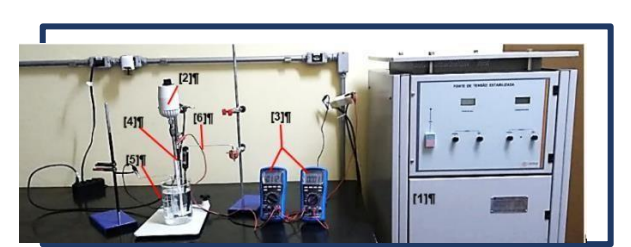


Fig. 1. Photo of the experimental arrangement - LaPE.



Fig. 2. Nb sample sanded with 1000 grit sandpaper.

3. Results and Discussions

In figure 3 end 4 Sample performed by SEM analysis with 50x and 1000x magnification, respectively, at 400V, 20 minutes in a 50% Deionized H2O Glycerol solution at pH 5.



Fig. 3. Nb sample 50x

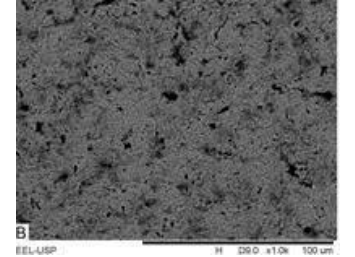


Fig. 4. Nb sample by SEM 1000x

4. References

- [1] P. Favia and R. D'Agostino, Surf. & Coat. Tech., 98, 1102-1106, (1998).
- [2] H. Yasuda "Plasma Polymerization", 2nd edition, Academic Press, USA, (1980).

^{*}Corresponding author: jorge.rosa2@fatec.sp.gov.br

EVALUATION OF THE RELATIONSHIP BETWEEN ROUGHNESS AND WETTING OFDIFFERENT IMPLANTS SURFACES.

Jorge Luiz Rosa^{1*}, Douglas Sampaio², Rogério de Lima Romeiro³ e Sandra G. Schneider⁴

^{1,4}Escola de Engenharia de Lorena – EEL-USP ^{2,3}Faculdade São Leopoldo Mandic – Campinas-SP.

1. Introduction

The objective of this study is to analyze the level of surface roughness and wettability of three different types of commercially available implant surfaces, in addition to identifying whether there is a direct or indirect relationship between these characteristics [1]. The roughness and degree of hydrophilicity of 4 implant surface samples, in disc formats, will be analyzed: 1. Machined Ti, 2. Sandblasted Ti (with titanium oxide blasting), 3. Nano Ti (with double attack acid + heat treatment + layer of hydroxyapatite nanocrystals), 4 Ti DSP Calcium Phosphate, (surface with addition of calcium phosphate) and 5. TiAIV produced by additive manufacturing [2].

2. Experimental

The figures 1a-e show the disc-shaped samples used in the figure 2, contact angle and roughness measurement experiments. .



Fig. 1. Photo of the disc-shaped samples used.

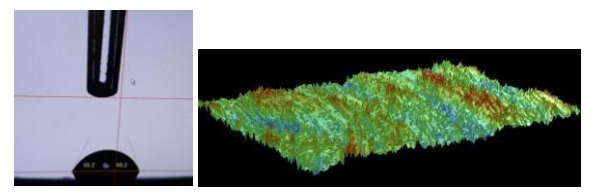


Fig. 2. contact angle and roughness.

3. Results and Discussions

In an initial analysis, it was possible to observe that the sample 4 Ti DSP Calcium Phosphate, (surface with addition of calcium phosphate), was the one that presented the lowest contact angle (Fig. 3) and with an average roughness of Ra: 761 nm (Fig. 4).

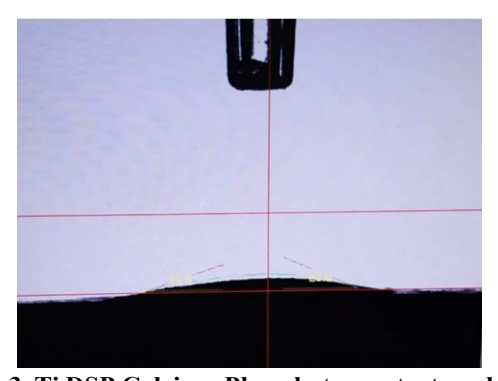


Fig. 3. Ti DSP Calcium Phosphate, contact angle

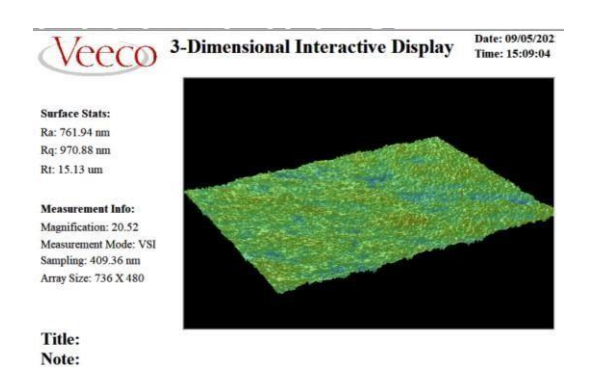


Fig. 4. Average roughness of Ra: 761 nm

4. References

- [1] Lampin M, Warocquier-Clerout R, Legris C, Degrange M, Sigot-Luizard MF. Correlation between substratum roughness and wettability, cell adhesion, and cell migration. J Biomed Mater Res 1997;36(1):99–108.
- [2] Keller JC, Draughn RA, Wrightman JP, Dougherty WJ. Characterization of sterilized CP titanium implant surfaces. Int J Oral Maxillofac Implants 1990;5:360–369.

5. Acknowledgments

Acknowledgments a Unesp., campus de Guaratinguetá-SP and INPE., de São José dos Campos-SP.

^{*}Corresponding author: jorgerosa@usp.br

EXPLORING PHYSICOCHEMICAL PROPERTIES OF BACTERIAL NANOCELLULOSE POLYMERIC FILMS DERIVED FROM ORGANIC RESIDUES

Amanda Nunes Duarte¹, Elen Gabriele dos Santos Braz¹, Milena Chanes², Alcides Lopes Leão², André Luiz Reis Rangel³, Ana Paula Rosifini Alves Claro¹

¹São Paulo State University (Unesp), School of Engineering, Guaratinguetá. ²São Paulo State University (Unesp), College of Agricultural Sciences, Botucatu. ³São Paulo State University (Unesp), Material Science Program, Ilha Solteira.

1. Introduction

Bacterial nanocellulose (BNC) represents a promising biopolymer with a broad spectrum of applications spanning multiple sectors, including the biomedical industry [1]. Despite its numerous advantages, there exist certain limitations, such as production costs and the challenge of achieving consistent BNC properties on a larger scale [2]. Recognizing this, the pursuit of natural polymers derived from organic waste emerges as a promising field due to its blend of economic viability and environmental sustainability [3]. Serving as a biomaterial, BNC boasts properties suitable for diverse applications owing to its notable purity, making it an appealing candidate for uses like wound dressings, tissue engineering, and drug delivery systems [4]. This endeavor aims to delve into the attributes of bacterial nanocellulose sourced from vinasse, an organic waste byproduct of ethanol production, for potential applications in the realm of biomaterials.

2. Experimental

The polymeric films were produced by the bacteria *Komagataeibacter xylinus*, cultured with a mix of vinasse (20 to 80%) and alabam. The films were characterized using scanning electron microscopy (SEM), contact angle, water retention, thermogravimetric analysis (TGA), and Fourier-transform infrared spectroscopy (FTIR).

3. Results and Discussions

The FTIR analysis revealed similar chemical structure in all film samples. SEM characterization suggested the possible existence of encapsulated bacteria in specific samples, as indicated by rod-like structures. The thermogravimetric assay (TG) identified three primary thermal events: initial water loss, a significant mass reduction attributed to cellulose degradation, and eventual degradation of carbonaceous residues. Wettability tests showed a transition in behavior between films produced with 20% and 60% vinasse. The latter also exhibited higher water retention capacity.



Fig. 1. SEM images performed on the polymeric films with varying concentrations of vinasse.

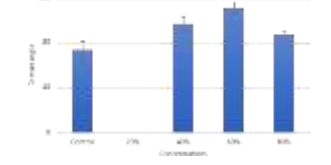


Fig. 2. Contact angles for polymeric films.

4. References

[1] Souza, L. O. Rheological and morphological characterization of cocoa husk nanocellulose for application in the development of biodegradable films. State University of Southwest Bahia - UESB. Graduate Program in Food Engineering and Science, 2021.

[2] Cacicedo, M. L., Castro, M. C., Servetas, I., Bosnea, L., Boura, K., Tsafrakidou, P., & Castro, G. R. (2016). Progress in bacterial cellulose matrices for biotechnological applications. Bioresource technology, 213, 172-180. [3] Borro, J. A. Production of bacterial cellulose using alternative substrates in the culture medium. São Paulo

State University 'Júlio de Mesquita Filho' - Botucatu Campus, 2021.

[4] Fischer, M. R., Garcia, M. C. F., Nogueira, A. L., Porto, L. M., Schneider, A. L. D. S., & Pezzin, A. P. T. (2017). Biosynthesis and characterization of bacterial nanocellulose for tissue engineering. Matéria (Rio de Janeiro), 22.

Acknowledgments: The authors would like to thank Prof. Edson Cocchieri Botelho research group for the thermal analysis.

^{*}Corresponding author: André Luiz Reis Rangel, al.rangel@unesp.br

EXPLORING THE PHYSICAL AND CHEMICAL ATTRIBUTES OF PLASMA-ACTIVATED WATER AND ITS ANTIMICROBIAL POTENTIAL

Michaela Shiotani Marcondes¹, Luan Gonçalves de Lima¹, Felipe S. Miranda^{1,2}, Lady.D.P. Leite², Victória K.F. Tavares², Clodomiro Alves Junior^{1,3}, Cristiane Yumi Koga Ito², Rodrigo Sávio Pessoa¹

¹ Aeronautics Institute of Technology (ITA), São José dos Campos-SP, Brazil ² São Paulo State University (UNESP), São José dos Campos-SP, Brazil ³ UFERSA, Mossoró-RN, Brazil

1. Introduction

The application of non-thermal plasma to water results in the creation of a liquid termed plasma-activated water (PAW). This liquid has gained significance across various sectors, including agriculture, industry, and healthcare. Importantly, in the medical and dental fields, PAW acts as an effective antimicrobial agent, highlighting its contribution to health promotion [1]. In this study, our goal is to undertake a comprehensive physicochemical characterization and microbiological evaluation of plasma-activated water produced with a surface-wave microwave plasma jet, emphasizing its effects on *S. aureus*, *E. coli*, and *C. albicans*.

2. Experimental

The experiment employed a surface-wave microwave plasma jet that operates at 2.45 GHz with a continuous argon gas flow. Microwave power, reaching 200 W, was supplied by a solid-state power source, and experiments were conducted at 70 W. Deionized water (DI) was activated at intervals of 10 and 30 minutes using 40 mL volumes. The pH was subsequently measured using a Metrohm 913 pH Meter. The antimicrobial assessment consisted of three groups: DI water (control), PAW activated for 10 minutes, and PAW activated for 30 minutes. A microbial suspension (750 μ L) was combined with 1250 μ L of PAW, then incubated for 10 and 30 minutes. Serial dilutions were made in sterile saline, and 100 μ L aliquots were spread on tryptic soy agar (for *S. aureus* and *E. coli*) and Sabouraud dextrose agar (for *C. albicans*). The plates were aerobically incubated at 37°C for 24 hours, after which CFU/mL was determined based on colony counts.

3. Results and Discussion

The pH decreased post-activation and remained stable up to the point of use, as illustrated in Figure 1. In terms of mycobiological tests, the bacterium *S. aureus* showed a reduction of 99.41%; *E. coli* exhibited a decrease of up to 95%. However, the fungus *C. albicans* did not display any reduction, as indicated in Table 1. Research links the oxidative stress induced by high ORP to this antimicrobial activity, similar to the low pH observed in the samples [1,2]. Thus, it's evident that PAW offers an affordable and effective method for inactivating bacteria. However, under the present conditions, it doesn't demonstrate the same efficacy against fungi.

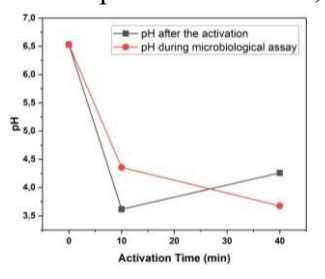


Fig. 1 pH changes post-activation and throughout the microbiological assay as related to the duration of activation.

C.albicans			E.coli		
Grupos	Percentual de redução (%)		Grupos	Percentual de redução (%)	
DI 10min/10min	-4,00	allion are	DI 10min/10min	-10,00	
DI 10min/40min	-8,49		DI 10min/40min	80,00	
DI 30min/10min	-1,42		DI 30min/10min	62,50	
DI 30min/40min	-2,36	ij	DI 30min/40min	95,00	
Di 10 min	controle		Di 10 min	controle	
Di 30 min	controle		Di 30 min	controle	
	S.a	ure	ıs		
	Grupos F	Percentual de redução (%)			
	DI 10min/10min	-3,09			
	DI 10min/40min		39,75		
	DI 30min/10min	18,24			
	DI 30min/40min	99,41			
	Di 10 min	controle			
	Di 30 min		controle		

Tab. 1 Percentage reduction of the microorganisms S. aureus, E. coli, and C. albicans.

4. References

- [1] N. Milhan, W. Chiappim, A. Sampaio, M. Vegian, R. Pesoa, C. Koga-Ito, Int. J. Mol. Sci., 23(8), 4131. (2022).
- [2] W. Chiappim. A. Sampaio. F. Miranda. G. Petraconi, *Plasma Process, Polym.* 18.11 (2021)

Acknowledgments

The authors gratefully acknowledge the financial support provided by the São Paulo State Research Foundation (FAPESP, grants 2019/05856-7 and 2022/13141-0).

^{*}Corresponding author: marcondes.micaela5@gmail.com

EXTRACTION OF LIGNIN FROM CORNCOB USING DEEP EUTECTIC SOLVENTS

Bruna Green Rodrigues^{1*}, João Vitor dos Santos Motta¹, and Rita de Cássia Lacerda Brambilla Rodrigues¹

¹ Department of Biotechnology, Lorena Engineering School, University of São Paulo

1. Introduction

The impending shift away from models reliant on non-renewable resources and the growing global emphasis on environmental concerns has underscored the need for ecologically responsible alternatives [1]. Lignocellulosic materials, such as corncobs (CC), which primarily consist of cellulose, hemicellulose, and lignin, offer the potential to simultaneously extract valuable product streams, including sugars and lignin, as part of a biorefinery framework [2]. Deep eutectic solvents (DES) have emerged as a novel pretreatment method, designed to selectively dissolve biomass [3]. These solvents are not only environmentally friendly but also more cost- effective than other solvents falling within the same category of ionic liquids. In DES, one component functions as a hydrogen bond acceptor (HBA), while the other acts as a hydrogen bond donor (HBD). Choline chloride (ChCl) is a commonly utilized hydrogen bond acceptor (HBA) in the formulation of deep eutectic solvents (DES)[4]. It is frequently paired with hydrogen bond donors (HBDs) of the carboxylic acid and alcohol classes inDES compositions. This study's objective was to assess a deep eutectic solvent (DES) system composed of cholinechloride and lactic acid (in a 1:5 molar ratio) for lignin extraction from corncobs.

2. Experimental

The initial stage involved the preparation of the DES by mixing ChCl and lactic acid (LA) in a molar ratio of 1:5 within a flask, followed by maintenance under magnetic stirring at 80°C until a homogeneous solution was achieved.

Subsequently, the corn cob was added to the flask containing the DES ChCl/LA (1:5) at a 1:20 (w/w) ratio and subjected to an oil bath under reflux and magnetic stirring at 500 rpm, 110°C for 4 hours. After the pretreatment, the mixture of biomass and solvent was centrifuged, and the solid fraction (Solid 1) was washed with ethanol and water. The liquid fraction, which was rich in lignin, was transferred to a 1-liter centrifuge tube, and water was added at a 1:3 solvent-to-water ratio. It was left overnight in a refrigerator to allow lignin precipitation. Subsequently, the tube was centrifuged, and the solid phase was washed with water until a neutral pH was achieved (Solid 2 - lignin). The process is illustrated in Figure 1. The extraction of lignin (%L) followingDES pretreatment was determined using the formula [6] shown in Equation 1:

Corncobs (CC) in their natural state and pretreated corncobs, obtained under the conditions of DES ChCl/LA (1:5), were subjected to chemical characterization in order to determine their cellulose, hemicellulose, lignin, and extractive contents, following the Laboratory Procedures (LAP) as established by the National Renewable Energy Laboratory (NREL) [5]. The extraction of lignin (%L) following DES pretreatment was determined using the formula [6] shown in Equation 1:

$$\%L = \left[1 - \left(\left(\frac{y_L}{y_{Lnative}}\right) \times \frac{m_{sr}}{m_{initial}}\right)\right] \times 100 \tag{1}$$

%L: Yield of lignin in extracted solid (%)

m_{sr}: mass of solids recovered in the sample (g)

m initial: dry mass of lignocellulosic biomass at the beginning of pretreatment (g)yL

native = native lignin content in natura lignocellulosic biomass (%)

y_L= lignin content in pretreated lignocellulosic biomass (%)

3. Results and Discussions

The DES pretreatment demonstrates selectivity in extracting lignin and hemicellulose, while preserving the cellulose fraction. Table 1 below provides the chemical characterization of both fresh and pretreated corn cobs, including the average percentage of extracted lignin.

Sample	Cellulose % (w/w)	Hemicellulose % (w/w)	Lignin % (w/w)	Extractives % (w/w)	%L
CC-In natura	38,69±0,6	37,26 ±0,1	20,38±1,6	3,67±0,3	-
ChCl/LA (1:5)	68,89±0,74	18,60±0,79	12,66±2,91	-	67,22±1,82

Table 1- Compositional analysis of corncob in natura and after pretreatment with ChCl/LA at 110 °C for 4 hours as well asthe average percentage of lignin extracted.

Under the conditions of 110°C for 4 hours, compositional analysis revealed a significant reduction in

hemicellulose and lignin percentages. Utilizing DES ChCl/LA (1:5) in this context, the average lignin extraction reached 67.22% when compared to untreated corncobs (CC). This outcome underscores the potential of the pretreatment method to efficiently extract lignin. Deep Eutectic Solvents (DES) are widely recognized for their environmental friendliness and their non-inhibitory effect on microorganisms. Furthermore, they can be employed for the extraction of valuable sugar derivatives downstream. By extracting lignin and repurposing it into high-value products such as nanolignin and hydrogels, as opposed to conventional incineration, this approach offers the prospect of making the biorefinery economically sustainable.

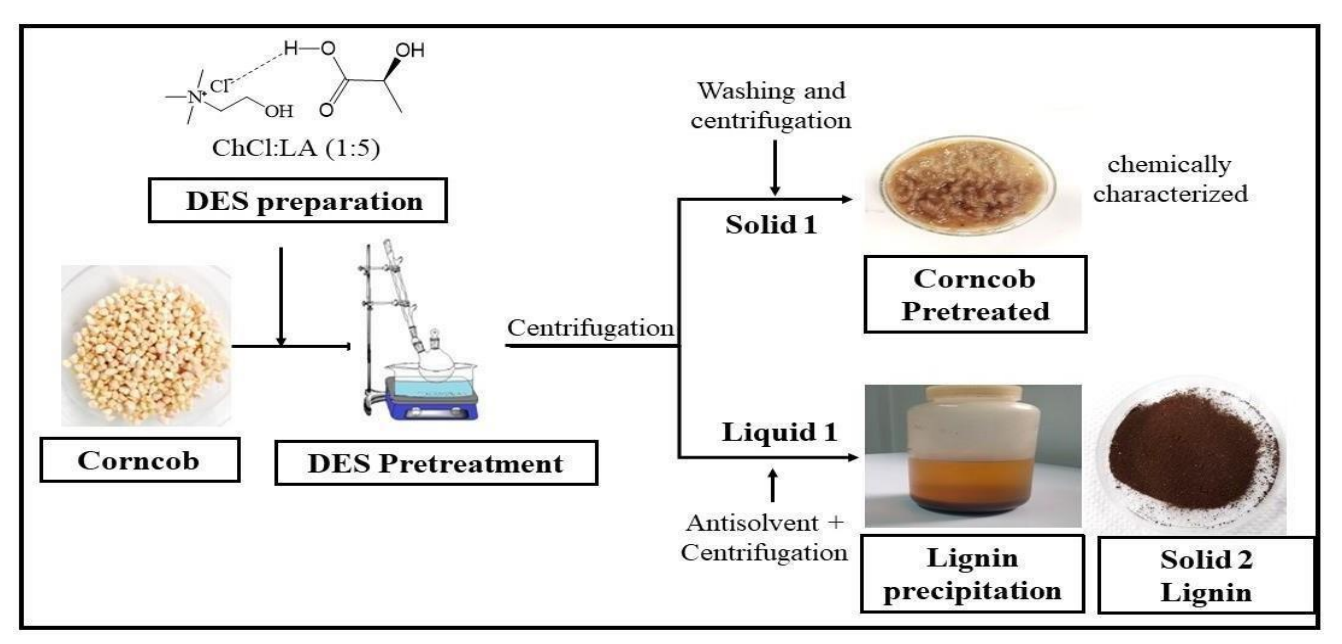


Figure 1 - The flowchart of the DES pretreatment process.

4. References

- [1] Urmetzer S, Lask J, Vargas-Carpintero R, Pyka A. Learning to change: Transformative knowledge for building a sustainable bioeconomy. Vol. 167, Ecological Economics. 2020.
- [2] Ponnusamy VK, Nguyen DD, Dharmaraja J, Shobana S, Banu JR, Saratale RG, et al. A review on lignin structure, pretreatments, fermentation reactions and biorefinery potential. Bioresour Technol. 2019;271(September 2018):462–72.
- [3] Procentese A, Johnson E, Orr V, Garruto Campanile A, Wood JA, Marzocchella A. Deep eutectic solvent pretreatment and subsequent saccharification of corncob. Bioresour Technol. 2015 Sep 1;192:31–6.
- [4] Zhang Q, De Oliveira Vigier K, Royer S, Jérôme F. Deep eutectic solvents: syntheses, properties and applications. Chem Soc Rev 2012;41(21):7108–46. Available from: http://www.ncbi.nlm.nih.gov/pubmed/22806597
- [5] SLUITER A et al. Determination of Structural Carbohydrates and Lignin in BiomassLaboratory analytical procedure. 2008;1–16.
- [6] Xu GC, Ding JC, Han RZ, Dong JJ, Ni Y. Enhancing cellulose accessibility of corn stover by deep eutectic solvent pretreatment for butanol fermentation. Bioresour Technol. 2016;203:364–9.

Acknowledgments

The authors would like to express their gratitude for the support provided by CAPES, CNPQ, andFAPESP (Grant Number 2022/03904-7), Brazilian research agencies.

^{*}Corresponding author: bgreen@usp.br

FLUID SIMULATION OF GLOW DISCHARGES GENERATED BY BIPOLAR PULSED POWER SUPPLIES

Júlio César Costa, Julio César Sagás*

¹Laboratory of Plasmas, Films, and Surfaces, Santa Catarina State University (UDESC), Joinville-SC, Brazil

1. Introduction

Bipolar pulsed power supplies (BiPPS) are a versatile tool to create ingenious voltage waveforms in the kHz frequency range [1]. Such waveforms affect the plasma potential and the energy distribution of ions, which modifies the energy transfer to surfaces, including substrates under plasma treatment. Despite the increased use of BiPPS, some observed effects are not fully understood, especially when asymmetric short positive pulses are used. The comprehension of such phenomena demands diagnostic and simulation studies. In this work, we propose the use of fluid plasma simulation to investigate some aspects of the plasma generated, particularly, the temporal behavior of plasma potential and the role of electron-induced secondary electrons.

2. Theory

The simulations were performed using the plasma module of the Comsol Multiphysics software. The fluid equations for electrons (particle, mass, and energy conservation) are solved using the finite element method in a 2D mesh. An argon plasma was modeled considering a Maxwell-Boltzmann distribution at a pressure of 0.5 Torr in a typical glow discharge reactor. For electron transport properties a reduced mobility of 10^{25} m⁻¹V⁻¹s⁻¹ was assumed, while the work function of electrodes was set to 5 eV. One electrode is grounded and the power supply is connected to the driven electrode through a RC circuit. Three heavy species were assumed: neutral, metastable, and ionized Ar. We use the default set of the software for argon plasma reactions. Ion-induced (ISEE) and electron-induced electron emission (ESEE) were considered on both electrodes.

3. Results and Discussions

In all simulations performed so far, the plasma potential oscillates in phase with the applied voltage, as expected once the plasma frequency is much higher than the frequency of the voltage signal. Also, the plasma potential remains above or very close to the driven electrode potential, indicating that even during the positive pulse, there is a potential barrier for electrons to reach the driven electrode. The inclusion of ESEE has a negligible effect on plasma properties at the conditions simulated.

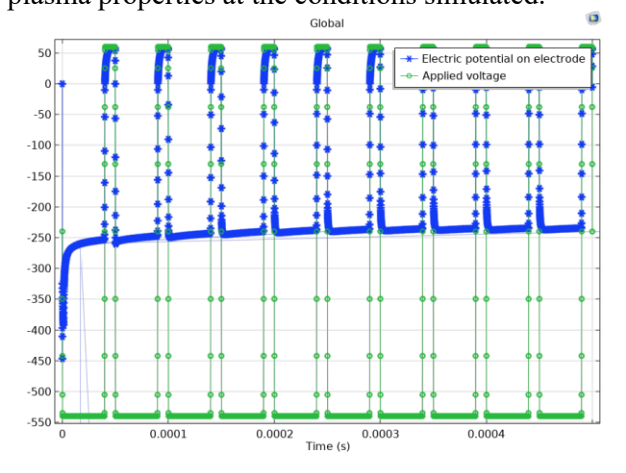


Fig. 1. Applied and driven electrode potential as a function of time.

Fig. 2. Temporal evolution of plasma potential at a point 5 cm above the center of the driven electrode.

4. References

[1] J. W. Bradley and T. Welzel, J. Phys. D: Appl. Phys., 42(9), 93001, (2009).

Acknowledgments

Thanks to FAPESC (grants 2021TR000563 and 2023TR000258) and CNPq (grant 304053/2021-0).

^{*}Corresponding author: julio.sagas@udesc.br

FULL AUTOMATION OF VACUUM, PLASMA AND DEPOSITION SYSTEMS USINGFRIENDLY, LOW-COST AND OPEN-SOURCE HARDWARE AND SOFTWARE

Alessandro Lima¹, Isabela M. Horta¹, Rodrigo S. Pessoa¹, André L. J. Pereira¹, Argemiro S. da Silva Sobrinho¹, Douglas M. G. Leite¹*

¹ Laboratório de Plasmas e Processos, Instituto Tecnológico de Aeronáutica, São José dos Campos/SP, Brazil

1. Introduction

Much of the basic research in materials science relies heavily on home-assembled vacuum systems, encompassing a wide range of processes, including plasma-assisted techniques and film deposition systems. The manual operation of systems such as sputtering deposition can be exceptionally intricate, often comprising multiple subsystems like vacuum, plasma sources, gas flow controllers, and more. The demands of atomic layer deposition (ALD) are even more challenging, requiring ultra-fast, precise, and repetitive pulses of precursors, rendering manual operation impractical. Unfortunately, the commercially available automated vacuum/plasma/deposition systems tend to be prohibitively expensive and lack the flexibility for easy maintenance, modifications, or upgrades.

In this work we present a low-cost automation solution designed to fully automate home-assembled systems like ALD and sputtering deposition systems. The solution is based on open-source platforms like Arduino and Node-Red, eliminating the need for extensive computational or electronic expertise. This approach opens up new possibilities for researchers to enhance the efficiency and reliability of their experiments while keeping costs manageable and the maintenance/modifications/upgrades to local staff.

2. Experimental

Arduino boards serve as the primary interface for real-time interaction with the system, utilizing various sensors like thermocouple modules, electrical relays for activating pumps or pneumatic valves, and motors/drivers for controlling mechanisms such as gate valves. Simultaneously, Arduino maintains continuous communication with the computer through a direct serial protocol connection to a Node-Red server. This server, in turn, establishes direct communication and control digital devices and equipment, such as plasma power sources, mass spectrometers, pressure sensors and vacuum pumps controllers, etc. The Node-Red server also integrates all these subsystems, providing a user-friendly interface and facilitating script execution within a Python shell for real-time data analysis for example. Figure 1 presents the schematics of the employed solution.

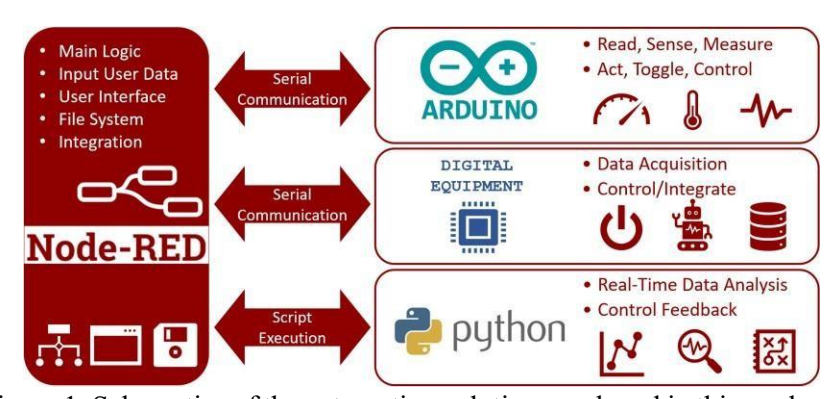


Figure 1: Schematics of the automation solution employed in this work

3. Results and Discussions

The described automation solution was successfully employed in an ALD system and in a UHV magnetron sputtering system. Among the several advantages of the automation on both systems are: i) access the dashboard over network (great for clean room systems); ii) line-after-line script programming allowing an entireprocess to be executed with "one click"; iii) possibility to pulse, ramp, repeat and fast operate processes as gas flow, plasma power, pressure, temperature, among others; iv) safety, reproducibility, repeatability, and quality improvement of the deposited films.

Acknowledgments

We thank the funding agencies: FAPESP, CNPq, CAPES and FINEP.

^{*}Corresponding author: leite@ita.br

FUNCTIONALIZED MULTI-WALLED CARBON NANOTUBES POTENCIALIZE EFFECT OF PHOTODYNAMIC THERAPY OF MURINE MELANOMA IN 2D AND 3D CULTURE.

Kaique G. Hergesel¹, Keren A. S. Moura¹, Larissa S. Almeida³, Daiane M. Lima¹, Diego V. Neves¹, Maria Vitória F. Fragoso¹, Juliana P. Santos^{1,4}, Amanda Lima³, Breno B. Ferrari³, Leonilda M. B. Santos³, Marcos D. Manfrinato¹, Luciana S. Rossino^{1,3}, Elaine C. Oliveira^{1,2*}

¹Faculty Technology of Sorocaba – FATEC, CEETEPS-SP ²University of Campinas – UNICAMP ³Federal University of São Carlos – UFSCar ⁴Universidade Paulista - UNIP Sorocaba

1. Introduction

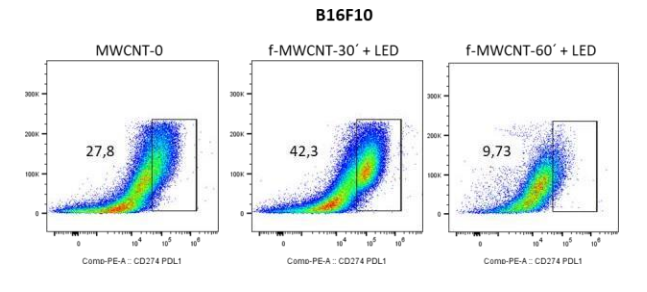
Photodynamic therapy is a minimally invasive health technology used to treat cancer and other non-malignant diseases [1]. Multi-walled carbon nanotubes (MWCNTs) have wide biomedical application prospects but exhibit notable biotoxicity associated with your hydrophobic character. In this study, we functionalized the MWCNT by plasma ablation process for use in photodynamic therapy with LED.

2. Experimental

Carbon nanotubes were functionalized by 30 and 60 seconds (f-MWCNT-30' and 60') using 3 sccm of O2 with 800 V, and the nanotubes not functionalized (MWCNT-0) were internalized by mouse melanoma (B16F10) and non-tumor control cells (mouse fibroblast cells - L929) in 2D and 3D culture. After 24h, cells were exposed to the LED 660 nm for 5 minutes for two consecutive days. Cell viability, qPCR, and flow cytometer were used to evaluate the cells after treatments. In 3D culture, we evaluated de internalization of f-MWCNT and MWCNT-0, spheroids morphology, size, and invasion and migration capability in vitro.

3. Results and Discussions

The results showed that the plasma ablation process increased the dispersion of f-MWCNT 30' and 60' in an aqueous medium without affecting its crystalline structure. Plasma treatment reduced the hydrophobic character of f-MWCNT-30' and f-MWCNT-60', therefore, they were more internalized by cell lines. LED treatment decreases cell viability. Treatment of f-MWCNT 60'+ LED decreases the expression of PDL-1 in B16F10 cells (Fig. 1). Gene expressions revealed that there was a decrease in TGF- β cytokines and VEGF after treatment in the tumor cells (Fig. 2). In 3D melanoma tumor models, the treatment with f-MWCNT 30'+LED and f-MWCNT 60'+ LED resulted in morphological alterations and decreases migration capability of the spheroids in vitro. The results are interesting to understand how functionalized MWCNT and LED can be used how cancer therapy in the future.



TGF p1

Correct

MMCNTr.0

FAM/CNTr.0s

Fig. 1. PDl-1 decreases expression after f-MWCNT-60'internationalization and LED treatment.

Fig. 2. Relative expression of $TGF\beta$ and VEGF genes decreases after functionalized MWCNT and LED exposition.

4. References

[1] Lagos KJ et al. Carbon-Based Materials in Photodynamic and Photothermal Therapies Applied to Tumor Destruction. Int J Mol Sci. 2021 Dec 21;23(1):22...

Acknowledgments

Financial support: Paula Souza Center, FAPESP and CNPq

^{*}Corresponding author: elaine.oliveira10@fatec.sp.gov.br

GROWTH OF BORON-DOPED DLC FILMS ON DIFFERENT SUBSTRATES

Saulo R. Ferreira^{1*}, Elver J. D. M. Pillaca², Funsho O. Kolawole², Lais G. Vernasqui², Vladimir J. Trava-Airoldi²

¹Federal University of São Paulo – Campus São José dos Campos ²National Institute of Space Research – São José dos Campos, São Paulo - Brazil

1. Introduction

DLC (Diamond Like-Carbon) film is a material used as a coating for other materials, due to its excellent properties such as high hardness, excellent wear resistance, high corrosion resistance, low coefficient of friction, etc. In this work, boron incorporated DLC films were grown on different substrates in a PECVD (Plasma Enhanced Chemical Vapor Deposition) reactor with an additional cathode.

2. Experimental

The growths of the boron doped DLC films were carried out in a pulsed PECVD reactor with an additional cathode system and a bubbler (Fig. 1). Characterization techniques such as RAMAN spectroscopy and High-Resolution Scanning Electron Microscopy (FEG-SEM) were used. Boron is obtained from trimethylborate vapor (CH₃)₃BO₃. This was produced at 240 kppm from a mixture of B₂O₃ and CH₃OH. C₂H₂ gas was used as a carrier gas to transport (CH₃)₃BO₃ from the bubbler to the PECVD reactor for plasma production. The growth stages canbe seen in Table 1.

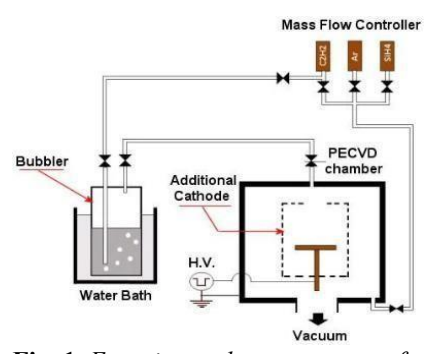


Fig. 1. Experimental arrangement of growth system.

Table 1. (frowth steps of boron doped DLC f	ilm.

Etapa	Gas	Flow rate (sccm)	Pressure (mTorr)	Voltage (kV)	Time (min)
Cleaning	Ar	2	3	-0.60	30
Interlayer	SiH ₄	2	3	-0.75	15
DLC + dopant	C ₂ H ₂ + (CH ₃) ₃ BO ₃	6	3	-0.90	60

3. Results and Discussions

Table 2 presents the average roughness value (Ra) of the DLC films deposited on silicon, Ti6Al4V and glass samples. The results showed that there were no changes in Ra when compared to samples prior to growth. Through RAMAN analyzes it was possible to confirm the presence of DLC grown in all materials. The I_D/I_G ratiowas measured (Fig. 2). A higher I_D/I_G ratio was found for the glass sample and a lower one for the silicon samples. An increase in the I_D/I_G value can be interpreted as a tendency towards graphitization of the film.

Table 2. Roughness measurement (Ra)

Substrate	Roughness (Ra)
Ti6Al4V	$(24,97 \pm 1,90)$ nm
Silicon	$(10,97 \pm 5,88)$ nm
Glass	$(11,09 \pm 4,28) \ nm$

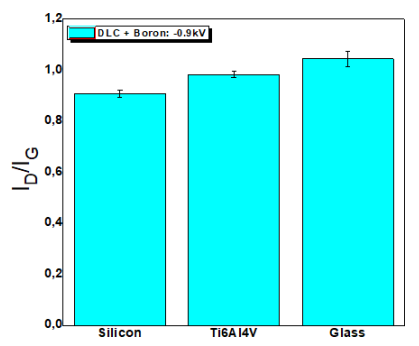


Fig. 2 I_D/I_G ratio for samples coated.

^{*} Corresponding author: s.ferreira02@unifesp.br

HYPERSONIC HEAT FLUX EVALUATION FOR SHAPE MEMORY ALLOY THERMO-MECHANICAL CHARACTERIZATION

Felipe Jean da Costa^{1,3}*, Alana Aíres da Rocha Brito², Gustavo Jean da Costa³ and Milton Sergio Fernandes de Lima⁴

¹Instituto Federal de Ciência e Tecnologia de São Paulo – Campus São José dos Campos ²Instituto Tecnológico de Aeronáutica ³BRENG Engenharia e Tecnologia ⁴Instituto de Estudos Avançados

1. Introduction

The Brazilian Aerospace Startup BRENG Engineering and Technology, is studying Hypersonic Airbreathing Propulsion (HAP) Systems as integrating part of INCT-PRO-HYPER (National Institute of Science and Technology in HAP) efforts, a research network involving universities, research centers, companies and headed by the Institute for Advanced Studies (IEAv) from the Brazilian Air Force. Also, BRENG is a player in the PROCAD DEFESA academic cooperation, headed by IEAv, to collaborate with the Human Resources training in HAP areas aiming the space access [1].

The HAP system studied by BRENG, named Vector Hypersonic Vehicle (VHV), is based on the supersonic combustion (scramjet) and a laser propulsion combined cycle, such as suggested by Costa (2018). The VHV (Fig. 1) is a technological demonstrator designed to demonstrate, during the hypersonic flight speed corresponding to Mach number 7 through the Earth's atmosphere at 30 km altitude, three innovative technologies: i) waverider technology, to obtain lift from conical shock wave during the supersonic or hypersonic flight; ii) scramjet engine that consists in a hypersonic airbreathing propulsion system based on supersonic combustion, using hydrogen as fuel, and iii) laser propulsion concept, where the air breakdown phenomenon promotes the aerospace vehicle thrust and accelerates it up to supersonic/hypersonic conditions. During the hypersonic flight the scramjet engine promotes the compression and deceleration of freestream at the inlet station of the scramjet, throughout the oblique/conical shock waves. The scramjet is an aeronautical engine without moving parts and integrated as part of the aerospace vehicle, in order to conditioning the air in supersonic speeds and then to burn fuel (Hydrogen) in the combustion chamber.

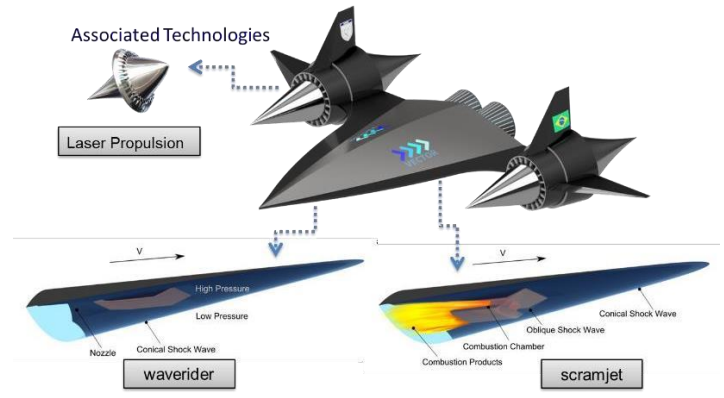


Fig. 1. The Vector Hypersonic Aerospace Vehicle with waverider, scramjet and laser propulsion concepts.

2. Theory

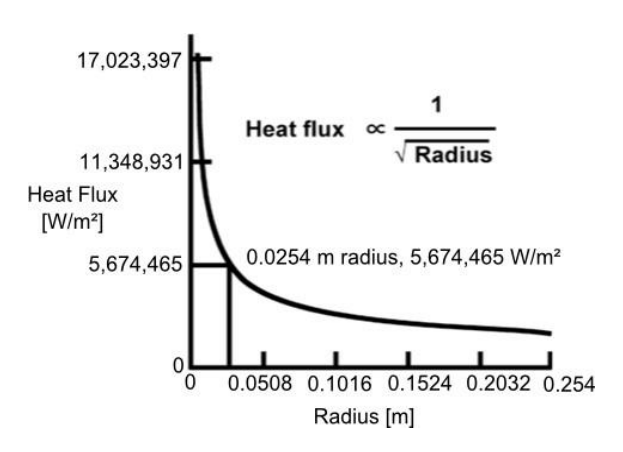
When the air reaches supersonic/hypersonic conditions, the shock waves and the viscous forces in the boundary layer, established over a vehicle body, are responsible to decelerate the air and it yields the phenomenon called aerodynamic heating. In this case, occurs a friction between the fluid filaments and the body or the compression at the stagnation regions of leading edge that convert the kinetic energy into heat within a thin layer of air which blankets the body, where the temperature in this layer increases with the square of the speed of the vehicle, and this high temperature is concentrated in the boundary-layer, where heat will flow readily from the boundary-layer to the vehicle's surface [2].

The aerodynamic heating is affected by a possible dissociation and ionization of the air that occurs at finite rates, and implies that the thermochemical equilibrium cannot be achieved in the flow field (Fay and Riddell, 1958), because there is a high static temperature in the shock layer. Furthermore, the atoms and ions release a high specific energy, if they are diffused on the surface and consequently recombined at the wall, which causes a significantly increase in the heat transferred by conventional molecular conduction. Using a non-catalytic surface will be possible to eliminate the fraction of heat transfer that is transported by atomic diffusion into the wall

followed by recombination at the surface. Although, to an effective use of a non-catalytic surface, the atoms cannot recombine firstly in the gas before reaching the wall. If the wall is catalytic, the concentration of atom is reduced to the equilibrium value of the wall temperature. If the atoms recombine in the boundary layer or at the wall there will be no major effect on convective heat transfer [3].

For the aerodynamic heating are applied two theories, the Fay and Riddell theory to the stagnation point due the existence of a blunted nose formed at the vehicle's leading edge during the manufacturing process; and the Eckert's reference enthalpy theory applied to the vehicle's surface assuming the air flow in the conical surfaces as a flow over a flat plate [4].

In terms of thermo-structural challenges, typically the extreme thermal loads on the leading edges of the vehicle have a significant magnitude in terms of heat flux, where the heat flux increases inversely to square root of the nose radius, as stagnation heat transfer theory, develop by Fay and Riddell [5]. The heat flux as function of the nose radius can be seen in the Figure 2(a), where for 1-inch (25.4 mm) nose radius, the heat flux is approximately 500 Btu/ft2-sec (5674.47 kW/m²). For a large leading-edge radius, one may obtain a lower heat flux, but several airbreathing vehicles require a small nose radius and therefore, the heat flux is significantly high [6]. Figure 2(b) shows the aerodynamic heating for the ballistic and 1 g reentry vehicles, respectively [7]. In the ballistic reentry trajectory, one may observe an extreme heat flux, about 10,000 (Btu/ft2 s) (113,489,317 W/m²) for a short time period (20s). In other hand, the heat flux for the lifting reentry vehicle is 1% of the ballistic reentry vehicle, around 100 (Btu/ft2 s) (1,134,893.17 W/m²), but with a longer time period. Therefore, it is necessary keep in mind what type of the trajectory will be used to demonstrated any new hypersonic aerospace vehicle.



Ballistic reentry $q_{w} = 100000$ $q_{w} = 1000$ Lifting reentry t[s]

Fig. 2. Heat flux function of the nose radius, adapted from [6].

Fig. 3. Ballistic and lifting reentry heat flux function of the trajectory, adapted from [7].

So a numerical thermo analisys will be conducted.

3. Results and Discussions

Results will be provided for the final paper.

4. References

- [1] Costa, F.J., Rocha, A.A.R., Costa, G.J., and Lima, M.S.F. Aerodynamic Heating Calculation for a Hypersonic Airbreathing Propulsion System at Mach Number 7. In: 19th Brazilian Congress of Thermal Sciences and Engineering. November 06-10th, 2022, Bento Gonçalves, RS, Brazil.
- [2] Driest, E.R.,1956. The Problem of Aerodinamic Heating. Aeronautical Engineering Review, p 26-41.
- [3] Eckert, E.R.G., April, 1954. Survey on Heat Transfer at High Speeds. WADC Technical Report, p 54-70.
- [4] Costa, F.J., Rolim, T.C., Rêgo, I.S., Minucci, M.A.S., Oliveira, A.C., and Toro, P.G.P. Aerodynamic Heating of the Brazilian 14-X Hypersonic Waverider Scramjet Vehicle at Mach Numbers 7 And 10. In: 16th Brazilian Congress of Thermal Sciences and Engineering. November 07-10th, 2016, Vitória, ES, Brazil.
- [5] Fay, J.A. and Riddell, F.R., 1958. Theory of Stagnation Point Heat Transfer in Dissociated Air. Journal of The Aeronautical Sciences.
- [6] Glass, D.E. Ceramic Matrix Composite (CMC) Thermal Protection Systems (TPS) and Hot Structures for Hypersonic Vehicles. In: 15th AIAA International Space Planes and Hypersonic Systems and Technologies Conference, 28 April 1 May 2008 (AIAA 2008-2682), Dayton, Ohio USA.
- [7] Hankey, W.L. Re-Entry Aerodynamics. AIAA Education Series, J.S. Przemieniecki, Series Editor-in-Chief, 1988, AIAA, ISBN 978-0-930403-33-1

Acknowledgments: The first author would like to express his gratitude to INCT PRO-HYPER (INCT - MCTI/CNPq/CAPES/FAPs n. 16/2014), CAPES PROCAD/DEFESA n.15/2019, and to UNIVAP Technological Park

*Corresponding author: felipejean@brengtrein.com.br

HYPERSONIC PLASMA SETUP FOR OXIDATION TESTING OF ULTRA-HIGH TEMPERATURE CERAMIC COMPOSITES

Cristian Cley Paterniani Rita^{1,2}, Felipe de Sousa Miranda¹, Alexei Mikhailovich Essiptchouk³, Gilberto Petraconi Filho¹

¹ITA- Technological Institute of Aeronautics, LPP, S. J. Campos, SP, Brazil ²FATEC – Technology College – Pinda^{ba}, SP, Brazil ³UNESP – Paulist State University – S. J. Campos, SP, Brazil

1. Introduction

Materials known as thermal protection systems are used as coatings for space vehicles that are subject to aggressive thermal environments, mainly in the process of atmospheric reentry. In this study, it is proposed to simulate and investigate the ablative properties of the Ultra High Temperature Ceramic composite (UHTC) inside the plasma tunnel – LPP – ITA, using a hypersonic plasma torch as an ablative system. The UHTC materials based on Zirconium Diboride (ZrB₂) doubled with Silicon Carbide (SiC), with 10%, 20% and 30% by volume (vol) subjected to hypersonic thermal flow, showed interesting and different behaviors for each percentage by volume of SiC. The highlight is the composition doped with 20% vol, presenting better behavior when subjected to thermal wear in the proposed simulated system.

2. Experimental

The ablation tests were performed in the Plasma Tunnel located in LPP - ITA (Fig. 1), using an non transferred arc DC plasma torch fed with a low pressure air reactive atmosphere of P = 75 Pa. plasma working at a power of 35 kW, coupled to a hypersonic Mach 5 nozzle under a thermal flux of 2.2 MW / m^2 and average Enthalpy of 18.61 MJ / kg. Microstructural and chemical analyzes of the UHTC composites doped with SiC were carried out, before and after the SEM/EDS ablation process, to analyze the microstructural behavior and the chemical composition of the UHTC composite materials.

3. Results and Discussions

This study confirmed that it is possible to simulate steady-state conditions for atmospheric re-entry necessary for the development of materials for spacecraft thermal protection systems. The results of the oxidation tests showed that the ZS10 and ZS30 samples undergo active oxidation and form ZrO₂ oxide, causing an accentuated mass loss. For these samples, the protective oxide layer was partially volatilized with the time of exposure to the plasma jet. Passive oxidation occurred in ZS20, and the reactions in this mechanism favor the formation of a passivation layer of ZrSiO₄, a stable oxide, promoting mechanical strength and, consequently, low degradation rate. These results can be associated with variation in SiC composition, which demonstrates that there is an ideal ratio of ZrB₂ and SiC and influences oxidation mechanisms to produce a protective surface layer.

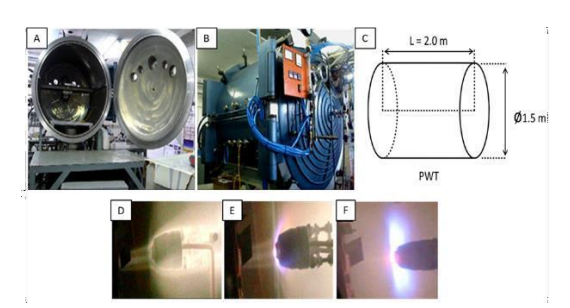


Fig. 1. (Experimental PWT - ITA: (a) Front and (b) rear view of the vacuum chamber and (C) main dimensions of the vacuum chamber. Sample test after (d) 5 s, (e) 10 s, and (f) 40 s.)

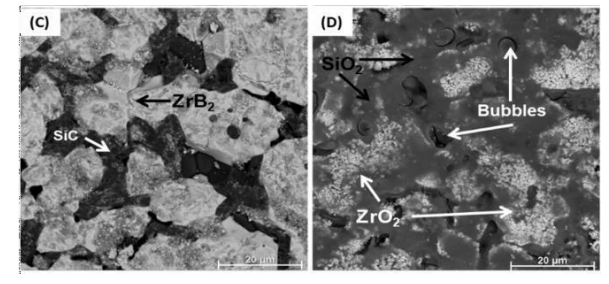


Fig. 2. (Micrographs (c) ZS20 before the oxidation tests. The micrographs (d) ZS20 after the oxidation tests.)

4. References

[1] F. Monteverde, A. Cecere, R. Savino, "Thermo-chemical surface instabilities of SiC-ZrB2 ceramics in high enthalpy dissociated supersonic airflows", J. Eur. Ceram. Soc. **37** (2017) 2325–2341. doi:10.1016/j.jeurceramsoc. (2017).

[2] C. Rita, F. Miranda, F. Caliari, R. Rocha, A. Essiptchhouk, L. Charakhovski, G. Petraconi. "Hypersonic Plasma Setup for Oxidation Testing of Ultrahigh Temperature Ceramic Composites", J. Heat Transfer. **142**(8): 082103. https://doi.org/10.1115/1.4047150, (2020).

Acknowledgments This work was supported by FAPESP, CNPq, AEB and Capes

^{*}Corresponding author: cpaterniani@yahoo.com.br

IMPACTS OF THE PRESENCE OF COMMERCIAL MWCNT ON THE TERRESTRIAL ECOSYSTEM

Vitória C. Pereira¹; Larissa S. Almeida²; César A. Antônio Jr³; Elidiane C. Rangel³; Francisco T. Degasperi⁴; Silvia P. Irazusta^{1,5*}

¹Faculdade de Tecnologia de Sorocaba – CEETEPS – SP; ²Programa de Pós-graduação em Ciências de Materiais – UFSCAR-SP; ³ Instituto de Ciência e Tecnologia de Sorocaba- UNESP -SP ⁴Faculdade de Tecnologia de São Paulo – CEETEPS -SP; ⁵Programa de Mestrado Profissional em Gestão e Tecnologia dos Sist. Produtivos CEETEPS-SP

1. Introduction

Carbon nanotubes (CNT) stand out because of their high mechanical resistance, capillarity, and optical and electronic properties [1]. However, because of these properties, the great volume of production, and applications, there is still no evidence of its potential impacts on different environmental matrices. This work aimed to study the possible environmental impacts of the deposition of CNTs in the terrestrial matrix, by ecotoxicological tests, using the species Eisenia andrei.

2. Experimental

Commercial Multi-walled Carbon Nanoparticles (MWCNT), Helix® were incorporated into a standard soil in concentrations of 6.25; 12.5; 25.0; 50.0, and 100.0 mg/Kg of soil. Adult earthworms of the E. andrei, weighing 310.9 ± 33.4 mg, were inserted into the soil plus NTCs, according to the protocol by Nunes et al. (2019) [1]. After 14 days the organisms were evaluated for mortality and body weight. After that, the earthworms were euthanized, and subjected to freeze-drying, metallization with Au/Pd, and scanning electron microscopy (SEM).

3. Results and Discussions

Fig. 1 shows no CNT effect on mortality (A) and an increase in body mass of the organisms exposed to 100 mg/Kg of soil (B) was observed. In Fig. 2, significant alterations in the body tissue surfaces of the exposed organisms (C, D) in relation to controls (A, B) can be observed. There was a hardening and dehydration of the cuticle of earthworms.

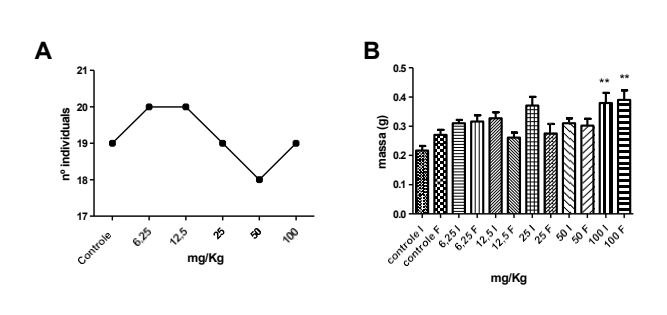


Fig. 1. CNT effects on survival and weight.

Fig. 2. CNT effects on body tissue (A and B) control and (C and D) exposed earthworms.

4. References

[1] Nunes, M. E; Alves, P, R; Segat, J. C; Cardoso, E. J; et al. Ensaios de letalidade. In: NIVA, C. C (ed.); BROWN, G. G (ed.). Ecotoxicologia Terrestre: Métodos e aplicações dos ensaios com oligoquetas. Brasília:EMBRAPA. p. 167-174,(2019).

[2] HERBST, M. H.; MACEDO, M. I. F.; ROCCO, A. M. Tecnologia dos nanotubos de carbono: tendências e perspectivas de uma área multidisciplinar. Química Nova, v. 27, n. 6, p. 986992, 2004.

Acknowledgments: The authors thank the institutions involved.

 $[\]hbox{*Corresponding author: silvia.pierre@hotmail.com}\\$

INFLUENCE OF THE ABRASIVE WEAR MODES ON THE VOLUME OF WEAR OF THIN FILMS

Jorge Thiago de Sousa Lima Wilcken¹, Jorge Humberto Luna-Domínguez², Vikas Verma³, Ronaldo Câmara Cozza^{1,4}*

¹ University Center of FEI – Educational Foundation of Ignatius "Priest Sabóia de Medeiros" – Brazil

² Universidad Autónoma de Tamaulipas – Mexico

³ Aqila Technologies and Integration Solutions – India

⁴ CEETEPS – State Center of Technological Education "Paula Souza" – Brazil

1. Introduction

The micro-abrasive wear test by rotative ball is an important method adopted to study the abrasive wear behavior of materials (Figure 1) [1,2]. "Wear craters" are generated on the specimen and two abrasive wear modesare usually observed on the surface of the worn crater: "grooving abrasion" is observed when the abrasive particles slide on the surface, while "rolling abrasion" results from abrasive particles rolling on the specimen. The purpose of this work is to measure the volume of wear in coated systems submitted to micro-abrasive wear, using the "ball-cratering" wear test method.

2. Experimental procedure

Experiments were conducted with thin films of TiN, CrN, TiAlN, ZrN, TiZrN, TiN/TiAlN, TiHfC and TiHfCN. For counter-body, it was adopted one ball made of AISI 52100 steel, with diameter of D = 25.4 mm. The normal force value defined for the wear experiments was N = 0.4 N, with two abrasive slurries concentrations(C), $C_1 = 5\%$ SiC + 95% glycerin and $C_2 = 50\%$ SiC + 50% glycerin (volumetric values). The average particle size of the SiC is 3 µm. The volume of wear (V) was calculated using the equation $V = \pi d^4/64R$ – where d is the diameter of the wear crater and R is radius of the ball (Figure 1).

3. Results and Discussions

Figure 2 shows the behavior of the wear volume (V) as a function of the micro-abrasive wear modes – the maximum error observed was $V = 0.4 \times 10^{-3} \text{ mm}^3$.

The values of the volumes of wear reported under conditions of "rolling abrasion" (high abrasive slurry concentration $-C_2$) were higher than the values of the volumes of wear reported under conditions of "grooving abrasion" (low abrasive slurry concentration $-C_1$). This tribological behavior can be justified because under the occurrence of "rolling abrasion", there is a larger amount of abrasive particles acting between the test sphere and the specimen, participating of the micro-abrasive wear process and, consequently, generating a higher wear volume. In other hand, in "grooving abrasion", the abrasive particles are fixed on the counter-body (in the case, on the ball), limiting then, their movements and requiring higher tangential forces.

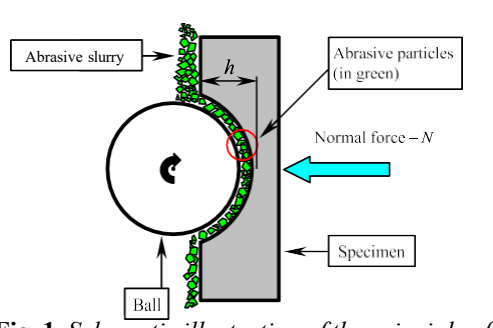


Fig. 1. Schematic illustration of the principle of the micro-abrasive wear test by rotating ball [1].

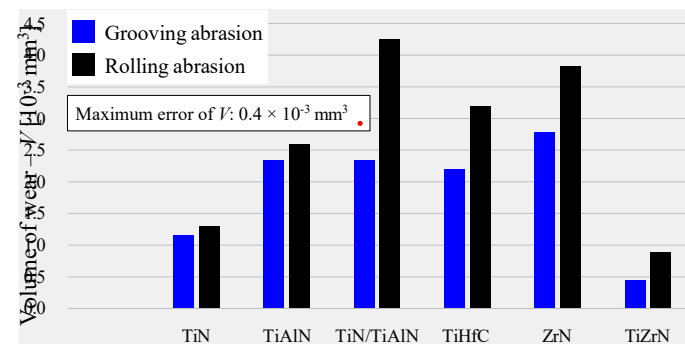


Fig. 2. Wear volume of (V) as a function of the micro-abrasive wear modes "grooving abrasion" and "rolling abrasion".

4. Conclusions

The volume of wear increased with the increase of the abrasive slurry concentration – from $C_1 = 5\%$ SiC + 95% glycerin to $C_2 = 50\%$ SiC + 50% glycerin), i.e., from "grooving abrasion" to "rolling abrasion".

5. Reference

- [1] R.C. Cozza, Surface & Coatings Technology **215** (2013) 224-233.
- [2] M.M. Macedo, J.H. Luna-Domínguez, V. Verma, C.G. Schön and R.C. Cozza, Wear 476 (2021) 203664.

^{*}Corresponding Author: rcamara@fei.edu.br, ronaldo.cozza@fatec.sp.gov.br

INTERACTION OF OXYGEN PLASMA ACTIVATED WATER WITH CALCITE

Pedro César Fortuna Cupertino Vianna de Souza¹, Felipe Sampaio Alencastro¹, Renata Antoun Simão¹

¹ DMM/PEMM/COPPE, Universidade Federal do Rio de Janeiro, Rio de Janeiro, RJ, Brazil

1. Introduction

The study of the interaction between plasma activated water (PAW) and calcium carbonate stands at the intersection of innovation and practical necessity [1]. As industries grapple with the challenges posed by calcium carbonate in processes utilizing hard water, the potential of PAW emerges as a compelling avenue for exploration. Calcium carbonate precipitation, a ubiquitous phenomenon in hard water systems, poses a significant impediment to operational efficiency and product quality [2]. Therefore, the pursuit of effective and sustainable solutions has prompted an investigation into the unique characteristics of PAW and its potential in mitigating the adverse effects of calcium carbonate.

2. Experimental

PAW was synthesized by activating deionized water with a plasma pen (PlasmaPen, PVA Tepla) supplied with O_2 gas, kept at 5 mm over the water surface, for both 5 and 15 minutes. $10\mu L$ droplets of PAW were applied to calcite crystal (CaCO₃) freshly cleaved surfaces and left to air-dry. Samples were analyzed via atomic force microscopy (AFM) and UV-Vis spectrophotometry. Results were compared to untreated samples.

3. Results and Discussions

AFM topography of cleaved calcite surface (Fig. 1) initially presented a smooth appearance. However, following contact with PAW, subsequent topography (Fig. 2) revealed a distinct transformation, characterized by the emergence of notable formations on the calcite crystal surface. This result prompts the hypotheses that during contact with PAW, the calcite crystal locally dissolved, releasing calcium and carbonate ions into the droplet. As the droplet air-dried, the ion concentration increased, leading to supersaturation and precipitation on the crystal surface, forming the observed features. This implies PAW's ability to dissolve calcium carbonate.

The process of plasma activation significantly altered the solution's pH, reducing it to 4.3. This reduction in pH is a factor of considerable influence on the dissolution of calcite. Overall, this study indicates PAW's potential to dissolve calcium carbonate, requiring further investigations to understand the intricacies and efficiency of this process, including experiments with different solutions.

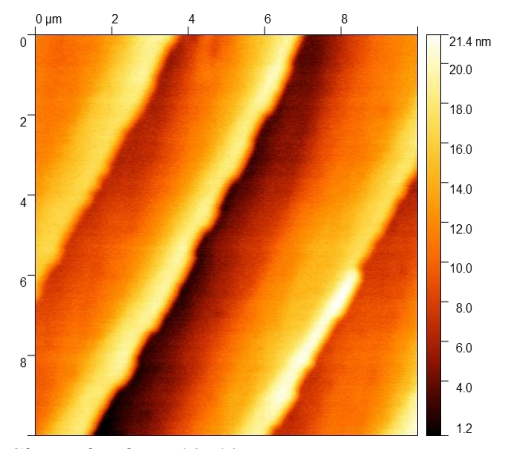


Fig. 1. Cleaved calcite 10x10nm.

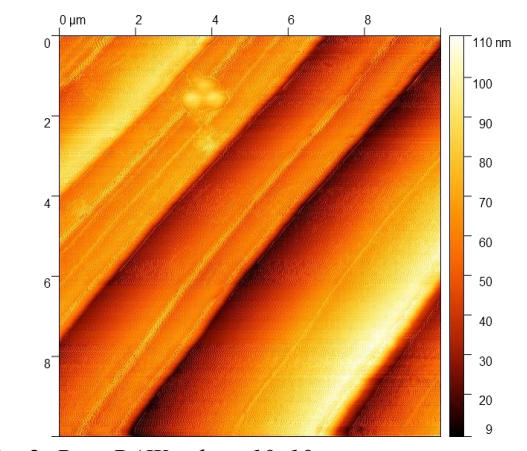


Fig. 2. Post-PAW calcite 10x10nm.

4. References

- [1] M. Wartel, Journal of Applied Physics, **129**, 233301, (2021).
- [2] R. Ketrane, Desalination, **249**, 1397–1404, (2009).

Acknowledgments

This work was partially funded by FAPERJ - Fundação Carlos Chagas Filho de Amparo à Pesquisa do Estado do Rio de Janeiro - process SEI-260003/019684/2022 and by CNPq.

^{*}Corresponding author: pedro.fortuna@poli.ufrj.br

INVESTIGATION OF POWDER METALLURGY TECHNIQUE FOR FABRICATING MG-ZN ALLOYS FOR BIOMEDICAL APPLICATIONS

William Souza^{1*}, Viviane Costa², Durval Rodrigues Junior³

¹Undergraduation student, Engineering Physics, Lorena School of Engineering (EEL), University of São Paulo (USP), Lorena-SP-Brazil

² Doctoral Student of the Postgraduate Program in Materials Engineering (PPGEM), Lorena School of Engineering (EEL), University of São Paulo (USP), Lorena-SP-Brazil;

³ Full Professor, Lorena School of Engineering (EEL), University of São Paulo (USP), Lorena-SP-Brazil

1. Introduction

The present study proposes an analysis of the potential of Mg-Zn alloys in biomedical contexts. Biodegradable magnesium alloys have exhibited properties comparable to those of natural bone, mitigating the occurrence of the phenomenon of bone density loss (stress shielding). The impact of zinc (Zn) incorporation in different proportions, notably up to 3% by mass, on the mechanical properties and corrosion resistance of these alloys was investigated. However, it is important to note that higher concentrations of Zn can lead to the formation of intermetallic precipitates, with significant effects on the corrosion rate. For alloy fabrication, mechanical alloying with highenergy ball milling was adopted, an approach that aligns with the requirements of biomedical applications [1,2].

2. Experimental

First, elemental powders of magnesium (Mg) and zinc (Zn) were weighed in the desired proportions: 99% Mg / 1% Zn, 98% Mg / 2% Zn, and 97% Mg / 3% Zn (by mass). High-energy ball milling was performed using a SPEX mill with tungsten carbide jar and balls with different sizes. A total of 3.5 g of powder per sample was processed, with a 5:1 ratio of balls to powder masses, and milling times of 1, 2, and 4 hours. The samples were labeled MgZn-1h, MgZn-2h, MgZn-4h, Mg2Zn-1h, Mg2Zn-2h, Mg2Zn-4h, Mg3Zn-1h, Mg3Zn-2h, and Mg3Zn-4h. Characterization was performed using scanning electron microscopy with energy-dispersive spectroscopy (SEM+EDS) and X-ray diffraction (XRD).

3. Results and Discussion

Through this research project, it was possible to observe that the utilization of the mechanical alloying dry technique for obtaining powders intended for Mg-Zn systems is a viable production route. The reproducibility of the samples could be ensured, and through analyses using scanning electron microscopy with energy dispersive spectroscopy (SEM+EDS) and X-ray diffraction (XRD), it was verified that the obtained powders present low concentrations of contaminants and a flake-like morphology. This natural flakes morphology will provide porosity to the conformed structure, eliminating the need for spacing agents. This highlights that the samples developed in this project exhibit desired characteristics for applications in the field of biomaterials.

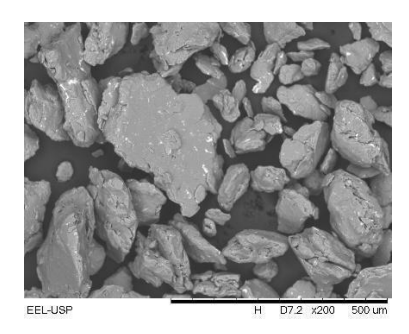


Fig. 1. Example of micrograph sample Mg2Zn-2h, magnification of 200X.

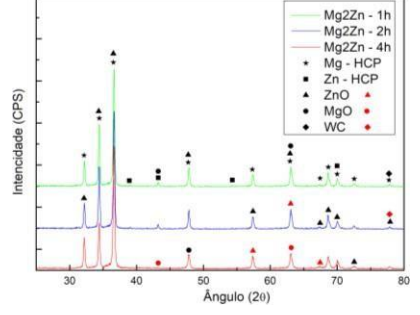


Fig. 2. *X-ray diffractograms of sample powders:* Mg2Zn - 1h, Mg2Zn - 2h, Mg2Zn - 4h

4. References

- [1] Youwen Yang, et al. Mg bone implant: Features, developments and perspectives. Materials & Design, (2020).
- [2] M. Sherif El-Eskandarany. "Mechanical Alloying", 3nd edition, William Andrew Publishing, (2020).

^{*} Corresponding author: willsouza@usp.br, durvalrj@usp.br

METAL ADSORPTION FROM CONTAMINATED SOIL USING SODIUM POLYACRYLATE

Alana Maria Corá^{1*}, Silvia Pierre Irazusta², Maira de Lourdes Rezende³, Ana Paula Paglione Aniceto⁴

^{1,3} Faculdade de Tecnologia de Sorocaba "José Crespo Gonzales"
^{2,4} Programa de Mestrado Profissional em Gestão e Tecnologia em Sistemas Produtivos

1. Introduction

Environmental liabilities are understood to mean deposits and contaminated sites that pose risks to society and/or the environment [1]. This work seeks to remediate environmental liabilities contaminated by heavy metals, using a permeable reactive barrier of sodium polyacrylate (NaPA), a substance known for its ability to bind heavy metals and mitigate their harmful effects.

2. Experimental

The experiment consisted of six samples containing polymer in two forms: powder and swollen, along with different water volumes for each condition for the leaching. A control soil layer was positioned directly underthe polymer layer, while the layer of contaminated soil was placed above of the polymeric one. Before the experiment, initial ICP (Inductively Coupled Plasma) analyses were conducted on both the soils and the polymerto assess the feasibility of the study's aim. Furthermore, the polymer was analyzed by Fourier Transformed Infra-Red (FTIR) before and after the assay. After a period of 30 days, the system was disassembled, and both the soiland polymer samples were subjected to analysis using ICP to quantify the metal content in each material.

3. Results and Discussions

Figure 1 represent the polymer FTIR before and after the assay. The peak present in 3368 cm⁻¹ show the hydroxyl group (-OH), in 2950 cm⁻¹ CH₂ aliphatic, in the swollen NaPA possibly hidden because of the intensive peak of hydroxyl. The carboxyl acid peak (-COO) are observed in 1566 cm⁻¹, and -CO in 1407 cm⁻¹ band, only the characteristics peaks NaPA [2] are present demonstrating that any alteration occurred after the leaching assay. The ICP results showed a reduction in the levels of metals in the contaminated soil by transferring it to the NaPA, where the metals were retained. The highest transfer and adsorption occurred in the assembled system with the polymer in powder form, as Figure 2 represent. In this way, the (NaPA) proved to be efficient in the removal of contaminating metals from the soil, such as a PRB, at least for these metals analyzed. The resulting polymer residue, studies shows that this residue could be used in the cement industry, in line with circular economy principles, aiming the right discard of this polymer [3].

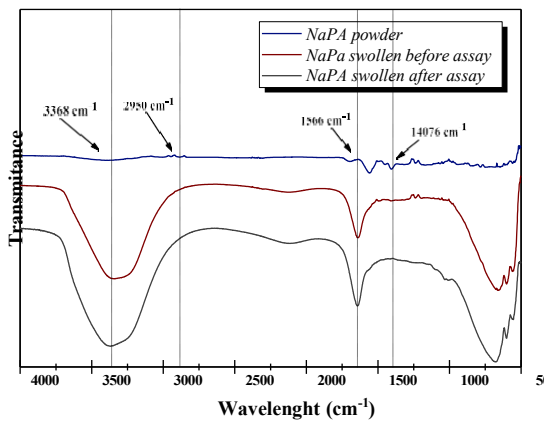


Fig. 1. FTIR polymer analysis before the	leaching assay.
--	-----------------

METALS	POWDER PO	LYMER	SWOLLEN POLYMER		
mg/Kg	INITIAL (Q.L.)	FINAL	INITIAL (Q.L.)	FINAL	
Ba	<20	95,41	<20	<20	
Pb	<1	3.534,50	<1	3663,6	
Fe	<20	7.640,35	<20	3475,44	
Ni	<2	7,05	<2	<2	
Cr	3,32	48,69	3,32	4,64	
Mn	<5	185,37	<5	9,67	

Fig. 2. Tabel of the results before and after the assay.

4. References

- [1] C. A. B. Galdino, et al. Revista Produção, 14, 54 63, (2004).
- [2] C. Yu, et al. Journal of Cleaner Production, 213, 242–250, (2019).
- [3] X. Li, et al. RSC Adv., 7, 32842–32849, (2017).

Acknowledgments: To FAPESP for financial support (Process No. 2022/13496-3) and to the Faculdade de Tecnologia de Sorocabafor provide the necessary equipment.

^{*} Corresponding author: alana.cora@fatec.sp.gov.br

METALLOGRAPHIC STUDY OF LOW-CARBON STEELS API 5L X70 MO AND API 5L MS

Élida Mariana Almeida Alves^{1*}, Pietra Alice Marcelino Soares², Rafael Resende Lucas¹, Rosinei Batista Ribeiro², Heloisa Andréa Acciari¹, Eduardo Norberto Codaro¹

¹Unesp - Câmpus de Guaratinguetá, Av. Dr. Ariberto Pereira da Cunha, 333, Portal das Colinas, CEP 12516-410, Guaratinguetá - SP

²CEETEPS – UPEP - FATEC- Guaratinguetá, Av. Prof. João Rodrigues Alckmin, 1501, Jardim Esperança, CEP 12517-475, Guaratinguetá - SP.

1. Introduction

API 5L pipelines can suffer localized or generalized corrosion depending on the steel, oil and operating conditions such as pressure, temperature and flow dynamics. The nature of the corrosion products depends on the occurrence and extent of oxygen contamination during the primary and secondary oil recoveries. In this first stage, the objective of this work was to study the microstructure of the low carbon steels API 5L X70 MS and API 5L X70 MO, which will subsequently be subjected to corrosion tests by immersion in NACE 177B solution.

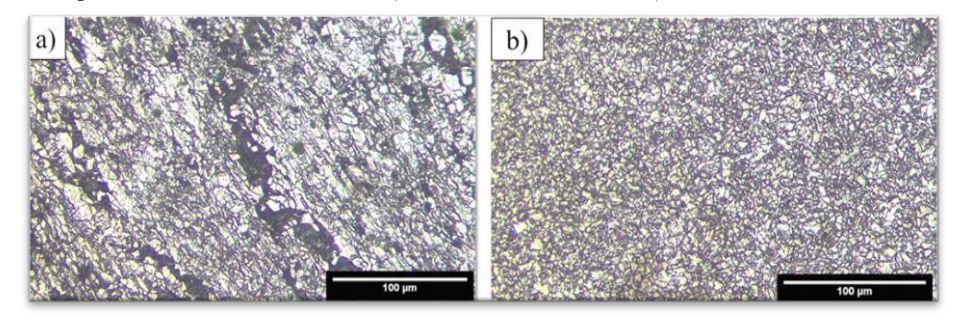
2. Experimental

Samples of API 5L MO and API 5L MS steels were taken from the cross section of tubes manufactured by Tenaris S.A. Metallographic preparation was carried out in accordance with ASTM E 3, 2017 [1] and 2% Nital was used to reveal the microstructure. Metallographic analysis was carried out using a Zeiss® optical microscope equipped with a digital camera and IMAGE J® image analysis software [2]. Microhardness tests were carried out on the polished surface with a Wilson® 401 MVD Microindentation Tester.

3. Results and Discussions

The microstructures of API 5L X70 M0 and API 5L X70 MS steels are shown in figure 1. The former (Fig. 1a) shown a coarse-grained ferritic microstructure with the presence of bands (identified by the darker areas). Banding is mainly caused by the microsegregation of alloying elements during steel solidification. Subsequent hot work operations result in an alignment of microsegregation in the work direction, which results in the emergence of outlined bands in the microstructure. The later (Fig. 1b) revealed a ferritic matrixcomposed of randomly oriented polygonal grains (light areas) and intergranular pearlite (black spots). The high grain refinement is resulting from the low carbon content, and the thermomechanical treatment (controlled rolling and accelerated cooling). The high refinement of the grand is resulting from the carbon content and from the thermomechanical treatment (control lamination and accelerated cooler). Both steels exhibited similar average grain sizes. MO and MS steels have ferritic grain sizes of $6 \pm 3 \mu m$ and $5 \pm 2 \mu m$, respectively. In Vickers microhardness tests, twenty microindentations were made on the surface. MO and MS steels also presented similar microhardnesses, $76 \pm 2 \, \text{HV}$ and $75 \pm 1 \, \text{HV}$, respectively. However, the average grain sizes and standard deviation values of microhardness in MO steel are larger than in MS steel, probably due to a more refined and homogeneous microstructure in the latter.

Figure 1: Steel microstructure: a) API 5L X70 MO and b) API 5L X 70 MS



4. References

- [1] ASTM E 3. Standard Guide for Preparation of Metallographic Specimens 1., 2017.
- [2] ASTM E1382. Standard Test Methods for Determining Average Grain Size Using Semiautomatic and Automatic Image Analysis. **ASTM International**, v. 97, Reapproved 2010, p. 1–24, 2014.

^{*}Corresponding author: elida.alves@unesp.br

METHODOLOGY FOR APPLYING SHAPE MEMORY ALLOY IN HYPERSONIC VEHICLES SIMULATED IN A PLASMA TUNELL

Alana Aíres da Rocha Brito^{1*}, Felipe Jean da Costa², Cristian Cley Paterniani Rita³ and Milton Sergio Fernandes de Lima⁴

¹Instituto Tecnológico de Aeronáutica (ITA) – PG-CTE, São José dos Campos - SP

²Instituto Nacional de Pesquisas Espaciais (INPE), São José dos Campos - SP

³Faculdade de Tecnologia (FATEC), Pindamonhangaba - SP

⁴Instituto de Estudos Avançados (IEAv), São José dos Campos – SP

1. Introduction

During the hypersonic flight of a vehicle equipped with hypersonic air-breathing propulsion system technology operating in a wide range of flight conditions, it must withstand severe conditions of thermal flow gradients, shock waves and pressure in a short exposure time. The aim of the work is to simulate the ablative environment in which the Shape Memory Alloy (SMA) present in the fairing will be exposed to in the real conditions of a hypersonic flight inside a hypersonic plasma tunnel.

2. Experimental

Throughout the experiment, it is possible to simulate and study the thermal flow conditions in the most critical process of the mission: atmospheric reentry. The tunnel, seen in figure 1, has a vacuum chamber with an integrated refrigeration system, providing a controlled atmosphere, a plasma torch and a sample holder. The vacuum system consists of two mechanical vacuum pumps and a roots pump. To reach the hypersonic regime, the geometry of the torch nozzle simulates a rocket nozzle, in which its geometry converges and diverges the compressed air that is being introduced, reaching hypersonic speeds. [1].

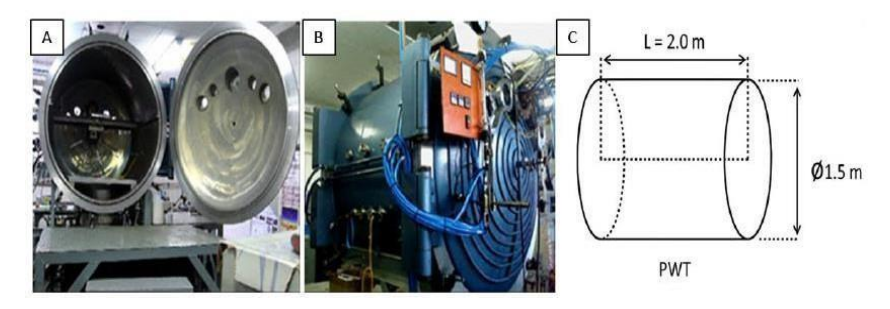


Fig. 1. Plasma tunnel A) frontal profile of the tunnel B) isometric profile of the tunnel with analog panel and cabling C) dimensions of the tunnel [1].

3. Results and Discussions

During the simulation, it was possible to record the configurations at the end of the thermal flow calculation using a calorimeter and a thermocouple fixed close to the sample holder, the mach number using the pressure ratio P0/P considering the disposable system and the enthalpy according to ASTM standard. To know the crystalline structure of the SMA sample after the simulation, optical metallography, XRD diffraction and hardness were used.

4. References

[1] C. Paterniani, F. Miranda, F. Caliari, R. Rocha, A. Essiptchouk, L. Charakhovski, G. Petraconi, Hypersonic Plasma Setup for Oxidation Testing of Ultra-High Temperature Ceramic Composites. Journal of Heat Transfer. 142. 10.1115/1.4047150. (2020).

Acknowledgments

This study was financed in part by the Coordenação de Aperfeiçoamento de Pessoal de Nível Superior – Brasil (CAPES) – Finance Code 001. Thanks, are also due to the ITA and IEAv for the support and availability of the laboratories and material.

^{*} Corresponding author: alanarb21@gmail.com

METROLOGY IN VACUUM TECHNOLOGY BY THE STATIC EXPANSION METHOD

João Pedro Cappeletti Andreatta¹, Alicia Fernanda Rubio Pinheiro², Francisco Tadeu Degasperi³

^{1,2}microelectronics students at FATEC-SP, São Paulo College of Technology ³Doctor by electrical engineering and computer college UNICAMP, professor in FATEC-SP

1. Introduction

Metrology is the science of measurement and its applications, covering all theoretical and practical aspects, being crucial to improve the precision and reliability of the measuring instruments. This project seeks thecreation of a primary vacuum standard in Brazil using the static expansion method. Thus, the project that is currently being developed out in a partnership of the National Institute of Metrology, Quality and Technology (INMETRO) aims to expand the graph of measured pressures relative to calculated pressures, based on the collection of more empirical data.

2. Theory

The methodology utilized during this project consists in the method of the static expansion, whereupon utilizes an ideal gas volume, which is conserved during the whole process of expansion.

By the ideal gas model and the volume conservation, can be used the Boyle-Mariotte law, which derives from the ideal gas equation: p. V = n. R. T

Where in this case, assuming that the system doesn't have any gas leak, the number of moles is preserved, and just the pressure, volume and temperature changes during the process of gas expansion. So, these three variables can be equated in only one equation $\underline{p_i v_i} = \underline{p_f v_f}$, where: p_i , V_i e T_i – Initial pressure (mbar), volume (m³), and

temperature (K), before the expansion. pf, Vf, e Tf – Final pressure (mbar), volume (m³), and temperature (K), after the expansion.

4. Results and Discussions

Analyzing the figure 1, that brings an average between the values measured by the three pressure meters, is possible to see that the measured and the calculated points shows a good collinearity, that can be confirmed when verifying the equation of the straight line present on the left top corner of the graphic. Where the value thatmultiplies the X variable must be closest to 1, and the next value, which is summed to the X, must be close to 0, so that the tendency line is exactly at 45°, proofing that the experimental arrangement is in a perfect condition.

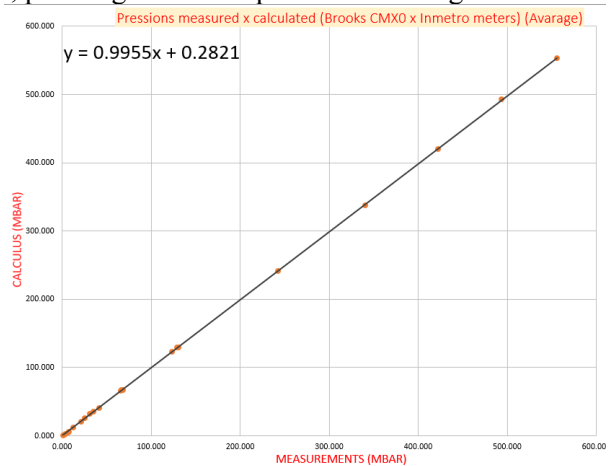


Fig. 1. Graph of the experimental curve with the averagevalue of the three meters.

5. References

[1] G. Dantas; K. Cesar. Criação do padrão primário de Vácuo no Brasil pelo método de Expansão Estática. FatecSão Paulo, São Paulo, 2022.

Acknowledgments: For the institution FATEC-SP for the support, the vacuum technology laboratory (LTV) and the CNPq instution for the scientific initiation scholarship.

^{*} Corresponding author: Joao.andreatta@fatec.sp.gov.br

MICRO ABRASION WEAR OF HOMOGENEOUS AND GRADED TITANIUM NITRIDE FILMS

Felipe Carneiro da Silva^{1,2}, Ronaldo C. Cozza³, Julio César Sagás⁴, Luis César Fontana⁴, Claudio Geraldo Schön¹

¹ CEETEPS – Centro Estadual de Educação Tecnológica "Paula Souza" - Brazil
 ² Universidade de São Paulo, Department of Metallurgical and Materials Engineering - Brazil
 ³ Centro Universitário FEI – Fundação Educacional Inaciana "Padre Sabóia de Medeiros" - Brazil
 ⁴ Laboratory of Plasmas, Films and Surfaces, Universidade do Estado de Santa Catarina- Brazil

1. Introduction

Titanium nitride (TiN) have been used in the last decades to enhance wear resistance of surfaces. TiN stands outdue to its excellent mechanical, great chemical stability optical, electrical properties, corrosion resistance and highwear resistance [1]. Using the GAMS technique, it is possible to produce functionally graded TiN thin films by varying the N_2 supply during deposition [2]. The aim of this work is to analyze the micro abrasive wear resistance and quantify wear coefficient (k) of graded and homogeneous TiN films by GAMS.

2. Experimental

Homogeneous and graded TiN films were deposited onto AISI M2 tool steel substrates. Micro abrasion tests were carry out using the counter-body of AISI 52100 bearing steel sphere of diameter D = 25.4mm. The abrasive slurries were prepared with abrasive particles of black silicon carbide (SiC) and distilled water. For each specimen, three experimental repetitions were conducted for each sliding distance, totally 18 micro abrasive weartests on each specimen (homogeneous and graded).

3. Results

Table 1 presents the values of the wear coefficient (k) for both homogeneous and functionally graded thin films. It is possible to assert that the functionally graded TiN thin film exhibited a wear resistance 33.3% higher than thehomogeneous TiN film. Figure 1 shows the wear volume behavior (V) plotted as a function of sliding distance(S) - V = f(S). It can be observed that, for both film types (homogeneous and graded), the wear volume (V) increased with the increase in sliding distance (S). Therefore, graded TiN films exhibit a greater increase in wearresistance compared to homogeneous TiN films, which could be of interest for engineering applications.

Condition	Wear coefficient (mm ³ /N.m)
Homogeneous	$(1.2 \pm 0.2) \times 10^{-4}$
Functionally graded	$(9.0 \pm 1) \times 10^{-5}$

Table 1- Values of the wear coefficient (k) [1].

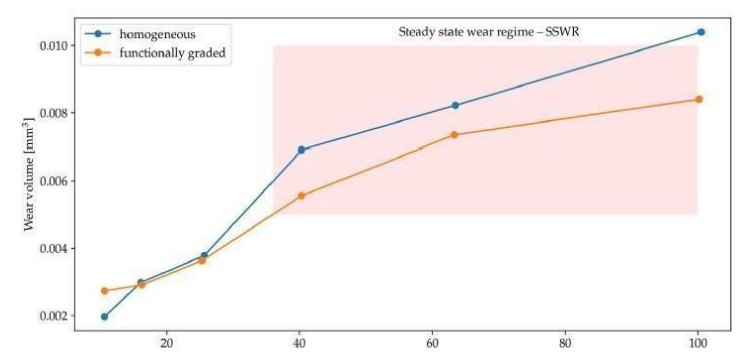


Figure 2- Behaviour of the wear volume - V as a function of the sliding distance -S-V = f(S). Maximum standard-deviation of V, SDV= 0.00018 mm³ [1].

4. References

- [1] F.C. Silva et al, JMR&T 22 54-65 (2023).
- [2] F.C. da Silva et al, SN Appl. Sci. 2 865 (2020)

Nb-DOPED TiO2 FILMS FOR APPLICATION AS TRANSPARENT CONDUCTIVE OXIDE

Francisco Alfaro^{1*}, Rafael G. Delatorre¹, Julio C. Sagás² and Diego A. Duarte¹

¹Universidade Federal de Santa Catarina, Joinville Center of Technology, Laboratory of Surface Treatments.

²Universidade do Estado de Santa Catarina, Laboratory of Plasmas, Films and Surfaces.

1. Introduction

Transparent conductive oxides (TCOs) such as ITO and FTO have been traditionally used in photovoltaic (PV) technology for their optical and electrical properties [1]. Specifically, ITO typically has a resistivity on the order of $10^{-4} \,\Omega$ ·cm [2]. Nb-doped TiO₂ (TNO) emerges as a promising alternative with similar high transmittance and low sheet resistance [3]. In such technology, these properties must be conciliated through a complex electronic structure optimization [3]. Plasma-assisted methods such as magnetron sputtering can be employed to achieve these goals due to its ability to control the material properties in atomic scale.

2. Experimental

TNO films were deposited by grid-assisted magnetron sputtering on glass substrates from a 4 inch target composed by Ti and different Nb inserts positioned along the target erosion zone. During the deposition, the substrate was maintained at floating potential. Depositions were made at room temperature and 300°C with one (0.8% Nb) and four (3.0% Nb) inserts. TiO₂ films were also obtained at the same temperatures for comparison. Target current, DC power, target-to-substrate distance, working gas, film thickness *t*, Ar and O₂ mass flow rate was kept, respectively, at 2.00 A, 1.0 kW, 6 cm, 0.80 Pa, 100 nm, 1.5 and 4.4 sccm. Films were evaluated by two-point probe method and spectrophotometry in the 190-1600 nm range.

3. Results and Discussions

Fig. 1 shows the transmittance for samples deposited at 300°C. Average transmittance for TiO₂ is 75% in the visible and 70% in the infrared range. Nb-doped samples have averages of 75% (visible) and 63% (infrared) for 1 Nb insert, and 73% (visible) and 63% (infrared) for 4 Nb inserts. Non-heated Nb samples averaged 78% in the visible and 66% in infrared. Resistivity for heated Nb samples was around $10^{-2} \,\Omega \cdot \text{cm}$ ($\rho = R_{\text{sh}}t$) whereas nonheated ones were close to $10^3 \,\Omega \cdot \text{cm}$. The data suggests that Nb doping and heating conditions significantly impact both transmittance and resistivity.

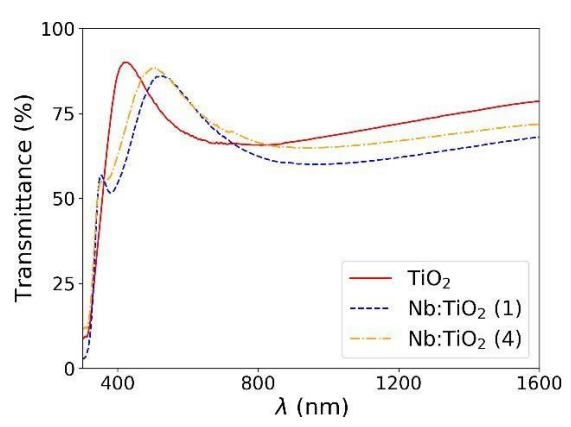


Fig. 1. Transmittance for TiO_2 and Nb-doped TiO_2 films, deposited at 300°C using targets with 1 and 4 Nb inserts.

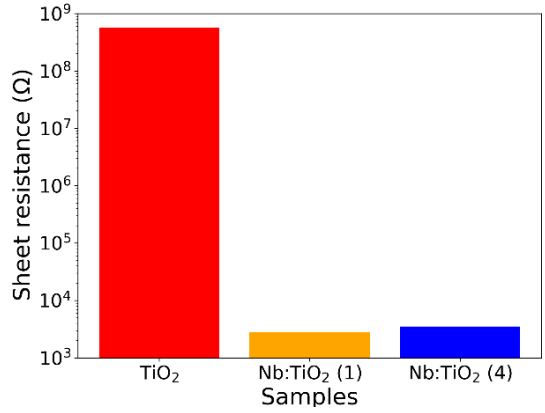


Fig. 2. Sheet resistance (R_{sh}) for TiO_2 and Nb-doped TiO_2 films, deposited at 300°C using targets with 1 and 4 Nb inserts

4. References

- [1] P. Basumatary, P. Agarwal. Materials Research Bulletin, 149 (2022) 111700.
- [2] M.S. Farhan, et al. International Journal of Precision Engineering and Manufacturing. 14 (2013) 1465.
- [3] Y. Furubayashi, et al. Applied Physics Letters, 86 (2005) 252101.

Acknowledgments

The authors thank FAPESC (PAP-UDESC) and CNPq (grants 307408/2021-3 and 406376/2022-0).

^{*}Corresponding author: alfaro.professor@gmail.com

NITROGEN-DOPED DIAMOND FILMS APPLIED TO THIN-FILM TRANSISTORS

Evaldo Chagas Gouvêa^{1*}, Joelma de Oliveira¹, Júlia Corrêa Reis¹, Thais Santos Castro¹, Teófilo Miguel de Souza¹

¹São Paulo State University (UNESP), Guaratinguetá Campus, Brazil

1. Introduction

Thin-film transistor is a type of FET transistor with simple, planar structure. It shows good electrical performance and can be used in displays [1], for example. To assemble it, several compounds could be used, such as Ga₂O₃ [2] and SiO₂ [25]. However, there is no relevant information in the literature about the use of nitrogen-doped diamond layers in thin-film transistors. Thus, in this work we describe how nitrogen-doped diamond filmsinfluence the behavior of thin-film transistors.

2. Experimental

The diamond films were produced with a hot-filament CVD reactor, using HPHT boron-doped p-type silicon substrates with crystalline orientation (100). The HFCVD reactor worked with 20 torr of internal pressure and total gas flow of 200 sccm. Methane (1.5%), nitrogen (1%) and hydrogen (mass balance) gases were used. Tungsten filaments heated the substrate between 1000-1070 K for 4-5 hours. The structural characteristics of the films were obtained using scanning electron microscopy (SEM) and Raman spectroscopy. Electrical characteristics of the transistors were obtained using current-voltage curves.

3. Results and Discussions

The films have grown uniformly over the substrate surface, according to SEM images. Raman graphs (Fig. 1) showed that only crystalline diamond was formed (1333 cm⁻¹ peak) and that interstitial nitrogen was incorporated to the films, since there is no Raman peak at 1190 cm⁻¹, reducing the quantity of charge carriers and thus raising the electrical resistivity of the material. If there was a 1190 cm⁻¹ peak in Fig. 1, then substitutional nitrogen was formed and the diamond film would be electrically conductive.

The output curves of the thin-film transistor (Fig. 2) show that the component presents a supra-linear behavior due to the high amount of traps formed in the nitrogen-doped diamond film. Supra-linear regions are described by an exponential increase in the drain current when drain-source voltage (V_{DS}) is increased, especially for low values of V_{DS} . Also, the presence of nitrogen significantly reduced the drain current magnitude in the transistor to microamps at room temperature. Therefore, nitrogen-doped-diamond thin-film transistors seem suitable for low-power circuits. Despite that, nitrogen-doped films could be useful in other components, such as insulating layers in capacitors, due to its high electrical resistivity.

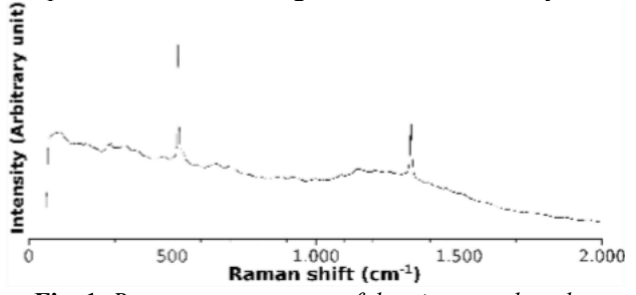


Fig. 1. Raman spectroscopy of the nitrogen-doped diamond film.

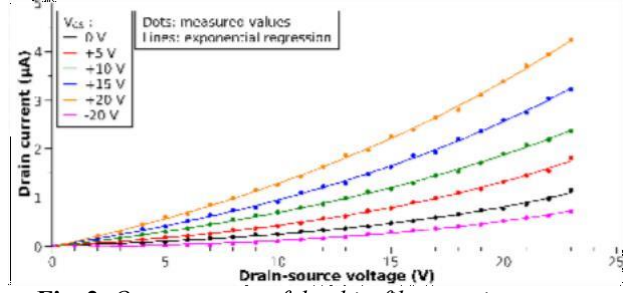


Fig. 2. Output curves of the thin-film transistor.

4. References

- [1] H. Jung et al., J. Vac. Sci. Technol. A, 35, 031510, (2017).
- [2] Y. Gong et al., Micro Nano Lett., 14, 1052–1055, (2019).
- [3] K. Yang et al., Phys. Status Solidi, 217, 1900556, (2020).

Acknowledgments

This study was financed in part by the Coordenação de Aperfeiçoamento de Pessoal de Nível Superior – Brasil (CAPES) – Finance Code 001.

^{*}Corresponding author: evaldo.gouvea@unesp.br

NUMERICAL EVALUATION OF PEROVSKITE SOLAR CELLS USING Nb₂O₅/AZO AS FRONT CONTACT LAYER

Christof Zickenheiner¹, Raul Ramos², José Roberto Ribeiro Bortoleto²

¹ Clausthal University of Technology, Clausthal-Zellerfeld, Germany ² Institute of Science and technology, São Paulo State University (UNESP), Sorocaba, Brazil

1. Introduction

To gain deeper insights into the impact of the optical properties of the AZO and Nb_2O_5 layers on the overall performance of the photovoltaic device, simulations with the software "OghmaNano" have been performed. This software employs a comprehensive numerical model which is capable of simultaneously simulating both the electrical and optical characteristics of the perovskite solar cell (PSC).

2. Methodology

For this simulation, a standard MAPbI₃ PSC nip configuration was chosen. To simulate the transport and electrostatic effects within the device, the model solves Poisson's equation and the bipolar drift-diffusion equations in one dimension. Critical for this simulation are the device parameters, which serve as input for the model. These were extracted from literature to represent an ideal PSC [1]. To accurately represent the optical field distribution within the device, the model further employs the transfer matrix method [2]. This approach incorporates the wavelength dependent complex refractive index and the continuity condition to calculate reflections at material interfaces and optical losses for planar light waves at normal incidence. Several scenarios were simulated to shed light on the influence of the different material layers and interfaces on the optical behavior of the PSC.

3. Results and Discussions

Upon conducting this series of simulations, the resulting J-V curves (Fig. 1) exhibited a noticeable variation in short-circuit current (Jsc) when considering the optical parameters of the different layers, consequently impacting the power conversion efficiency (PCE) of the PSC. The drops in Jsc can be primarily attributed to reflections occurring at material interfaces, which can be concluded from the reflection profiles (Fig. 2). While the Nb₂O₅ layer initially increases the overall reflectivity of the stack, the subsequent addition of the AZO and SLG layers results in a reduction of reflectivity while introducing strong interference patterns. These patterns arise due to the superposition of a multitude of phase shifted reflected light waves. The phase changes are in turn caused by a difference in optical path length through the materials and reflection induced phase shifts at interfaces. This has a significant wavelength dependent impact on the quantum efficiency of the PSC. The gradual increase in refractive index of the material layers prevents an abrupt change in the optical properties at the interfaces, minimizing the reflection that would typically occur.

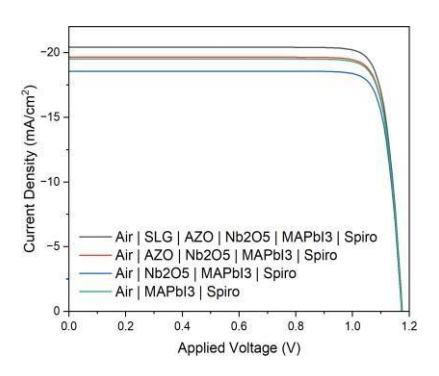


Fig. 1. J-V curves

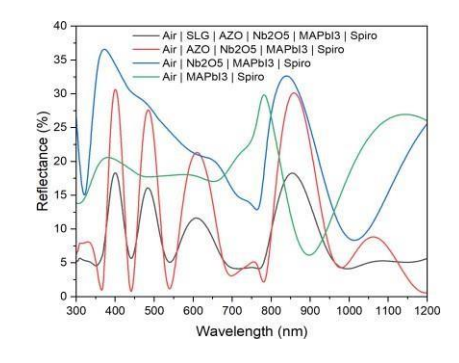


Fig. 2. Reflectance profiles.

4. References

- [1] Yassine Raoui et al, Solar Energy, **193**, 948-955, 2019.
- [2] Sachchidanand, Anil Kumar, Pankaj Sharma, Solar Energy, **259**, 63-71, 2023

Acknowledgments: The authors thank CAPES, CNPq for financial support and CBMM Company for niobium metallic target.

^{*}Corresponding author: jose.rr.bortoleto@unesp.br

NUMERICAL MODELING OF A RESONANT CAVITY LINEAR ACCELERATOR USING MONTE CARLO METHOD

Vinicius Carvalho Morais¹, Henrique Chaves Gulino², Francisco Tadeu Degasperi³

^{1,2,3} Laboratório de Tecnologia do Vácuo – LTV – Faculdade de Tecnologia de São Paulo - CEETEPS

1. Introduction

Understanding and comprehending the interaction and limitations imposed by residual gases present in the atmosphere of an accelerator structure on charged beams allows for the avoidance of undesirable events such as deceleration and particle loss [1]. The use of vacuum system modeling makes events more predictable and ensures that these types of systems are operated correctly. In this work, computational modeling was employed using the Molflow+ tool (Monte Carlo), developed by CERN, to study the pressure field along a linear accelerator structure with resonant cavities, enabling the determination of pressure values for each position in the vacuum system.

2. Experimental

The vacuum system structure was based on five resonant cavities, each formed by a spherical geometry with a radius of 100 mm and cylindrical tubes with a radius of 15 mm and a length of 40 mm. The total length (between each end) is 1240 mm, with a sticking factor equal to 1 at both ends. This sticking factor is a parameter used to simulate the vacuum pump by considering the probability of particles colliding with the surface (in this case, the ends of the system) being absorbed. Stainless steel was used as the material for constructing the resonant cavity linear accelerator, with a degassing rate per unit area of $q = 5.10^{-8}$ mbar.l.s⁻¹.cm⁻².

3. Results and Discussions

Molflow+ is a Windows program that allows you to calculate the steady-state pressure in an arbitrarily complex geometry when ultra-high vacuum condition is met. The name comes from molecular flow, the condition when the mean free path of molecules is so long compared to the geometry size that collisions can be neglected. In this case, particles fly independently, which makes this physics particularly suitable for Monte Carlo simulations [2].

From the simulation performed in Molflow+, using the parameters described in the previous section, the final pressure values were obtained for each position in the vacuum system. Figure 1 demonstrates the pressure values for each point on the system's surface, characterized by a gradient that shows a color for each pressure value. In Figure 2, a pressure field graph along an axis starting from one end and ending at the other end was obtained.

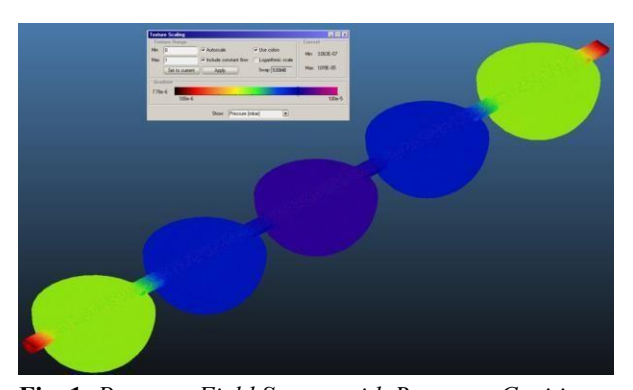


Fig. 1. Pressure Field System with Resonant Cavities During Monte Carlo Simulation.



Fig. 2. Pressure Field as a Function of Position along the Axis between One End and the Other of the Resonant Cavity Vacuum System.

4. References

- [1] MALYSHEV, Oleg. Vacuum in particle Acellerators. WILEY-VCH, 2020.
- [2] ADY, Márton; KERSEVAN, Roberto. MolFlow+ user guide. CERN, 2014.

Acknowledgments

To CNPq for the PIBIC scholarship.

^{*}Corresponding author: henriquegulino550@gmail

O IEAMAR NAS ESCOLAS DE ENSINO BÁSICO DA REDE PÚBLICA ESTADUAL

Giovanna Marcal Pereira*, Fernando Luiz de Campos Carvalho e Eduardo do Valle Ricardo

Departamento de Engenharia Ambiental e IEAMar

1. Introdução

A extensão universitária é uma abordagem interdisciplinar e interativa com a comunidade. Esse processo abrange aspectos culturais, educacionais, científicos e políticos, buscando transformações positivas entre a universidade e a sociedade [1]. O presente trabalho busca promover o letramento científico das comunidades escolares participantes, acerca da UNESP e do Instituto de Estudos Avançados do Mar(IEAMar), e proporcionar o contato social entre os participantes e a universidade por meio de visitas direcionadas nas/das escolas. Como objetivo específico, realizar demonstração do uso do microscópio eletrônico de varredura (MEV)abordando os princípios de funcionamento com ênfase na importância do vácuo para a qualidade das imagens.

2. Metodologia

A metodologia se dividiu em etapas: reuniões para definir como seria a abordagem dos estudantes do ensino médio e desenvolver um material didático; preparação e validação de dois questionários para avaliar o conhecimento pré e pós-implementação das atividades junto à universidade e ao IEAMar. A etapa posterior consistiu em visitas direcionadas às escolas, com palestras sobre a universidade e o IEAMar. A terceira foi a visita dos alunos à universidade, incluindo visitas aos departamentos e ao IEAMar, com apresentação do MEV eseu funcionamento, bem como de outros equipamentos e suas aplicações. A quarta etapa, em nova visita ao IEAMar, consistirá na apresentação sobre importância do vácuo para diferentes equipamentos de pesquisa, partindo do MEV e da qualidade das imagens geradas nesse equipamento.

3. Resultados e Discussões

Os resultados após a visita à Unesp/IEAMar podem ser discutidos a partir das nuvens de palavras geradas, mostrando que os estudantes foram positivamente impactados, e despertou o interesse em ingressar na universidade. Professores das escolas participantes passaram a buscar parcerias com a UNESP e o IEAMar para o desenvolvimento de trabalhos de iniciação científica com seus alunos do ensino médio. Por sua vez, os estudantes interessados em ciências exatas e da natureza manifestaram interesse em participar de projetos no IEAMar, discutindo o funcionamento do MEV em suas respostas. Os princípios físicos de funcionamento do MEV serão abordados com foco na importância do vácuo, e, para instigar a curiosidade e interesse dos alunos, as imagens a seguir (Fig. 3 e 4) foram apresentadas durante a visita à Unesp.



capacidademelhor entender
microrganismos microscópica
golho aumentar partículas
ampliador potentes
imagem observar
avançado forma visão pesquisa grandes ampliação
tecnologia microscopio superficies

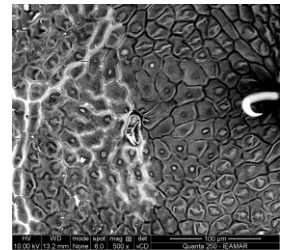




Fig. 1. Nuvem de palavras

Fig. 2. Nuvem de palavras

Fig. 3. Folha em baixo vácuo (50Pa).

Fig. 4. Folha em alto $v\acute{a}cuo(10^{-4}Pa)$.

4. Referências

[1] Fórum de Pró-Reitores de Extensão das Universidades Públicas Brasileiras – FORPROEX, 2010, Belo Horizonte. Extensão Universitária: organização e sistematização. Belo Horizonte: COOPMED, 2010

^{*}Corresponding author: giovanna.marcal@unesp.br

OPTIMIZATION OF ALUMINUM-THERMOPLASTIC COMPOSITE ADHESION THROUGH MICROARC OXIDATION TREATMENT

Rafael R. Lucas¹*; Luis Felipe B. Marques¹; Edson C. Botelho²; Ana Beatriz R. M. Abrahão³; Rogério P. Mota¹

¹Department of Physics, Faculty of Engineering and Sciences (UNESP), Guaratinguetá Campus ²Department of Materials and Tech., Faculty of Engineering and Sciences (UNESP), Guaratinguetá Campus ³Laboratory of Electrochemistry and Corrosion, Faculty of Technology of Pindamonhangaba

1. Introduction

Joining different materials through welding can be challenging due to their distinct mechanical and thermal properties. For an effective union, it is crucial to consider factors such as the welding method, surface preparation, temperature control, pressure management, and the use of additional materials [1, 2]. In this study, we carried out the joining of 1100 aluminum alloy, which had been previously surface-treated using electrolytic plasma, with a thermoplastic composite of glass fiber-reinforced polyetherimide, using the oxyacetylene welding (OFW) process. The objective was to characterize these joints and determine their Lap Shear values.

2. Experimental

Strips of the 1100 alloy and the PEI/Fiberglass composite were cut to dimensions of 100 x 25 mm, following ASTM D1002:10 standards. They were cleaned using ultrasonic treatment with distilled water and a neutral detergent for 900 seconds, followed by a cleaning with isopropyl alcohol for the same duration. The study employed a system comprising a stainless steel (AISI 430) electrolytic tank and an AC voltage variator with a rectifier/doubler circuit. The treatment was conducted using a 2³ factorial design, varying time, voltage, and the electrolyte concentration (sodium tetraborate), as detailed in Table 1.

	Levels					
v ariabie	Coaea —	-α	-1	0	+1	$+\alpha$
Time (s)	X1	95	300	600	900	1105
Voltage (V)	X2	150	200	275	350	400
Concentration (g/L)	X3	0,6	3,0	6,5	10	12

Table 1. Encoded values of the applied variables.

The gas pressures were set at 0.5 kgf/cm² for acetylene and 1.0 kgf/cm² for oxygen, with the torch nozzle positioned approximately 70 mm from the aluminum sample. The shear test (LSS) of the joined samples was conducted using a Shimadzu AG-X universal testing machine, equipped with a 50 kN load cell, operating at a speed of 1.5 mm/min, following the standards specified in ASTM D1002.

3. Results and Discussions

The Lap Shear Strength (LSS) test results ranged from 5.4 to 10.7 MPa, with control samples averaging 5.2 MPa. This indicates the effectiveness of the treatment, resulting in significant increases ranging from 4% to 104%. An analysis of variance (ANOVA) revealed that immersion time, process voltage, and electrolyte concentration (sodium tetraborate) contributed 1.23%, 9.53%, and 0.20%, respectively, to the variation in shear strength. However, approximately 20.52% of the total variability in the response variable (Lap Shear) was attributed to "Pure Error" or "Unexplained Variability," which may be influenced by various factors in the PEO and OFW processes.

4. References

- [1] R. Lucas, et al., MRS Communication, 12, 266-271, (2022)
- [2] J. Reis, et al., Welding in the World, 65, 1145-1160, (2021)

Acknowledgments

The authors express their gratitude to CNPq and CAPES for the financial support provided for this study, as well as for the funding of the graduate program.

^{*}Corresponding author: rr.lucas@unesp.br

OPTIMIZING WETTING PROPERTIES OF POLYPROPYLENE NON-WOVEN VIA ATOMICLAYER DEPOSITION OF TiO2

Júlia Karnopp^{1*}, Ngoc Le Trinh², Han-Bo-Ram Lee², Rodrigo S. Pessoa¹

¹Plasmas and Processes Laboratory, Aeronautics Institute of Technology, São José dos Campos, Brazil ²Department of Materials Science and Engineering, Incheon National University, Incheon, Korea

1. Introduction

Face masks are used to reduce the transmission of respiratory illnesses. However, commonly used masksare not completely effective. The textile material of masks, the polypropylene non-woven, can be functionalized by thin film deposition as a potential way to improve the efficiency. Oxides metallic films deposited by atomic layer deposition (ALD) can improve wetting and electrostatic effects properties of polymer fibers [1, 2]. ALD consists in a deposition layer by layer through surface chemistry reactions. Initially in this study, TiO₂ thin films were deposited on polypropylene non-woven using ALD to investigate the changes in wettability and morphology.

2. Experimental

TiO₂ thin films were deposited by ALD for the range of 100 to 700 cycles at 100°C. Two sample types were employed: one consisting of a single layer of polypropylene non-woven, and other with three layers like the commercial triple-layer mask. Titanium(IV) isopropoxide (TTIP) and H₂O were used as the precursor and oxidant, respectively. One ALD cycle was composed of the filling step pulse of N₂ (7s, 30 sccm) used to carry the TTIP, TTIP pulse (6s), N₂ purge (20s, 100 sccm), H₂O pulse (3s), and N₂ purge (20s, 100 sccm). The samples mass variation due the deposition, wettability and morphology were analyzed.

3. Results and Discussions

The initial results revealed that for low number of ALD cycles, the sample mass remained unchanged after deposition, indicating a nucleation process (Fig. 1). After 300 cycles the film's mass began to increase linearly with the cycles. The mass variation for the triple layer sample is greater than for single layer because it has a larger surface area available for deposition. The deposition also occurred in the intermediate layer.

In the conditions that the mass did not change after the depositions, the water contact angle also remains nearly constant. As the TiO_2 film thickness increased in the samples, the water contact angle decreased. After 500 cycles, the single-layer sample became hydrophilic, while the triple-layer sample became super hydrophilic (Fig.2). Importantly, the deposition process did not damage or alter the polypropylene fibers in the samples.

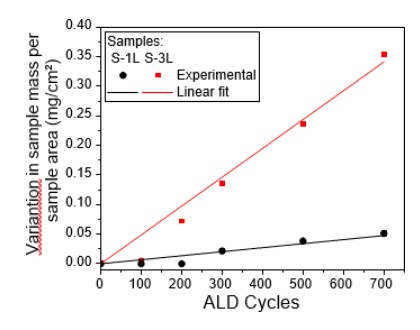


Fig. 1. Variation in sample mass per sample area as function of ALD cycles for single layer, S-1L, and triple layer, S-3L, samples

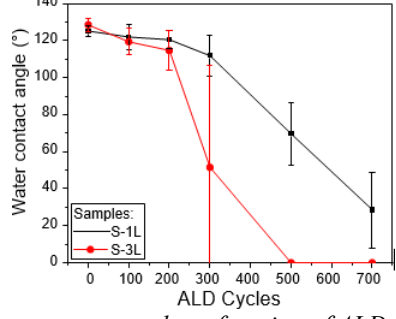


Fig. 2. Water contact angle as function of ALD cycles for single layer, S-1L, and triple layer, S-3L, samples. The error bars correspond to the standard deviation of measurements at different points in the sample.

4. References

- [1] A. H. Brozena, et al., J. Vac. Sci. Technol. A, 34, 010801, (2016)
- [2] C. Li, et al., Adv. Mater. Interfaces, **8**, 2001485, (2021)

Acknowledgments

Júlia Karnopp thanks CAPES (Finance Code 001) and CNPq for the PhD and SWE scholarships, respectively.

^{*}Corresponding author: julia_karnopp@outlook.com

OVERVIEW OF BRAZILIAN NATIONAL WIND ENERGY, HIGHLIGHTING THE NORTHEAST REGION

Marcus V.S. Dias¹; Joel A.S. Ferraz¹; Wilson Santos Júnior¹; Anselmo C. de Araújo¹; Rafael R. Lucas¹; Rogério P.Mota¹

¹Faculty of Engineering and Science of Guaratinguetá, São Paulo State University (FEG/UNESP), Av. Dr. Ariberto Pereira da Cunha, 333, Guaratinguetá, São Paulo, Brazil.

1. Introduction

The energy matrices of Brazil and other countries have undergone significant changes, reducing dependence on oil and increasing other energy sources, due to oil price shocks and awareness about climate change. This reflects a pursuit of greater sustainability in the energy sector [1, 2]. This study aims to conduct an exploratory literature review to gather data and information, as well as analyze information provided to governmental bodies and energy sector agencies regarding sustainable energy sources.

2. Theoretical Study

According to the Global Wind Energy Council - GWEC (2022), 2021 was the second-best year for wind energy growth, with an addition of approximately 94 GW to global capacity, second only to 2020, which had a 1.8% increase compared to 2022. Brazil stands out in this growth, contributing 4.06% to the global addition of 93.6 GW, as shown in Figure 1.

3. Results and Discussions

This results in a global wind capacity of 837 GW, reducing the emission of 1.2 billion tons of CO2 into the atmosphere, which corresponds to the annual emissions of the entire South America. However, the growth of wind energy is not reaching the necessary speed for a safe and resilient global energy transition aiming to achieve the climate target of a temperature increase of 1.5°C by 2050. To attain this goal, the growth of wind energy should be four times greater than the current and projected growth until 2030, as depicted in Figure 2.

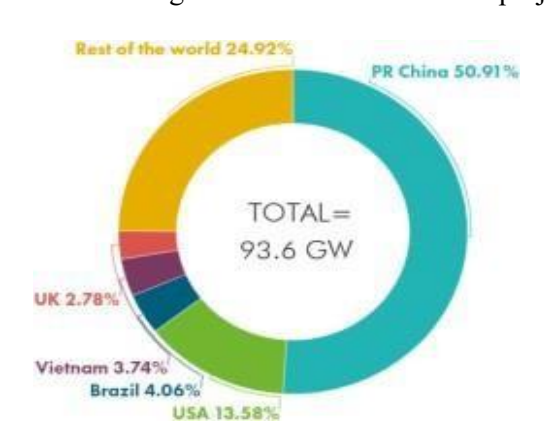


Fig. 1. Capacidade mundial de produção de energia eóica (em GW) – Fonte: GWEC/2022.

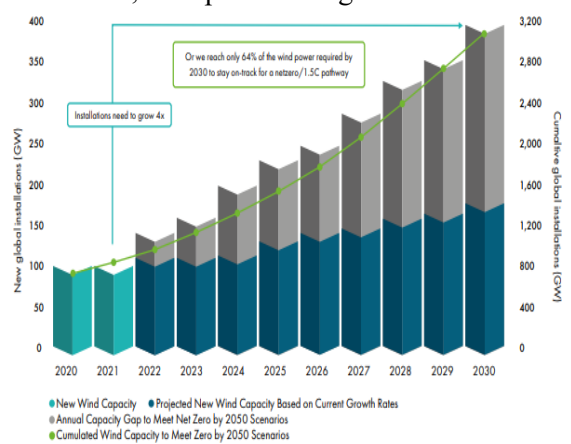


Fig. 2. Installed Wind Capacity and Future Need – Fonte: GWEC/2022

4. References

[1] SILVA, S. et al. Wind energy and energy complementarity: strategy and challenge for sustainable development in the northeast region of Brazil. Qualitas, v. 19 (3), (2018). http://dx.doi.org/10.18391/req.v19i3.5640.

[2] CASTRO, M. et al. Renewable energy: Wind energy, its effects and environmental gains. Journal od Engineering and Technology for Industrial Applications, v. 5, n. 19, p. 103-108, 2019.

 $[3] \ GWEC. \ Global \ Wind \ Report \ 2022. \ https://gwec.net/wp-content/uploads/2022/03/GWEC-GLOBAL-WIND-REPORT-2022.pdf$

^{*}Corresponding author: rogerio.mota@unesp.br

PESQUISA 3IP REALIZADAS NO BRASIL NAS ÚLTIMAS DUAS DÉCADAS

Abreuçon Atanasio Alves*1, Ana Carla de Paula Almeida1, Rogério Pinto Mota1

¹Universidade EstadualPaulista "Julio de Mesquita Filho" – Campus de Guaratinguetá

1. Introdução

A busca por novos materiais e os filmes finos poliméricos depositados por meio de processos a plasma são altamente valorizados em diversas aplicações. Assim, o desenvolvimento de técnicas capazes de modificar a superfície de materiais vem sendo exploradas para serem utilizadas em várias aplicações industriais e científicas, abrangendo setores como eletrônica, mecânica, revestimentos e biomateriais, entre outras. Isso ocorre devido às suas propriedades atrativas, como a capacidade de aderir bem à superfície subjacente, uma estrutura interligada, de fina espessura e uniformidade, entre outras características benéficas.O processo de modificação de superfícies por meio de plasma vem sendo explorado devido a sua rapidez, eficiência e ausência de resíduos tóxicos.A Implantação Iônica por Imersão em Plasma (3IP) é uma técnica avançada de modificação de superfície que melhora as propriedades da superfície do material sem afetar sua estrutura interna.

2. Teoria

Na técnica 3IP, uma amostra é colocada em uma câmara de vácuo e imersa em plasma. O processo de implantação iônica se dá ao aplicar um pulso elétrico de tensão negativa no substrato, expulsando os elétrons e, em seguida, atraindo os íons contra o substrato. Os ions colidem com o substrato, sendo nele implantados, alterando sua estrutura.

3. Discussões

Esse trabalhos tem como motivação apresentar uma revisão sobre trabalhos realizados no Brasil que utilizam a técnica 3IP. As pesquisas realizadas no Brasil que utilizam essa técnica, apontam como vantagens a sua capacidade de tartar amostras com geometrias complexas, uma vez que todas as regiões de sua superfície são cercadas pelo plasma e, portanto, podem ser atingidas pelo bombardeio iônico. Além disso, trabalhos apontam que esse método é caracterizado por seu baixo custo e tempos de tratamento reduzidos. A técnica 3IP aplicada nas fibras de carbono mostraram que não houve alterações significativas na estrutura cristalina das suas fibras, entretanto, notouse uma alteração namorfologia superfícial e na composição química das mesmas, ocasionando o aumento da resistência ao cisalhamento interlaminar.

De forma geral, a 3IP desenvolvida no Brasil, por pelo menos duas décadas, é estudada nos grupos de plasma/materiais alocados no INPE, em São José dos Campos; do Grupo de Plasma, da UNESP, em Guaratinguetá; do Grupo de Plasma/Materiais da UNESP de Sorocaba; na Universidade Estadual de Ponta Grossa (UEPG); na Universidade Federal de São Paulo (UNIFESP), em São José dos Campos; no Grupo de Materiais/ Processos de fabricação da UNICAMP, em Campinas.

4. Referências

- [1] KODAIRA, F.V.P. Implantação iônica por imersão em plasma e deposição de filmes finos poliméricos provenientes da mistura hexametildisilazano/argônio. 2013. 33 f. Trabalho de conclusão de curso (Bacharelado -Física) Universidade Estadual Paulista, Faculdade de Engenharia de Guaratinguetá, 2013.
- [2] C.-H. Yang, Y.-T. Wang, W.-F. Tsai, C.-F. Ai, M.-C. Lin, and H.-H. Huang, "Effect of oxygen plasma immersion ion implantation treatment on corrosion resistance and cell adhesion of titanium surface," Clin. Oral Implants Res., vol. 22, no. 12, pp. 1426–1432, 2011
- [3] C. B. Mello, "DEPOSICÃO DE FILMES FINOS BASEADA EM IMPLANTAÇÃOIÔNICA POR IMERSÃO EM PLASMA COM DESCARGA LUMINESCENTE EMAGNETRON SPUTTERING," Instituto Nacional de Pesquisas Espaciais, 2011

Agradecimentos:

Este trabalhos foi apoiado pela CAPES

^{*}Corresponding author: abreucon.alves@unesp.br

PHASE AND CHEMICAL COMPOSITION EFFECT ON THE GROWTH OF MAO COATING IN NOVEL BIO-HEAS.

Tiago dos Santos Pereira de Sousa^{1*}, Jhuliene Elen Torrento¹, Diego Rafael Nespeque Correa¹, Carlos Roberto Grandini¹

¹Universidade Estadual Paulista. Laboratório de Anelasticidade e Biomateriais

1. Introduction

Titanium and its alloys are widely used for biomedical implants due to their excellent mechanical properties. Similarly, high entropy alloys (HEAs) are a new class of materials that have gained attention in the field of biomedical applications due to their high strength, ductility, and corrosion resistance [1,2]. Micro-arc oxidation (MAO) is a surface treatment method that involves anodic reaction and dielectric barrier breakdown on the surface, resulting in a porous and thick oxide layer that is strongly bonded to the substrate. Therefore, MAO treatment can be an effective way to enhance surface properties and create low-cost metallic biomaterials with suitable biofunctionality. This work aims to develop bio-multifunctional surfaces in HEAs samples composed of non-toxic elements (Ti, Nb, Zr, Mo, Ta, and Fe).

2. Experimental

The HEAs ingots were created via an argon arc melting process using a tungsten electrode and a water-cooled copper crucible. The MAO treatment was carried out at three different voltages (100V, 200V, and 300V) with electrolytes rich in calcium, phosphorus, and magnesium. Structural and microstructural analyses of the bulk and film were carried out using optical and scanning electron microscopy (SEM) and X-ray diffraction (XRD). The composition of the film was analyzed by X-ray Photoelectron Spectroscopy (XPS).

3. Results and Discussions

The X-ray diffraction (XRD) analysis of the substrate revealed the bulk phases and some peaks related to the oxides formed on the surfaces. The SEM images showed (Fig.1) that the morphology of the oxides varied between the voltages used in this study. The XPS analysis indicated that the films were composed of the elements present in the bulk and some elements present in the electrolyte.

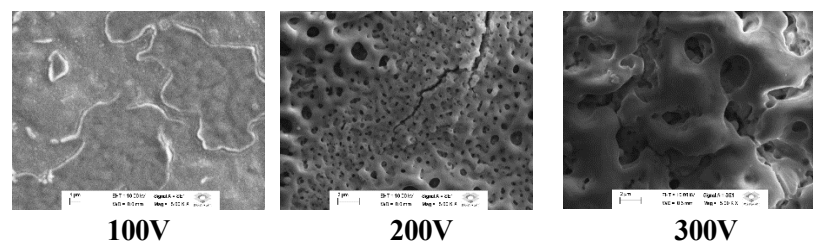


Figure 1: SEM images of TiZrNbFeMo alloy with MAO treatment in 100V, 200V and 300V

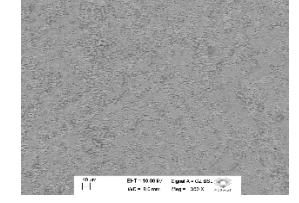


Figure 2: The backscattered electron (BSE) SEM images at 200V

The backscattered electron (BSE-SEM) images at 200V (Fig. 2) revealed the influence of substrate elements on film formation, as well as the preferential growth of oxides along distinct regions of the dendritic structures formed on the bulk material.

4. References

- [1] Torrento, J. E. et al., APL Materials: v 10, n. 8, 081113,2022
- [2] Sousa, T. S. P., et al. Materials Research, v.22, 2019

Acknowledgments

CNPq (grant #407251/2018-9) for the financial Support.

PHYSICAL AND CHEMICAL CHARACTERISTICS OF PLASMA ACTIVATED WATER GENERATED BY A COMBINATION OF DIELECTRIC BARRIER DISCHARGE AND GLIDING ARC TECHNIQUES

Nilton Francelosi Azevedo Neto^{1*}, Felipe Miranda², Pedro W. P. Moreira Júnior¹, Alessandro de Lima¹, Douglas M.G. Leite¹, Cristiane Y. Koga Ito², Rodrigo S. Pessoa¹

¹Instituto Tecnológico de Aeronáutica ²Universidade Estadual Paulista

1. Introduction

The development of non-thermal atmospheric plasma (NTAPP) to produce plasma activated water (PAW)has paved the way for the rapid advancement of new procedures that align with the demands of the biological sciences. This has opened exciting applications in fields such as agriculture, medicine, and dentistry, which were not achievable with just water or chemical products alone. Studies have shown that treating water with plasma isa promising technique for devising next-generation solutions for tooth-related diseases, bacterial inactivation, cancer treatments, and cement twinning [1].

2. Experimental

The experimental setup for plasma generation and water treatment is depicted in Figure 1. We utilized a combination of gliding arc and dielectric barrier discharge plasma reactors for the water treatment process. The airflow was adjusted between 1.0 and 10.0 L/min, and the experiments were conducted with a constant volume of 40 mL of deionized water. Parameters such as pH, total dissolved solids (TDS), oxidation-reduction potential (ORP), and conductivity were measured using a pH Meter from Metrohm, Herisau, Switzerland. Absorbance spectra, ranging from 190 to 500 nm, were obtained using a Perkin Elmer spectrophotometer. All water plasma samples from each experiment were analyzed immediately after collection.

3. Results and Discussion

The pH during water plasma activation shows a linear decline as flow increases to 5 L/min, then stabilizes. The pH drops from 8.06 to 2.65, attributed to nitrites [2]. The concentration of TDS in the treated water showeda significant increase. This elevation in TDS underscores that plasma-activated water treatment is instrumental inion generation. Notably, a peak TDS value is observed at 5 L/min, after which it tends to stabilize. This stabilization suggests a balance in the chemical reactions that produce new compounds from the existing chemical species in the water. The ORP analysis, a crucial metric indicating the efficiency of electron transfers in chemical reactions [2], yielded encouraging findings. For the untreated water, the ORP was measured at -38.5 mV, which might suggest that oxygen atoms predominantly act as electron acceptors. Once treatment commenced, there was a swift rise in ORP values, implying that plasma treatment of deionized water bolsters its oxidative potential. Mirroring the TDS findings, the ORP values also showed a trend of stabilization from a flow rate of 5 L/min onward. Increasing flow rates might produce more oxidizing agents in the plasma, such as nitrous acid, which contributes to the pH decline. UV-Vis spectroscopy was utilized to identify the presence of NO₂, NO₃, and H Q species in the treated water. Qualitative analysis of the spectra revealed a growing absorbance intensity with increasing airflow, suggesting a rise in the concentration of NO₂, NO₃, and H₂ Q species. Additionally, the broadened absorbance spectra, resulting from heightened airflow, can be linked to the enhanced presence of H₂O₂. The exact physical and chemical processes leading to the generation of H₂O₂ in activated water are still debatedin scientific circles. However, several theories have been put forth, one of which suggests the recombination of dissolved hydroxyl radicals (•OH) in the water.

4. References

[1] N.V.M. Milhan, W. Chiappim, A. da G. Sampaio, M.R. da Cruz Vegian, R.S. Pessoa, C.Y. Koga-ito, Int. J. Mol. Sci., 23, 4131-4148, (2022).

[2] N. Bolouki, W.H. Kuan, Y.Y. Huang, J.H. Hsieh, Appl. Sci., 11, 6158-6170, (2021).

Acknowledgments

We acknowledged the financial support of the São Paulo Research Foundation (FAPESP), grant's #2019/05856-7, 2023/02268-2, 2023/02273-6 and 2021/14181-3.

^{*}Corresponding author: nilton.azevedo@unesp.br

PHYSICAL AND MATHEMATICAL MODELING AND MEASUREMENT OF VACUUM LEAK DETECTION SYSTEM

Hernandes Miranda Alves¹, Thiago Ricardo Braga Silva², Francisco Tadeu Degasperi³

^{1, 2,3}Departamento de Sistema Eletrônico - DSE Faculdade de Tecnologia de São Paulo – FATEC-SP - CEETEPS

1. Introduction

Leak detection is a critical part of vacuum technology, with broad applications in industries and research that require vacuum to ensure the quality of their processes. It is also important in high-pressure systems, where leaks can contaminate the surrounding environment with harmful substances. In addition, the growing demand for technological innovations provides an opportunity for vacuum technology to improve and seek standards that are more precise. Therefore, the creation of new methods and validation tools for leak detection is necessary. In this context, our project aims to calibrate leak detectors with an accuracy of (10⁻⁵ to 10⁻⁶) mbar·L/s.

2. Theory and Materials

Based on vacuum technology theory, we model the throughput (Q) of a Leybold TL-4 capillary, which, through the choked flow effect, generates a continuous leak in the vacuum system, predetermined by the manufacturer. By analyzing the pressure in two chambers with the TL-4 capillary between them, a pressure difference will increase over time. This forms a graph of pressure over time.

Initially, the throughput (Q) is determined only for helium (He) gas, but various other gases, such as N2 and CO2, will calibrated the TL-4 and the mathematical modeling of the system have been performed by the Scilab program. The assembly was made with two vacuum chambers (vacuum chamber #1 on the left and vacuum chamber #2 on the right), as shown in Figure 1. The supports manufactured at LTV, using PLA, a polymer used in 3D additive manufacturing. Polystyrene tubes chosen to provide flexible connections, allowing freedom to make changes to the arrangement. The setup have been used two vacuum pump, one being a vane pump and a turbo-drag pump.

3. Results and Discussions

Using the gas accumulation method, in which the vacuum system is closed and the pressure of the system is allowed to increase over a long period. It is possible to calculate the intrinsic leak rate of the system and test the simplest leak detection method, as shown in the graph obtained by plotting the pressure over time, as shown in Figure 2. The graph shows that there is linearity, which allows us to calculate the slope of the line and thus calculate the actual leak rate of our vacuum system. The next step of the project will use a helium mass spectrometer to test new vacuum leak detection methods available on the market. This work will help to establish a reliable leak standard for the calibration of leak detectors.

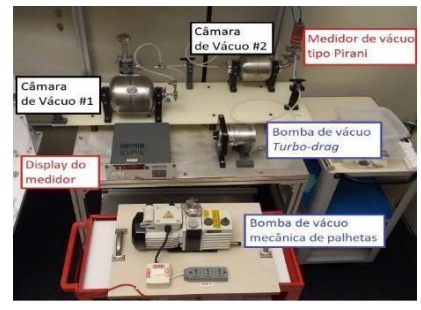


Fig. 1. The experimental setup used

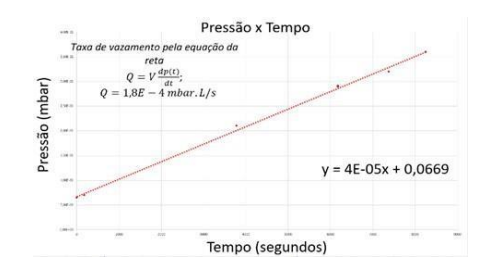


Fig. 2. Gas accumulation method graph.

4. References

- [1] Pfeiffer, The Vacuum Technology Book, Pfeiffer Vacuum GmbH, 2018.
- [2] A. Roth, Vacuum Technology, 3rd ed., Elsevier Science, 1990.

Acknowledgments: We acknowledge the support of the CNPq through the PIBIC undergraduate research grant.

^{*}Corresponding author: hernandes.alves@fatec.sp.gov.br1, thiago.silva440@fatec.sp.gov.br, ftd@fatecsp.br

PLASMA POWER SOURCES INFLUENCE ON CARBON NANOTUBES FUNCTIONALIZATION

Teresa Tromm Steffen^{1*}, Peter Hammer², Julio César Sagás¹, Luis César Fontana¹, and Daniela Becker¹.

¹Laboratory of Plasmas, Films, and Surfaces, Santa Catarina State University (UDESC), Joinville, SC, Brazil ²Laboratory of Photoelectron Spectroscopy, São Paulo State University (Unesp), Araraquara, SP, Brazil

1. Introduction

Carbon nanotubes (CNTs) functionalization through plasma has aroused interest in academia and industry (nowadays), since it is a fast and eco-friendly technique that allows a wide range of surface modifications on nanoparticles, depending on selected parameters such as the power source, reactor configuration, type of functionalizing agent, and so on [1]. Since there is still a gap in the understanding of those plasma parameters in CNTs functionalization, this work aims to verify the influence of using radio frequency (RF) or Asymmetric Bipolar Pulsed Plasma Source (ABiPPS) as discharge generators on the CNTs functionalization degree.

2. Experimental

Samples were treated in a capacitively coupled plasma (CCP) reactor, equipped with stainless steel electrodes and a cylindric glass wall. First, CNTs were premixed with solid maleic anhydride (MA) [2] and treated with argon gas (33.3 sccm) at 1 Torr. The reactor was fed with argon for 15 min and then the glow discharge was maintained for 30 minutes, provided by RF or ABiPPS. The discharge conditions were analyzed using an oscilloscope. After treatment, the samples were washed with methanol and oven-dried to remove chemically unreacted MA molecules and then samples were characterized by X-Ray Photoelectron Spectroscopy (XPS).

3. Results and Discussions

The standard sample (CNTs premixed with solid MA, washed with methanol, and oven-dried) presents an atomic composition of 96.9 % C and 3.1 % O. After RF plasma treatment, the O atomic content increased only slightly to 3.5 %, while for ABiPPS plasma treatment 7.0 at.% were detected. The CNTs functionalization degree (evidenced by the increase of the C 1s O-C=O component) achieved in each treatment can be related to discharge power. In the case of RF, 35 W was applied, limited by impedance matching; while for ABiPPS, a rms power of 389 W was recorded. Therefore, it can be concluded that the ABiPPS treatment led to more oxygen dissociation and radical creation on the CNTs surface, resulting in a higher functionalization degree.



Fig. 1. CNTs samples mixed with MA being treated in glow discharge provided by ABiPPS in CCP reactor.

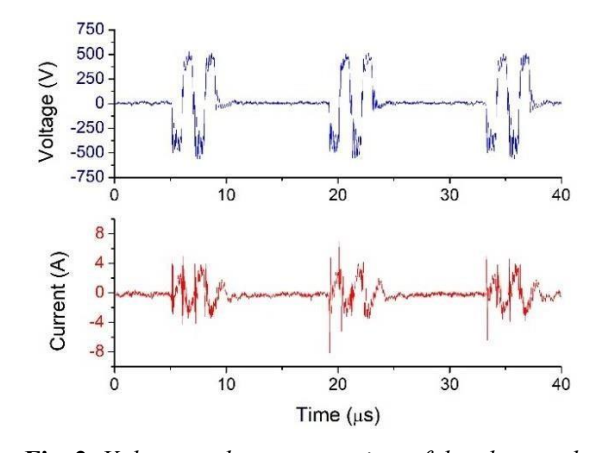


Fig. 2. Voltage and current vs. time of the plasma glow discharge powered by ABiPPS.

4. References

- [1] H. Hosseini, M. Ghaffarzadeh. Inorg. Chem. Commun., 138, 109276, (2022).
- [2] T. T. Steffen et al. Appl. Surf. Sci., 491, 405-410, (2019).

Acknowledgments

The authors would like to thank LabPasma and Multi-User Facility infrastructure from UDESC/CCT and FAPESC for financial support (grant 2023TR000258).

^{*}Corresponding author: teresa.ts@udesc.br

PRODUCTION AND CHARACTERIZATION OF NOVEL ZrTiNb-BASED HIGH-ENTROPY ALLOYS BY ARGON ARC MELTING FOR BIOMEDICAL APPLICATIONS

Jhuliene Elen Torrento ^{1,*}, Carlos Roberto Grandini ¹, Diego Rafael Nespeque Correa ¹

¹Univ. Estadual Paulista, Laboratório de Anelasticidade e Biomateriais

1. Introduction

In recent years, high entropy alloys (HEAs) have been researched for their potential applications in the biomedical field due to their simple crystalline structure, such as HCP, BCC, and FCC, associated with superior mechanical strength [1]. Although there is significant potential for their use in biomedical applications [2,3], the actual HEAs do not possess the necessary mechanical, electrochemical, and biological properties for use in the human body. Therefore, there is a promising opportunity for developing new HEAs in this field. This study aims to create novel Bio-HEAs utilizing non-toxic, low-cost, and low-melting elements, including Ti, Zr, Mn, Al, Nb, and Fe.

2. Experimental

HEAs ingots were produced by argon arc melting using a water-cooled copper crucible and tungsten electrode. The melting chamber was previously evacuated in a low vacuum (10⁻² Torr) and purged with high-purity argon gas. The chemical composition was previously assessed by density measurements and EDS (energy dispersive X-ray spectroscopy). Structural and microstructural analyses were carried out using X-ray diffraction (XRD) and optical and scanning electron microscopy (SEM). Finally, Vickers microhardness measurements were taken to preliminary evaluate the mechanical properties.

3. Results and Discussions

The as-cast samples were obtained with complete incorporation of all alloying elements and density close to the theoretically determined value, around 6.0 g·cm-³. The XRD patterns exhibited the formation of a dual phase composition (BCC and HCP), similar to the results found in the literature and predicted by the theoretical predictions. The micrographs (Fig.1) depicted dendritic microstructure with non-uniform sizes due to the cooling gradient inside the melting chamber. Vickers microhardness measurements showed an overall value of around 450 HV of all samples, higher than some commercial biometals (commercially pure grade 2 Ti, Ti- 6Al-4V alloy, and 316L stainless steel). However, it was possible to notice greater microhardness values in the matrix than those from the dendritic structures.

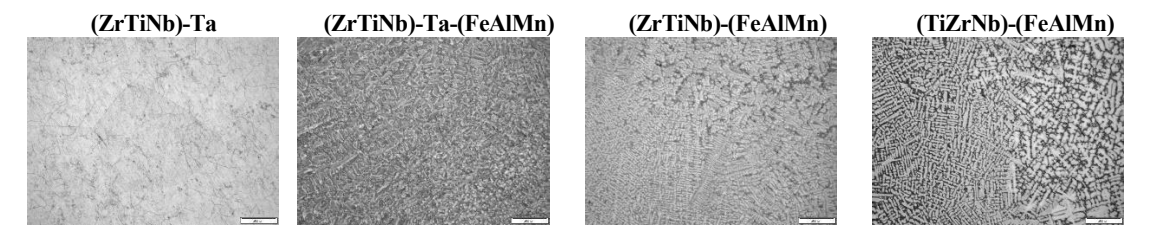


Fig. 1. Micrographs of the alloys in the raw melt condition.

The ingots produced by argon arc melting presented a dual phase composition with non-uniform microstructure and high Vickers microhardness, indicating that the samples can exhibit good mechanical strength after proper thermomechanical processing, having potential for use in biomedical applications.

4. References

- [1] Hori, T.; Nagase, T.; Todai, M.; Matsugaki, A. et al. Scripta Materialia, 172, 83-87, (2019).
- [2] Motallebzadeh, A.; Peighambardoust, N. S.; Sheikh, S.; Murakami, H. et al. Intermetallics, 113, (2019).
- [3] Torrento, J. E. et al., APL Materials, v 10, n. 8, 081113, (2022).

Acknowledgments

CNPq (grant #407251/2018-9) and FAPESP (grant #2021/13921-3) for the financial support.

^{*}Corresponding author: jhuliene.torrento@unesp.br

PRODUCTION OF ULTRATHIN FILMS AND NANOSTRUCTURES FROM CARBON DIOXIDE

Olavo Teixeira Neto^{1,2}, Augusto Oliveira Korukian¹, Bernardo Vieira Magaldi¹, Braulio Archanjo² and Renata Antoun Simão¹*

¹Programa de Engenharia Metalúrgica e de Materiais - PEMM, COPPE - UFRJ ²Divisão de Metrologia de Materiais - DIMAT - INMETRO

1. Introduction

With the development of societies and consumption patterns, inevitably, an inherent need for technological development capable of meeting their needs also arises. New materials and surfaces have become key players in today's society, being not only necessary but indispensable for everyday activities, whether personal, in industry, in research, in everything.

It is in this context that the proposal to use carbon dioxide (CO₂) arises as a gas used for the deposition of carbon on different surfaces. CO₂ is a gas that is cheap, abundant and popularly famous only for its harm to the environment, not being widely used as a raw material in the production of thin films. In addition to the ecological and financial factor of choosing this gas, there is the technical factor that, with other gases, at the same time as carbon deposition is promoted, plasma ions are bombarded on the surfaces, causing damage to the films, while, when CO₂ is used in the plasma, free oxygens are formed, which are capable of reacting with the carbons weakly bounded to the substrate, obtaining a better quality film. There is few reports in the current literature on the use of CO₂ as a precursor gas for the deposition of carbon species via PECVD, but all of them involves high temperature deposition [1,6]. This work was to define the best conditions for the deposition of a better quality carbon film using CO₂, varying the PEVCD power used, the deposition time and the substrate. Films were evaluated through scanning electron microscopy (SEM), Raman spectroscopy and atomic force microscopy (AFM).

2. Experimental

Niobium, and silicon were used as substrates. Niobium plates were prepared by grinding. Substrates were placed inside a tubular reactor and prior to PECVD of carbon dioxide, argon plasma was used to prepare the surface for deposition. Different times both for argon plasma and CO₂ plasma were employed and samples were not intentionally heated. The Raman analyzes were carried out in the National Laboratory of non-Destructive testing, Corrosion and Welding (LNDC) through a Bruker 40 Raman Microscope Senterra. Samples were analyzed by scanning electron microscopy (SEM) using a VEGA3 microscope from Tescan, located in the Electronic Microscopy Center at COPPE. Atomic force microscopy (AFM) was performed using a JPK I microscope.

Another batch of substrates was prepared by reactive magnetron sputtering from a niobium target using a mixture of argon and oxygen in a ratio equivalent to that used by Fridriksson et al. [5] to form niobium oxide (NbO). These new substrates were placed inside a cathode reactor and carbon was deposited by PECVD from carbon dioxide. In the laboratories of the INMETRO Materials Metrology Division, images of the second samples were taken by SEM on a Nova nanolab 600 where their chemical compositions were also analyzed by energy dispersive X-ray spectroscopy (EDS).

3. Results and Discussions

Different deposition conditions were tested for carbon deposition in silicon surfaces. Most of them let to the formation of massive flakes on the surface or continuous amorphous carbon layer. Best results are presented in **Fig.** 1 and **Fig.** 2. Figures show two deposition conditions without previous argon treatment. Deposition was carried on in two different powers and both resulted in the formation of layered structured flakes that can resemble graphene like layers.

When niobium surfaces were considered, two different surfaces were considered: polished ones as well as surfaces with native oxide. **Fig. 3** shows the Raman spectra obtained for both samples. It is clear that when naturally oxidized samples are concerned a Raman spectrum typical of graphene is observed and when this oxide layer is removed the formation of a layer composed of other types of carbon is observed.

Other deposition conditions can lead to the formation of amorphous carbon and it is observed also that the nature of the oxides present on the surfaces. It is still a question whether the CO₂ plasma changes the original oxide on the surface or different oxide states of the metal will induce different carbon growth.

On NbO substrates deposited by magnetron sputtering, the color change of samples after PECVD deposition can be seen with the naked eye. The EDS results show a ratio of 1:1 between Niobium and oxygen before PECVD deposition and 1:2 after deposition, **Fig. 4b**, indicating a possible oxidation of niobium by CO₂ plasma. The SEM images, **Fig. 4a**, show the appearance of carbon particles.

This way, our study clearly demonstrates the feasibility of depositing carbon nanostructures that resemble

graphene flakes at room temperature, while also highlighting the influence of deposition parameters and substrate characteristics on the morphology of the resulting structure. This new knowledge not only enhances our understanding of the processes of graphene deposition, but also provides valuable information to optimize the fabrication of carbon-based materials with tailored properties.

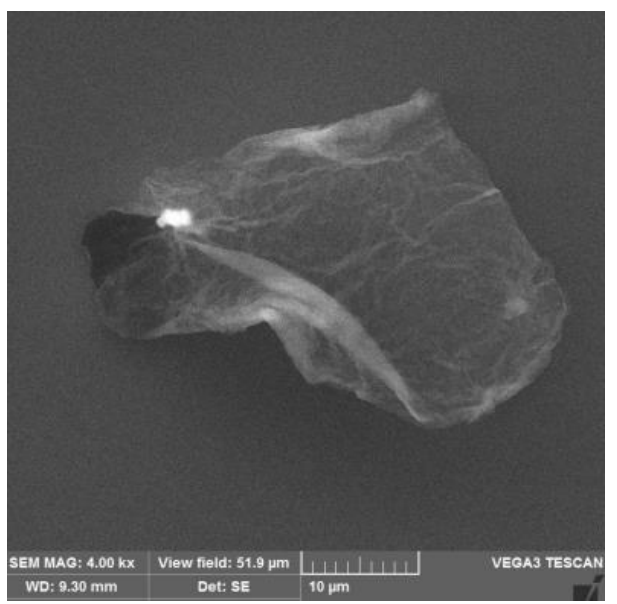


Fig. 1. Carbon dioxide deposited by PECVD for 2 h at 41 W and pressure of 0.2 mbar

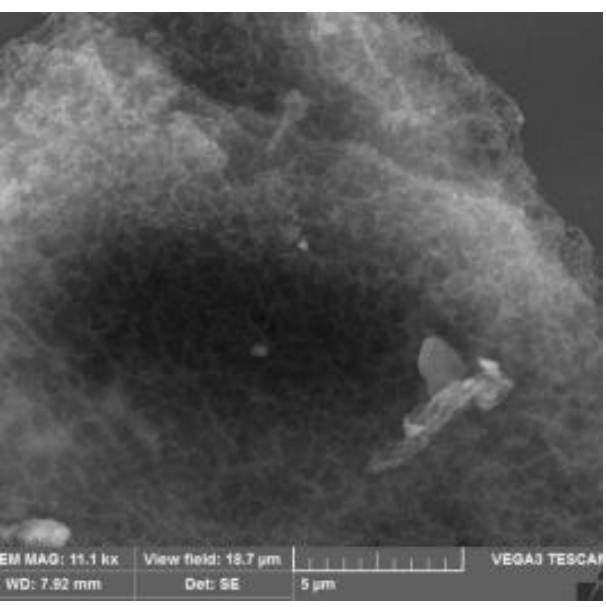


Fig. 2 Carbon dioxide deposited by PECVD for 1 h at 79 W and pressure of 0.08 mbar.

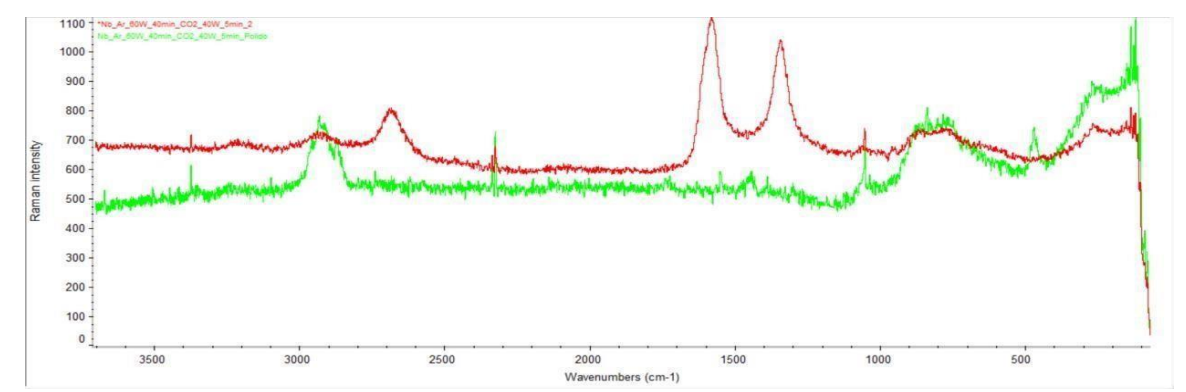


Fig. 3. Raman spectroscopy of niobium plates after argon and CO_2 plasma. Argon at 60W for 40 minutes followed by CO_2 at 40W for 5 minutes. In red, naturally oxidised, and in green polished niobium

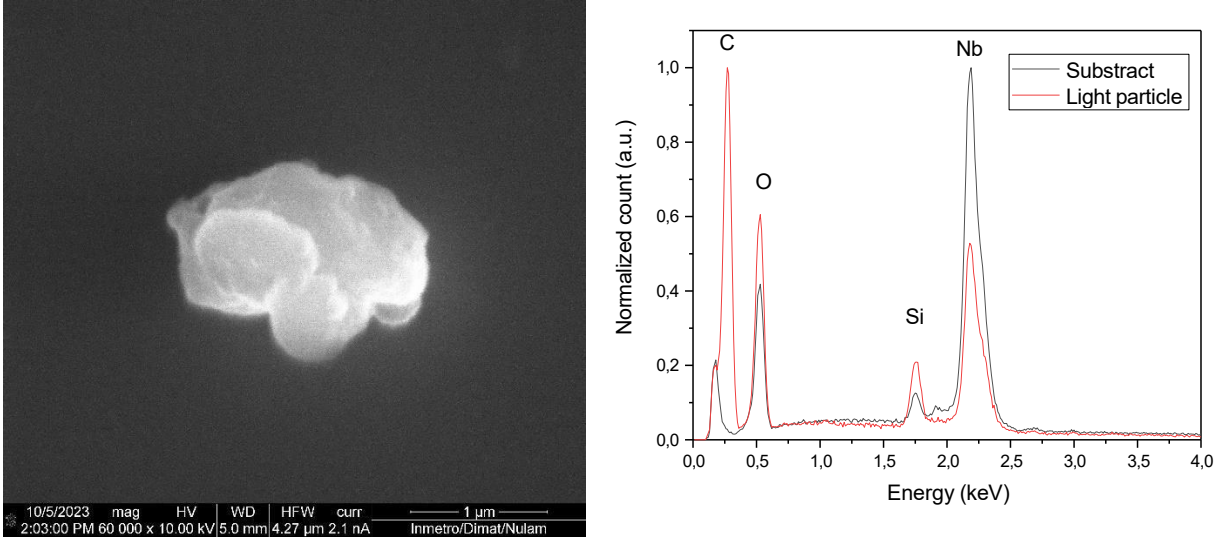


Fig. 4. SEM image from carbon structures deposited (a). EDS spectrum from the light particle in red, and the substrate in black (b).

4. References

- [1] P. Favia and R. D'Agostino, Surf. & Coat. Tech., 98, 1102-1106, (1998).
- [2] V. CAROZO et al; , Raman signature of graphene superlattices. Nano Letters, v. 11, n. 11, p. 4527–4534, 2011.
- [3] HAN, Linzhi et al. Two-step method preparation of graphene without hydrogen on methanol pretreatment copper substrate by PECVD at low temperature. Physica E: Low-Dimensional Systems and Nanostructures, v. 84, p. 249–257, 2016. Disponível em: http://dx.doi.org/10.1016/j.physe.2016.04.013.
- [4] HONG, Hyo Ki et al. Synthesis of high-quality monolayer graphene by low-power plasma. Current Applied Physics, v. 19, n. 1, p. 44–49, 2018. Disponível em: https://doi.org/10.1016/j.cap.2018.11.003.
- [5] E. G. Fridriksson et al.; Growth of NbO, NbO2 and Nb2O5 thin films by reactive magnetron sputtering and post-annealing. Vacuum, v. 202, p. 111179, 2022.
- [6] C. Molina-Jirón, et al.; Direct Conversion of CO2 to Multi-Layer Graphene using Cu-Pd Alloys, ChemSusChem, v. 12, p. 3509-3514, 2019

(Leave one empty line, if possible, between section 4 and the acknowledgments)

Acknowledgments

The author would like to express their gratitude to CNPq, CAPES and FAPERJ for their financial support.

PRODUCTION, CARACTERIZATION AND APLLICATION OF LOW-COST HIGH VOLTAGE POWER SOURCE IN PLASMA ACVATED WATER (PAW)

Alessandro Lima^{1,2*}, Felipe S. Miranda¹, Marcelo P. Gomes¹, Nilton Francelosi Azevedo Neto¹, Rodrigo S. Pessoa¹, Argemiro S. da Silva Sobrinho¹, Douglas M. G. Leite¹

¹ Laboratório de Plasmas e Processos, Instituto Tecnológico de Aeronáutica, São José dos Campos/SP, Brazil

² Instituto Federal de São Paulo, São José dos Campos/SP, Brazil

1. Introduction

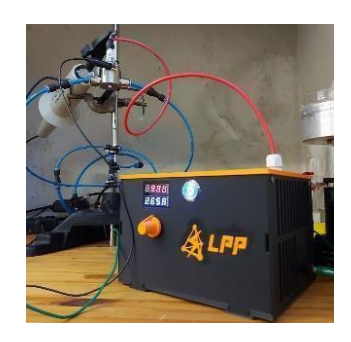
The strong dependence of plasma science and technology research on high-voltage power sources is widely recognized. However, such equipment is often quite expensive and may not be domestically produced or readily available in Brazil. In response to this challenge, the Laboratório de Plasmas e Processos at ITA has taken the initiative to design and manufacture simple, low-cost power sources tailored for use in specific plasma experiments. These power sources possess specialized capabilities, particularly in applications such as ozone production and Plasma-Activated Water (PAW). In this study, we present the utilization of a straightforward homemade power source for PAW production. We provide a detailed account of the assembly and characterization of the power source, aiming to gain insights into its capabilities and limitations.

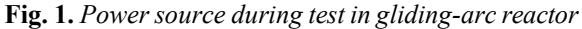
2. Experimental

The power source was designed to provide a nominal power of 60 W, being able to maintain free electric arc of at least 20 mm in atmospheric pressure (air) for more than 2 hours and control the output power from 50 to 100%. It is assembled from: i) 12 V, 5A switched DC power source; ii) DC current and voltage controller; iii) high frequency (150 kHz) generator; and iv) flyback high voltage transformer. The power source's characteristics were assessed using a Keysight DSOX1202A digital oscilloscope, in conjunction with a high-voltage Tektronix P6015A probe. The PAW was produced by reacting the discharge gas with deionized water using a gliding arc reactor for plasma generation. Throughout all experiments, the airflow and sample volume were consistently maintained at 5 L/min and 40 mL, respectively. Treatment durations ranged from 1 to 30 minutes. Following each PAW treatment, the pH of the samples was immediately measured using a Metrohm pH meter.

3. Results and Discussions

The assembled power source was capable of maintaining a 40 mm free arc in atmospheric pressure (air), and worked very well with gliding arc reactors. The characterization show that the output is an asymmetric peak... with $25 \text{ kV}_{\text{peak-peak}}$ at frequency of 35 kHz the average delivered power at maximum output is around 20 W. Figure 1 show a picture of the power source feeding a gliding arc reactor. The results of pH observed in PAW over the course of the treatment time highlight a significant reduction in pH value, reaching 3.1 after 30 minutes of treatment. In contrast, the initial pH value of the untreated sample stands at 7.24. The decrease in pH can be attributed to reactions between NO₂ and deionized water, yielding nitric acid as a resulting product [1].





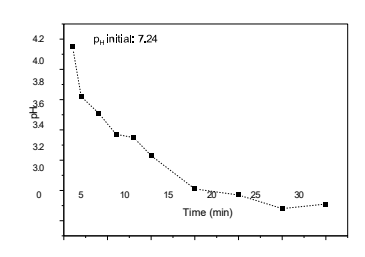


Fig. 2. *Graph of the pH versus treatment time*

4 References

[1] N. Bolouki, W.H. Kuan, Y.Y. Huang, J.H. Hsieh, Appl. Sci., 11, 6158-6170, (2021).

Acknowledgments

We acknowledged the financial support of the São Paulo Research Foundation (FAPESP), grant #2023/02268-2.

^{*}Corresponding author: alessandrolima10396@gmail.com

PROMOTING MAKER AND STEAM EDUCATION ON VACUUM: EVALUATION OF COMPLEXMIDIA FOR HEARING AND DEAF STUDENTS IN AN INCLUSIVE AND MULTIMEDIA APPROACH

Marco Aurélio Alvarenga Monteiro^{1*}, José Silvério Edmundo Germano², Carolina Savedra Vargas³

^{1,2}Universidade Estadual Paulista – UNESP – Campus Guaratinguetá ²Universidade de São Paulo - Escola de Engenharia de Lorena - EEL – USP

1. Introduction

Contemporary education is faced with the paramount challenge of preparing students for an increasingly complex, technological, and globalized world [1]. Globalization has expanded competition on a global scale, necessitating educational systems to empower individuals capable of competing in an increasingly internationalized economy, where skills and knowledge are assessed globally. Simultaneously, rapid scientific and technological progress has generated swift social and economic changes, demanding educational systems to adapt in order to equip students not only with information, but also with transferable competencies such as criticalthinking, problem-solving, and effective communication [2].

Within this context, science education plays an even more fundamental role, as Science and Technology constitute the pillars of the societal framework in which we live. Science education enables students to comprehend the scientific changes and advancements shaping contemporary society, enabling them to make informed decisions and actively participate in a perpetually transforming world [3].

To meet this educational challenge, practice-centered teaching approaches like the maker movement and the STEAM approach have gained prominence for their potential to stimulate creativity, interdisciplinary learning, and the development of essential 21st-century competencies [4,5]. The maker movement, born from the "do-it- yourself" culture, advocates for students to take an active role in their own learning, engaging in creative and constructive projects. As per [6], this approach aligns with the new industrial revolution that values people's capacity to create and produce their own ideas.

The STEAM approach, on the other hand, promotes the integration of Science, Technology, Engineering, Arts, and Mathematics disciplines, seeking comprehensive and interdisciplinary learning. Based on Seymour Papert's constructivist principles, this approach values creativity, critical thinking, and collaboration, allowing students to explore diverse skills and knowledge to tackle the complex challenges present in society, which all citizens face [6].

Considering these conclusions, this research aims to evaluate the use of ComplexMidia on the topic of vacuum, for both hearing and deaf students. ComplexMidia is a multimedia tool that integrates various educational resources such as video lectures, simulations, texts, and activities, aiming to facilitate conceptual understanding, promote active learning, and stimulate student engagement. Amid the challenges many Brazilian schools face in implementing effective educational strategies, especially those related to maker and STEAM education, this research seeks to investigate the efficacy and accessibility of ComplexMidia as a viable and inclusive alternative.

Given the reality of deaf students, whose inclusion in education is supported by legislation and norms aiming for equal opportunities [7 and 8], the research will seek to understand how the use of ComplexMidia can address the specific needs of these students, contributing to the development of their conceptual understanding and STEAM skills while aiding in overcoming challenges faced by teachers.

2. Research Methodology

The Complexmidia_Vacuum encompasses various media and pedagogical elements to effectively conveythe concept of vacuum. It has been designed to be inclusive, catering to both deaf and hearing students, and aimsto offer a transdisciplinary and challenging perspective on the topic. Additionally, it seeks to apply the scientific concept in real-world contexts.

The resource contains different components, such as contextualization videos, interactive simulations, video lectures, digital books, and hands-on activities. Each component aims to address a specific facet of the vacuum concept, promoting a deep and practical understanding.

The Complexmidia_Vacuum underwent an evaluation with 10 high schools where classrooms had both hearing and deaf high school students. The results were compared against a control group. A pre-test and a post-test were administered to compare the performance of students exposed to teaching with Complexmidia_Vacuumversus those who learned through traditional teaching methodologies. Interviews were conducted with the teachersof the classes exposed to Complexmidia_Vacuum. The analysis of these interviews was carried out using ContentAnalysis methodology [9].

3. Results and Discussions

The assessment revealed that students who utilized the resource exhibited a more robust understanding of the vacuum concept, along with an increased ability to apply it in everyday situations. Furthermore, there was greater interaction between deaf and hearing students.

The interviewed teachers showed significant interest in incorporating the resource in the classroom and highlighted that Complexmidia_Vacuum greatly enhanced the instructional process for both hearing and deaf students' learning experiences.

4. References

- [1] SANTIAGO, M. C.; ANTUNES, K. C. V.; AKKARI, A. Educação para a cidadania global: desafios para a BNCC e formação docente. Rev. Espaço do Currículo (online), João Pessoa, v.13, n. Especial, p. 687-699, dez. 2020.
- [2] GOBBO. A. A quarta revolução industrial e seus impactos na civilização e na educação 4.0: muitas variáveisde uma nova e complexa equação civilizatória. São Paulo: Pimenta Cultural, 2022. 299p.
- [3] MONTEIRO, M.A.A. Um estudo sobre as contribuições para o process de ensino e de aprendizagem de conceitos de física a partir de experimentos controlados remotamente. Tese (livre-Docência) Universidade Estadual Paulista (UNESP), Faculdade de Engenharia de Guaratinguetá, 2017.
- [4] DA SILVA VIEIRA, S.; SABBATINI, M. Cultura Maker na educação através do scratch visando o desenvolvimento do pensamento computacional dos estudantes do 5 ano de uma escola do campo da cidade de Olinda-PE. Revista Docência e Cibercultura, v. 4, n. 2, p. 43-66, 2020. Acesso em: 27 de julho. 2022.
- [5] CARVALHO, A. B. G.; BLEY, D. P. Cultura Maker e o uso das tecnologias digitais na educação: construindo pontes entre as teorias e práticas no Brasil e na Alemanha. Revista Tecnologias na Educação, v. 26, p. 21-40, 2018. Acesso em: 11 de maio. 2022.
- [6] BACICH, L.; HOLANDA, L. STEAM: integrando as áreas para desenvolver competências. STEAM em salade aula: a aprendizagem baseada em projetos integrando conhecimentos na educação básica. Porto Alegre: Penso,2020. Acesso em: 04 de abril. 2022
- [7] BRASIL. Instituto Nacional de Estudos e Pesquisas Educacionais Anísio Teixeira (Inep). Resumo Técnico: Censo Escolar da Educação Básica 2021. Brasília, DF: Inep, 2021.
- [8] SCHNEIDER, M. F.; SILVA, G. N. da. Inclusão escolar de alunos surdos: avanços, desafíos e perspectivas. Educação e Pesquisa, São Paulo, v. 43, n. 4, p. 1155-1172, 2017. Disponível em: http://www.scielo.br/pdf/ep/v43n4/1678-4634-ep-43-04-01155.pdf. Acesso em: 31 mar. 2023.
- [9] BARDIN, L. Análise de conteúdo. Edições 70, 2016

RAMAN SPECTROSCOPY ANALYSIS OF $\alpha\textsc{-}Bi_2O_3$ STRUCTURAL DEFECTS POST ATMOSPHERIC ARGON PLASMA EXPOSURE

Claudio Andrés Téllez Zepeda¹, Helen Caroline de Souza Barros¹, Rafael Nunes Segantine¹, Clodomiro Alves Junior.^{1,2}, André Luís de Jesus Pereira¹, Rodrigo Sávio Pessoa¹

¹ITA – Instituto Tecnológico de Aeronáutica ²UFRN – Universidade Federal do Rio Grande do Norte

1. Introduction

Metal oxides are widely used materials due to their properties, such as high chemical, thermal, and mechanical stability. Among them, bismuth oxide stands out as a p-type semiconductor with significant potential for applications in optoelectronics and photonics. In this context, this study focused on the formation of structural defects (oxygen vacancies) in monoclinic α -Bi₂O₃ through atmospheric Ar plasma treatment. Such vacancies function as active centers for increasing the surface activities of nanomaterials [3]. Our work is justified because, although there are successful reports in the literature regarding the use of Ar plasma to produce oxygen vacancies in oxide materials similar to α -Bi₂O₃ [4], and despite the advantages inherent to plasma techniques, the literature still lacks studies addressing plasma treatment as a strategy to produce oxygen vacancies in α -Bi₂O₃.

2. Experimental

The synthesis of the powder material was carried out using the conventional hydrothermal method [3]. The powder obtained was used to prepare pastes that were deposited on FTO substrates using the spin-coating technique with the equipment Laurell – Model WS-650MZ-23NPP [4]. The α -Bi₂O₃ pastes were treated directly by Ar plasma during an exposition time of 60s, using a Surfatron (SWD) equipment operating at 2.45 GHz at a power of around 70 W. The equipment was adjusted to avoid a reflected power greater than 5%. We fed the quartz tube with a continuous flow of argon gas with a purity of 99.95% at a fixed flow rate. The material (before and after atmospheric plasma treatment) was characterized using Raman spectroscopy using a Horiba LabRAM HR Evolution Raman Spectrometer with 532 nm laser. The spectra were taken at room temperature, with a grade of 1800, range of 50-800 cm⁻¹, time of 30s, 3 accumulations, spectral resolution of 1 cm⁻¹, and filter of 5%.

3. Results and Discussions

In studies involving α -Bi₂O₃ ceramics, existing literature indicates a correlation between the characteristic bands of the α -Bi₂O₃ phase (space group P2₁/c), specifically the 210 cm⁻¹ and 535 cm⁻¹ Raman bands, and oxygen-related defects [5]. These peaks correspond to vibration modes involving the same oxygen atoms in the α -Bi₂O₃ crystal structure [6]. From the spectroscopic analysis of the experimental Raman spectra of the material before and after exposure to the Ar plasma, we observed a marked change in the shape of the bands between 280 and 315 cm⁻¹, suggesting alterations in the crystalline structure related to the displacement of oxygen atoms (modes above 150 cm⁻¹) [7]. We also observed changes in the shape and intensity of the peaks around 200 cm⁻¹ and between 500 and 550 cm⁻¹, indicating our success in generating oxygen vacancies through treatment with Ar plasma. Our preliminary results indicate that the treatment with atmospheric Ar plasma, under the experimental conditions employed, effectively induced the expected structural defects in the material.

4. References

- [1] H.Liu, P.Chen, X.Yuan, Y.Zhang, H.Huang, L.Wang, F.Dong, Chinese J. Catal. 40 (2019).
- [2] L.Xu, Q.Jiang, Z.Xiao, X.Li, J.Huo, S.Wang, L.Dai, Angew. Chem. 55 (2016).
- [3] Z.Long, G.Xian, G.Zhang, T.Zhang, X.Li, Chinese J. Catal. 41 (2020).
- [4] C.J.Brinker, A.J.Hurd, G.C.Frye, P.R.Schunk, C.S.Ashley, J. Ceram. Soc. JAPAN, 99 (1991).
- [5] M. Vila, C. Díaz-Guerra, J. Piqueras, Mater. Chem. Phys. 133 (2012).
- [6] S.N. Narang, N.D. Patel, V.B. Kartha, J. Mol. Struct. 327 (1994).
- [7] V.N. Denisov, A.N. Ivlev, A.S. Lipin, B.N. Mavrin, V.G. Orlov, J. Phys.: Condens. Matter 9 (1997).

Acknowledgments

We would like to express our gratitude to CNPq (131920/2023-5, 141620/2023-4) and FAPESP (2022/02994-2, 2022/01901-0, 2023/10449-7) for their financial support. Our thanks also extend to ITA and to the entire LPP - ITA team for their valuable support.

^{*} Corresponding author: tellez@ita.br

RECOVERING OF A VACUUM SYSTEM USED IN PLASMA TREATMENT

André Ricardo Marcondes*and Samantha F.M. Mariano.

¹ National Institute for Space Research, CGIP/COPDT, São José dos Campos, SP, Brazil

² National Institute for Space Research, CGIP/COPDT, São José dos Campos, SP, Brazil

Abstract

This article presents the work carried out at the National Institute for Space Research to recover an entire vacuum system used in plasma immersion ion implantion treatments. It is shown what type of problems can occur when a vacuum system is used for many years and what can be done to improve the performance of the vacuum system.

1. Introduction

There are currently four plasma immersion ion implantation (PIII) systems in operation at the National Institute for Space Research's plasma laboratory. The oldest system called 3IPLAP has been in operation since the early 1990s and during this long period no significant maintenance has been carried out on its vacuum system. In short, only the oils of the mechanical and diffusion pumps were replaced during this period.

The 3IPLAP system worked properly for many years, and several works were published based on experiments carried out on this system [1, 2, 3, 4]. Recently it was noted that it was difficult to achieve a satisfactory base pressure and the system required many hours of pumping to reach a pressure of 10⁻⁴ mbar. As expected, several parts of the vacuum system had suffered degradation due to age and use. In Figures 1 and 2, one can see the 3IPLAP vacuum system as it was before the improvements.



Fig. 1. Mechanical pump connected to the 3IPLAP vacuum chamber and to the diffusion pump.



Fig. 2. Hoses, ball valves and bellows used in the 3IPLAP vacuum system.

Figs 1 and 2 show that many connections were not adequate to work in vacuum. There were hoses made of rubber and pipes made of copper, and metal clamps were used to tighten the rubber hoses to the copper pipes. Some of the ball valves connections were made by using PTFE sealing tape, which is not in use nowadays for such application. So, it was necessary to review the entire vacuum system, perform a detailed inspection of all its parts, and replace all the compromised materials and components in order that the base vacuum could reach pressures below 10⁻⁵ mbar. It is known that the lower the base pressure, the cleaner the treatment chamber which means fewer contaminants in the treated sample.

2. Experimental

The vacuum system used in the 3IPLAP vacuum chamber consists of 1 Edwards mechanical pump model E2M8, 1 Edwards diffusion pump model Diffstak 100/300Mxxx, 2 ball valves, 4 bellows 1' \varnothing_{in} (5), 20 rubber orings, 2 glass windows, and 1 lever valve between the diffusion pump and the vacuum chamber. In the vacuum chamber, there are 8 rubber o-rings, 4 copper rings, 1 Alcatel pressure gauge, 1 Pfeiffer coarse gas dosing valve, 1 Edwards needle gas valve, 2 feedthroughs (electron shower and high voltage pulses, and 1 gas hose for the gas feed. The 3IPLAP system is detailed elsewhere [1]. The procedure to improve the system's vacuum consisted of step-by-step disassembly of the entire system which was carried out in six months. We started with the pumps. The mechanical pump has been thoroughly cleaned and its oil replaced. The diffusion pump was removed from the vacuum system, disassembled, cleaned, reassembled and filled with new oil. In Figures 3 and 4 we can see the

diffusion pump disassembly to be completely cleaned.



Fig. 3. Diffusion pump removed from the vacuum system.



Fig. 4. The diffusion pump was dismantled. The internal parts were covered with a thick layer of burnt oil. The removal of the deposited layer involved mechanical and chemical cleaning.

In the following, all the rubber and copper o-rings were replaced. The lever valve between the diffusion pump and the chamber was disassembled and cleaned and its o-ring was replaced and lubricated with vacuum grease. Vacuum grease was applied in a very thin layer, just enough to provide lubrication to the o-rings so that it seats properly during the assembly process. After that, the 2 ball valves were replaced with new ones. Due to the long period of use, all rubber and copper sealing rings and bellows also had to be replaced, except for the two largest rubber sealing rings in the chamber. Since these sealing rings could not be replaced because new sealing rings of the same specification were not available, the old sealing rings were removed, inspected, cleaned, and lubricated with high vacuum grease. During inspection, it was found that these sealing rings showed minor deformation and degradation. Alcatel pressure gauge was removed, cleaned and its pressure indication was compared with the pressure indication of a new pressure gauge installed in the chamber. The pressure gauge was considered approved and was reinstalled in the chamber. One of the feedthroughs was defective and had to be replaced with a new one. The gas hose, needle gas valve, coarse gas dosing and the two glass windows were also replaced by new parts. The glass windows have become darkened due to the accumulated deposition from multiple plasma treatments and this type of deposited layer proved very difficult to remove. Figures 5 and 6 show the new vacuum connections.



Fig. 5. All bellows were replaced with new ones. The system no longer has rubber hoses and copper pipes.



Fig. 6. The ball valves were replaced with new stainless steel ones. All connections and clamps are new.

3. Results and Discussions

Before recovery work, the vacuum system required 3 to 4 hours to reach a base pressure of only 10⁻⁴ mbar, which is a high pressure for good plasma immersion ion implantation treatment and other plasma treatments in general. After the recovery work, the vacuum system has improved significantly and currently requires approximately 1 hour to reach the base pressure of 8 x 10⁻⁶ mbar. During the 6 months of work a lot of practical knowledge was acquired, mainly related to the operation of the pumps, the quality of the pump oils, the correct installation and use of feedthroughs and copper rings, and the procedure for detecting leaks in the system. Regarding the type of oil, it was observed that the performance of the diffusion pump is much better when using SANTOVAC® oil compared to the Dow Corning (DC 704). SANTOVAC is more viscous and more heat resistant, which means less contamination in the treatment chamber. In Figure 7 one can see the new base pressure of the system after one hour of pumping.

he new system hase pressure after I ho

Fig. 7. The new system base pressure after 1 hour of pumping.

It is worth mentioning that in addition to the system being able to reach a much lower pressure in less time, it is now able to maintain the vacuum for longer when the pumping is turned off.

4. References

- [1] UEDA, Mario et al. Plasma immersion ion implantation experiments at the Instituto Nacional de Pesquisas Espaciais (INPE), Brazil. **Surface and Coatings Technology**, v. 136, n. 1-3, p. 28-31, 2001.
- [2] GOMES, Geraldo Francisco; DE ANDRADE NONO, Maria do Carmo; UEDA, Mario. Estudo da formação de austeníta expandida em função da quantidade de íons de nitrogênio implantados nas superfícies de aço inox 304. **São Pedro–SP**, 2000.
- [3] UEDA, Mário et al. Overcoming sheaths overlapping in a small diameter metallic tube with one end closed and using a high density plasma from a high power pulsed hollow cathode discharge. **AIP advances**, v. 8, n. 8, 2018.
- [4] MARCONDES, André Ricardo et al. Improvements of ultra-high molecular weight polyethylene mechanical properties by nitrogen plasma immersion ion implantation. **Brazilian journal of physics**, v. 34, p. 1667-1672, 2004.

Acknowledgments: The authors would like to thank the Brazilian Ministry of Science, Technology and Innovation.

^{*}Corresponding author: andre.marcondes@inpe.br

RESPOSTA ESPECTRAL DE DRONE UTILIZANDO ESPECTRORADIÔMETRO E EMISSÃO DE INFRAVERMELHO PRÓXIMO

Kaleb Duarte Costa¹, Vinícius Ormianin Arantes Sousa¹, Ivan Carlos Caetano da Silva², Alvaro José Damião³

¹Instituto Tecnológico de Aeronáutica ² Instituto de Aeronáutica e Espaço ³Institudo de Estudos Avançados

1. Introdução

O conflito entre a Rússia e a Ucrânia tem mostrado a utilização de drones na linha de frente dos campos de batalha, os quais estão se apresentando como elementos fundamentais no êxito de missões. A dificuldade de detecção, baixo custo e fácil operação contribuem para o uso cada vez mais frequente desses vetores. O

Sabe-se, ainda, que a utilização de drones por parte das Forças Armadas Ucranianas foram e ainda pode estar sendo responsável pelo atraso e até mesmo interrupção do avanço russo. Mesmo os drones ucranianos muito simples parecem ter imposto uma necessidade pedagógica significativa nas defesas aéreas e logísticas russas. 0

Foi apresentado um relatório em um Workshop da ONU, em 2022, no qual cita-se que drones armados com letalidade cada vez maior, com carga útil e alcance estão sendo cada vez mais usados. Além disso, drones de asa fixa e quadricópteros armados ou desarmados, de vários tamanhos, fornecem uma gama de capacidades ameaçadoras. Inclusive, em um nível tático, drones menores aparecem com destaque em inteligência, vigilância, medidas de guerra eletrônica e aquisição de alvo para aumentar a letalidade de precisão de sistemas terrestres. 0

A operação desses dispositivos não tripulados está diretamente relacionada com os princípios da guerra adotados pelas forças armadas.

Os princípios de guerra como o Objetivo, Ofensiva, Manobra, Economia de Meios, Simplicidade, Surpresa e Segurança são facilmente afetados pela capacidade dos drones de possuírem baixo custo, fácil operação e simplicidade na cadeia logística. 0

Em fevereiro de 2023 alguns portais de notícias na Europa publicaram que o Vice Primeiro-Ministro da Ucrânia, Mikhailo Fedorov, que é o responsável pela pasta da Transformação Digital informou que as Forças Armadas Ucranianas possuem um exército de Drones com 1765 aeronaves não tripuladas.

Os drones que estão sendo utilizados, em grande maioria, são os drones HESA Shahed 136 ou Geran-2 utilizado pela Rússia. Possuem 3,5 m comprimento e 2,5 m de envergadura, pesando entre 30 e 50 kg. Considera- se que a característica mais importante é a baixa Radar Cross Section (RCS). [5]

Já os drones mais utilizados pelas forças armadas ucranianas são os Drones Bayraktar TB2 de fabricação Turca. Maiores que os drones russos, possuem 12 m de envergadura e 6,5 m de comprimento e capacidade de carga útil de 150 kg. [6]

Pelo tamanho do vetor e mesmo não havendo uma preocupação em torná-lo furtivo à detecções, estes dispositivos possuem uma Seção Reta Radar (RCS) pequenas para os radares utilizados pelo controle do espaço aéreo. Como já foi apresentado, essas caraterísticas favorecem a utilização de drones com capacidade de vigilância, comunicações, repetidoras de dados e até de içamento de carga explosiva.

Diante do vasto emprego de drones com fins civis e militares, este artigo tem o objetivo de apresentar um estudo da reflectância eletromagnética de drones quando iluminado por uma fonte de emissão na faixa do infravermelho. Pretende-se com este estudo fundamentar uma possível alternativa para a detecção de drones utilizando um iluminador.

2. Experimental

Para atingir o objetivo proposto neste artigo, utilizou-se no cenário desenvolvido o Espectrorradiômetro RS-5000, utilizando o sensor sanduíche de Si (25 °C) e InGaAs (25 °C) que cobre a faixa de 0,4 µm a 2,4 µm, com a capacidade de gerar a curva de emissão eletromagnética dentro da faixa supramencionada. No campo de visão (FOV) do sensor foi configurado para operar em 6 mrad, de maneira que a reflectância capturada seja proveniente das proximidades das hélices do drone. [7]

O drone utilizado é do tipo quadricópetro de dimensões (27 x 27x 5,5) cm, ele foi suspenso por um fitilho de 5mm de espessura preso tanto no teto quanto no chão do laboratório, a uma altura de 1,23 m. O drone permaneceu com a vista lateral direita a 45° exposta para a câmera e para o sensor do espectroradiômetro.

Foi utilizado como iluminador uma câmera de segurança da marca Ípega com 10 led infravermelho emitindo energia no comprimento de onda com pico em 0,87 µm. A câmera permaneceu em todo o ensaio suspensa por um tripé a 0,85 m do chão, com a ideia de manter a câmera sempre em uma posição inferior ao drone.

Todas as medições ocorreram em laboratório, o qual se manteve com temperatura constante de 24 °C e com todas as luzes apagadas no momento de cada medição.

Para medir a refletância usamos um gráfico Volts/Gain, gerado pelo espectrorradiômetro, indicando a

relação entre a amplitude do sinal medido em volts e o ganho do sistema de medição de forma a gerar uma escala de amplificação aplicada ao sinal para torná-lo mais visível no gráfico, dessa forma, quanto maior o valor do Volt/Gain, maior será o sinal proveniente da refletância causada pelo drone.

3. Resultados e Discussões

Inicialmente, observou-se que o drone ligado ou desligado não apresentou diferença na resposta espectral obtida pelo sensor do espectroradiômetro quanto à reflectância da iluminação no drone.

Verificou-se que entre a primeira e a segunda medida a razão entre a quantidade de energia recebida pelo espectroradiômetro e a emitida pela câmera de segurança foi maior que na primeira vez, 36 %, o que não se repetiu nas medidas seguintes. O que identifica que a posição que a câmera está do drone mesmo que maior pode resultar em uma melhor aquisição pelo detetor. Outra possibilidade é que uma melhor distribuição da matriz dos LED's pode contribuir para melhorar a detecção, ou a reflectância da energia no drone.

Em seguida os resultados apresentaram quedas à medida que as distâncias foram aumentando, ou seja, quanto mais distante, menor a razão entre a emissão direta da câmera e a refletida pelo drone e medida pelo espectroradiômetro.

Conclui-se, portanto, que utilizando o espectrorradiômetro SR-5000 e as emissões de infravermelho da câmera de segurança e seguindo a metodologia proposta, é possível verificar que esta pode ser útil para auxiliar na detecção de drones com dimensões bem reduzidas como a utilizada no artigo, o qual possui 0,0143 cm² de RCS, inclusive em ambientes noturnos.

4. Referências

- [1] D. Kunertova, The war in Ukraine shows the game-changing effect of drones depends on the game. The Bulletin of the atomic scientists, v. 79, n. 2, 95–102, (2023).
- [2] R. Dalsjö e M. Jonsson, A brutal examination: Russian military capability in light of the Ukraine war. Survival, v. 64, n. 3, 7–28, (2022).
- [3] J. Kunertova, The Vulnerabilities of the Drone Age Established Threats and Emerging Issues out to 2035. [s.l: s.n.]. Disponível em: https://css.ethz.ch/content/dam/ethz/special-interest/gess/cis/center-for-securities-atudies/pdfs/NATO VDA Policy Report.pdf >.
- [4] COMANDO DA AERONÁUTICA, Doutrina Básica da Força Aérea Brasileira, vol. 1.,31–38. (2020)
- [5] BBC News Brasil, Guerra Ucrânia: o que se sabe sobre ataques com drones a alvos estratégicos dentro da Rússia. 2022 Disponível em:
- < https://www.bbc.com/portuguese/internacional-63914427> Acessado em 29/06/23.
- [6] Aeroflap, Bayraktar TB2: o drone turco que está destruindo tanques do Exército Russo na Ucrânia. 2022. Disponível em: https://www.aeroflap.com.br/bayraktar-tb2-o-drone-turco-que-esta-destruindo-o-exercito-russo-na-ucrania/ Acessado em: 29/06/23.
- [7] Spectroradiometer, Operation and Maintenance Manual, Israel, (2004).

Agradecimento

Agradecemos ao Instituto de Aeronáutica e Espaço por nos ceder o laboratório da ASD, junto com os profissionais capacitados, para podermos executar as medidas para o experimento.

^{*} Corresponding author: kalebduarte@hotmail.com

ROTATIONAL TEMPERATURES OF N₂ MOLECULES PRODUCED BY COLD PLASMA JETS INSIDE MONTGOMERY TUBES

Ana Carla de Paula Leite Almeida*, Ananias Alves Barbosa, Fellype do Nascimento, Konstantin Georgiev Kostov

¹Universidade Estadual Paulista "Julio de Mesquita Filho" – Campus de Guaratinguetá

1. Introduction

Atmospheric pressure plasma jets (APPJs) are used to generate cold plasma plumes in open space. APPJs produce chemically active species that can interact with material surfaces making them suitable for many applications. Plasma jets are employed in environmental, biological, and biomedical applications as they can address many types of targets and different treatment requirements [1]. This is because APPJs have the capability to produce reactive species (with high oxidation potential), therefore helping in the pathogen inactivation process. In this work, we present results of rotational temperatures (T_{rot}) measurements obtained from N_2 molecules and optical characterization of plasma jets applied inside a Montgomery tube (T-tube). Such kind of tube is used in tracheostomy procedures with different configurations.

2. Experimental

In this study a plasma jet was produced at the tip of a nasoenteral probe, which is connected to a dielectric barrier discharge (DBD) reactor. The DBD reactor has cylindrical geometry and uses a pin-electrode configuration, to which high voltage pulses are applied. Then, the plasma plume was inserted into the T-tube through its transverse branch and optical analyzes were performed in the caudal branch, as depicted in Fig.1. T- tubes with different branch diameters were investigated. Helium was used as the working gas and the flow rate varied from 1.0 to 3.0 l/min in all experiments. Spectroscopic measurements were performed using an Avantes spectrometer (model AvaSpec-ULS-RS-TEC), with a spectral resolution of (0.784) nm. The rotational temperature values were estimated using the MassiveOES software. For this purpose, optical emission spectroscopy measurements of N₂ molecular bands were performed in the wavelength range of 360 to 382 nm.

3. Results and Discussions

According to the experiments, the rotational temperature values of He remained stable regardless of the increase in gas flow rate and tube diameter T. The average rotational temperature when He gas is used was (306 ± 51) K (Fig.2). The jet obtained by this method is cold enough to be placed in direct contact with human skin.

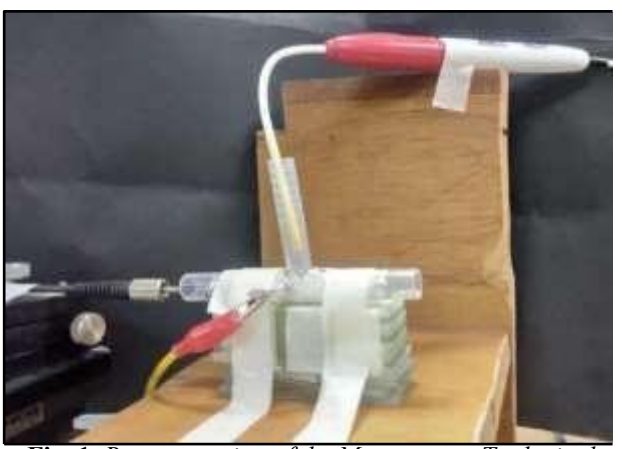


Fig. 1. Representation of the Montgomery T tube in the patient.

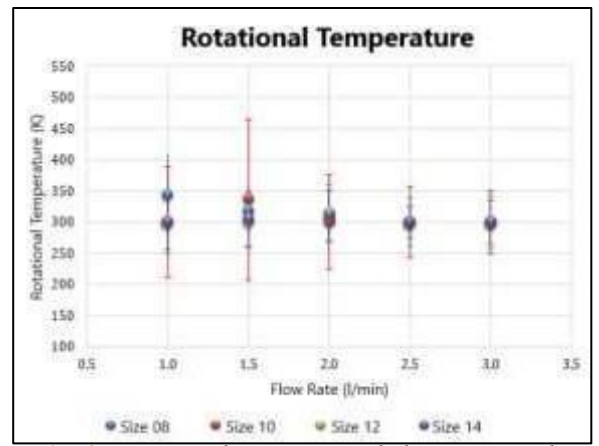


Fig. 2. Rotational temperature behavior according to the variation of gas flow inside the Montgomery T tube for its different sizes.

4. References

[1] P. Bourke, D. Ziuzina, L. Han, P. J. Cullen, B. F. Gilmore, J. Appl. Microbiol. 123, 123, 308–324, (2017)

Acknowledgments: This work was supported by CAPES and FAPESP.

^{*}Corresponding author: ana.c.almeida@unesp.br

SIMULAÇÃO DE PERDA DE REFLEXÃO DE MATERIAIS ABSORVEDORES DE RADIAÇÃO ELETROMAGNÉTICA

Mariana Aparecida de Assis Souza^{1,2}, Glauber Rogério Lanziloti^{1,2}, Ana Paula Oliveira¹, Braulio Haruo Kondo Lopes¹, Mauricio Ribeiro Baldan^{1*}, Divani Carvalho Barbosa²

¹Instituto Nacional de Pesquisas Espaciais, Av. dos Astronautas, 1758, São José dos Campos, SP, Brasil ²Faculdade de Tecnologia de Taubaté, Av. Tomé Portes Del Rei, 525, Taubaté, SP, Brasil

1. Introdução

Esse trabalho tem como foco a linha de pesquisa e desenvolvimento de materiais para controle e Interferência EletroMagnética (EMI). O estudo da prevenção e mitigação de EMI é de grande interesse científico, pois, refere-se ao controle, através de revestimento de diferentes materiais, da interferência indesejada de sinais eletromagnéticos em eletrônicos e antenas, o que pode ocasionar distorções ou mau funcionamento [1]. Aqui propõese o desenvolvimento de um software em linguagem de programação Python que seja capaz de simular omaterial Ferro Carbonila para controle e interferência eletromagnética (EMI).

2. Experimental e Teórica

A amostra de Ferro Carbonila é analisada pelo equipamento VNA (Analisador de Rede Vetorial) para a obtenção dos parâmetros eletromagnéticos experimentais [1], essa análise fornece os dados que serão usados como parâmetros de entrada no software, o processamento faz cálculo da perda por reflexão das amostras, a descrição matemática da perda por reflexão (*RL*) é feita a partir das propriedades do meio material conforme proposto no trabalho de Xu et. al. [2] e retorna de resultado a plotagem de gráficos com as propriedades eletromagnéticas do material como: permeabilidade magnética relativa, permissividade elétrica relativa e a perda por reflexão que são calculadas inicialmente em função da frequência e espessura da amostra (2 mm). Posteriormente, o software simula computacionalmente a perda por reflexão em função da espessura do material de maneira que o usuário possa definir qual apresentaria melhor absorção de EMI.

3. Resultados e Discussões

A Figura 1 apresenta o gráfico das propriedades da amostra de Ferro Carbonila obtida através do equipamento VNA, modelo N5232A da empresa Agilent Technologies. A Figura 2 apresenta a interface do software desenvolvido nesse trabalho, onde tem-se o gráfico representando a perda de reflexão calculada versus a frequência. A princípio esse gráfico é plotado com a espessura da amostra obtida experimentalmente, nesse caso2 mm, depois é permitido ao usuário alterar a espessura da amostra de forma que consiga simular qual apresentariamenor perda por reflexão. Aqui encontramos o valor mínimo de perda por reflexão em aproximadamente -40 dBindicando que a amostra ideal de Ferro Carbonila para operar na faixa de frequência 8,2-12,4 GHz pode ser projetada com uma espessura de 10 mm para aplicações de controle e mitigação de EMI.

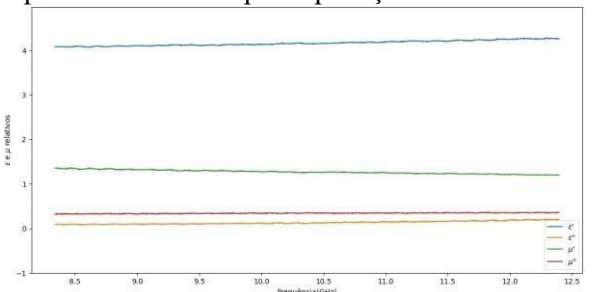


Fig. 1. Permeabilidade magnética relativa (μ) e permissividade elétrica relativa (ε) versus frequência (GHz) para Ferro Carbonila

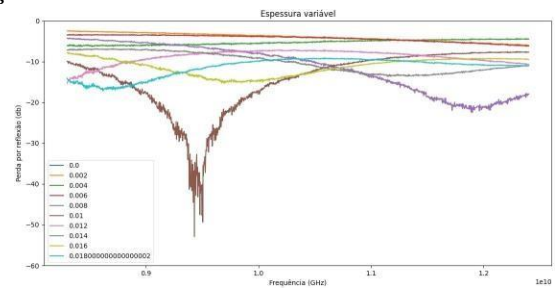


Fig. 2. Frequência (GHz) versus Perda por Reflexão (dB) com espessuras simuladas computacionalmente para amostra de Ferro Carbonila.

4. Referencias

[1] H.K.L. Braulio, Estudo da capacidade de absorção de onda eletromagnética por particulados de ferrita MnZne ferrocarbonila dispersos em matriz de borracha de silicone na faixa de frequência referente à banda X (8,2-12,4GHz). 2020. Dissertação Mestrado em Engenharia e Tecnologias Espaciais, Instituto Nacional de Pesquisas Espaciais, São José dos Campos, São Paulo.

[2] W. Xu, G. Wang, P. Yin. Designed fabrication of reduced graphene oxides/Ni hybrids for effective electromagnetic absorption and shielding. Carbon, v. 139, p. 759–767, 2018.

Agradecimentos: Programa PIBIC/INPE CNPq, processo nº 158140/2023-0.

^{*} Corresponding author: mauricio.baldan@inpe.br

SIMULATION AND INVESTIGATION OF THE THICKNESS OF CARBONYL-IRON MATERIALS IN THE KU BAND.

Ana Paula S. Oliveira¹, Aline F. Batista¹, Plinio I.G. Tenorio¹, Miguel A. do Amaral Junior¹, Sergio L. Mineiro¹, Mauricio R. Baldan¹

¹Instituto Nacional de Pesquisas Espaciais, Av dos Astronautas 1758, Jd Granja, SJCampos.

1. Introduction

Radiation absorbing materials (RAM) have attracted great interest from the scientific community due to factors associated with industrial standards of compatibility and electromagnetic interference, marine radar systems, aerospace and aeronautic areas [1]. It stands out among them as an absorber material of electromagnetic waves, especially in the frequency range between 2 - 40 GHz, the carbonyl iron (CI) that has a relatively low electrical conductivity coupled to a high Curie temperature and high saturation magnetization. To overcome the difficulties mentioned, an alternative approach consists in developing a calculation routine using Nicolson-Ross-Weir (NRW). Data generated from theoretical approach allow prediction of materials with tailored proprieties suitable to aeronautical and aerospace applications (work frequency 12.4-18GHz) without making a great many samples. The permittivity and permeability of materials are extracted from the S-parameters generated by a Vector Network Analyzer (VNA) coupled to a coaxial cable and a Ku- band waveguide. The objective of this work was to develop a Python code capable of simulating the ideal thickness for the material, according to its permittivity and permeability properties.

2. Experimental or Theory

Samples were prepared using the magnetic additive carbonyl iron (CI), by BASF, and a polymeric epoxy matrix. The CI powder was homogenized manually with a mass ratio of 60:40, 70:30, and 80:20 of additive concentration on epoxy and the thickness of the sample produced varied from 1 to 3 mm. The electromagnetic characterization was performed in a rectangular waveguide. The electromagnetic wave absorption performance of materials is generally characterized by the reflection loss (RL). The simulated reflection loss (RL) was calculated from the measured parameters according to the transmission line theory with. Through these models was developed a program with graphical interface to realize the adjustments of the reflectivity using the permittivity and permeability extract the measurement in the VNA, and estimated the better reflectivity for the CI samples. The programming language used to create the program was Python version 2.7.

3. Results and Discussions

In Figure 1, you can see two points of absorption one close to 12 GHz, Ku-Band limit, with 2 mm thickness, and another at approximately 17 GHz for a thickness of 1.5 mm, with an absorption close to -36 dB. If we compare the contour curves shown it is possible to observe that for the 1.5 mm sample, the curves are closer, revealing a narrower band absorber. The 1.5 mm sample made showed a maximum absorption of -37 dB at 16.8 GHz, that is, an excellent attenuation (99.9% of incident radiation). It is possible to observe that the data obtained through the thickness mapping, corroborate the experimental data.

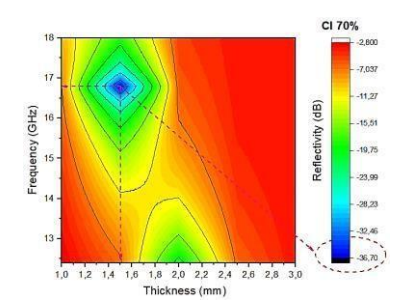


Fig. 1. Trend map of CI 70 wt. % reflection of samples as a function of frequency and thickness

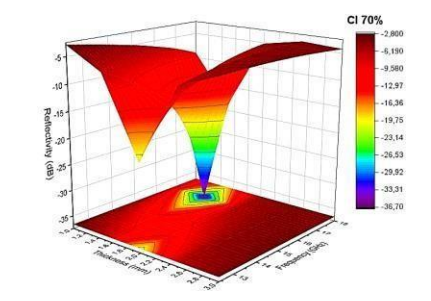


Fig. 2. Reflectivity for CI 70 wt. % sample with 1.5 mm

4. Referencies

[1] AMARAL, Miguel Angelo Junior et al. Influence of the Permittivity on Carbon Fiber Particulates Applied in Radiation Absorbing Materials. Global Journal of Research In Engineering, 2018.

^{*}Corresponding author: mauricio.baldan@inpe.br

SIMULATION OF PLASMA GENERATION IN A CATHODIC CAGE SYSTEM

Gabriel C. Camargo, Julio C Sagás*

Laboratory of Plasmas, Films, and Surfaces, Universidade do Estado de Santa Catarina, Joinville-SC

1. Introduction

Low-pressure plasma is commonly used for material treatment [1], aiming to enhance the surface properties of metals, ceramic, polymers and composites. However, the energy imparted by the charged particles can lead to excessive heating of polymers, causing degradation. To mitigate this issue, one strategy is to employ a cathodic cage system, where the sample is positioned within an electrical discharge hollow cathode. Depending on the pressure and the cage geometry, the plasma can be generated either inside or outside the cage, allowing for the treatment of thermally sensitive substrates. This study deals with simulations of DC argon plasma generated in a cathodic cage system. Specifically, we investigate the spatial distribution of the plasma at various working pressures to identify the pressure range at which plasma is formed outside the cage.

2. Theory

Simulations were conducted using the Plasma module of the *COMSOL Multiphysics Software*, employing the solutions of the moments of the Boltzmann equation. The adopted model treats electrons as a fluid within a 2D geometry representing a laboratory-installed reactor. The electron energy distribution (EEDF) is considered Maxwellian, and only three heavy species are taken into account: neutral Ar, ionized Ar, and metastable Ar.

3. Results and Discussions

At lower pressures, the plasma forms outside the cathodic cage, but higher pressures enable plasma to penetrate the grid. This penetration is linked to the product of pressure and grid hole size (pd). As the product pd increases, the chances of plasma forming within the cage also rise. Moreover, plasma density is higher within the cage due to the hollow cathode effect, which confines electrons, boosting ionization. Simulations reveal that when plasma is outside the cage, the cage's interior potential approaches negative values similar to the applied voltage, consistent with prior experiments. The different potential distributions within the grid indicate a change in predominant incident particle type according to the plasma spatial distribution.

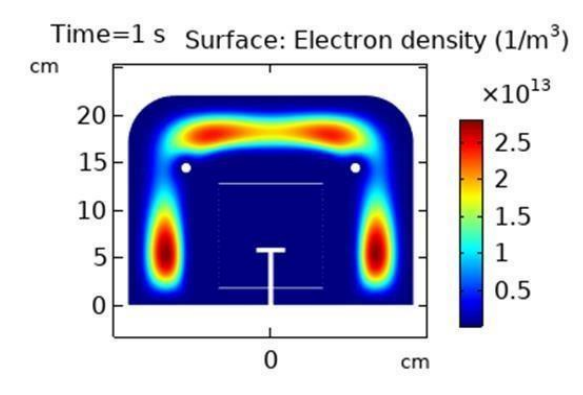


Fig. 1. Plasma distribution for a 100 mTorr working pressure.

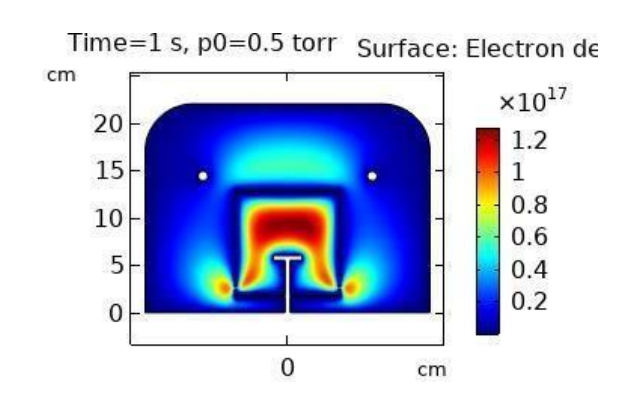


Fig. 2. Plasma distribution for a 500 mTorr working pressure.

4. References

[1] Gudmundsson, J. T., & Hecimovic, A. (2017). Foundations of DC plasma sources. *Plasma Sources Science and Technology*, 26(12), 123001.

Acknowledgments

Thanks to FAPESC (grants 2021TR000563 and 2023TR000258) and CNPq (grant 304053/2021-0).

^{*}Corresponding author: julio.sagas@udesc.br

SÍNTESE E ESTUDO DA ATIVIDADE ANTIMICROBIANA DA MOF DE COBALTO

Isabelle Goulart dos Santos¹, Maria Tereza Fabbro^{1,2}, Felipe De Moraes Yamamoto², Luis Presley Serejo³, Maurício Ribeiro Baldan²

¹Instituto Federal de São Paulo – Campus São José dos Campos ²Instituto Nacional de Pesquisas Espaciais ³Universidade Federal de São Paulo

1. Introduction

As estruturas metal-orgânicas (MOFs), também denominadas como polímeros de coordenação porosos, têm despertado um interesse substancial nos domínios de armazenamento de energia, separação de gases e catálise, além de serem flexíveis e possuírem a capacidade de incorporar funcionalidades e espécies ativas sem modificar sua estrutura principal, oferecendo alta porosidade, ampla área superficial interna, sítios coordenadamente insaturados e uma forte interação entre os metais e os ligantes orgânicos. Recentemente, tem- se observado uma crescente pesquisa sobre o potencial bactericida desses materiais. Este estudo destaca-se a síntese e caracterização de MOF de cobalto preparada pelo método hidrotérmico assistido por microondas (MAH), assim como verificou-se a atividade fungicida contra *Candida albicans* e bactericida contra *Staphylococcus aureus* e *Escherichia coli*.

2. Experimental e Teórica

Dissolveu-se ácido benzeno tetracarboxílico (H₄BTC) em uma solução mista de dimetilformamida (DMF) e água deionizada e adicionou-se Co(NO₃)₂ e CTAB. Em seguida introduziu-se a um reator de micro-ondas em 180°C por 30 minutos. O precipitado formado foi lavado em centrífuga por 3 vezes com água deionizada e etanol e foi seco em estufa em 60°C por 24 horas. O material preparado foi caracterizado a partir de difração de raios-X (DRX), microscopia eletrônica de varredura com campo de emissão (FEG-MEV) e espectroscopia com energia dispersiva (EDS).

3. Resultados e Discussões

Os resultados apresentam picos nítidos e claros que demonstram boa cristalinidade, demonstrando efetiva formação do material, correspondendo aos planos cristalográficos do padrão de difração teórico de um MOF-Co obtidos do The Cambridge Crystallographic Data Centre (CCDC 638866). Os picos de difração (Figura 1) estão de acordo com os observados ao difratograma teórico coletado no CCDC, que correspondem aos planos cristalográficos. A morfologia dos materiais obtidos revela uma forma de bastões, diferentes aos encontrados na literatura, que geralmente apresentam morfologia cúbica (Figura 2), podendo ser justificado pela utilização do surfactante CTAB.

Fig. 1. Difratograma da MOF-Co sintetizado

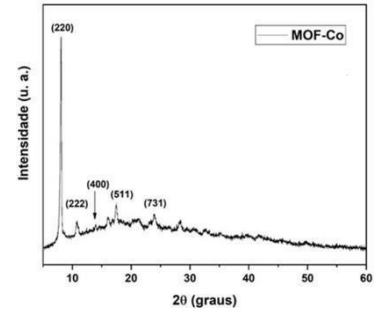
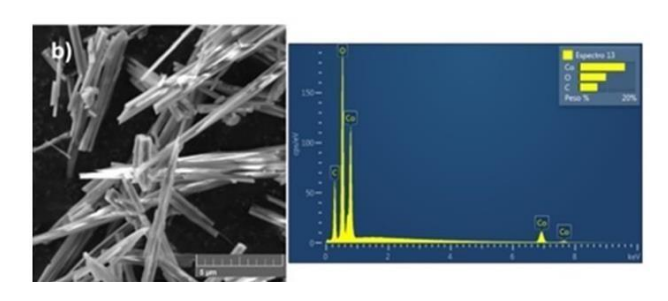


Fig. 2. Micrografia e análise de EDS da MOF-Co



Os valores de MIC obtidos contra as cepas de bactérias Gram negativas *E. coli* foi maior que 22 μg/mL e Gram-positivas *S. aureus* 44 μg/mL, enquanto a cepa fúngica *C. albicans* 87 μg/mL.

4. Agradecimentos

(FINEP/N° 16.01.0076-00) e ao Programa Wash e ao Conselho Nacional de Desenvolvimento Científico e Tecnológico (CNPq – Processo n° 4033506/2020-4. Ao Instituto Nacional de Pesquisas Espaciais (INPE), à Universidade Federal de São Paulo (UNIFESP) e ao Instituto Federal de São Paulo - Campus São José (IFSP).

^{*}Autor correspondente: isabellegoulart9@gmail.com

SOUND WAVE PROPAGATION IN WET STEAM

Paloma H.P. Eleuterio¹, Marcelo P. Gomes², Alexei M. Essiptchouk^{1*}

¹Department of Environment Engineering, Institute of Science & Technology, São Paulo State University, UNESP, São José dos Campos, 12247-004, Brazil

²Plasma and Processes Laboratory, Technological Institute of Aeronautics, São José dos Campos, 12228-900, SP, Brazil

1. Introduction

Rapid economic growth increases waste volume, necessitating environmentally friendly technologies like thermal plasma treatment, which is currently underutilized due to a shortage of reliable plasma generators. The plasma torch, which utilizes water vapor for both electrode cooling and plasma generation, demonstrates exceptional thermal efficiency and yields a plasma jet with elevated enthalpy. The electrode cooling is achieved through the utilization of latent heat during the phase transformation from liquid to vapor. To ensure optimal performance in such a system, precise control over steam quality (the proportion of saturated vapor in a saturated two-phase liquid/steam mixture) is essential.

2. Theory

A method of measuring the steam quality based on ultrasound is described in [1] and based onmeasuring the speed of sound in wet steam. It was shown theoretically in [2] that the isentropic speed of sound depends on saturation temperature T, pressure p, and steam quality. Rigorous consideration of the thermodynamic properties of steam is necessary for calculations. Nonetheless, in [3], it was outlined that sound propagation through the equilibrium wet steam depends on acoustic wave frequency. No experimental measurements of the speed of sound have been reported.

3. Results and Discussions

Analytical and numerical analyses on the governing equations for sound speed in wet steam within the pressure range of 0.1 to 0.5 MPa allows to simplify the formula for steam quality: $x = Ac^2 p^B$, where A = 4.09 ·10⁻⁶ and B = -0.088, c – sound speed (m/s) and p – pressure (MPa). The difference between the approximate function and the theoretical outcomes is minimal and only impacts the low vapor quality range (x < 0.1). Experimental verification will be carried out.

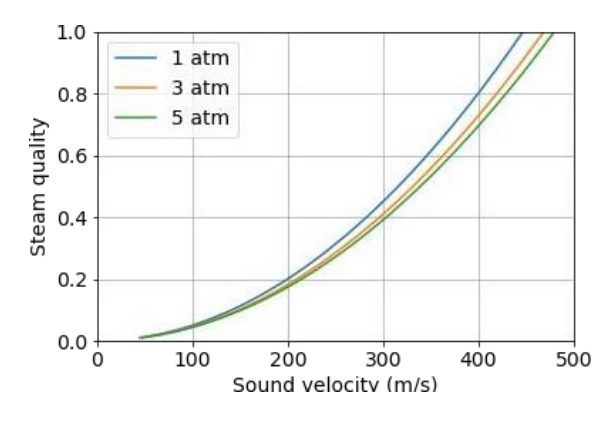


Fig. 1. Steam quality versus sound velocity at various pressure levels.

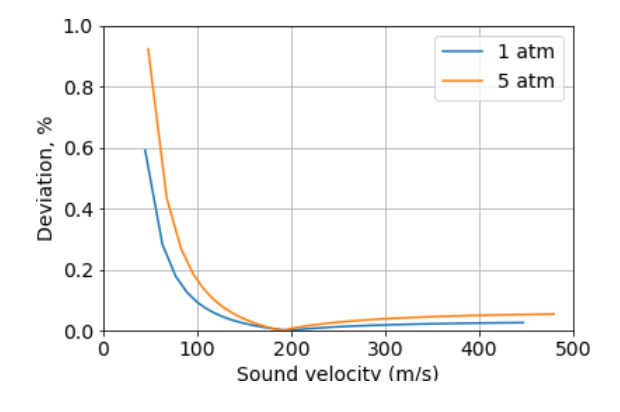


Fig. 2. Deviation of the theoretical value of steam quality from approximated function.

4. References

- [1] J. J. S. Shen, Journal of Energy Resources Tech., 121, 172-175, (1999).
- [2] E.E. Michaelidis and K.L. Zissis, int. J. of Heat & Fluid Flow, 4, 2, 79 84 (1983)
- [3] V. Petr, J. Mechanical Engineering Science, **218**, Part C, 871 882, (2004)

Acknowledgments

We would like to thank the São Paulo Research Foundation (FAPESP) for financial support: 2022/00271-3.

^{*}Corresponding author: alexei.essiptchouk@unesp.br

STRUCTURAL ANALYSIS OF HEO-BASED COATING ON Ti-6Al-4V ALLOY PRODUCED BY PEO FOR POTENTIALBIOMEDICAL APPLICATION

Karine Stefany Coan^{1*}, Carlos Roberto Grandini¹, Diego R. Nespeque Corrêa¹

¹São Paulo State University (UNESP), School of Sciences, Bauru-SP

1. Introduction

Metallic biomaterials, such as titanium alloys, play a crucial role in Medicine to repair or replace tissues and organs in the human body. However, the release of toxic ions at long-term has driven research into improving surface properties. Surface modification techniques, such as plasma electrolytic oxidation (PEO), havestood out in the biomedical area due to the formation of porous oxide coatings, strongly adhered to the substrate, and enriched with specific chemical species from the electrolyte. An interesting and scarcely explored possibility is the formation of high entropy oxides (HEO), composed of five or more oxides and which have resulted in interesting properties for several current technological applications [1,2].

2. Experimental

Samples of the Ti-6Al-4V alloy (2 × 2 cm) were cleaned with isopropyl alcohol and an ultrasonic bath, after later were treated by PEO. For the treatment, an electrolyte solution composed of calcium acetate, β -glycerol phosphate and metal oxides (Fe, Al, Ti, Mo, Mn) was used at a concentration of 61 g/L, 6 g/L and 1 g/L respectively. The process involved the use of a DC power source with a voltage of 300 V, for 1 minute, under constant stirring. After this, an analysis of the surface phase composition was carried out by X-ray diffractometry(XRD), with monochromatic CuK radiation (λ = 0.1544 nm), potential of 40 kV, current of 30 mA, fixed time mode, step of 0.02° and collection time of 1.6 s. Diffraction peaks were compared with crystallographic datasheetsfrom the ICDD database.

3. Results and Discussions

The diffraction patterns of the substrate and the treated sample are presented in Figure 1. A preliminary analysis reveals peaks characteristic of the substrate phases, represented by the α -Ti and β -Ti phases, with HCP and BCC crystalline structures, respectively. For the treated sample, it was possible to identify an amorphous oxide region at low angles, with small oxide peaks, mostly based on Ti and Fe oxide compounds. Therefore, the preliminary results offer important insights to understand the structure and composition of the samples, indicating that the PEO technique may be promising for the development of multicomponent oxide films with potential application in the biomedical area.

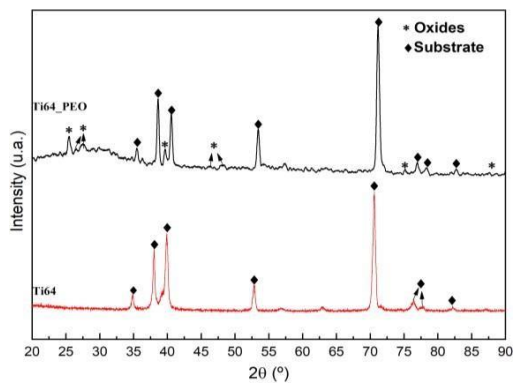


Figure 1. XRD profile of the sample with and without PEO treatment.

4. References

[1] MARCUZ, N. *et al.* The effect of PEO treatment in a Ta-rich electrolyte on the surface and corrosion properties of low-carbon steel for potential use as a biomedical material. **Metals**, v. 13, p. 520 – 563, 2023.

[2] AAMLID, S. S. et al. Understanding the Role of Entropy in High Entropy Oxides. *J. Am. Chem. Soc.* 2023, 145, 11, 5991–6006.

Acknowledgments

The authors thank FAPESP, CNPq, and Capes for their financial support.

^{*} Corresponding author: karine.coan@unesp.br

STUDY OF HYBRID TiO2–WOX THIN FILMS DEPOSITED VIA CO-SPUTTERING: EVALUATION OF THE PHOTOCATALYTIC ACTIVITY

Giovana Fazenda^{1,2}, Douglas Marcel Gonçalves Leite², Argemiro Soares da Silva Sobrinho², André Luis de Jesus Pereira²

¹Instituto Federal de São Paulo – Campus São José dos Campos (IFSP-SJC), São José dos Campos-SP ² Laboratório de Plasmas e Processos (LPP), Instituto Tecnológico de Aeronáutica (ITA), São José dos Campos-SP

1. Introduction

Among semiconductor materials, TiO_2 has several advantages in addition to photocatalytic activity, including its natural abundance, low toxicity, thermal and chemical stability and resistance to photocorrosion. TiO_2 has the property of acting as both an oxidant and a reductant [1]. However, TiO_2 has a bandgap of ~ 3.2 eV and the energy of the visible light spectrum (< 2.75 eV) is not enough for the formation of electron-holes, so the oxide is inefficient in this range of light that represents $\sim 40\%$ of the light that reaches Earth [2]. In order to contribute to the increase in the photocatalytic activity of TiO_2 , in this work we will present a study of the production and characterization of hybrid films of TiO_2 and WO_x grown using a Dual Magnetron Sputtering aiming their application in the photodegradation of organic contaminants.

2. Experimental

All depositions were carried out in a DC Dual Magnetron Sputtering chamber where for each of the targets (metallic Ti and W) there is an independent DC source. During depositions, parameters such as power on the Ti target (300 W), Ar flow (10 sccm), O₂ flow (2 sccm), substrate temperature (ambient) and pressure (3.0 mtorr) were kept constant. Six films were grown with different powers applied to the W target: 0W, 5W, 10W, 15W, 20W and 30W. After deposition, the films, growth on Si(100), glass and FTO, were annealed at 450 °C for 2h. The films obtained were characterized by Raman Scattering, X-ray Diffraction (XRD), Energy Dispersive X-ray Spectroscopy (EDS), mechanical profilometry, UV-VIS spectrophotometry and photocatalysis tests with Methylene Blue using UV light.

3. Results and Discussions

The characterizations indicate a linear increase in the concentration of W incorporated into the films with the power applied in the tungsten target, reaching a value of \sim 45% for a power of 30 W. Figs 1 and 2 show that, up to 10 W, the films crystallize in the anatase phase of TiO_2 . Above this power, the films present an amorphous structure. Furthermore, we did not observe any significant variation in the bandgap value of the films, remaining around 3.2 eV. Despite this, there were significant variations in the photocatalytic efficiency of the films with variation in W incorporated.

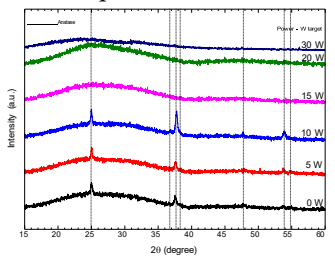


Fig. 1. X-ray diffraction measurements of TiO_2+WO_x films deposited with different DC powers on the W target.

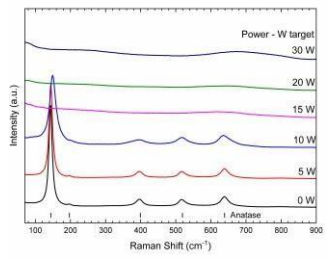


Fig. 2. Raman Scattering measurements of TiO_2+WO_x films deposited with different DC powers on the W target.

4. References

- [1] Y. H. Chiu, T. H. Lai, M. Y. Kuo, P. Y. Hsieh and Y. J. Hsu, **APL Mater.**, 2019, 7, 080901.
- [2] J. Schneider, et Al., Chem. Rev., 2014, 114, 9919–9986.

Acknowledgments

We thank the FAPESP (2022/02994-2, 2023/10449-7) for the financial support.

^{*}Corresponding author: andrelpereira@gmail.com

STUDY OF LOW-POWER DIELECTRIC BARRIER DISCHARGE AT ATMOSPHERIC PRESSUREAND CYTOTOXICITY TEST AND ANTIMICROBIAL ACTIVITY

Thayna F. Tavares¹, Felipe Kodaira¹, Gisele Soares de Castro², Diego Morais da Silva², Konstantin G. Kostov¹, Cristiane Y. Koga Ito^{2,4}, and William Chiappim¹*

¹Laboratory of Plasmas and Applications, Department of Physics, Faculty of Engineering and Sciences, São Paulo State University (UNESP), Guaratinguetá 12516-410, Brazil

²Science Applied to Oral Health, Graduate Program of Institute of Science and Technology, São Paulo State University (UNESP), São José dos Campos 12245-000, Brazil

and ³Departmente of Environment Engineering, Institute of Science and Technology, São Paulo State University (UNESP), São José dos Campos 12245-000, Brazil

1. Introduction

The COVID-19 pandemic underscores the vital need for widespread antimicrobial techniques. Initially limited to medical, pharmaceutical, and food sectors, this imperative now spans surfaces used daily and personal items. Recent decades witnessed swift progress in cold atmospheric plasma (CAP), particularly in bacterial, fungal, and viral inactivation [1] and surface disinfection [2]. In this context, the present study explores a cost-effective, low-power dielectric barrier discharge device operating at atmospheric pressure using air as gas for antimicrobial inactivation.

2. Materials and Methods

In the assessment of antimicrobial efficacy, two clinically significant microbial species were selected: Candida albicans, a fungus responsible for both superficial and widespread human infections, and Staphylococcus aureus, a gram-positive bacteria associated with various diseases. Vero cells—a commonly used cell lineage in cultures—were employed to evaluate cytotoxicity. Subsequently to preparation, microbial species and cells were exposed to low-power dielectric barrier discharge for 1, 3, 5, and 10 minutes. The antimicrobial activity and cytotoxicity tests were performed using a previously reported methodology [3].

3. Results and Discussions

The percentage reduction of Candida albicans and Staphylococcus aureus treated with the plasma device were of 99.9% (not showed). All the groups showed viability above 70% [Fig. 2], indicating that the treatment performed at times varying between 1 and 10 min is not cytotoxic.



Fig. 1. Exposure of microbial species and Vero cells in a 24-well plate to the plasma generated by the equipment.

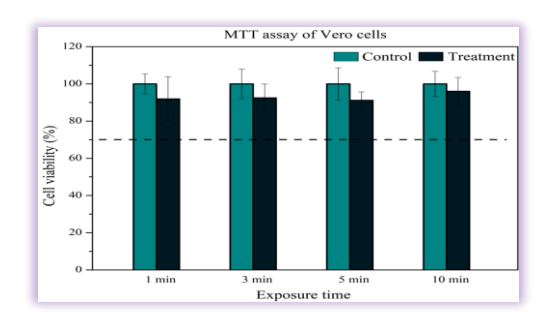


Fig. 2. Results obtained from MTT assay using Vero cells. Cell viability (%) of cells exposed to plasma at 1, 3, 5, and 10 min and the respective controls.

4. References

- [1] G.M.G. Lima et al., Appl. Sci., 12(14), 7247, (2022).
- [2] A. Sakudo et al., Int. J. Mol. Sci., **20(20)**, 5216, (2019).
- [3] W. Chiappim et al., Plasma Process Polym., **18(11)**, 202100010, (2021).

Acknowledgments

This work was supported by the São Paulo State Research Foundation (FAPESP) [2019/05856-7; 2020/10450-7].

^{*}Corresponding author: william.chiappim@unesp.br

STUDY OF NON-LINEAR OPTICAL PROPERTIES USING THE Z SCAN TECHNIQUE OF QDs NANOFLUIDS OBTAINED BY GREEN SYNTHESIS

Ruben Gutiérrez-Fuentes¹, Jose. L. Jiménez-Pérez^{2*}, Jose L. Luna-Sánchez², Zormy N. Correa-Pacheco³, Misha J. del Castillo-Aguirre², Mauricio A. Algatti^{4*}

¹Tecnológico de Estudios Superiores de Villa Guerrero, Carretera Federal Toluca Ixtapan de La Sal. Km. 64.5,Col. La Finca, Villa Guerrero, Mexico State, Mexico

²Unidad Profesional en Ingeniería y Tecnologías Avanzadas, IPN. Avenida Instituto Politécnico Nacional No. 2580, Col Barrio la Laguna Ticomán, Gustavo A. Madero, Mexico City, C.P. 07340, Mexico.

³Centro de Desarrollo de Productos Bióticos, IPN. Carretera Yautepec-Jojutla, Km. 6, calle CEPROBI No. 8, Col. San Isidro, C.P. 62731, Yautepec, Morelos, Mexico.

⁴Faculdade de Engenharia e Ciências, UNESP-Campus de Guaratinguetá, Av. Ariberto P. Cunha 333,12516-410 Guaratinguetá, SP, Brazil

1. Introduction

Carbon quantum dots (CQDs) have attracted special attention in recent research due to their nonlinear optical properties in applications in electronics, energy, and biomedicine [1]. However, new organic sources such as banana peel, glucose sucrose, orange peel, must be sought. In this work, QDs were synthesized from QDs nanofluids obtained by green synthesis as precursors. Distilled water-based nanofluids were prepared using different QDs concentrations. The nonlinear optical properties of the nanofluids were measured using the Z-scan technique.

2. Experimental

QDs were synthesized obtained by green synthesis as precursors by dehydration y carbonization. Two different centrifugation speeds. For the Z scan experimental setup, a diode laser (488 nm) The sample was placed in a quartz cuvette and the beam was focused using a lens of 15 cm and the cuvette was moved across the focal region along the Z-axis. Also, the QDs nanofluids were characterized by UV-vis spectroscopy and transmission electron microscopy (TEM).

3. Results and Discussions

From the results, UV-vis showed absorption bands at 200 and 330 nm. Mean diameter size was 5 nm and spherical morphology was observed by TEM. The optical nonlinear refractive index for the QDs values were between 4.51×10^{-9} cm²/W (PAN- QDs), -2.97×10^{-9} (WQDs) and -3.45×10^{-9} (OQDs) for 8000 rpm. Therefore, organic QDs greatly improve the nonlinear optical properties of the sample being a very promising nonlinear medium for optoelectronic applications.

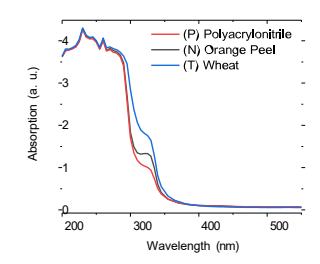


Fig. 1. *UV-vis spectra of organic QDs,*.

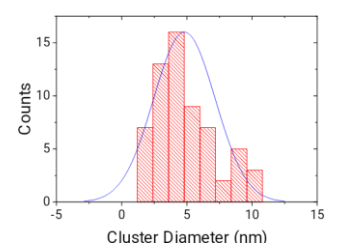


Fig. 2. Size distribution QDs measured by TEM.

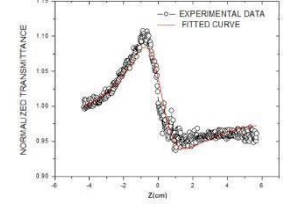


Fig. 3. Z-Scan for the OQDs at 12,000 rpm.

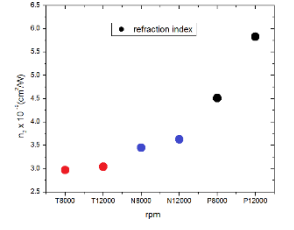


Fig. 4. *Non-linear refractive index as afunction of rpm for QDs.*

4. References

[1] M. Cotta, ACS Appl. Nano Mater., **3(6)**, 4920-4924, (2020).

Acknowledgements

One of us, M. A. A., would like to thank FAPESP for financial support.

^{*}Corresponding authors: jimenezp@fis.cinvestav.mx and mauricio.algatti@unesp.br

STUDY OF PROCEDURES FOR 3D PRINTING OF POLYMERIC STRUCTURES AIMING BIOMEDICAL APPLICATIONS

Vinicius dos Santos*, Fábio H. C. Bernardes, Durval Rodrigues Junior.

Department of Materials Engineering (DEMAR), Lorena School of Engineering (EEL), University of São Paulo (USP), Lorena-SP-Brazil

1. Introduction

Research in 3D printing of polymeric scaffolds for biomedical applications has gained prominence due to its potential. The evaluation of the morphology and porosity of these structures is crucial to ensure their quality. To achieve this, characterization techniques have been applied, allowing for a comprehensive analysis. Based onthis, this research explores the analysis of surface and structural characteristics of these scaffolds, employing advanced characterization techniques [1,2]. These approaches provide valuable insights for optimizing these structures for biomedical applications.

2. Experimental

Porous polymeric samples were employed in the conducted experiment. The samples were prepared using GTMax model A4 3D printer, using ABS and PLA polymeric filaments. The porosity was introduced using different printing schemes and morphologies. The procedures to characterize the porosities included the determination of dry weight, saturation of samples under vacuum, evaluation of suspended and saturated weights, calculation of external volume, and determination of open pore volume and impermeable portion of the specimen.

3. Results and Discussions

The realization of the tests on 3D printed polymeric samples subjected to vacuum yielded remarkable outcomes. The utilization of vacuum allowed for a more precise measurement of weights compared to the Archimedes test, due to the complete filling of pores with isopropyl alcohol. This led to density calculations that approached the desired accuracy, demonstrating the efficacy of the technique in evaluating sample porosity. The significance of this approach becomes evident when contrasted with the metallic samples studied by the DEMAR-EEL-USP research group. This comparison provided valuable insights into the influence of porosity onliquid absorption and retention, emphasizing the intricate interplay between porous structure and saturating liquid. These findings suggest a promising potential for enhancing the properties of porous polymeric materials and contribute to advancements in characterizing and understanding such structures.



Fig. 1. Porous polymeric samples, as tested.



Fig. 2. Characterization of samples using vacuum.

4. References

[1] ABBASI, Naghmeh et al. Porous scaffolds for bone regeneration. Journal of science: advanced materials and devices, v. 5, n. 1, p. 1-9, 2020.

[2] BISHT, Bharti et al. Advances in the fabrication of scaffold and 3D printing of biomimetic bone graft. Annalsof Biomedical Engineering, v. 49, n. 4, p. 1128-1150, 2021.

Acknowledgments

Thanks to Unified Scholarship Program (PUB) of USP, for funding the work of the undergraduate student.

^{*} Corresponding author: vini.santos@usp.br, durvalrj@usp.br

STUDY OF THE EFFECT OF BORETATING AGENT 70%Na2B4O7 + 30%SiC ON THE MICROWEAR RESISTANCE OF AISI 420 STAINLESS STEEL

Leandro Almeida Silva¹, Rogério Varavallo², Omar Maluf³, Marcos D. Manfrinato^{1,4}, Luciana S. Rossino^{1,4}

¹Sorocaba Technological College- FATEC, Sorocaba, SP, Brazil ²Technical School of Sylvio de Mattos Carvalho – ETEC, Matão-SP, Brazil 3 Sertãozinho Technological College – FATEC, Sertãozinho, SP, Brazil. ³Federal University of São Carlos (UFSCar), Sorocaba Campi, Sorocaba, SP, Brazil

1. Introduction

Boridation is a thermochemical surface hardening treatment in which boron atoms are diffused onto the surface of steel. Boron atoms react with the base material and form several borides that increase the hardness of the boride layer. The formation of the boride layer on the surface produces a positive effect in reducing the rate of corrosion, oxidation, or formation of fatigue cracks and reducing the rate of wear [1,2,3]. The aim of this work is to evaluate the influence of the mix $70\%Na_2B_4O_7 + 30\%SiC$ in the formation of a borated layer and microwear resistance of the AISI 420 martensitic stainless steel.

2. Experimental

The solid boretation in the AISI 420 martensitic stainless steel is carried out using 70% Na₂B₄O7 + 30%SiC dust in muffle furnace keeping the time of 2 and 5 hours, the temperature 950°C. The material characterization with and without treatment was carried out by metallography and microhardness Vickers. The microabrasive wear by fixed ball was carried out with a load of 20 N, time test of 5 to 30 min. and 150 RPM, using abrasive paste consisting of F-1200 SiC (4-5 μ m) particles dissolved at 20% (80 g / 100 ml of deionized water). The solution was constantly stirred with a magnetic stirrer to avoid the particle precipitation.

3. Results and Discussions

Solid Boridation for 2 and 5 hours produces layers of thicknesses of 10 μ m and 80 μ m, respectively. The untreated AISI 420 stainless steel presented a surface microhardness of 350 HV, while the borided steel at 2 hours presented a surface microhardness of 1360 \pm 35 HV and at 5 hours a microhardness of 2240 \pm 28 HV. The borided layers showed greater resistance to abrasive microwear than the base material, as shown in Fig. 1. The borided layer for 5 hours showed a lower wear rate due to the greater hardness of the layer and thickness in relation to the 2-hour treatment, as presented in Table 1.

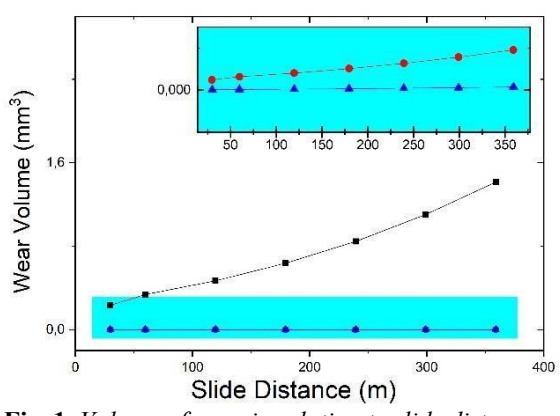


Fig. 1. Volume of wear in relation to slide distance

Tab. 1 - Wear rate calculated by linear regression with respective standard deviations.

	k (mm³/N.m)	Standard Deviation	R²
BM	1,7261x10 ⁻⁴	0,11x10 ⁻⁴	0,97966
2 hours	1,04228x10 ⁻⁷	0,049x10 ⁻⁷	0,98907
5 hours	9,66059x10 ⁻⁹	0.07×10^{-8}	0,96972

4. References

[1]- Y. Kayalli, I. Gunes and S. Ulu, Vaccum, 86, 1428-1434, (2012).

[2]- C.D.R. Calderon, G.A.R. Castro, A.M. Amador, I.E.C. Silva, J.A. Adame, M.E.P. Pardavé, E.A.G. Hernández. Journal .Mat. Eng. Perf, **26(11)**, 5599-5609, (2017).

[3]- I.C. Silva, M.E.P. Pardavé, R.P.P. Borja, O.K. Feridum, D.B. Bárcenas, C.L. García, R.R. Helguera. Surf. Coat. Tech., 349, 986-997, (2018).

^{*}Corresponding author: leandro.silva326@fatec.sp.gov.br

STUDY OF THE EFFECT OF GAS FLOW VARIATION ON THE WEAR RESISTANCE OFPLASMA NITRIDED ASTM F138 STAINLESS STEEL

João Gabriel Velo Danesi¹, Luciana Sgarbi Rossino^{1,2}, Marcos Dorigão Manfrinato¹

¹Faculdade de Tecnologia - Fatec- Sorocaba ²Universidade Federal de São Carlos - UFSCAR – Sorocaba

1. Introduction

The parameters determined to carry out the plasma nitriding treatment, such as time, temperature, proportion, and gas flow, can influence the characteristics of the layer formed [1]. In particular, the gas flow influences the type of nitride formed without significantly changing the thickness of the layer formed [2]. This work aimed to study the wear resistance of ASTM F138 stainless steel subjected to plasma nitriding at different gas flows.

2. Methods

ASTM F138 stainless steel was subjected to plasma nitriding treatment, maintaining the fixed parameters of 80% N2 and 20% H2 for 6 hours at 415°C, varying the gas flow by 500 sccm (4,1 torr), 750 sccm (5,7 torr), 1000 sccm (5,9 torr), and 1200 sccm (6,4 torr). After treatment, the samples were subjected to metallographic analysis, Vickers microhardness testing, and micro-abrasive wear testing by fixed ball.

3. Results and Discussions

Regardless of the treatment conditions, plasma nitriding considerably increased the hardness and wear resistance of ASTM F138 stainless steel. must be considered that the hardness of the substrate is 204.4 HV. The variation in treatment flow influenced the uniformity, thickness, and hardness of the layers formed (Fig.1), the result of which is different from that obtained by Sholtz et al. (2018) [2], who state that layer thickness is mainlyinfluenced by treatment time and temperature. As a result, the influence of the gas flow on the wear resistance ofthe treated material was observed (Fig. 2). It can be seen that the 750 and 1200 sccm treatments had greater wear resistance at longer test times, and the 500 and 1000 sccm treatments had greater wear resistance in the 5-minutetests. The treatments with greater thickness and hardness showed an increase in wear volume after 5 minutes, while the treatments with lower thickness and hardness showed stability in wear volume even as the test time increased. It can be concluded that the treatment pressure, defined by the gas flow, has an influence on the surface properties of the steel studied.

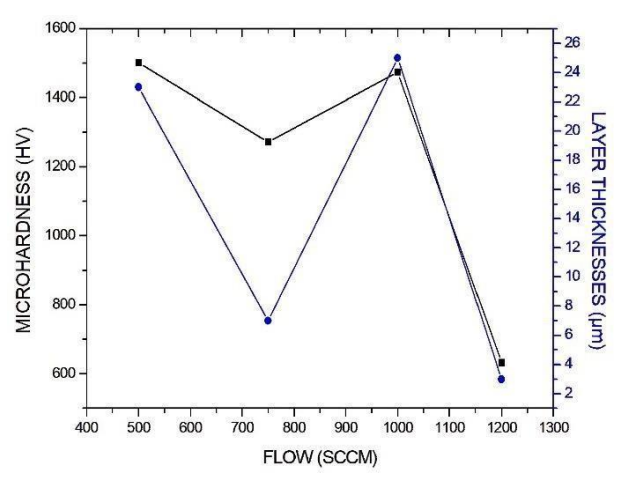


Figure 1- Microhardness and thickness as a function of treatment gas flow

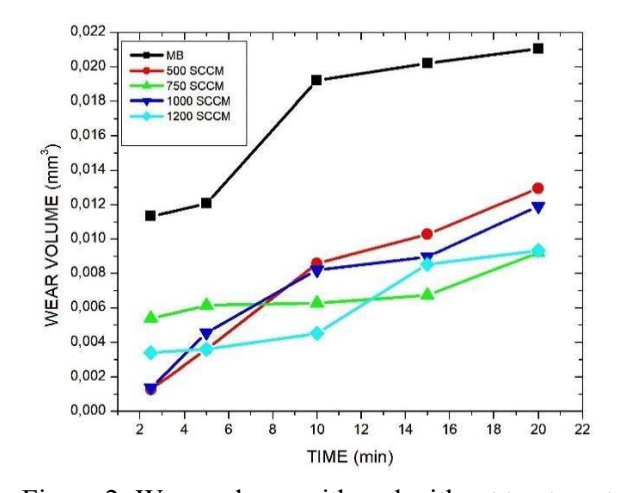


Figure 2- Wear volume with and without treatment

4. References

- [1] Danelon, M. R, Revista Brasileira de Aplicações de Vácuo, (2020). 39(2).
- [2] J. S. Scholtz et al. Metal. Mater. Min., 15 (2018) 110-114

^{*} Corresponding author: joaogabrielvelodanesi@gmail.com

STUDY OF THE ELECTRICAL PROPERTIES OF POLY-O-METHOXYANILINE (POMA) FOR APPLICATIONS IN ELECTRONIC DEVICES

Bruno E. P. Nogueira da Gama¹; Silmar A. Travain^{2*}

¹Laboratório de Química, Departamento de Alimentos da Escola de Nutrição (ENUT)

Universidade Federal de Ouro Preto (UFOP)

²Departamento de Física (DFI), Faculdade de Engenharia e Ciências de Guaratinguetá (FEG)Universidade

Estadual Paulista Júlio de Mesquita Filho (UNESP)

1. Introduction

In recent decades, research in the area of conjugated polymeric materials has attracted considerable attention. These materials, depending on the degree and type of doping, can vary their electrical conductivity by about 10 orders of magnitude [1]. Among these, the semiconductor polymer poly-o-methoxyaniline (POMA) and its derivatives, appear as a potential candidate from the technological point of view, in view of its low cost and ease of processing. Outstanding due to their electrical and optical properties, these polymers are widely used for application in shields, optical and electronic devices, and sensors.

2. Experimental

The o-methoxyaniline monomer was synthesized via oxidative polymerization, using the reducing agent ammonium peroxydisulfate ((NH4)2S2O8). The polymers obtained showed a dark green color, which is characteristic of POMA polymers doped Emeraldine Salt (ES). The dedoping of the polymers was performed with ammonium hydroxide solution (NH4OH). The undoped polymers obtained showed a bluish color (BE). The materials obtained were dried in a vacuum oven for 24 hours at a temperature of 30°C. Subsequently to study the electrical properties a variation in the concentration of the 1 mol/L HCl solution was performed for redoping the polymer.

3. Results and Discussions

We can observe a greater variation in the actual electrical conductivity as the variation in the concentration of the H+Cl- doping agent increases (Fig. 1). The addition of the dopant agent in the POMA polymer mass favors the formation of conductive islands in the polymer volume, resulting from the polymer doping (emeraldine salt), reducing the energy required for jumps between the established islands. This result is very important, since, as mentioned in the literature [2] the random free energy (Random Free-Energy Barrier Model – RFEB) relates the value of maximum jump energy of the charge carriers involved in the transport process in the volume of the polymer. In Fig. 2 (undoped POMA UV spectrum - 0.001g/mL) the presence of a band in the 300nm region was observed, which can be attributed to the π - π * electronic transition of the conjugated aromatic systems present in the POMA polymer. In the region of 620nm another absorption band is observed, which is attributed to the electronic transition of the n- π * type resulting from the transfer of charge from the benzenoid rings to the quinoid ring.

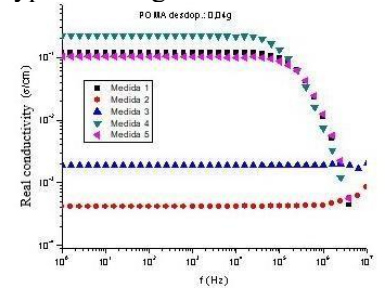


Fig. 1. Real electrical conductivity of POMA doped in different concentrations of H+Cl-.

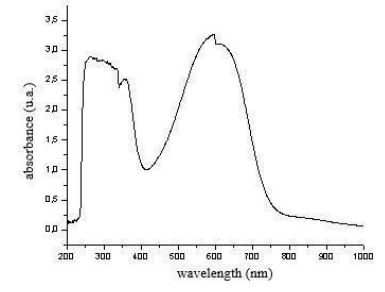


Fig. 2. UV-Visible Spectrum Undoped POMA.

4. References

- [1] Shirakawa, H. et al; Physical Review Letters, **39**, n.17, 1098-1101, (1977).
- [2] Dyre, J. C.; Disordered Solids; Journal Applied Physics, **64**, n.5, 2456-2468, (1988).

Acknowledgments: The authors would like to thank FAPESP and INEO/CNPq for encouraging the development of this work.

^{*}Corresponding author: silmar.travain@unesp.br

STUDY OF THE INFLUENCE OF DC POWER ON THE PROPERTIES OF WO₃ FILM GROWN BY MAGNETRON SPUTTERING

Rafael da Silva Leal¹, Giovana Fazenda², Helen Carolina de Souza Barros¹, Argemiro Soares da Silva Sobrinho¹e André Luis de Jesus Pereira¹.

¹ Laboratório de Plasmas e Processos (LPP), Instituto Tecnológico de Aeronáutica (ITA), São José dos Campos;

² IFSP – Instituto Federal de Educação, Ciência e Tecnologia de São Paulo, Campus São José dos Campos.

1. Introduction

Due to their wide range of applications, including catalysis and energy storage, metal oxides, particularly tungsten trioxide (WO₃), are considered promising materials due to their distinct properties. WO₃, an n-type semiconductor, is particularly useful in gas sensors and optoelectronic devices [1,2]. Magnetron Sputtering is one of many techniques that can be used to make WO₃ films [2]. The study aims to determine how the DC potency variation applied to the target affects the characteristics of the WO₃ films created by this method.

2. Experimental

The WO₃ films were grown using a magnetron sputtering system, with a 100 mm diameter tungsten target (99.9%purity), deposited on Si (100) and glass substrates. Controlling the concentration of WO₃ incorporated into the films was carried out by varying the DC power applied to the metallic WO₃ target. Five different powers were used: 30W, 50W, 100W, 150W and 200W. Subsequently, the films underwent heat treatment at 450 oC for 2 h, with a heating ramp of 5° C/min. The films were characterized by Energy Dispersive X-ray Spectroscopy (EDX) and Mechanical Profilometry measurements.

3. Results and discussions

All films showed good mechanical properties and homogeneity, even at low power. Optical transmittance measurements suggest that the films have a thickness and refractive index with a high degree of homogeneity. Regarding thickness, it can be seen that the growth is proportional to the increase in power. Therefore, in the next stages of the work, WO₃ films will be grown by varying the oxygen and argon flow ratio $(\phi Ar/O_2)$ in order to obtain films with other concentrations.

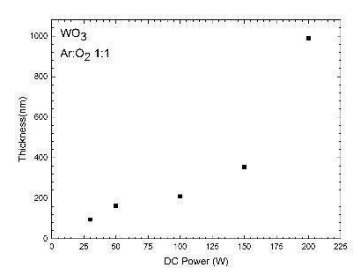


Figure 1. Thickness of the WO_3 film deposited at different DC power.

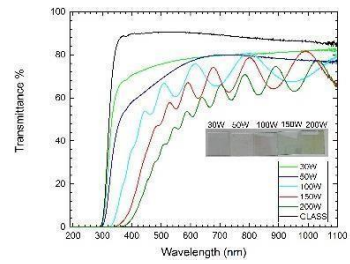


Figure 2. Transmittance spectrum in the UV-Vis region of the WO_3 films.

4. References

- [1] W.J. Ong, L.L. Tan, Y.H. Ng, S.T. Yong, S.P. Chai, Chem. Rev. 116 (2016) 7159–7329.
- [2] Z. Chen, S. Zhang, Y. Liu, N.S. Alharbi, S.O. Rabah, S. Wang, X. Wang, Sci. Total Environ. 731 (2020).

Acknowledgments

We thank Plasmas and Processes (LPP – ITA) for providing the infrastructure used during the execution of the work.

^{*}Corresponding author: leal.rafael@aluno.ifsp.edu.br

STUDY OF THE INFLUENCE OF O₂ FLOW VARIATION ON THE DEPOSITION OF WO₃ FILMS BY THE MAGNETRON SPUTTERING TECHNIQUE

Helen Caroline de Souza Barros^{1,2}, Giovana Fazenda^{1,2}, Rafael da Silva Leal^{1,2}, Marcilene Cristina Gomes², Douglas Marcel Gonçalves Leite¹, Argemiro Soares da Silva Sobrinho¹, André Luís de Jesus Pereira¹

¹ITA – Instituto Tecnológico de Aeronáutica ²IFSP – Instituto Federal de Educação, Ciência e Tecnologia de São Paulo, Câmpus São José dos Campos

1. Introduction

Metal oxides, especially tungsten trioxide (WO₃), are promising materials due to their various applications, such as in catalysis and energy storage. WO₃, an n-type semiconductor, is particularly useful in optoelectronic devices and gas sensors due to its unique properties, including a wide optical band gap[1,2]. Various techniques can be used to develop WO₃ films, with Magnetron Sputtering standing out for its advantages such as high deposition rate and uniformity [2]. The goal of the work is to evaluate how the variation in oxygen flow affects the properties of WO₃ films produced by this technique.

2. Experimental

WO₃ films were deposited on pre-cleaned Si (100) and glass substrates using a dual sputtering technique with a 100 mm tungsten target of 99.9% purity. Mass flow controllers regulated the injection of argon and oxygen gases, and the oxygen flow was varied over a 60-minute deposition to create six different samples. After deposition, the samples underwent thermal treatment at 450°C for two hours to ensure crystallinity, followed by characterization through mechanical profilometry and Raman spectroscopy.

3. Results and Discussions

In order to evaluate the influence of the oxygen flow on the behavior of the bias voltage (V_b) during the deposition process, measurements were taken every five minutes, as illustrated in **Figures 1** and **2**. These measurements reveal that an increase in oxygen flow causes the tungsten target to oxidize, leading to a rise in V_b .

The crystalline phase of the films was assessed by Raman scattering measurements (**Figure 3**). Samples WO₃-0 and WO₃-2 exhibit no defined peaks, suggesting an amorphous structure. In contrast, samples WO₃-4, WO₃-6, WO₃-8, and WO₃-10 display intense and distinct peaks, attributable to the vibrational modes of the monoclinic phase, as indicated in **Figure 3**. This suggests that oxygen flow influences the obtention from an amorphous to a crystalline structure of the material.

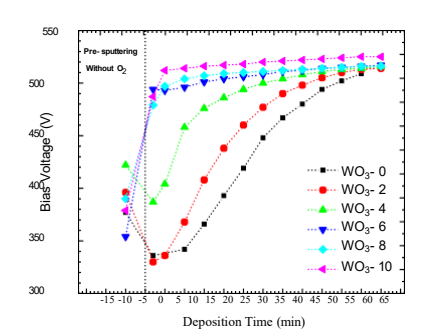


Fig. 1. Evolution of bias voltage during deposition.

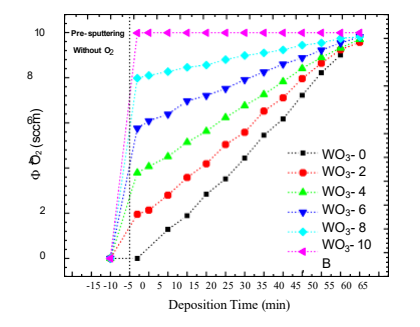


Fig. 2. Evolution of O_2 flow during deposition.

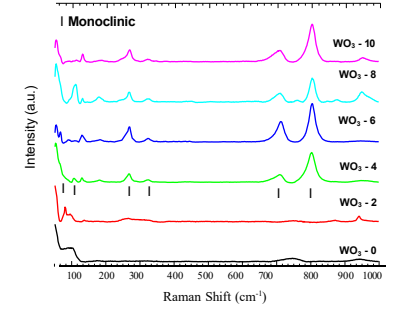


Fig. 3. Raman spectroscopy of the WO_3 samples.

4. References

- [1] M. Modak, S. Rane, S. Jagtap, Bull. Mater. Sci. 46 (2023).
- [2] L. Zhang, J. Guo, B. Hao, H. Ma. Opt. Mater. (Amst). 133 (2022)

Acknowledgments: We thank the CNPq (131920/2023-5). and FAPESP (2022/02994-2, 2022/01901-0, 2023/10449-7) for the financial support. To the ITA and to the whole team of the LPP - ITA for the support.

^{*}Corresponding author: helencssb@gmail.com

STUDY OF THE PHYSICOCHEMICAL PROPERTIES OF BACTERIAL NANOCELLULOSE POLYMERIC FILMS PRODUCED FROM PHYTOTHERAPEUTIC AGENTS.

Brunna Cristina Guimarães Nunes¹; Gustavo Oliveira dos Santos¹; Milena Chanes², Alcides Lopes Leão², André Luiz Reis Rangel³, Ana Paula Rosifini Alves Claro¹

¹São Paulo State University (Unesp), School of Engineering, Guaratinguetá. ²São Paulo State University (Unesp), College of Agricultural Sciences, Botucatu. ³São Paulo State University (Unesp), Material Science Program, Ilha Solteira.

1. Introduction.

As per the World Health Organization, approximately 265,000 deaths occur each year worldwide due to burn injuries. More effective burn wound dressings could be a great instruments for those patients recovery and the bacterial nanocellulose films emerges as an alternative. This biopolymer, produced by *Komagataeibacter xylinus* bacteria, boasts promising attributes for effective treatment, notably its purity, water absorption capacity, and biocompatibility. Moreover, its nanoscale fibers exhibit robust mechanical and tensile strength, facilitating the creation of polymeric films integrated with sources possessing phytotherapeutic benefits, such as aloe vera, extensively employed in burn treatment applications.

2. Experimental.

The polymeric films were produced by the bacteria *Komagataeibacter xylinus*, cultured with a mix of aloe vera (20 to 80%) and alabam. The films were characterized using scanning electron microscopy (SEM), contact angle, water retention, thermogravimetric analysis (TGA), and Fourier-transform infrared spectroscopy (FTIR).

3. Results and Discussions

The wettability assay uncovers hydrophilic tendencies across a range of aloe vera concentrations—specifically at 20%, 40%, and 80%. This hydrophilicity can be attributed to the presence of surface hydroxyls, a fact confirmed by FTIR analysis, and holds the potential to foster cell growth. Thermal analysis points to a distinct pattern, encompassing water loss at approximately 100°C, followed by cellulose degradation. Notably, the 80% aloe vera concentration group exhibits the least significant thermal degradation. The microstructure analysis reveals insights into fiber arrangement, and the potential encapsulation of bacteria

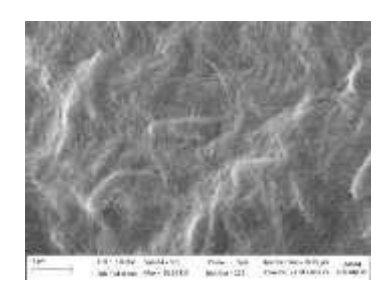


Fig. 1. SEM images performed on the polymeric films

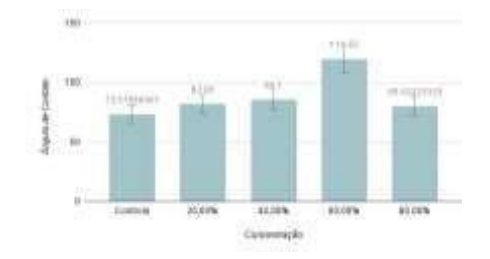


Fig. 2. Wettability results

4. References.

[1] BHATIA, A., O'BRIEN, K., CHEN, M., et al., "Dual therapeutic functions of F-5 fragment in burn wounds: preventing wound progression and promoting wound healing in pigs", **Molecular Therapy - Methods & Clinical Development**, pp. 1 - 11, Jun. 2016.

[2] DAI, T., HUANG, Y., SHARMA, S.K., et al., "Topical Antimicrobials for Burn Wound Infections" **Recent Pat Antiinfect Drug Discov**, v. 5, n. 2, pp. 124-151, Jun. 2010.

[3] LOPES, R. de. Funcionalização de celulose bacteriana com peptídeo RGD para reparação tecidual da pele. 2015. 106f. Dissertação (Mestrado em Biotecnologia) - Instituto de Química de Araraquara, Universidade Estadual Paulista, Araraquara, 2015.

Acknowledgments.

The authors would like to thank Prof. Edson Cocchieri Botelho research group for the thermal analysis.

^{*}Corresponding author: André Luiz Reis Rangel, al.rangel@unesp.br

STUDY OF THE PROPERTIES OF DLC THIN FILMS DEPOSITED IN TI-6AL-4V BY THE PIII&D TECHNIQUE INSIDE TITANIUM TUBES OF DIFFERENT DIMENSIONS

Beiker M. Rueda^{1*}, Mário Ueda ² and Nazir M. Santos²

¹ Federal University of Santa Catarina (UFSC), Florianopolis, SC, Brazil ²National Institute for Space Research (INPE), São José dos Campos, SP, Brazil

1. Introduction

Surface treatments of metallic biomaterials are a simpler, more cost-effective, and more technologically efficient option for increasing wear resistance, which increases device life by minimizing the release of wear debris and corrosion. To improve the properties of these materials and study their structural characteristics, Diamond-Like Carbon (DLC) thin films were deposited on Ti-6Al-4V titanium alloy samples (biomaterial) by the Plasma Immersion Ion Implantation and Deposition (PIII&D) system using methane and hydrogen plasmas. The properties of the deposited films generally depend on the deposition conditions, which determine their microstructure, mainly the respective proportions of sp³ and sp² carbon, therefore in this work was analyzed the structure of the DLC thin films by Raman Spectroscopy, scanning electron microscopy (SEM) and X-rayDiffraction (XRD).

2. Experimental

The PIII&D reactor used consists of a cylindrical stainless-steel chamber with an internal volume of 20 liters, a gas system with flow controllers, a high voltage pulser with a maximum capacity of 17KV, a mechanical pump that reaches up to 10^{-1} mbar (manometric pressure) inside the reactor, a diffusion pump that reaches a vacuum in the order of $4x10^{-5}$ mbar. For the deposition process, the samples were fixed inside of two titanium tubes (sample holders) with a length of 150mm, a thickness of 2mm and external diameters of 11mm and 40 mmeach, with one end closed and introduced inside the reactor. The tubes were cleaned in argon plasma for 10 min (2.5kV, 12A, $20\mu s$, 500Hz). The films were produced using a gas mixture of methane (organic precursor) and hydrogen, by driving Hollow Cathode (HC) discharges inside the tube attached to the top part of the chamber for 120 minutes (6.12kV, 16A, $20\mu s$, 500Hz) in each tube, maintaining the same deposition parameters. The properties of the films were studied considering two positions of the samples at the ends inside the tubes (positions#1 and #7) and the interference of the tube diameter on the deposition results.

3. Results and Discussions

In the films synthesized in the 40mm diameter tube, the SEM results showed a morphology with discontinuities and agglomerations, the Raman spectra exhibited bands of the vibrational mode of titanium carbide (TiC) and the C-H bond in the amorphous carbon phase, agreeing with what was obtained in XRD. In the films synthesized in the 11mm diameter tube, the results showed a good appearance of morphology and adhesion to the substrate, the XRD showed a greater contribution of TiC in the film at position #1, agreeing with the bands shownin Raman spectroscopy. In the diffractograms of the sample at position #7, a range of peaks is observed that may include graphite, diamond, and amorphous carbon, agreeing with Raman spectroscopy that showed two (D and G) bands in the DLC films. The diameter of the tubes and the position of the samples interfered with the results, which is evident the obtaining of specific microstructures for each tube.

4. References

- [1] S.F.M. Mariano, M. Ueda, R.M. Oliveira, E.J.D.M. Pillaca, N.M. Santos, Magnetic-field enhanced plasma immersion ion implantation and deposition (PIII&D) of diamond-like carbon films inside tubes. Surface & Coatings Technology. **312**, 47-54, (2017).
- [2] N. M Santos, S. F. M. Mariano, M. Ueda, Carbon films deposition as protective coating of titanium alloy tube using PIII&D system. Surface & Coatings Technology, **375**, 164-170, (2019).
- [3] J. Robertson, Diamond-like amorphous carbon, Materials Science and Engineering, 37, 129-281, (2002).

Acknowledgements

This study was financed in part by the Coordenação de Aperfeiçoamento de Pessoal de Nível Superior – Brasil (CAPES) – Finance Code 001.

^{*} Corresponding author: b.m.rueda@posgrad.ufsc.br

SURFACE FUNCTIONALIZATION OF TI15ZR15MO ALLOY - INCORPORATION OF NANOPARTICLES

Reginaldo T. Konatu, Carlos Roberto Grandini, Ana Paula Rosifini Alves Claro

¹São Paulo State University, School of Engineering and Sciences, Guaratinguetá Campus, Sao Paulo, SP, Brazil

²São Paulo State University, School of Sciences, Bauru Campus, Sao Paulo, SP, Brazil

1. Introduction

The selection of a biomaterial to replace a specific function in the human body depends on its volume and surface properties. Among the metallic materials used, titanium and its alloys stand out for their volumetric properties, whichmake them suitable for replacing hard tissues. Surface modification techniques can be used to enhance theresponse of these materials in terms of cell adhesion and proliferation of specific cells. Among these techniques, anodic oxidation stands out because it utilizes simpler and cheaper equipment and reagents, while also providing better control over the morphology of the formed structure. By studying the process parameters, it is possible to form various structures, ranging from porous layers [1] to ordered nanotubes. The formation of these structures depends on factors such as the composition of the material, potential, electrolyte, and other parameters, which will vary according to the alloy composition [2-5]. Despite the bactericidal activities attributed to TiO2 nanotubes in the literature, incorporating drugs and applying bactericidal coatings to these surfaces may be more effective in combating the adhesion and proliferation of bacteria [6]. The use of oxide nanoparticles is an alternative to using drugs, as it provides the material with bactericidal properties. Some metallic oxides have been studied for application and among them, zinc oxide (ZnO) is one of the alternatives, which is already used in medicines and has bactericidal and non-toxic characteristics. Using the layer-by-layer (LBL) technique, it is possible to combine different materials, thereby leveraging their unique properties. The combination of chitosan and hyaluronic acid has already been used as a bactericidal film, as it combines the antimicrobial properties of chitosan and the surface formed by hyaluronic acid, as well as being non-toxic [7]. In this way, it is possible to obtain a thin film composite consisting of multiple layers of hyaluronic acid, chitosan, and intercalated ZnO particles. The aim of this study was to deposit a polymeric film made up of polyethyleneimine (PEI), hyaluronicacid (HA), and chitosan (CHI) with ZnO nanoparticles by dip coating (LBL) after anodic oxidation on the surface of the Ti15Zr15Mo alloy.

2. Experimental

The processing and anodization of the Ti15Zr15Mo alloy were carried out according to our previous studies [8]. Briefly, ingots were obtained from an arc melting furnace and cold forged using a rotary swage. Samples were anodized in an electrolyte prepared by mixing water, glycerol (50% v/v), and ammonium fluoride (NH4F) at a concentration of 2.7 g/L. The anodization process was carried out at a voltage of 30 V, with a voltage rate of 2 V/min, for a duration of 24 hours. After the anodization, all samples were annealed at 450 °C for 1 hour to stabilize the crystalline phase. After the anodic oxidation of the alloy, polymeric films such as polyethyleneimine (PEI), hyaluronic acid (HA), chitosan (CHI), and LBL (layer by layer) were deposited using the dip coating technique. The surfaces of the samples were characterized using scanning electron microscopy (NovaNano). The contact angle was evaluated using the sessile drop method, with drops of 1 μ L of deionized water, using a Ramé- Hart 300-F1 goniometer. In vitro studies were conducted to evaluate the adhesion and bacterial proliferation of Staphylococcus aureus on the samples.

3. Results and discussion

The use of bilayers of hyaluronic acid and chitosan as a method of incorporating ZnO nanoparticles was found to be effective. Although the ZnO particles were detected in low concentrations, they were present on the coated samples (Fig. 1). In light of the results obtained from scanning electron microscopy, contact angle measurements, and surface energy analysis, the condition with two bi-layers was selected. This condition exhibited partial coating of the nanotubes (with no complete closure), incorporation of the particles, and demonstrated low wettability. The study investigated bacterial adhesion using the bacterium Staphylococcus aureus on samples under various conditions. These conditions included: untreated alloy, alloy with nanotube formation, and samples coated with two bi-layers of hyaluronic acid, chitosan, and ZnO nanoparticles at concentrations of 1 mM, 3 mM, and 5 mM. The studies led to the conclusion that the conditions examined in this research did not exhibit any significant difference in bactericidal properties. Further study is needed on the film formation parameters and the incorporation of nanoparticles.

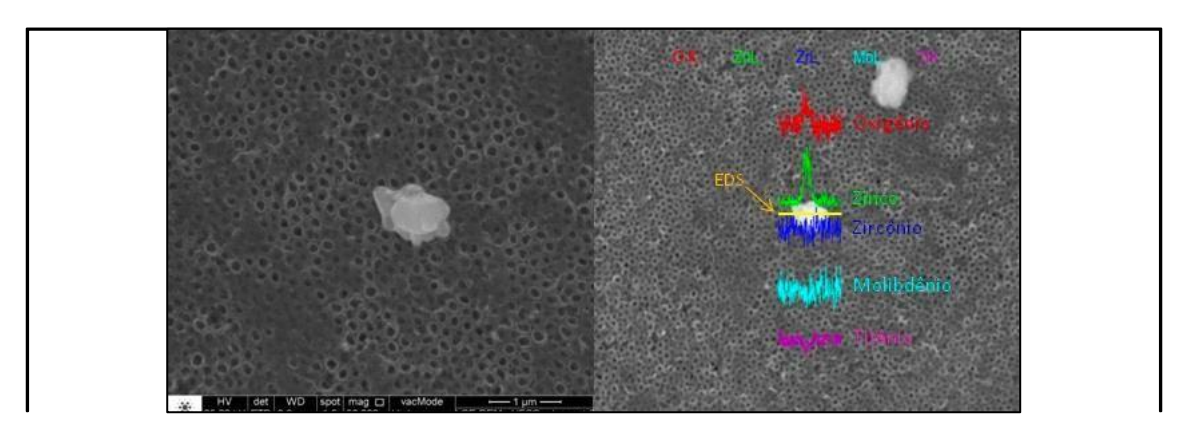


Fig. 1 - Micrograph of the surface of the Ti15Mo15Zr alloy after anodic oxidation and deposition of the LBL polymers [HA/CHI/ZnO]. a) image of the particle, b) analysis of the chemical composition by EDS of the particle, identifying the intensity of each element present on the surface of the nanotube

3. References

- [1] Carobolante, J. P. A., da Silva, K. B., Chaves, J. A. M., Netipanyj, M. F. D., Popat, K. C., & Claro, A. P. R.A. (2020). Surf. & Coat. Tech, **386**, 125467.
- [2] do Amaral Escada, Ana Lucia, Javier Andres Muñoz Chaves, and Ana Paula Rosifini Alves Claro. Materials Science Forum. Vol. 869. Trans Tech Publications Ltd, (2016)
- [3] Capellato, P., Sachs, D., Vasconcelos, L. V., Melo, M. M., Silva, G., Ranieri, M. GClaro, A. P.A. Metals, 10(8), 1059, (2020).
- [4] Chaves, J. M.; Esacada A. L. A.; Rodrigues, A. D.; Alves Claro, A. P. R. **Applied Surf. Science**, v. 370, p. 76–82, (2016)
- [5] Rangel, A. L., Chaves, J. A., Escada, A. L., Konatu, R. T., Popat, K. C., & Alves Claro, A. P. R. Journal of Applied Biomaterials & Functional Materials, 16(4), 222-229 (2018).
- [6] Sirelkhatim, A., Mahmud, S., Seeni, A., Kaus, N. H. M., Ann, L. C., Bakhori, S. K. M, Mohamad, D. Nanomicro letters, 7, 219-242. (2015)
- [7] Hernandez-Montelongo, J., Lucchesi, E. G., Gonzalez, I., Macedo, W. A. D. A., Nascimento, V. F., Moraes, A. M., ... & Cotta, M. Colloids and Surfaces B: Biointerfaces, 141, 499-506.(2016).
- [8] Konatu, R. T., Domingues, D. D., Escada, A. L. A., Chaves, J. A. M., Netipanyj, M. F. D., Nakazato, R. Z., ... & Claro, *Surfaces and Interfaces*, 26, 101439. . (2021).

 $[\]hbox{*Corresponding author: paula.rosifini@unesp.br}$

TEMPORAL EVOLUTION OF SPATIAL DISTRIBUTION OF HYDROGEN AT TCABR-UPGRADE

João Vitor Araya Kobayashi de Sousa^{1*}, Francisco Tadeu Degasperi², Gustavo Paganini Canal³, Juan Iraburu Elizondo⁴

^{1,3,4}Instituto de Física – Universidade de São Paulo ²Faculdade de Tecnologia - FATEC-São Paulo

1. Introduction

For a long time, the Plasma Physics Study in Brazil had the TCABR, a Tokamak at Plasma Physics Laboratory of the Institute of Physics at the Universidade de São Paulo. In need to elevate Brazil to innovation, the TCABR will upgrade, in direction to improve the plasma study. For this upgrade, it demands simulations and calculations. An important part of this upgrade is the vacuum chamber. Understanding the behavior of the gas in temporal evolution in a vacuum system motivates an analysis of the spatial distribution of hydrogen during the process of plasma synthesis.

2. Experimental:

The challenge is the residual gas inside the chamber, which can change the plasma properties. To avoid this problem, the chamber demands a vacuum system. With the difference of the pressure it would be able to maintain the chamber approximately without this residual gas. To build the analysis, the MolFlow developed for simulations with geometries in High-Vacuum Systems would be used to analyze the vacuum chamber and the special distribution of hydrogen. A theoretical model would be constructed to compare the results of the simulation. Having the theoretical model, it would be possible to analyze the results with a toroidal geometry. MolFlow Software's analysis method is the Monte Carlo Method.

3. Results and Discussions

At this moment, the project is concentrated in the improvement of the stationary regime in simple geometries, trying to start the analyses in the transitory regime. The theoretical model. As the simulation is concentrated in simpler systems, however it is important to emphasize that the theoretical model is being constructed using the model results clearly.

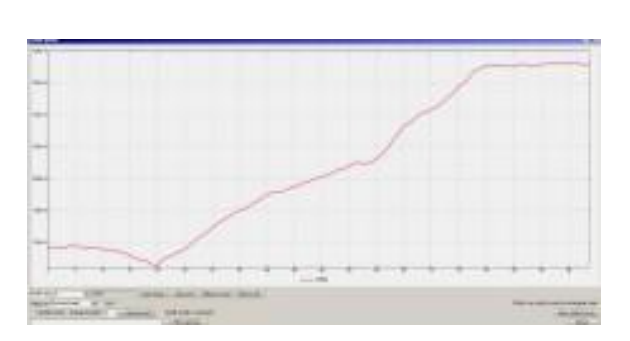


Fig. 1. Vacuum system analyses of pressure distribution, based on the work of J.Howell and B. Wehrle.

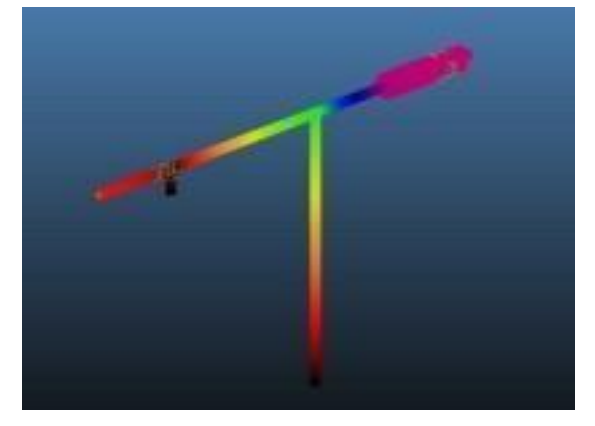


Fig. 2. Graphic of Pressure made by the student with the Monte Carlo Method in the MolFlow.

4. References

[1] A. Roth "Vacuum Technology", 3rd edition, Elsevier Science B.V., Netherlands (1990)

[2] M. ADY, R. KERSEVAN, MolFlow+ User Guide, France (2014)

^{*}Corresponding author: jvaks_345@usp.br

THERMAL PLASMA APPLICATION FOR METHANE REFORMING

Alexei M. Essiptchouk^{1,2*}, Felipe de Souza Miranda², Marcelo P. Gomes², Gilberto Petraconi Filho²

¹Department of Environment Engineering, Institute of Science & Technology, São Paulo State University, UNESP, São José dos Campos, Brazil

1. Introduction

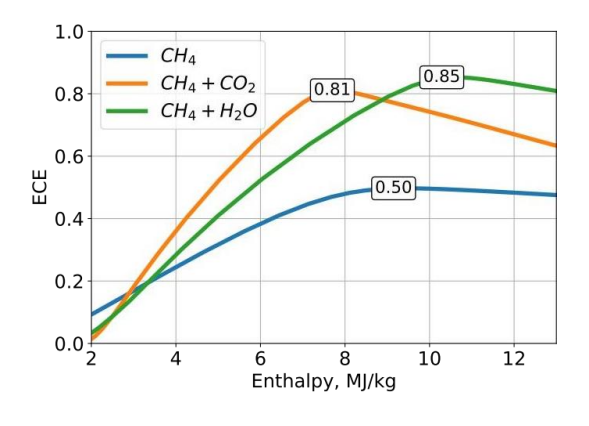
Methane (CH4) is a simple organic compound with high hydrogen content among hydrocarbons, and its reforming has gained significant attention from both industrial and research communities due to the possibility of converting it into more energy-dense fuels or high-value chemicals [1]. Compared to non-thermal plasma, thermal plasma offers several advantages, including high temperature, high enthalpy, high energy density, and high chemical reactivity, making it a more suitable option for certain chemical reactions [2]. This work evaluates the potential of thermal plasma technology to produce clean hydrogen from methane.

2. Theory

A comparative analysis of the three cases of methane processing (pyrolysis, dry reforming, and steam reforming) was carried out, applying a thermodynamic equilibrium model. The chemical composition of the system was evaluated seeking the maximum entropy under the assumption of thermodynamic equilibrium. One of the dimensionless key characteristics is Energy Conversion Efficiency (ECE) was defined as the useful energy output (carried by the outgoing gases) divided by the energy input (chemical energy contained in initial CH4 and energy spent by plasma torch). ECE indicates how much of the LHV of the raw material was converted to thermal energy contained in the CO and H2 mixture, taking into account the energy required to maintain the system at a specific temperature.

3. Results and Discussions

In comparing CO2 and H2O as compounds for CH4 reform, it can be concluded that the use of H2O requires a lower energy consuming (88 kJ mol⁻¹) than CO2, which requires 116 kJ mol⁻¹. Although the ECE values for all cases are very similar, the highest efficiency was achieved using water vapor (0.85) compared to CO2 (0.81). At temperatures above 1200K (~10 MJ/kg) the concentrations of principal products, CO and H2, reach their maximum values: 73%vol of H2 and 25%vol of CO.



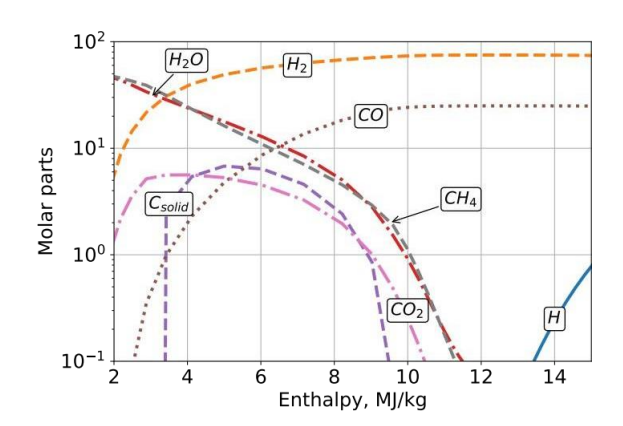


Fig. 1. Energy conversion efficiency, ECE, in function of enthalpy of the system.

Fig. 2. Equilibrium composition of gases (in %vol) forsteam methane reforming as a function of enthalpy.

4. References

[1] Bilera IV, Lebedev YA. Petroleum Chemistry. 62, 4, (2022)

[2] Y. Vadikkeettil et al. Renewable and Sustainable Energy Reviews, 161, 112343, (2022)

Acknowledgments: We would like to thank the São Paulo Research Foundation (FAPESP) for financial support: 2022/00271-3.

²Plasma and Processes Laboratory, Technological Institute of Aeronautics, São José dos Campos, SP, Brazil

^{*}Corresponding author: alexei.essiptchouk@unesp.br

THERMAL STUDY OF Fe₃O₄ MAGNETIC NANOFLUIDS USING TWO PHOTOTHERMAL TECHNIQUES FORBIOMEDICAL APPLICATIONS

Usiel O. García-Vidal¹, Jose L. Jiménez-Pérez¹, Zormy N. Correa-Pacheco², Mauricio A. Algatti^{3*}

¹Unidad Profesional en Ingeniería y Tecnologías Avanzadas, IPN. Avenida Instituto Politécnico Nacional No. 2580, Col Barrio la Laguna Ticomán, Gustavo A. Madero, México City, C.P. 07340, México. ²Centro de Desarrollo de Productos Bióticos, IPN. Carretera Yautepec-Jojutla, Km. 6, calle CEPROBI No. 8, Col. San Isidro, C.P. 62731, Yautepec, Morelos, Mexico. ³Faculdade de Engenharia e Ciências, UNESP-Campus de Guaratinguetá, Av. Ariberto P. Cunha

333,12516-410 Guaratinguetá, SP, Brazil

1. Introduction

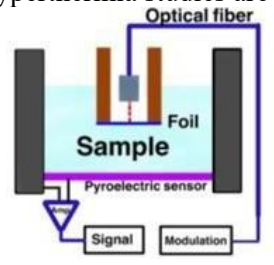
The thermal characterization of magnetic nanofluids is of key importance for its application on magnetic hyperthermia in cancer therapy. Therefore the accurate measurements of thermal diffusivity for different nanoparticles concentrations in aqueous solutions is essential for tailoring the use of magnetic nanofluids in cancer hyperthermia. To reach this goal this paper deals with the use of two photothermal techniques, i.e.; thermal lens spectroscopy (TLS) and thermal wave resonant cavity photopyroelectric spectroscopy (TWRC-PPE) for measuring the thermal diffusivity of magnetic Fe₃O₄ nanofluids with concentrations ranging from 0.01 mg/ml to 1 mg/ml.

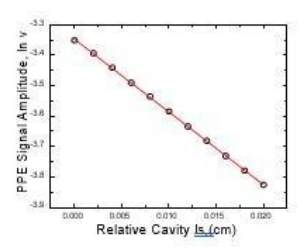
2. Experimental

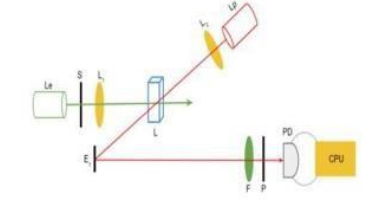
Thermal diffusivity of Fe₃O₄ nanofluids were measured using the experimental TWRC technique with a pyroelectric sensor. The experimental setup is shown in figure 1 (right). A modulated laser beam (660 nm 40 mW power) at a fixed frequency of f=0.25 Hz, is guided into a cylindrical cavity of stainless-steel (2 cm length, diameter of 10 mm and 50 um thick) with one end covered by an Al foil. The Al foil heated by laser radiation acts as a heat source for the nanofluid sample. The heat generated in the sample diffuses through the liquid medium and reach the pyroelectric sensor (PZT of 50 microns) that generates a signal that is sent to apreamplifier and then to a second lock-in amplifier (model SR810 DSP). The signal amplitude and phase are measured as a function of the length L. Thermal lens setup is shown in figure 2 (right). An Ar⁺Xe laser creates the thermal lens that is probed by a HeNe laser. One of the TL results is shown in figure 2 (left).

3. Results and Discussions

Both techniques gave quite similar results. These techniques are widely applied to measure the thermal properties of various kinds of nanoliquids. Among the advantages of the TWRC technique, all types of transparent and opaque samples with different thicknesses, thermally thin and thick can be measured. The experimental results showed that the semitransparent Fe₃O₄ nanoliquid samples have a linear behavior for low concentrations and for samples with higher concentrations (or thermally thick and opaque) the thermal lens signal is completely attenuated, making difficult to obtain a reliable TL signals. The TWRC technique is useful for substances with strong absorbance and higher concentrations, non-transparent and with different thicknesses. On the other hand, the TLS technique is useful when you need versatility and speed for semi-transparent samples. Finally, both techniques can undoubtedly be very useful for different nanoliquids such as Fe₃O₄ for medical applications where hyperthermia studies are required.







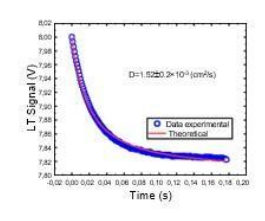


Fig. 1- Experimental setup for TWRC thermal diffusivity measurements (left) and the PPE signal amplitude versus relative cavity length (right)

Fig. 2- Experimental setup for TL thermal diffusivity measurements (left) and the TL signal amplitude versus time (right)

4. References

- [1]- V. R. Khabibullin, L. O. Usoltseva, I. V. Mikheev, M. A. Proskurnin, Nanomaterials, 13, 1006, (2023).
- [2]- E. Shahriari, M. G. Varnamkhasti, R. Zamiri, Optik, 126, 2104-2107, (2015).
- [3]- V. R. Khabibullin, M. Franko, M. A. Proskurnin, Nanomaterials, 13, 430, (2023).

^{*}Corresponding author: mauricio.algatti@unesp.br

THERMAL TREATMENT OF DAIRY SLUDGE BY DC-TRANSFERRED ARC PLASMADISCHARGE

Pedro William Paiva Moreira Júnior¹*, Felipe de Souza Miranda² Gilberto Petraconi Filho¹

¹Instituto Tecnológico de Aeronáutica ²Universidade Estadual Paulista

1. Introduction

The dairy industry's growth has led to increased wastewater and dairy sludge production, which poses disposal challenges [1]. Due to dairy sludge composition, including minerals, solids, and organic matter like fats and proteins, the traditional disposal methods, including land spreading and anaerobic digestion, have faced limitations like environmental contamination and oversupply [2]. Thermal plasma treatment, especially DC-transferred are plasma, offers a solution due to its ability to handle diverse waste streams, making them ideal for the treatment of complex materials like dairy sludge. This study examines dairy sludge, exploring thermal processing and DC plasma treatment. The goal is to transform dairy sludge into valuable products, understanding the temperature's role in degradation. This study's findings offer sustainable solutions for dairy waste management, reducing environmental impact.

2. Experimental

Dairy sludge was subjected to various tests to understand its composition and thermal degradation processes. For material characterizations, the techniques of X-ray fluorescence spectroscopy (XRF), Proximate and Ultimate analyses, Thermogravimetric (TGA) and Differential Scanning Calorimetry (DSC), X-ray diffraction (XRD) and Fourier-transform infrared spectroscopy (FTIR) were applied. Conventional thermal treatment, i.e. pyrolysis, was carried out in a muffle furnace. A specifically designed DC-transferred are plasma reactor, equipped with graphite and carbon-composite electrodes, was used for plasma gasification.

3. Results and Discussions

The dairy sludge is characterized by a high volatile matter and ash content, with primary elements such as Al, P, Si, Ca, and Fe. The sludge shows significant mass and volume reductions before 600 °C pyrolysis temperature, a phenomenon further intensified during plasma gasification. TGA and DSC highlight the degradation of primary milk components like lactose, casein protein and fat. XRD analysis of sludge reveals broad diffusions at lower scattering angles, attributed to polymorph silicon, phosphorus and calcium compounds. As pyrolysis temperature approaches 1000°C, this broad diffusion vanishes, followed by the detection of crystalline structures like silicon dioxide, calcium silicon, dicalcium silicate and hydroxylapatite. Plasma gasified sludge features various oxide crystalline structures, Al₂O₃, CaO(Al₂O₃)₆, CaO(Al₂O₃)₂, Ca₂Al(AlSi)O₇, KFeO₂ and ZrO_{1.98}. FTIR analysis of sludge identifies a complex organic composition presenting alkanes, amines, amides and hydroxyl groups along with a fingerprint region populated by metallic and semi-metallic oxide bonds absorption. As pyrolysis temperature rises, these absorptions' relative intensity undergoes modifications, with integrated absorption results suggesting degradation of organic compounds and an increase in phosphorous and aluminum bonds, regarding silicon bonds content, especially after 600 °C. The vitreous slag from plasma gasification exhibits distinct composition characteristics based on absorptions observed, highlighting the potential of dairy sludge plasma treatment. As a result of the rapid heating during plasma discharge, the slag is in the absence of any organic bond, presenting a vitreous and metallic/ceramic matrix. The FTIR spectra of this slag are restricted to the fingerprint region, indicating the presence of phosphorous, aluminum, calcium, iron and silicon oxide bonds, reflecting the complex crystalline matrix formation during plasma gasification.

4. References

- [1] M. Kwapinska, A. Horvat, Y. Liu, J.J. Leahy, Waste and Biomass Valorization 11 (2020) 2887–2903.
- [2] A. Horvat, M. Kwapinska, J.J. Leahy, Energy Procedia 161 (2019) 66–74.

Acknowledgments

We acknowledged the financial support of the São Paulo Research Foundation (FAPESP), grants 2023/02273-6 and 2022/03522-7.

^{*}Corresponding author: pedro_kcond28@hotmail.com

TIME-RESOLVED DETECTION OF DIFFERENT SPECIES IN A CONICAL APPJ BY AN ICCD CAMERA

Felipe V.P. Kodaira^{1*}, Konstantin G. Kostov¹, Éric Robert²

¹School of Engineering, São Paulo State University (UNESP), Guaratinguetá 12516-410, SP, Brazil ²GREMI, UMR7344, CNRS/Université d'Orléans, Orléans, France

1. Introduction

Atmospheric pressure plasma jets (APPJ) are widely used to treat different materials, biological tissues, and surface sterilization. Several characteristics of plasma are interesting for such applications; various species are generated within it, such as ions, energetic electrons, radicals, UV radiation, among others. The generation of such species strongly depends on the parameters used for plasma generation, such as voltage, flow, gas composition, and system geometry. Since it's a customizable process, it ends up being very versatile. To better tailor the discharge for specific applications, it's necessary to understand how certain parameters influence the discharge. This work focuses on detecting the regions where active NO and N2 species are formed in the discharge of a conical Atmospheric Pressure Plasma Jet (APPJ) fueled by Argon gas (2SLM) and a pulsed power source with positive 9kV pulses at 500 Hz. The images were captured by a high-speed ICCD camera synchronized with the voltage signal sent by the plasma power source, to filter the light of different species, specific filters for the wavelength at which such species emit were used (NO at 236nm and N2 at 337nm). The images (250 frames) were obtained with a 20 ns interval over a voltage pulse lasting 5.4 µs. In Fig.1(a), the sum of the highest light intensity across all 250 frames is observed for NO (top), N2 (middle), and without a filter (bottom). In Fig. 1(b), it's possible to observe the signal intensity over time for each case. It can be seen that very little NO is generated in comparison to the total discharge, and it's generated only at the beginning of the discharge, while for N2 and for the images without a filter, the signal is more intense, and the generation of species is observed at two moments within the same pulse.

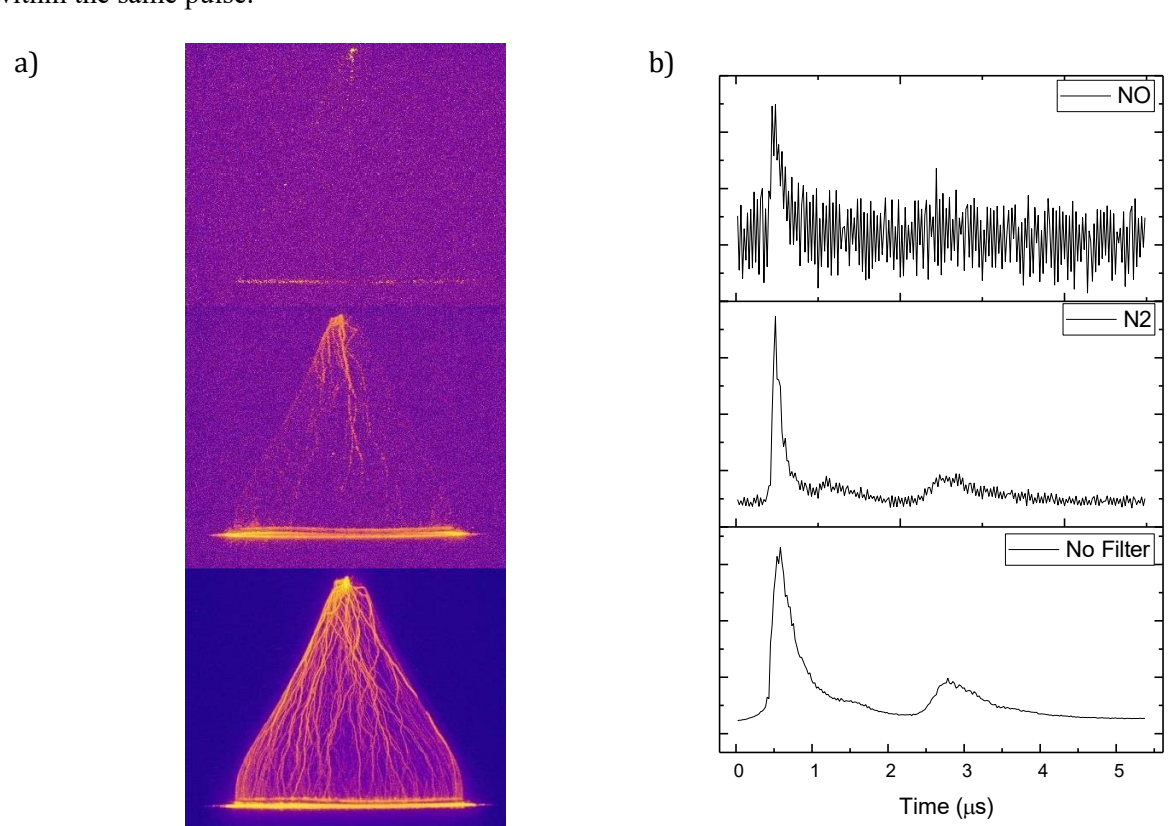


Fig.1 (a) sum of the highest light intensity across all 250 frames is observed for NO (top), N2 (middle), and without a filter (bottom); (b) the light intensity over time for each case.

^{*}Corresponding author: Kodaira.felipe@gmail.com

TITANIUM-TANTALUM ALLOYS OBTAINED BY LASER DEPOSITION FOR BIOMEDICAL APPLICATIONS

Odila Florêncio^{1*}, Romualdo Emílio^{1,2}, Rui Vilar³ and Amélia Almeida³

¹Universidade Federal de São Carlos, CEP 18052-780, Sorocaba-SP, Br ²Centro Paula Souza – ETEC Fernando Prestes, CEP 18040-810, Sorocaba-SP, Br ³Instituto Superior Técnico, Universidade de Lisboa, 1049-001, Lisboa, Pt

1. Introduction

Metallic materials for biomedical applications should have good biocompatibility, wear and corrosion resistance, suitable levels of stiffness, strength, fracture toughness, fatigue resistance and low elastic modulus [1]. Ti alloys are among the most used metallic biomaterials and can be found in the α , β or dual $\alpha+\beta$ phases. Asthe concentration of β -stabilizing is increased the β phase becomes dominant, and the martensitic structure α' (acicular martensite) tends to be replaced by α'' (orthorhombic martensite), the α'' phase being considered a transition from the α' to the β phase [2].

2. Experimental

Ti-Ta alloys with variable composition were synthesized by laser-assisted deposition. Laser treatment was done by feeding CP Ti and Ta powders with variable feed rates through a coaxial nozzle into a laser beam directed to the substrate. The compositions of Ti and Ta varied almost linearly along the distance, with compositions ranging from 3 to 86 wt% Ta. The composition and microstructure of the alloys were characterized by XRD and SEM, while the mechanical properties were assessed using depth-sensing ultramicroindentation tests.

3. Results and Discussion

Fig. 1 shows the dependence of ultramicrohardness, for Ti-Ta alloys, as a function of Ta composition and the corresponding microstructure. The Young's modulus decreases from 120 GPa to about 45 GPa with increasing the Ta content to 35 wt.%, corresponding to the region where the α " (orthorhombic) phase is predominant. The lowest value of Young's modulus (45 GPa) was obtained for the Ti-36wt.%Ta alloy, that has a ultramicrohardness of 2.3 GPa. Fig. 2 presents the microstructure of the Ti-36Ta alloy showing a very fine grain structure with predominance of the α " phase and a low content of β . Based on these results, samples of the Ti-40Ta alloy was produced by laser deposition, 8 layers high and 30 mm long, which will be characterized by continuing the survey of alloys with potential use as an orthopedic biomaterial.

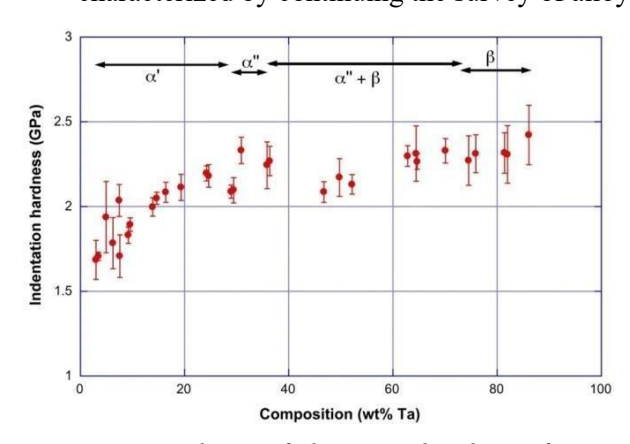


Fig. 1. Dependence of ultramicrohardness, for Ti-Ta alloys, as a function of Ta composition and corresponding phases.

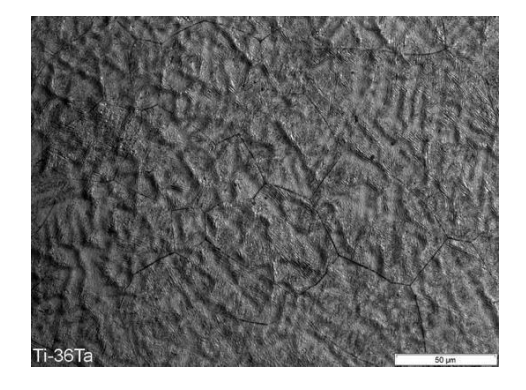


Fig. 2. Microstructure of Ti-36Ta alloy showing the predominance of the α'' phase (orthorhombic martensite) and a low content of β phase.

4. References

[1]- M. Niinomi, Mater. Sci. Eng. A. 483-484, 153 (2008).

[2]-G. Lütjering and J. C. Williams "Titanium", 1st edition, Springer, USA, (2003).

Acknowledgments: FAPESP (2011/20151-8 and 2022/04825-3)/Br, FCT (PTDC/CTM/09811/2008)/Pt.

^{*}Corresponding author: odila@df.ufscar.br

TRATAMENTO DE AMOSTRAS POLIMÉRICAS COM UM JATO DE PLASMA CÔNICO EM PRESSÃO ATMOSFÉRICA

Thayná F. Tavares*, Felipe V.P. Kodaira, Konstantin G. Kostov.

UNESP - Faculdade de Engenharia e Ciências - Campus Guaratinguetá

1. Introdução

O tratamento a plasma é comumente usado para modificar propriedades superficiais de polímeros [1]. Nesse trabalho usamos amostras de polietileno de alta densidade (HDPE). Através do tratamento a plasma, os polímeros podem ter propriedades superficiais modificadas, porém mantendo as do seu volume. O plasma usado nos tratamentos é capaz de mudar a estrutura molecular e até mesmo incorporar novos grupos funcionais na superficie do polímero; essas modificações criam mudanças em propriedades tais como molhabilidade, adesão e biocompatibilidade [2].

2. Experimental

O tratamento a plasma gerado em argônio foi aplicado na parte superior (up) das amostras de HDPE por 5 minutos cada, variando as distâncias do bocal do funil até a amostra em 3 mm, 5 mm e 8 mm, sendo assim possível analisar se há influência desta distância no tratamento. A fonte usada foi AC MINIPULS-6 acoplada a um gerador de funções a 25 kHz em modo burst com 12 ciclos e período de 2 ms. O gás de trabalho foi o argônio com 4L/ de vazão.

3. Resultados e Discussões

Analisando o centro das amostras em relação as bordas, nota-se uma diferença de ângulo de contato de até 60°, isso devido ao tamanho do bocal (75mm de diâmetro) sendo menor que as amostras poliméricas (100mm de comprimento) assim concentrando maior intensidade de tratamento nas partes onde as amostras ficam no limite da circunferência do jato. Contudo, existe também uma diferença entre as faces superiores e inferiores ao tratamento. Uma possível explicação é o polímero se comportar como como um dielétrico formando uma espécie de reator secundário de descarga DBD formado entre a face inferior e a base.

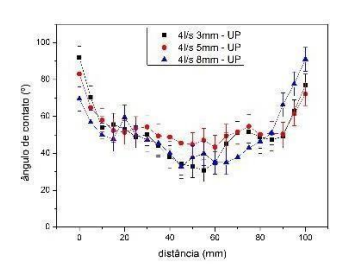


Fig. 1. Amostras de HDPE, parte superior medidas com as distâncias 3mm, 5mm e 8mm com fluxo de 4L/s.

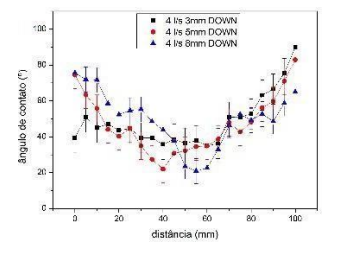


Fig. 2. Amostras de HDPE, parte inferior medidas com as distâncias 3mm, 5mm e 8mm com fluxo de 4L/s.

4. Referências

[1] R. Morent, Comparison between XPS- and FTIR-analysis of plasmatreated poly-propylene film surfaces, $2008\,$

[2] LAI, J., Non-linear Time-dependent Deformation Behaviour of High Density Polyethylene The Netherlands, Delft University of Technology, 1995.

[3] Kodaira, F.V.d.P.; Almeida, A.C.d.P.L.; Tavares, T.F.; Quade, A.; Hein, L.R.d.O.; Kostov, K.G. Study of a Conical Plasma Jet with a Cloth-Covered Nozzle for Polymer

Agradecimentos

Agradeço a CNPq pelo financiamento do projeto.

TREATMENT OF COMMERCIAL FABRIC WITH A CONICAL-SHAPED ATMOSPHERIC PRESSURE PLASMA JET

Bruno Henrique da Silva Leal*, Felipe Vicente de Paula Kodaira, Konstantin Georgiev Kostov

São Paulo State University (UNESP), Guaratinguetá, São Paulo.

1. Introduction

The textile industry is one of the largest and most developed industries in the world, requiring constant updates and modernizations in various processes [1]. One of the common and widespread practices in the industry is starching fabrics [2], which improves their resistance to friction and prevents unraveling of the textile structure. However, starch coating reduces the wettability of the textile fiber, making it difficult for subsequent finishing processes, such as painting. Typically, after the coating process, fabrics undergo further treatment to improve their wettability, aiding in the finishing processes of the textile production line [3].

The study aimed to investigate the effect of atmospheric plasma generated by a conical-shaped atmospheric pressure plasma jet. Cotton (CO) and polyester (PES), the two most commonly used textile materials, were used to create fibers, with both fabrics constructed using the Oxford method and distinct compositions. The first fabric was made entirely of cotton, and the second was a blend of 33% cotton and 67% polyester.

2. Experimental

The funnel-shaped jet was electrically characterized by its current and charge carried. Using the Lissajous figure technique, the power of the treatment was obtained, which enabled the energy dose of each treatment to be obtained.

To analyze the physical and chemical changes caused by the treatment, several surface characterization methods were used, including the vertical wicking test, Fourier-transform infrared spectroscopy (ATR-FTIR) with attenuated total reflection, scanning electron microscopy (SEM), and X-ray photoelectron spectroscopy (XPS).

3. Results and Discussions

The funnel-shaped plasma jet treatment can improve the wettability of CO and COPES and the increase is related to the treatment energy dose applied to it. When analyzing the wettability, the resistance of the treatment to washing was found, which suggests a low surface incorporation of weakly bound molecules. In addition, a hydrophobic regression analysis was performed, in which the samples showed a tendency to maintain wettability even after 168 hours of treatment. This may be related to the low presence of weakly bound molecules on the surface.

Analyzing the materials by ATR-FTIR, changes in the CH₂ stretching bands were detected in the samples, which were resistant to washing with distilled water. This again refers to low action of weakly bound molecules but still holds the possibility of functionalization or cleaning by plasma treatment. XPS analysis indicated the presence of N, Ca, K, Si, P, and S residues, possibly from cellulose complementary materials in the textile fiber. In addition, it allowed us to verify the incorporation of oxygen along the surface of the samples according to the dose of treatment applied. It was possible to observe an increase in the C-OH, C=O, and COOH bands, to the detriment of C-H, thus indicating an effective functionalization resulting from the treatment.

Finally, the morphological analysis of the surface of the samples showed the physical effect of the plasma on the opening of microcraters in the textile fiber. Moreover, the ability of the treatments to remove possible contaminants from the textile surface was reiterated.

Therefore, the treatment promoted surface cleaning of contaminants, increased surface roughness and functionalization, providing surface activation and increased wettability in a relatively regular way on the surface of the samples, according to the applied energy dose.

4. References

- [1] P. Frizoni, "PROCESSO ECOLÓGICO PARA O TINGIMENTO DO ALGODÃO purga ezimática", TCC, Americana, 2011.
- [2] L. Beltrame, "Caracterização de Efluente Têxtil e Proposta de Tratamento", 2000.
- [3] C. P. de R. H. CPRH, "ROTEIRO COMPLEMENTAR DE LICENCIAMENTO E FISCALIZAÇÃO PARA A TIPOLOGIA TÊXTIL", Recife, 2001, p. 1–10.

^{*} Corresponding author: silva.leal@unesp.br

TRIBOLOGICAL BEHAVIOR OF BORON DOPED DLC FILM GROWN VIA PULSED PECVD

Funsho Olaitan Kolawole, Elver Juan de Dios Mitma Pillaca¹, Saulo Ribeiro Ferreira², Lais Gimenes Vernasqui¹, Rebeca Falcão Correia¹, Evaldo José Corat¹, Vladimir Jesus Trava-Airoldi¹

¹Instituto Nacional de Pesquisas Espaciais ²Universidade Federal de São Paulo

1. Introduction

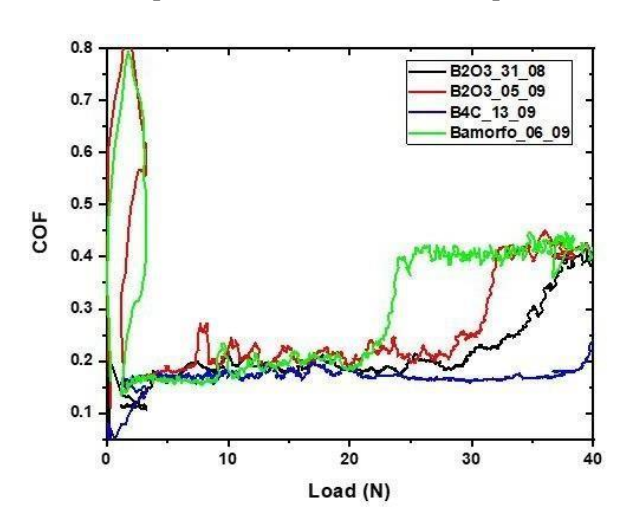
DLC coatings are known for their poor adhesion to metallic substrate, therefore leading to delamination during tribological applications [1]. Doping of DLC with metallic or non-metallic elements has been shown to improve adhesion to metallic substrate and tribological properties of DLC coatings [2].

2. Experimental

Plasma enhanced chemical vapour deposition (PECVD) with an additional cathode placed inside the reactor, to confine the plasma, and a bubbler, placed outside the reactor, to produce the boron solution was used to grow boron doped DLC on Ti-6Al-4V and Si substrates by varying the pressure and voltage, from 3mTorr to 7mTorr and from 0.7kV to 1.0kV, respectively. The mechanical properties and tribological properties were studied using nanoindentation, SEM, CETR-UMT Multi Specimen Test System equipment, WYKO NT1100 optical profiling system and Raman spectroscopy.

3. Results and Discussions

The COF and specific wear rates were obtained from scratch and wear test of the boron doped DLC film. The results present variation in COF and specific wear rate depending on the boron source used as dopant. The scratch track images were obtained using SEM. Fig. 1 shows the COF of boron doped DLC film, while Fig. 2 shows the specific wear rate of boron doped DLC film.



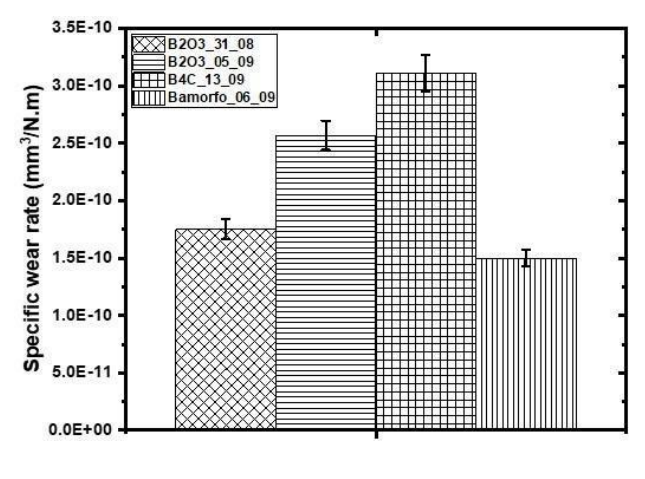


Fig. 1. COF for Scratch test for boron doped DLC film.

Fig. 2. Specific wear rate for boron doped DLC film.

4. References

- [1] J. Robertson, Mater. Sci. Eng. R. Reports., 37, 129–281, (2002).
- [2] A. Erdemir, C. Donnet, J. Phys. D Appl. Phys., 39, 18-24, (2006).

Acknowledgments

This work was supported by Fundação de Amparo à Pesquisa do Estado de São Paulo (FAPESP), grant # 2023/08065-6, 2017/08899-3, 19/18572-7 and Concelho Nacional de Desenvolvimento Científico e Tecnológico(CNPq) grants # 102497/2022-2 and 106517/2023-6.

TRIBOLOGICAL BEHAVIOR OF THE HYBRID NANOSTRUCTURE OF CNTs AND DLC FILM Premiado 1° Lugar OBTAINED BY PECVD

Larissa Solano de Almeida^{1*}, Renan Matos Monção³, Francisco das Chagas Silva Santos³, Conrado Ramos Moreira Afonso⁴, Rômulo Ribeiro Magalhães de Sousa³, Marcos Dorigão Manfrinato^{1,2}, Bartolomeu Cruz VianaNeto³, Luciana Sgarbi Rossino^{1,2}

1. Introduction

Studies focused on carbon nanostructures have intensified in recent decades, as they present specific physical and chemical properties that make them attractive for application in various areas. Structures such as carbon nanotubes (CNTs) are studied for application in biomedicine, due to their biocompatibility with the human body [1]. Diamond-like carbon (DLC) films have great potential to be competent in implant coating, due to their low coefficient of friction [2]. Therefore, the objective of this work is to study the tribological behavior of the hybrid carbon nanostructure of carbon nanotubes and DLC film (CNTs/DLC) obtained by the Plasma Enhanced Chemical Vapor Deposition (PECVD) technique on a nickel substrate.

2. Experimental

The synthesis of the hybrid carbon nanostructure on the nickel substrate was carried out using the PECVD technique with a pulsed DC source. The synthesis process began with plasma ablation of the nickel for cleaning. Then, the CNTs were grown with the precursor gases methane (CH₄) (25.5%), H_2 (12.8%) and Ar (61.7%) with a total gas flow of 235 sccm, at 800 V per 30 minutes. After the growth of the CNTs, the DLC film was deposited with the gases CH_4 (90%) and Ar (10%) at a total gas flow of 30 sccm, at 600 V for 60 minutes. Characterizations of the nanostructures were obtained by Raman spectrometry and fixed ball micro abrasive wear.

3. Results and Discussions

The Raman spectra in Fig. 1 (a and b). present the D, G, 2D e D+G bands, characteristic of carbon nanostructures. The hybrid nanostructure presents the characteristic bands of CNTs, however with the presence of bands characteristic of DLC films (Fig. 1(b)). In Fig. 2 (a and b) it is possible to observe the increase in wear resistance of nickel with carbon nanostructures. However, the hybrid nanostructure presents the best tribological behavior.

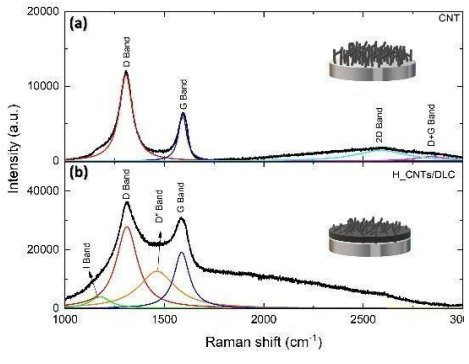


Fig. 1. Raman spectra (a) CNTs and (b) CNTs/DLC hybrid nanostructure.

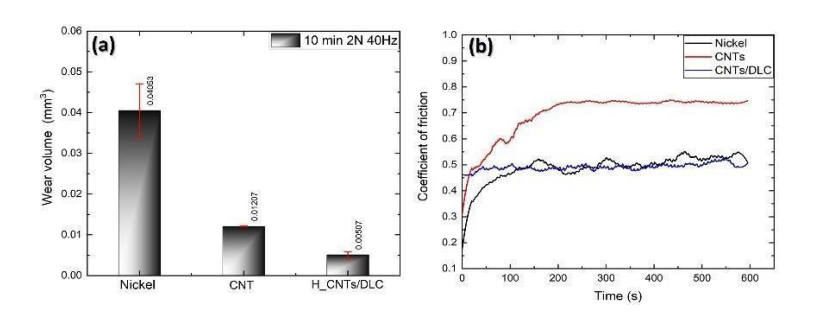


Fig. 2. (a) Wear volume and (b) Coefficient of friction.

4 References

- [1] M. Selvaraj et al. Journal of Water Process Engineering, v. 33, n. October 2019, p. 100996, (2020).
- [2] L. S. Almeida et al. Materials Research Express, v. 7, p. 1–19, (2020).

Acknowledgments

The authors acknowledge FATEC-SO, UNICAMP, DEMA, UFPI, and CAPES (001) for the financial support.

¹ Universidade Federal de São Carlos - UFSCar Campus Sorocaba

² Faculdade de Tecnologia do Estado deSão Paulo - Fatec Sorocaba ³ Universidade Federal do Piauí – UFPI,

⁴ Universidade Federal de São Carlos - UFSCar Campus São Carlos.

^{*}Corresponding author: solano.larissa@gmail.com

TRIBOLOGICAL STUDY OF AISI 304 NITROCEMENTED STEEL WITH DIFFERENT PERCENTAGES OF METHANE

Maria Fernanda Águas Schünemann ¹, Hugo Felipe da Silva Lopes ¹, Marcos Dorigão Manfrinato ¹, Luciana Sgarbi Rossino ^{1.2}

¹ FATEC Sorocaba, ² UFSCar Sorocaba

1. Introduction

The stainless steel is a widely used material in industry that operates in corrosive environments. However, its use is limited due to its low surface hardness and low wear resistance. It is possible improve your surface characteristics by thermochemical treatments, which maintain the tenacity of the core and the surface more resistant to wear [1]. Nitrocarburizing provides increase in hardness and wear resistance of the treated metal by the formation of the layer compound and diffusion zone produced by the diffusion of carbon and nitrogen into the treated substrate. The plasma nitrocarburizing treatment allows for better parameter and formed layer control. The objective of that study is to determine the effect of the percentage of methane (CH₄) in the 304 stainless steel surface properties nitrocarburized by plasma process.

2. Experimental

Polished and cleaned AISI 304 steel samples were nitrocarburized by plasma process. Plasma ablation was step was carried out with 80% Ar and 20% H₂ at 400°C and 450°C for 2 hours. After that, the plasma nitriding and nitrocarburizing step, whose parameters were 0%, 1%, 3% and 5% CH₄, was carried out with flows of 750 and 1000 sccm. The tribological study was carried out using a rotating fixed ball wear machine with normal load of 8N and 40Hz by 150, 300, 600, 900 and 1200 seconds. A hardness analysis was performed per Vickers microhardness with a load of 0.05 kgf.

3. Results and Discussions

Plasma nitriding and nitrocarburizing significantly increased the surface hardness and wear resistance of the treated material. It possible observe in Fig. 1 that the increase in substrate hardness is directly proportional to the increased CH₄ content at treatment atmosphere, in which nitrocarburizing with 3% and 5% CH ₄ provided bigger hardness values with an increase of approximately 430 % in relationship to the base material (BM). The wear volume presented in Fig. 2 shows the treatment carried out with 3% and 5% CH ₄ increased the wear resistance by 94% and 89%, respectively, in relation to BM.We conclude the increase in CH₄ at treatment atmosphere is beneficial for the surface characteristics of the steel, providing increase in hardness and wear resistance.

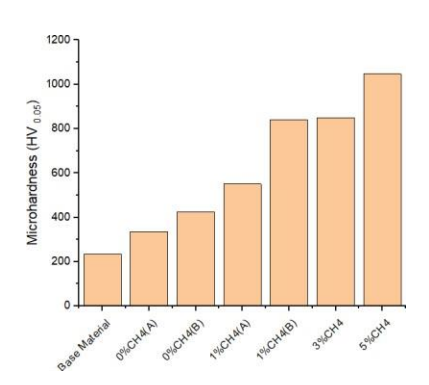


Figure 1 Graph of microhardness (b)

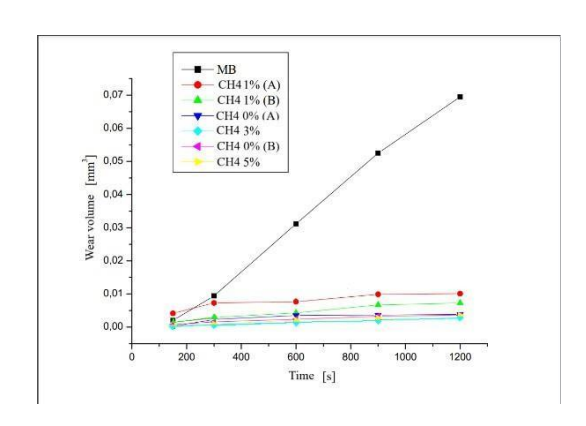


Figure 2 Worn volume graph

4. References

[1] GUEDES, Luis. Austenitic stainless steels. 1st edition. Brazil, 1994.

Acknowledgments

To the CPS for the scholarship.

^{*}Corresponding author: mariafernandaschunemann@gmail.com

UNDERSTANDING THE INTERACTION OF PLASMA JETS WITH THE HUMAN BODY FOR MEDICAL APPLICATIONS

Ananias Alves Barbosa*, Ana Carla de Paula Almeida, Fellype do Nascimento, Konstantin Georgiev Kostov

¹Universidade Estadual Paulista "Julio de Mesquita Filho" – Campus de Guaratinguetá

1. Introduction

Cold Atmospheric Pressure Plasma Jets (CAPPJs) have been successfully used in the biomedical field, with applications in wound healing, antimicrobial effects, improved blood circulation, and stimulation of tissue regeneration. To enable more effective use, it is necessary to better understand the physicochemical properties of CAPPJs, such as the electrical current to which the patient will be exposed during plasma treatment [1,2]. In this context, this study aimed to investigate two different configurations of an electrical device known as the Human Box, which is composed of an electrical circuit based on the IEC 60601-1 standard, to determine which one is more appropriated for simulating the interaction of CAPPJs with the human body.

2. Experimental

Two different models of the Human Box were assembled. Such a device is composed of a metallic target electrically connected to the ground through a $10~k\Omega$ resistor in series with a capacitor, with both in parallel witha $1~k\Omega$ resistor. The two Human Box models differ from each other only by the capacitance value of the capacitors(15 nF and 15 pF). The plasma jet was applied to the metallic target connected to the device, and the electrical current flowing through this system was measured using an electric current monitor. Subsequently, the electricalcurrent flowing through the capacitor of the system was calculated. Such current is known as Patient Leakage Current (PLC).

3. Results and Discussions

An experimental setup allowed us to measure the total current associated with each Human Box device, as well as the corresponding PLC values. The results show that the current that came closest to the value measured in parts of the human body was that of the Human Box with a 150 pF capacitance capacitor, the one suggested bythe IEC 60601-1 standard.

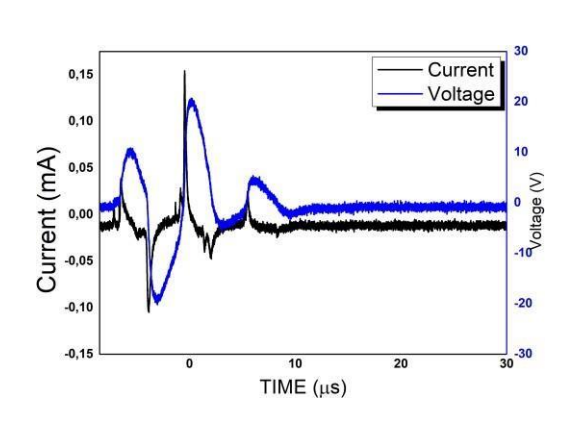


Fig. 1. Measuring electrical current and voltage signals using He, a 150 pF Human Box.

4. References

[1] STANCAMPIANO, Augusto et al. IEEE Transactions on Radiation and Plasma Medical Sciences, v. 4, n. 3, p. 335-342, 2019.

[2] TIMMERMANN, Eric et al. Journal of Physics D: Applied Physics, v. 54, n. 2, p. 025201, 2020.

Acknowledgments: This work was supported by CAPES and FAPESP.

^{*}Corresponding author: ananias.alves@unesp.br

USE OF DUPLEX TREATMENT OF NITROCARBURIZING AND SILICON DOPED DLC FILM AS A IMPROVEMENT OF USEFUL LIFE OF AISI M2 STEEL MACHINING TOOL

Miguel Rubira Danelon¹*, Larissa Solano de Almeida², Paulo Sérgio Martins³, Elhadji Cheikh Talibouya Ba⁴, Marcos Dorigão Manfrinato^{2,5}, and Luciana Sgarbi Rossino ^{2,5}

¹Departmetn of Materials and Metallurgical Engineering, University of São Paulo – USP, SP, Brazil

²Federal University of São Carlos – UFSCar – Sorocaba Campus, SP, Brazil

³University Center - UNA, MG, Brazil

⁴Federal University of Uberlândia – UFU – MG, Brazil

⁵Sorocaba Technological College – FATEC Sorocaba – SP, Brazil

1. Introduction

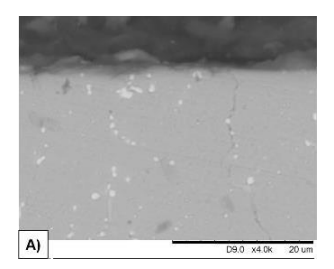
Duplex treatments consist of a combination of superficial treatments, which can combine nitrocarburizing with a DLC film promoting the formation of a hard ceramic compound layer and a lubricating amorphous carbon film, respectively [1]. The addiction of silicon in the DLC can stabilize the film structure allowing its application in situation of high temperature [2]. This work aims to study the effect of the duplex treatment (nitrocarburizing + Si-DLC) on the useful life of AISI M2 steel machining bits.

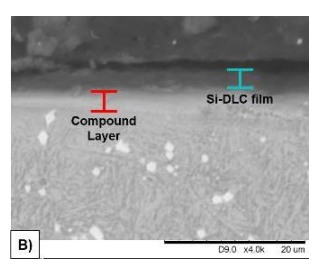
2. Experimental

Duplex treatments were performed on AISI M2 steel machining bits, with a pulsed-DC power supply. Plasma nitrocarburizing was performed with a gas mixture of 80%N₂/15%H₂/5%CH₄ at 450°C, 750 sccm gas flow by 6h. Right after, an organosilicon interlayer has been deposited with a gas mixture of 70%HMDSO/30%Ar, at 300°C by 15min. Finally, the Si-DLC film was deposited with a 90%CH₄/8%Ar/2%HMDSO gas mixture, at 300°C, 30 sccm gas flow by 2h. Images of the cross-section of tools and measurement of the built-up edge were performed by SEM. Microhardness Vickers tests were performed using a 0.1 kgf load. Al-Si-Mg 6351-T6 alloy was machined with cutting speed parameters of 37 and 147 m/min.

3. Results and Discussions

Fig. 1 shows the cross-section of untreated and treated tools. It is possible to observe the presence of a compound layer, indicated by a red line, and the Si-DLC film indicated by a blue line, with thicknesses of 2,60 and 2,01 μ m, respectively, which provided an increase in the hardness from 698 ± 64 HV to 1577 ± 273 HV. The duplex coating decreased the thickness of the built-up edge for cutting speeds of 37 and 147 m/min by 1.5 and 42.26%, respectively, as shown in Fig 2. This can be explained by the low coefficient of friction of the Si-DLC film with the high hardness and the thermal isolation provided by the coating between the tool and the milled material, which reduces the plastic deformation and the attachment of the material. It is possible to conclude that the duplex coating was effective to improve the machining useful life of the tools.





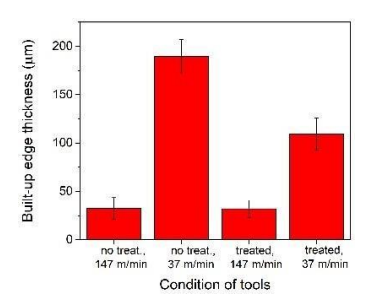


Fig. 1. Cross-section of tools A) without treatment and B) withtreatment NITC+Si-DLC

Fig. 2. Thickness of built-up edges as a function of tools with and without surface treatment

4 References

- [1] A. P. Tschiptschin "Duplex Coatings". Encyclopedia of Tribology. Springer US, 2013. p. 794 800.
- [2] W-J Wu and M-H Hon, Surf. & Coat. Tech., v. 111, n. 2-3, 134-140, (1999).

Acknowledgments

We would like to acknowledge FATEC Sorocaba, CEFET-MG and Capes (code 001).

^{*}Corresponding author: miguel.danelon@usp.br

USE OF HIGH-ENERGY BALL MILLING AND POROSITY CONTROL IN THE DEVELOPMENT OF ALLOYS OF THE MG-ZN SYSTEM AIMING BIOMEDICAL APPLICATIONS

Viviane Costa^{1*}, Durval Rodrigues Junior.²

¹ Program in Materials Engineering (PPGEM), Lorena School ofEngineering (EEL), University of São Paulo (USP), Lorena-SP-Brazil;

² Lorena School of Engineering (EEL), University of São Paulo (USP), Lorena-SP-Brazil

1. Introducion

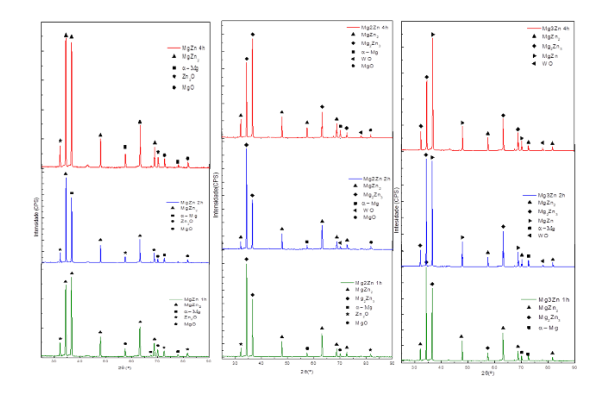
The scientific and technological development of today's society depends on materials that meet constantly evolving demands. This research focuses on biodegradable metallic materials, especially magnesium (Mg) and zinc (Zn) alloys, for medical applications such as load-bearing implants. These materials offer good biocompatibility, mechanical resistance and lightness, being useful in orthopedic and reconstructive surgeries. Powder metallurgy and high energy ball milling are employed to manufacture porous Mg-Zn system alloys with element distribution. The study explores the influence of these processes on the microstructure and properties of alloys, aiming at advances in customized biomedical materials for promising clinical applications [1].

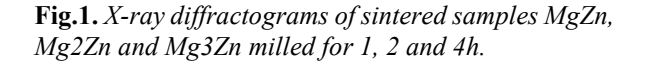
2. Experimental

At this stage, concerns are concentrated on the formation and densification of the powders, with a focus on the final properties and microstructure of the product. The selection of the powder production technique is crucial, being applied to several materials to create phases and dispersoids, increase solid solubility, refine grains (down to nanometric scales), generate new crystalline and amorphous phases, in addition to creating alloys with incompatible elements [2]. To study the solidification of Mg-Zn systems by powder metallurgy, with high-energy ball milling, a methodology was used that involves carrying out the characterization steps by X-ray Fluorescence (XRF) to verify contamination, X-Ray diffraction (XRD) and scanning electron microscopy (SEM) with EDS.

3. Results and Discussion

The study of the Mg-Zn system alloys presents results after high-energy ball milling of the powders, highlightingthe MgZn, Mg2Zn and Mg3Zn systems in milling times of 1, 2 and 4 h. X-ray analysis showed the formation of zinc solid-solution, generating secondary phases of MgZn2. SEM + EDS analysis observed white zinc particles, larger at 1 and 2 hours of milling. Milling generated irregularities in the particles due to attrition, causing deformations and fractures, notably in zinc. Magnesium powder milled with 1, 2 and 3% zinc, sintered at 580°C for 2 hours, showed advantages due to the possibility of pore formation, as shown in Figures 1 and 2.





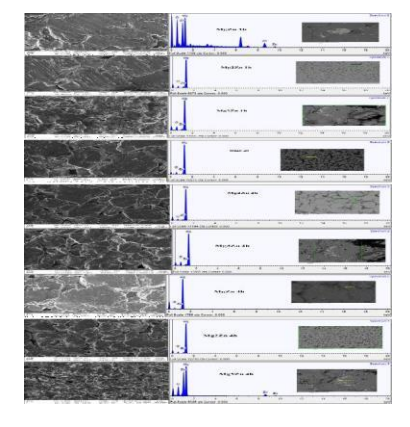


Fig.2. Analysis of scanning electron microscopy where the microstructure of the sample is observed, and their respectivechemical analysis by EDS spectrum for the alloys MgZn,Mg2Zn and Mg3Zn, milled for 1, 2 and 4h, respectively

4. References

[1] DAYAGHI, E. et al. Magnesium-zinc scaffold loaded with tetracycline for tissue engineering application: In vitro cellbiology and antibacterial activity assessment. Materials Science & Engineering C, v.102, p.53-65, 2019. Available at: https://doi.org/10.1016/j.msec.2019.04.010>.

[2] EL-ESKANDARANY, M. SHERIF. Biomedical applications of mechanically alloyed powders, Editor: M. Sherif El-Eskandarany, "*Mechanical Alloying*" (Third Edition), William Andrew Publishing, 2020, Pages 431-440, ISBN 9780128181805. Available at: https://doi.org/10.1016/B978-0-12-818180-5.00015-7>.

^{*} Corresponding author: vivianecosta@usp.br, durvalrj@usp.br

USING FOG COMPUTING: PROPOSING A PROBLEM-SOLVING ROADMAP FOR INDUSTRY 4.0 AND VACUUM TECHNOLOGY

Leandro Colevati dos Santos^{1,2}, Maria Lucia Pereira da Silva^{1,2}, Sebastião Gomes dos Santos Filho¹

¹Escola Politécnica da Universidade de São Paulo ²Faculdade de Tecnologia – Centro Paula Souza

1. Introduction

Vacuum technology is one of the pillars of Industry 4.0. and one of the main consequences of this industry is the enormous generation, and recurring need for evaluation, of data. Thus, several computational tools were born from this scenario, among them fog computing is one of the best alternatives because it addresses two fundamental issues: latency and immediate processing. In previous paper [1], an architecture was presented, which innovated through the use of Enterprise Service Bus (ESB), and which optimized these two commitments. Therefore, this work summarizes several case studies and uses them to propose a way of solving problems using such an approach. The final test is carried out with images with a high amount of noise.

2. Experimental

The previously developed architecture was used in addition to previous data from multiple, but specific, case studies. The images provided for the experiment, in addition to containing high noise, were always obtained over large portions of water and have information in the visible and infrared spectrum [2]. Environmental sensors are low-cost and data acquisition depends on a low-cost microprocessor.

3. Results and Discussions

Figure 1(a) presents the roadmap to be followed to verify data suitability for use in the Algorithmic Ignitor in Cloud Computing structure whereas Figure 1(b) shows an example. Therefore, after creating the structure [3], a conformity assessment is necessary, where a low amount of data is sufficient; conversely, optimization requires checking the compliance and quality of data, which can be, including images to be analyzed in a machine learning engine.

Once the functioning of the structure is understood, with data relevant to the process for the user, the offline verification of the system's behavior precedes decision making. An example, developed in this work, is an inservice image monitoring application with machine learning applied, returning more than 80% correction accuracy from Boolean image analysis in low time. If the architecture and performance are adequate offline, the system is used online and in the field. In this work, the case study developed was the use of environmental sensors for climate monitoring in the East Zone of São Paulo for days, allowing medium-term analysis. Thus, this approach is broad and applicable from specific cases (e.g. measurements in plasma) and broad information, such as environmental control.

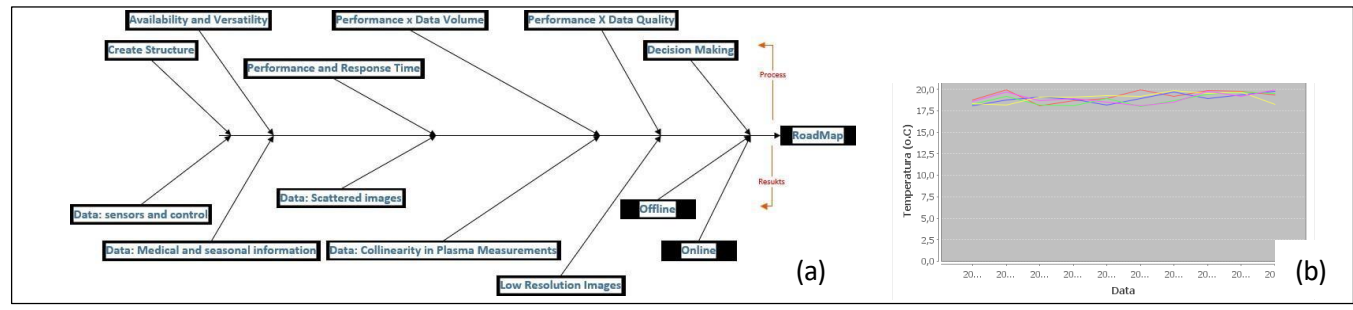


Figure 1: (a) Roadmap (in Ishikawa format) for applying the data structure to solve problems and (b) example of possible extracted data [1]

4. References

- [1] SANTOS, L. C. et al., "Anais do XXI ENGEMA", v. 1, p. 1-16, (2019).
- [2] Eick, F. B. L., "Dissertação de Mestrado", Instituto Tecnológico de Aeronáutica, (2021).
- [3] SANTOS, L. C. et al., "International Journal of Development Research", v. 10, p. 40875-40882, (2020).

Acknowledgments: M.Sc. Francisco Bernardo L. Eick and Ph.D. Alvaro José Damião for the data provided for this study.

^{*}Corresponding author: leandro.colevati@usp.br

VACUUM COMPONENTS OBTAINED BY 3D PRINTING USING BIODEGRADABLE PLASTIC

Ricardo Cardoso Rangel¹, Henrique Chaves Gulino², Francisco Tadeu Degasperi³

^{1,2,3} Laboratório de Tecnologia do Vácuo – LTV – Faculdade de Tecnologia de São Paulo - CEETEPS ¹Laboratório de Sistemas Integráveis – LSI – Escola Politécnica da Universidade de São Paulo – EPUSP

1. Introduction

Polylactic acid - PLA is a biodegradable polymer obtained from renewable sources and sold worldwide on a large scale. It is a safe material for human health and economically viable [1]. It has many advantages for use in FFF-type 3D printers (fused filament fabrication), due to its low fusing temperature (\sim 180°C). Therefore, several applications have been explored, however, the application as a material to form components of vacuum systems has been neglected so far.

It is well known that additive synthesis facilitates prototyping and is now a standard process in scientific and industrial development laboratories. The use of 3D printing to obtain vacuum components presents difficulties regarding the outgassing and permeability of the parts, however, the low cost and great flexibility can be attractive [2], especially in applications where the final pressure is around 1mbar.

2. Experimental

In this work blank flanges were produced in the KF-25 pattern of PLA using FFF type 3D printing. These components can be observed in Figure 1. The flanges were tested when replacing an aluminum flange of an Edwards auto 306 evaporator equipment from the Laboratory of Integrated Systems (LSI-USP). The flanges were printed using two different techniques, standard (braided) printing and unidirectional printing. The unidirectional flange even went through a polishing process to improve its performance. The pressure in the vacuum system wasobserved as a function of pumping time and the results are shown in Figure 2.

3. Results and Discussions

The final pressure obtained with an aluminum flange is used as a reference for comparison. The final pressure achieved is 10 times better with the unidirectional technique when compared to the traditional (braided) printing technique. When polishing the unidirectional flange the result was even better. This is due to the reduction of surface roughness, improving sealing with the o-ring. The results are promising and show that it is possible toapply PLA and additive synthesis in vacuum systems for pressures of a few mbar.

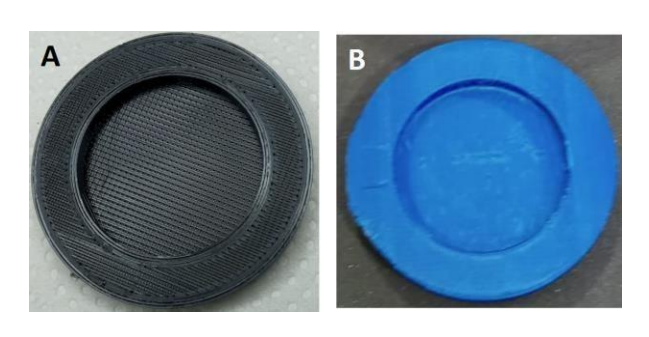


Fig. 1. Image of KF-25 3D printed PLA blind flanges. A) Using the standard (braided) technique and, B) Using the unidirectional technique.

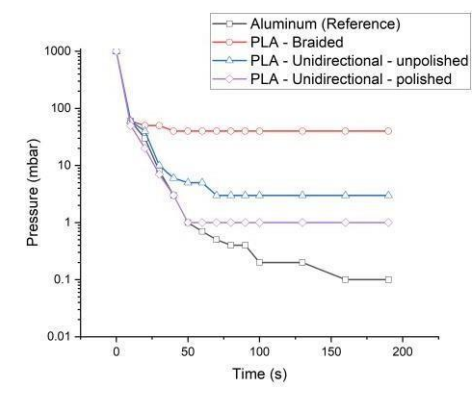


Fig. 2. Pressure as a function of time for the different flanges obtained. The unidirectional technique increased the pressure result.

4. References

[1] A. C. S. de Oliveira, et. al. - Poli (Ácido Lático) Aplicado para Embalagens de Alimentos: Uma Revisão - Revista Eletrônica deMateriais e Processos, v. 15, n. 1 (2020) 1-10 ISSN 1809-8797.

[2] T. Chaneliere. Vacuum compatibility of ABS plastics 3D-printed objects. [Research Report] CNRS, Laboratoire Aimé Cotton. 2017.

Acknowledgments: To FAPESP and CNPq for financial support.

 $[\]hbox{*Corresponding author: rrangel@lsi.usp.br}$

VACUUM PRESSURE METROLOGY BY THE STATIC EXPANSION METHOD - MORE RESULTS

1. Introdution

Continuing the metrology activities in vacuum technology, in the specific case, pressure metrology, are being developed, joint work between the *Laboratório de Tecnologia do Vácuo - LTV* of *FATEC-SP - CEETEPS* and the *Laboratório de Pressão -* LAPRE of the Instituto Nacional de Metrologia, Qualidade e Tecnologia - INMETRO, aims to improve a system that aims to be a standard vacuum primer in Brazil. Its operation uses the method of successive static expansion to make vacuum manometer metrology. In this way, these research activities are intended for the industrial area, but there is also the possibility of carrying out studies on metrology in vacuum and the interference that certain variables have in pressure measurement. In most industrial processes, the control over the variables that interact with the vacuum system becomes important, since a pressure variation can influence the manufacture of a product, therefore, the metrological quality must be maintained with pressure sensors, as well as gas transfer rate (*throughput*).

2. Methodology - Theoretical and experimental approaches

The experimental metrological arrangement is composed of a set of vacuum chambers with various volumes, which were determined with their measurement uncertainties. The determination of the volumes of the vacuum chambers, with small uncertainty, is fundamental to guarantee a high metrological quality. The largest vacuum chamber is called the expansion vacuum chamber, as illustrated in Figure 1. The concept relating to ideal gases, Boyle-Mariotte Law is applied to gas expansions, Equation 1. To carry out the measurements, the temperature is controlled through an air-conditioned environment, the temperature of 20 °C, with an uncertainty of 1 °C. Thus, with the injection of nitrogen gas - N_2 - in one of the vacuum chambers or in a combination between the starting vacuum chambers, with pressure p_1 , (with the volumes of the vacuum chambers determined). In this way, it is possible to find the value of the final pressure p_2 (after expansion of gas) of the vacuum system, after the expansion of the gas that was in the initial volume V_1 into the expansion chamber, with the final volume V_2 , this final volume being the sum of the volumes involved in expansion,

$$p_1.V_1 = p_2.V_2$$
 (1)

3. Results e Discussion

Using vacuum gauges from LAPRE - INMETRO and LTV - FATEC-SP, which capacitive membrane gauges are with calibrated 10⁵ Pa pressure gauges and two capacitive pressure gauges from LTV. Figure 1 shows the metrological system in LTV. Expansions were carried out that extended the measurements in relation to the measurements made in the year 2022. In principle, the Static Expansion Method can be a primary metrological arrangement that has the pressure range from 10⁵ Pa to 1 Pa. This pressure range is what corresponds to around the pressure in 70% of vacuum systems employed in industry.



Fig. 1. Vacuum system in LTV

4. Reference

[1] **ARAKAWA**, Rodrigo. **Caracterização do Padrão Primário de Vácuo pelo Método de Expansão Estática**. Orientador: Francisco Tadeu Degasperi. 2013. TCC (Graduação) — Curso de Tecnologia de Materiais, Processos e Componentes Eletrônicos, MPCE - FATEC-SP. São Paulo.

ZINC OXIDE FILM ON GLASS SUBSTRATES BY MEANS OF PLASMA IMMERSION ION IMPLANTATION AND DEPOSITION

Maxson Souza Vieira^{1*}, Eduardo Cezar Barbosa de Barros Aragão²

¹Instituto Federal da Bahia ²Universidade Federal dos Vales do Jequitihonha e Mucuri

1. Introduction

Zinc Oxide (ZnO) is a semiconductor material, which presents many interesting characteristics to the scientific community and the electronics industry[1]. Recently, researchers turned their attention to micro and nanostructures of ZnO. In the case of sensor, e.g., the efficiency or sensitivity is proportional to surface area of the sensing element [2]. Nano structures such as rods (nanorods) or wires (nanowires), for example, provide a high ratio of surface area to volume ratio, thus resulting in high sensitivity and efficiency [2]. This article reports the growth of ZnO micro and nano-structured on glass substrates by means of Plasma Immersion Ion Implantation and Deposition (PIII&D).

2. Experimental

The process of PIII&D was performed in a system called VAST [16,17,18] (acronym for Vaporization of Solid Targets). In this system an argon/oxygen (90% and 10% respectively) glow discharge is first switched-on at a pressure of 10-3 mbar. The vapor is partially ionized due to collisions with plasma particles and electrons drawn from the cathode. Zn ions are implanted into Glass when high negative voltage pulses (6-10 kV/250 Hz/40 µs) are applied to the sample holder.

3. Results and Discussions

Figure 1 and 2 shows high resolution X-Ray diffractogram pattern for as deposited state (a) and after annealing at 700 °C (b). Different diffraction peaks of a mixture of both metallic Zn and ZnO, were detected for the as deposited sample revealing a polycrystalline structure. The partial oxidation of Zn in this case is due to the percentage of oxygen in the composition of the plasma. The annealed sample shows only ZnO peaks, can be seen in figure 2. The (101) peak remained as the dominant one, but many other ZnO peaks arose, indicating that the annealing favored the oxidation of metallic Zn present in the film.

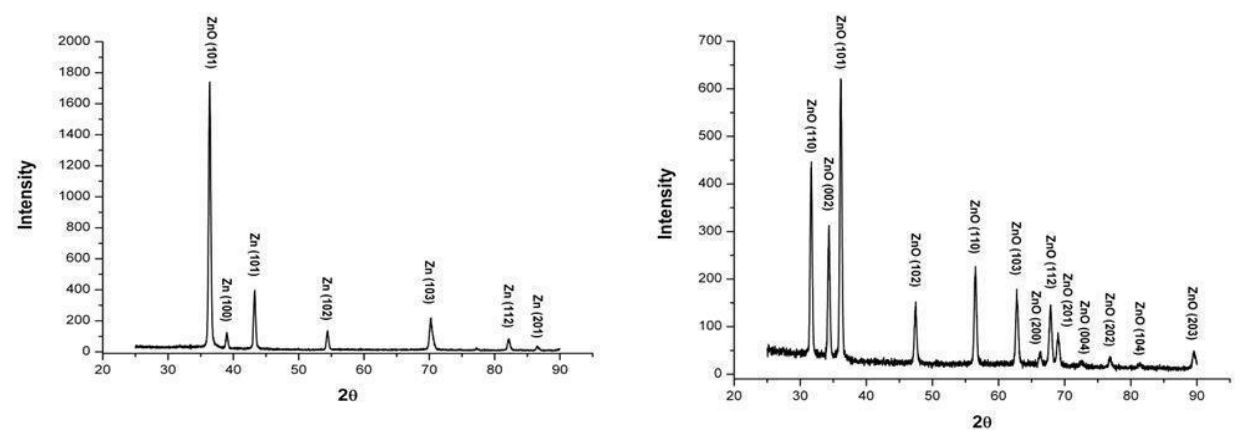


Fig. 1. XRD before annealing.

Fig. 2. XRD after annealing.

4. References

[1] P. MORKOÇ, H. OZGUR, U. Zinc Oxide: fundamentals, materials and device technology. 1 ed. Alemanha: Wiley-VCH. 2009. 490p

[2] FANG, Z. B. YAN, Z. J. TAN, Y. J. LIU, X. Q. WANG, Y. Y. Influence of post-annealing treatment on the structure properties of ZnO films. Applied Surface Science. v. 241, p. 303-308, 2005.

^{*}Corresponding author: eduardo.aragao@ufvjm.edu.br

SUMÁRIO DE AUTORES

Α

Abrahão

Ana Beatriz R.M., 120

Acciari

Heloisa A., 111

Afonso

Conrado R.M., 49, 170

Aguirre

Misha J.C., 150

Airoldi

Vladimir J.T., 102, 169

Alencastro

Felipe S., 108

Alfaro

Francisco, 72, 115

Algatti

Mauricio A., 150, 163

Almeida

Amélia, 166

Ana Carla P.L., 123, 141, 172

Felipe S., 89

Felipe S. de, 55

Larissa S., 64, 65, 73, 87, 101, 106, 170, 173

Alves

Abreuçon A., 123

Ana Paula R., 90

Élida M.A., 111

Fillip C., 92

Glauber R.L., 71

Hernandes M., 126

Alves Junior

Clodomiro, 31, 62, 96, 135

Amaral Junior

Miguel A., 143

Andreatta

João Pedro C., 113

Aniceto

Ana Paula P., 110

Antônio Jr

César A., 106

Aoki

Idalina V., 73

Aragão

Eduardo C.B.B., 178

Araújo

Anselmo C., 122

Archanjo

Braulio, 129

Azevedo Neto

Nilton F., 125, 132

В

Backes

Eduardo H., 59

Baldan

Mauricio R., 71, 142, 143, 145

Barbosa

Ananias A., 141, 172

Divani C., 71, 142

Barros

Helen C.S., 135, 155, 156

Batista

Aline F., 143

Becker

Daniela, 59, 70, 76, 127

Bento

R.T., 85

Bernardes

Fábio H.C., 63, 151

Bigansolli

Antonio R., *86*

Bimestre

Thiago A., 40

Bortoleto

José Roberto R., 60, 117

Bortolini Júnior

Celso, 90

Botan Neto

Benedito D., 62

Botelho

Edson C., 47, 92, 120

Braz

Elen G.S., *95*

Rrito

Alana A.R., 103, 112

Bueno

Maura A., 60

 \mathbf{C}

Caldas

Iberê Luiz, 53

Camargo

Gabriel C., 144

Canal

Gustavo P., 161

Canettieri

Eliana V., 40

Capellato

Patricia, 42 Carlobolante

Cariobolanii

João Pedro A., 90

Carvalho

Fernando L.C., 119

Castro

Gisele S., 149

Thais S., 116

Cavadas

Raiane, 80

Cavaleiro

Albano, 78

Ch

Chanes

Milena, 95, 157

Chiappim

William, 44, 149

Chiaradia

Carlos E., 80

C

Claro

Ana Paula R.A., 42, 46, 95, 157, 159

Coan

Karine S., 147

Codaro

Eduardo N., 111

Corá

Alana M., 73, 87, 110

Corat

Evaldo J., 169

Correa

Diego R.N., 124, 128

Corrêa

Diego R.N., 49, 81, 147

Mariana R., 54

Correia

Rebeca F., 169

Costa

Felipe J., 103, 112

Gustavo J., 103

Jílio C., 99

Kaleb D., 139

Lidiane C., 59

Michelle L., 92

Sidney C.Z., 38

Viviane, 109, 174

Cozza

Ronaldo C., 107, 114

Cruz

Nilson C., 30, 48, 56, 60, 69, 81, 88

D

Damião

Alvaro J., 19, 139

Danelon

Miguel R., 82, 173

Danesi

João Gabriel V., 64, 153

Degasperi

Francisco T., 35, 41, 106, 113, 118, 126, 161, 176

Delatorre

Rafael G., 115

Dias

Marcus V.S., 122

Domínguez

Jorge H.L., 107

Doria

Anelise C.O.C., 55, 89

Duarte

Amanda N., 95

Diego A., 72, 115

Dyer

Paulo P.O.L., 50

E

Eleuterio

Paloma H.P., 146

Elizondo

Juan I., 161

Emílio

Romualdo, 166

Escada

Ana Lúcia do A., 46

Essiptchouk

Alexei M., 105, 146, 162

F

Fabbro

Maria T., 145

Fazenda

Giovana, 148, 155, 156

Fermino

Júlio C.O., 67

Fernandes

Anderson C., 76

Ferrari

Breno B., 88, 101

Ferraz

Joel A.S., 122

Ferreira

Fábio E.S., 78

Marcelo J., 25

Saulo R., 102, 169

Florêncio

Odilia, 166

Fonseca

Wesley B.J., 86

Fontana

Luis C., 27, 59, 83, 114, 127

Fontes

Marcelo B.A., 35

Marcos A., 78

Fosca

Marco, 22

Fraceto

Leonardo F., 60

Fragoso

Maria V.F., 88

Maria Vitória F., 101

Fraile Jr

André C., 53

Freitas

Lília A. de, 40

Fuentes

Ruben G., 150

Fukutani

Katsuyuki, 16

G

Gama

Bruno E.P.N., 154

Germano

José S.E., *133*

Getnet

Tsegaye G., 56

Gobbi

Angelo L., 38

Goehr

Luiz Eduardo P., 72

Gomes

Anderson M., 54

Marcelo P., 132, 146, 162

Marcilene C., 156

Gonçalves

Gabriel A.C., 73

Vinícius R.M., 49

Gouvea

Evaldo C., 116

Gouvêa

Evaldo C., 68, 74

Grandini

Carlos R., 29, 49, 54, 61, 84, 124, 128, 147, 159

Grondona

Diana, 21

Guidi

Erick S., 39, 66

Gulino

Henrique C., 35, 118, 176

H

Hammer

Peter, 127

Hangai

Bruno V.A., 77

Harb

Samarah V., 59

Hein

Luiz R.O., 26

Hergesel

Kaique G., 88, 101

Hesse

Rubens, 67

Hirata

Anderson K., 50

Horta

Isabela M., 100

I

Irazusta

Silvia P., 65, 73, 106, 110

K

Karnopp

Júlia, 121

Kayama

Milton E., 56

Kodaira

Felipe V.P., 26, 47, 149, 165, 167, 168

Koga Ito

Cristiane Y., 28, 44, 45, 96, 125, 149

Kolawole

Funsho O., 102, 169

Kolowrotkiewicz

Julia, *30*

Konatu

Reginaldo T., 159

Korukian

Augusto O., 129

Kostov

Konstantin G., 26, 28, 79, 141, 149, 165, 167, 168, 172

Kressin

Eduardo, 72

Kruger

Cléber S., 72

L

Lanziloti

Glauber R., 142

Leal

Bruno H.S., 168

Rafael S., 155, 156

Leão

Alcides L., 95, 157

Lee

Han Bo Ram, 121

Leite

Douglas M.G., 100, 125, 132, 148, 156

Lady D., 96

Lady D.P., 44

Lemos

Lucas L.D., 38

Lima

Alessandro, 100, 125, 132

Amanda, 101

Amanda D.R., 88

Daiane M., 88, 101

Lais B.S., 76

Luan G., 62, 96

Milton S.F., 103, 112

Lisboa-Filho

Paulo N., 24, 49

Lopes

Braulio H.K., 71, 142

Hugo F.S., 171

Lourenço

Mariana L., 29

Lucas

Rafael R., 39, 47, 66, 80, 92, 111, 120, 122

M

Macedo

Waldemar A.A., 23

Machado

Raphaela C., 68, 74

Magaldi

Bernardo V., 129

Maluf

Omar, 152

Manfrinato

Marcos D., 64, 82, 87, 101, 152, 153, 170, 171, 173

Marcondes

Michaela S., 62, 96

Mariano

Samantha F.M., 136

Marques

Luis F.B., 120

Luís F.B., 39, 47, 66

Martins

Marcel G., 86

Paulo S., 173

Mastelaro

Valmor R., 38

Mauricio

Danilo C., 61

Milhan

Noala V.M., 28

Mineiro

Sergio L., 143

Miranda

Felipe S., 45, 62, 96, 105, 125, 132, 162, 164

Monção

Renan M., 170

Monteiro Marco A.A., 133

Montoro Sergio R., 93

Moraes

Carlos E., *92* Maria C.B., *60*

Morais

Vinicius C., 41, 118

Moreira Júnior

Pedro W.P., 125, 164

Mota

Rogério P., 39, 47, 66, 80, 120, 122, 123

Motta

João Vitor S., 97

Moura

Keren A.S., 88, 101

Myers-Ward

Rachael L., 20

N

Nakazato

Roberto Z., 90

Nascente

Pedro A.P., 38

Nascimento

Andreas, 37

Fellype do, 28, 79, 141, 172

Tayslâine B., 90

Neto

Aroldo M.P., 50

Nilton F.A., 36

Neves

Diego V., 88, 101

Nicollini

João V., *86*

Nishime

Thalita M.C., 79

Nunes

Brunna C.G., 157

Rhaysla T.R., 65

0

Oliveira

Ana Paula, 71, 142

Ana Paula S., 143

Elaine C., 88, 101

Joelma, 68, 116

Renata N., 86

P

Pacheco

Zormy N.C., 150, 163

Page

Laurence, 25

Pereira

André L.J., 100, 135, 148, 155, 156

Giovanna M., 119

Vitória C., 73, 106

Pérez

Jose L.J., 150, 163

Pessan

Luiz H., 59

Pessoa

Beatriz M., 86

Rodrigo S., 31, 44, 45, 55, 62, 96, 100, 121, 125, 132, 135

Petraconi Filho

Gilberto, 105, 162, 164

Petroski

Kléber A., *79*

Pillaca

Elver J.D.M., 102, 169

Pillis

Marina F., 85

inheiro

Alicia F.R., 113

Pintão

Carlos A.F., 49

Pouvesle

Jean-Michel, 18

Pradela

Fernando, 88

Q

Quade

Antje, 26

Quadros

Fernanda F., 84

R

Ramos

Raul, 117

Rangel

André L.R., 95, 157

Elidiane C., 30, 48, 56, 60, 69, 81, 88, 106

Ricardo C., 176

Rita C.C., 69

Rau

Julietta V., 17, 22

Recco

Abel A.C., 83

Reis

Jonas F., 39, 47, 66

Júlia C., 116

Rezende

Maira de L., 110

Ribeiro

Rafael P., 30

Rosinei B., 111

Ricardo

Eduardo V., 119

Ricotta

Regina M., 41

Rita

Cristian C.P., 93, 105, 112

Felipe L.P., 80

Robert

Éric, 18, 165

Roberto

Marisa, 53

Rocha

Lucas C., 31

Rodrigues

Bruna G., 97

Celio L.V., 86

Israel R., 61

Rita de Cássia L.B., 97

Rodrigues Junior

Durval, 63, 109, 151, 174

Romão

Maria Carolina F., 93

Romeiro

Rogério L., 94

Rosa

Jorge L., 93, 94

Luis Guilherme S.R., 59

Michel F.R., 87

Rossino

Luciana S., 64, 65, 73, 82, 87, 101, 152, 153, 170, 171, 173

Beiker M., 58, 158

S

Sachs

Daniela, 42

Sagás

Julio C., 67, 72, 76, 83, 99, 114, 115, 127, 144

Sampaio

Aline da G., 28

Douglas, 94

Sánchez

Jose L.L., 150

Sant'Anna

Luciana B., 89

Santos

Fernando V., 58

Francisco C.S., 170

Gustavo O., 157

Isabelle G., 145

Juliana P., 88, 101

Leandro C., 175

Leonilda M.B., 88, 101

Nazir M., 58, 158

Tuane S.R., 39, 66

Vinicius, 151

Vinícius dos, 63

Santos Filho

Sebastião G., 175

Santos Júnior

Wilson, 122

Schneider

Sandra G., 94

Schön

Claudio G., 114

Schünemann

Maria F.A., 171

Segantine

Rafael N., 135

Segat

Bruna, 70

Serejo

Luis P., 145

Shica

João Paulo M., 83

Sibelino

Sonia K., 55

Silva

Alex R., 64

Ana Maria R.da, 40

Diego F.G., 58 Diego M., 149

Elvis B., 72

Felipe C., 114

Gustavo H.R. da, 37

Ivan C.C., 139

João V.P., 82

José H. D. da, 36

Leandro A., 152

Lucas C., 92

Luiz G.C., 80

Maria Lucia P., 175

Maria Margareth da, 50

Raphael E. da, 19

Silvelene A., 50

Thiago R.B., 126

Simão

Renata A., 108, 129

Simões

Alexandre Z., 77

Soares

Pietra A.M., 111

Sobrinho

Argemiro S.S., 100, 132, 148, 155, 156

Sousa

João Vitor A.K., 161

Rômulo R.M., 170

Tiago S.P., 49, 124

Vinicius O.A., 139

Souza

Maria Eliziane P., 69

Mariana A.A., 71, 142

Pedro C.F.C.V., 108

Teófilo M., 68, 74, 116

William, 109

Stancampiano

Augusto, 18

Steffen

Teresa T., 127

Т

Talibouya Ba

Elhadji C., 173

Tavares

Thayna F., 26, 149, 167

Victoria K.F., 45

Victória K.F., 96

Teixeira Neto

Olavo, 129 Tenorio

Plinio I.G., 143

Torrento

Jhuliene E., 124, 128

Travain

Silmar A., 154 Trinh

Ngoc Le, 121

U

Ueda

Mário, 58, 158

Varavallo

Rogério, 152

Vargas

Carolina S., 133

Vasconcelos

Getúlio de, 50

Verma

Vikas, 107

Vernasqui Lais G., 102, 169

VianaNeto Bartolomeu C., 170

183

Vicente
Helder P., 50
Vidal
Usiel O.G., 163
Vieira
Maxson S., 178
Vilar
Rui, 166
Vilela
Filipe B., 42
Vitoriano

Jussier de O., 31

W

Wilcken Jorge T.S.L., 107 Yamamoto
Felipe M., 145

Zambuzzi Willian F., 54 Zanatta Antonio R., 36 Zepeda Claudio A.T., 135 Zickenheiner Christof, 117